

SOLIDIFICATION OF BINARY ALLOYS WITH
ONE DIMENSIONAL HEAT FLOW

A thesis
presented by
SHAM LAL MALHOTRA
for the
Degree of Doctor of Philosophy
in the
University of London

September, 1969.

John Percy Research Group
in Process Metallurgy,
Department of Metallurgy,
The Royal School of Mines,
Imperial College,
London, S.W.7.

ABSTRACT

A theory has been developed in this work to predict the progress of solidification of pure metals and binary alloys of the eutectic forming type, solidifying at zero or positive superheats with uni-directional heat flow. The solutions were developed using the integral profile method.

In order to verify experimentally the predictions made by the theory, solidification of pure lead, lead-antimony eutectic and lead-tin alloys was studied, under conditions of one dimensional heat flow with heat removed by convection with a constant heat transfer coefficient. The heat transfer coefficient was determined by independent steady state experiments. The progress of solidification was measured by thermal analysis.

Metallographic and solute segregation studies were undertaken to evaluate the various assumptions used in the development of the theory. Experiments were conducted to study the effect of purity and of morphology on the progress of solidification.

The agreement between theory and experiments have shown that the theory can be used to predict the rates at which a wide range of alloys solidify under a variety of different uni-directional cooling conditions.

CONTENTS

		PAGE
CHAPTER I	INTRODUCTION	9
CHAPTER II	REVIEW OF PREVIOUS WORK	11
II-1	REVIEW OF PRESENT KNOWLEDGE ON ALLOY SOLIDIFICATION	12
II-1-A	Different Morphologies Produced During Solidification	13
II-1-B	Factors affecting the type of morphology on solidification	15
II-1-B(i)	Planar to cellular transition in single phase alloys	15
II-1-B(ii)	Cellular to dendritic transition	15
II-1-B(iii)	Two phase alloys	16
II-1-C	Solute Segregation Produced During Solidification	16
II-2	PREVIOUS METHODS OF PREDICTING PROGRESS OF SOLIDIFICATION	18
II-2-A	Exact Solutions	18
II-2-B	Finite Difference Method	19
II-2-C	Integral Profile Method	20
II-2-C(i)	Hills' solution for the growth of a layer of solid metal	21
II-2-C(ii)	Other solutions for the growth of solid layer	27
II-2-C(iii)	Previous solutions for the solidification of freezing range alloys	28
II-3	EXPERIMENTAL TECHNIQUES	29
II-3-A	In Situ Techniques For Determining the Position of the Solidification Front	30
II-3-A(i)	Thermal analysis	30
II-3-A(ii)	Dip stick	31
II-3-A(iii)	Ultrasonic method	31
II-3-A(iv)	X-ray	31
II-3-A(v)	Direct visual techniques	32
II-3-B	Post Mortem Techniques	32
II-3-B(i)	Pour out method	32
II-3-B(ii)	Radio-isotopic	32
II-3-B(iii)	Addition of another metal	33
II-3-C	Selection of Method For Experimental Study	33
II-3-D	Solute Distribution	34

II-3-D(i)	Radio-isotopic method	34
II-3-D(ii)	Electron probe microanalyser	34
II-3-D(iii)	Spectroscopic	35
II-3-D(iv)	Selection of method for determining solute segregation	35
CHAPTER III	THEORETICAL TREATMENT OF UNI-DIRECTIONAL SOLIDIFICATION OF BINARY ALLOYS	36
III-1	STATEMENT OF THE PROBLEM	37
III-2	INTEGRAL PROFILE SOLUTION	38
III-3	THERMAL LAYER (COOLED LAYER)	40
III-3-A	General Equations	40
III-3-B	Convenient Forms	42
III-3-B(i)	Far bound moving at constant temperature, near bound stationary and cooling, and at variable temperature	43
III-3-B(ii)	Both bound stationary and cooling at variable temperatures	44
III-3-B(iii)	Both bounds moving at constant temperature	45
III-3-B(iv)	Far bound stationary, insulating and cooling near bound stationary	47
III-4	PARTIAL LAYER (LAYER OF PARTIALLY SOLIDIFIED METAL)	48
III-4-A	Liberation of Latent Heat	48
III-4-B	Variation of Thermal Conductivity	51
III-4-C	Derivation of General Equations	53
III-4-D	Convenient Forms	55
III-4-D(i)	Both bounds moving at fixed temperatures	55
III-4-D(ii)	Far bound stationary, insulating and cooling near bound at fixed temperatures and moving	57
III-4-D(iii)	Both bounds stationary, far bound insulated	58
III-4-D(iv)	Far bound insulated and moving at constant temperature, near bound stationary at variable temperature	59
III-4-D(v)	Far bound uninsulated moving at fixed temperature, near bound stationary at variable temperature	61
III-5	COOLING MODES FOR SOLIDIFICATION OF PURE METALS AND EUTECTICS IN PRESENCE OF SUPERHEAT	65

III-5-A	Mode 1 The Thermal Layer Growing Alone	66
III-5-B	Mode 1F Entire Liquid Region Cooling	69
III-5-C	Mode 2 The Solid and Thermal Layers Growing together	70
III-5-D	Mode 2F The Solid Layer is Growing after the Thermal Layer has reached the remote boundary	71
III-6	COOLING MODES FOR THE SOLIDIFICATION OF BINARY ALLOYS	71
III-6-A	Mode Z2 The Partial Layer is Growing into the Liquid at the Temperature	Liquidus 72
III-6-B	Mode Z2F Partial Layer Occupies Entire Region	75
III-6-C	Mode Z3 Partial Layer is Growing ahead of Solid Layer	76
III-6-D	Mode Z3F Partial Layer is Shrinking in front of Growing Solid Layer	77
III-6-E,F	Mode S1 Thermal Layer Growing and Mode S1F Entire Liquid Region Cooling	77
III-6-G	Mode S2 Partial Layer and Thermal Layer are Growing together	79
III-6-H	Mode S2F The Partial Layer is Growing after the Thermal Layer has reached the remote boundary	80
III-6-I	Mode S3 The Solid, Partial and Thermal Layers are Growing together	81
III-6-J	Mode S3F The Solid and Partial Layer has reached the remote boundary	81
III-7	VALUES OF THE PHYSICAL PROPERTIES AND OTHER VALUES USED IN THE THEORETICAL PREDICTIONS	85
III-7-A	Density, Thermal Conductivity and Specific Heat	85
III-7-B	Latent Heat	86
III-7-B(i)	Eutectic Metals	86
III-7-B(i)(a)	Lead Antimony	86
III-7-B(i)(b)	Lead-Tin Eutectic	86

III-7-B(ii)	Alloys	88
III-7-B(ii)(a)	Typical Calculation for the lead-tin system, Pb-20-Sn	89
III-7-C	Fraction Solid Present at Solidus Temperature (f_{SU})	89
III-7-C(i)	Typical calculations for the tin rich side of the lead-tin system	90
III-7-D	Liquidus and Solidus Temperatures	90
III-8-	NUMERICAL SOLUTION	91
CHAPTER IV	EXPERIMENTAL APPARATUS AND PROCEDURE	97
IV-1	DESCRIPTION OF THE APPARATUS	98
IV-1-A	The Casting Unit	98
IV-1-A(i)	The Crucible	98
IV-1-B	Measurement of Solidification Front	103
IV-1-C	The Cooling System	104
IV-2	HEAT FLOW CONDITION	106
IV-3	MEASUREMENT OF HEAT TRANSFER COEFFICIENT	108
IV-4	CALIBRATION OF THERMOCOUPLES	110
IV-5	PREPARATION OF ALLOYS	110
IV-6	SOLIDIFICATION OF LEAD-TIN ALLOYS AT ZERO-SUPERHEAT	111
IV-7	SOLIDIFICATION OF LEAD-TIN ALLOYS AT SUPERHEAT	112
IV-8	MORPHOLOGY AND SOLUTE SEGREGATION STUDIES	112
IV-9	CALORIMETRIC DETERMINATION OF LATENT HEAT OF LEAD-TIN EUTECTIC	113
IV-10	PURITY OF METALS USED	114
IV-10-A	COMMERCIAL METALS	114
IV-10-B	PURE METALS	114
CHAPTER V	RESULTS	115
V-1	HEAT TRANSFER COEFFICIENT	116
V-2	PROGRESS OF SOLIDIFICATION OF PURE METALS AND EUTECTICS	116
V-2-A	Lead	119
V-2-B	Lead-Antimony Eutectic	119
V-2-C	LEAD-TIN EUTECTIC	119

V-3	PROGRESS OF SOLIDIFICATION OF LEAD-TIN ALLOYS	120
V-4	VARIATION OF COOLED SURFACE TEMPERATURE	121
V-5	THERMAL BALANCES	121
V-6	LATENT HEAT OF LEAD-TIN EUTECTIC	152
V-7	SOLID STATE TRANSFORMATION	152
V-8	MORPHOLOGY AND SOLUTE SEGREGATION STUDIES IN LEAD ALLOYS	153
V-8-A	Lead-Antimony Eutectic	153
V-8-B	Lead-Tin Eutectic	154
V-8-C	Lead-Tin Alloy 20 wt. % Tin (Pb-20-Sn)	161
V-8-D	Tin-Lead Alloy 20 wt. % Lead (Sn-20-Pb)	169
V-8-E	Tin-Lead Alloy 10 wt. % Lead (Sn-10-Pb)	170
V-9	EFFECT OF MORPHOLOGY ON THE PROGRESS OF SOLIDIFICATION	170
CHAPTER VI	DISCUSSION	187
VI-1	INTEGRAL PROFILE METHOD	188
VI-2	ASSUMPTION USED IN THE PRESENT THEORETICAL TREATMENT	188
VI-2-A	Liquidus Temperature of the alloy is unique	189
VI-2-B	Solidus Temperature of the alloy is unique	191
VI-2-B	The Fraction of Solid Present in the partial layer is a function of temperature	192
VI-2-D	Fraction Solid Present at the solidus temperature is constant	195
VI-2-E	Liquid and Solid assumed to be of the same density	197
VI-3	ASSUMPTIONS MADE IN USING THE THEORY TO PREDICT SOLIDIFICATION RATES OF THE ALLOYS USED IN THIS INVESTIGATION	197
VI-3-A	Calculation of Density, Thermal Conductivity and Specific Heats of the Alloys	197
VI-3-B	Calculation of the Latent Heats of the Alloys	197

VI-3-C	Calculation of the Fraction Solid Present at Solidus Temperature	199
VI-3-D	Solidus Temperature of Lead-Tin Alloy containing 10 wt. % Tin	199
VI-4	Extent to which Experimental Apparatus reproduces Theoretical Conditions	200
VI-4-A	Unidirectional Heat Flow	200
VI-4-B	Absence of Convection Effects	200
VI-4-C	Accuracy of Experimental Results	201
VI-4-D	Solute Segregation Studies	202
VI-5	COMPARISON OF THEORETICAL AND EXPERIMENTAL RESULTS	202
VI-5-A	Eutectics and Pure Metals	202
VI-5-B	Tin Rich Alloys	203
VI-5-C	Lead Rich Alloys	204
VI-5-C(i)	Alloy composition more than maximum solid solubility	204
VI-5-C(ii)	Alloy composition less than maximum solid solubility	204
CHAPTER VII	CONCLUSIONS	206
APPENDIX I	DERIVATION OF DIFFERENTIAL EQUATION OF COOLED SURFACE TEMPERATURE IN MODES S2 and S2F	209
APPENDIX II	DETERMINATION OF THE LIMITING VALUE OF $\frac{dt_p^*}{d\bar{x}}$ WHEN THE PARTIAL LAYER IS EQUAL TO ZERO	212
APPENDIX III	COMPUTER PROGRAMME FOR THE SOLIDIFICATION OF METALS AND ALLOYS	215
APPENDIX IV	SPECIMEN THEORETICAL COMPUTED RESULTS	220
APPENDIX V	TENSILE STRENGTH OF PURE LEAD-TIN EUTECTIC	235
ACKNOWLEDGEMENTS		236
LIST OF FIGURES		237
LIST OF SYMBOLS		241
REFERENCES		247

I INTRODUCTION

The solidification of alloys has been a topic of intensive research, both from its industrial and fundamental aspects. In the main the fundamental research has two objectives. In the first place it is aimed at understanding the structure produced by solidification, the resulting solute segregation, and the effect of this structure and segregation on the mechanical properties of the alloy. In the second place it endeavours to predict the progress of solidification process as this information is required, for example, in the design of the continuous casting machines, and of feeder heads in the static casting process.

The work reported here deals with the later aspects and since the casting process is generally complex, involving among other factors multicomponent alloys and three dimensional heat flow; this work is limited to the simple cases of pure metals and binary alloys solidifying with unidirectional heat flow. Only the binary alloys which form eutectic with partial solid solubility are discussed.

The solidification of alloys involves unsteady state heat flow, so that the mathematical prediction of the solidification rates is a problem in unsteady state heat conduction. Since the problem involves a change of phase the partial differential equations involved are non-linear. The problem therefore can be solved by attempting an approximate mathematical solution for a particular case or by using simplifying assumptions and attempting an exact solution. Exact solutions have been obtained for only a few cases, approximate methods must be used for the more general cases.

There are two main approximate methods - the finite

difference method and integral profile method. In the finite difference method the partial differential equation is reduced to a suitable finite difference equation, (section II-2-B). This method suffers from the disadvantage that it is lengthy, tedious and time consuming. The integral profile method, on the other hand, reduces the ^{partial} differential equation to a non-linear ordinary differential equation which is much simpler to solve. The method is simple and flexible in its approach and has been used by various authors to predict the progress of solidification (section II-2-C). Recently Hills¹ has developed a generalised integral profile method for predicting the growth of a cooling solid metal layer and this method can be applied to a large number of cooling conditions. The aim of this work has been to extend Hills' solution so that it can be applied to the solidification of metals and alloys solidifying at various superheats and at various cooling conditions. The theoretical treatment is given in Chapter III.

The solidification of metals and alloys has been studied in an apparatus specially designed to produce unidirectional heat flow conditions. A short description of this apparatus and of the experimental procedure is given in Chapter IV. The experimental results obtained for the solidification of lead and tin alloys are compared with the predictions of the theory in Chapter V. Some of the results obtained for the solidification of lead-antimony eutectic alloys are also given. In a subsequent section the morphology and solute segregation that has been observed in these alloys are described.

The theoretical treatment developed in Chapter III is discussed critically in Chapter VI in the light of the experimental observations, and conclusions are drawn concerning the merits and limitations of the theory.

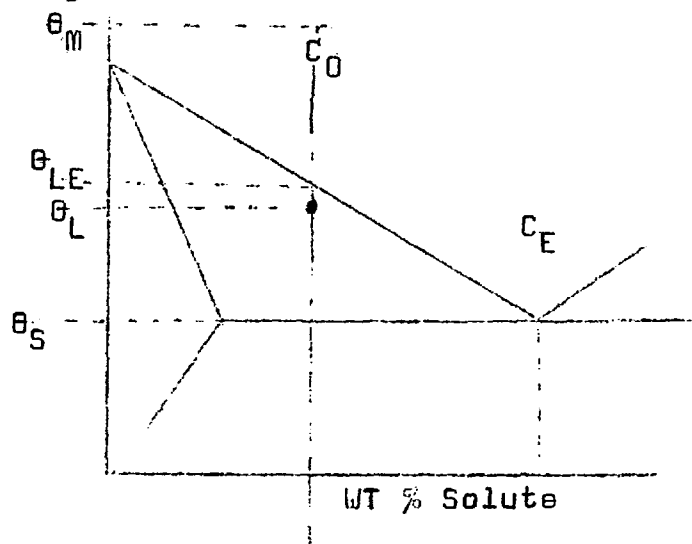
CHAPTER II
REVIEW OF PREVIOUS WORK

II REVIEW OF PREVIOUS WORK

The main aim of the work reported in this thesis has been to predict the rate of solidification of alloys and to compare the predictions with the results of relevant experiments. A short review of the previous literature is given in this chapter dealing with current knowledge regarding the solidification of alloys; various attempts made to predict the progress of solidification and the experimental techniques that have been used to measure solidification rates are also dealt with.

II-1 REVIEW OF PRESENT KNOWLEDGE ON ALLOY SOLIDIFICATION

The solidification of binary alloy that forms a eutectic can be explained with the help of a phase diagram as given below:



When an alloy of composition ' C_0 '^(a) is cooled from an initial temperature θ_M , the first solid will appear at the liquidus temperature, θ_L . This temperature will be lower than the equilibrium liquidus temperature, θ_{LE} , as given by phase diagram, by an

(a) This case discussed here is of an alloy of composition C_0 , when C_0 is greater than maximum solid solubility.

amount which depends upon the cooling rate. The first solid formed will contain a lower concentration of solute than bulk liquid. The solute rejected during solidification will thus enrich the remaining liquid so that subsequent solid will contain more solute than the solid that was formed first. The liquid will therefore become richer and richer in solute until the solidus temperature is reached when it will all solidify. The amount of liquid present at the solidus temperature will depend on the extent of solute rejection. This in turn, together with the resulting solute segregation will depend upon the rate of cooling, the temperature gradient and the composition and nature of the alloy. The segregation of solute influences the type of structure or morphology, produced during solidification. Thus, the morphology of the solidified metal may provide an insight into the nature of the solidification process.

II-1-A DIFFERENT MORPHOLOGIES PRODUCED DURING SOLIDIFICATION

A pure metal solidifies with a plane solid/liquid interface and the resulting microstructure will only show very thin grain boundaries. When a minute quantity of solute is present the solid/liquid interface will show small grooves and the resulting microstructure will show thick cell boundaries (cellular structure). When the amount of solute is no longer small, its rejection may lead to the formation of dendrites which can either be oriented in the heat flow direction (columnar dendrites) or **randomly oriented**. In some extreme cases this random oriented structure can give rise to an equiaxed structure. Under certain cooling conditions it has been possible to produce oriented two phase structures. Where the oriented phase does not form secondary arms the structures are

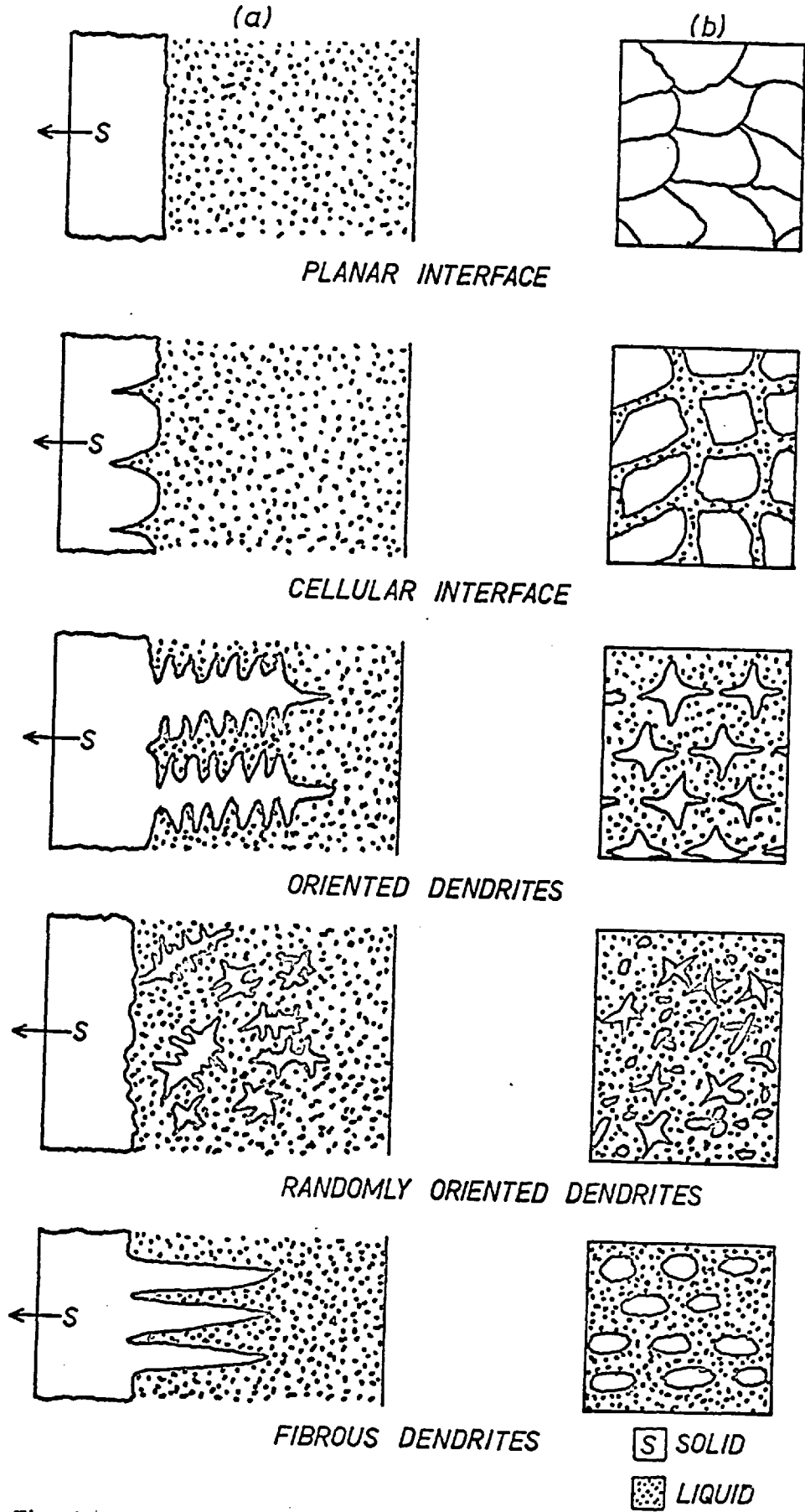


Fig. 11-1 VARIOUS MORPHOLOGIES OF ALLOY SOLIDIFICATION
 (a) along heat flow direction
 (b) microstructure normal to heat flow at solidus front

called composites or fibrous dendritic structures. The various morphologies discussed above are illustrated schematically in Fig. II-1.

II-1-B FACTORS AFFECTING THE TYPE OF MORPHOLOGY PRODUCED ON SOLIDIFICATION

The type of structure produced on solidification is mainly determined by the amount of solute, the solidification rate and the temperature gradient in liquid. Various authors have attempted to predict the type of structure produced once these factors are known.

II-1-B(i) Planar to cellular transition in single phase alloys

Various correlations have been suggested for the conditions under which a plane interface will transform into a cellular interface. The most satisfactory is that suggested by Rutter and Chalmers² which is based on constitutional supercooling. They say that the interface will remain plane if:

$$\frac{G}{R} > \frac{mC_0(1-k)}{D_f} \quad \text{II-1-1}$$

and this has been confirmed by various authors.

II-1-B(ii) Cellular to dendritic transition

Chalmers³ extended the hypothesis and proposed that increased constitutional supercooling leads to the breakdown of the cellular structure. Tiller and Rutter⁴ proposed on the other hand the criterion for the breakdown of the cellular structure can be represented as:

$$C_0 = \frac{AG}{R^2} \quad \text{II-1-2}$$

where 'A' is a constant. Tiller criterion has recently been questioned by many workers. Plaskett and Winegard⁵ and Coulhard and Elliot⁶ have modified Tiller criterion II-1-2, to include the effects due to cell size and liquid mixing.

Davies⁷ made a statistical analysis of the existing data on the solidification of alloys and their morphology, and found that no simple criterion could be valid for the transition from a cellular to a dendritic structure.

II-1-B(iii) Two phase alloys

Mollard and Flemings⁸ have predicted that during the growth of a two phase alloy from a single phase melt a plane interface should be stable if:

$$\frac{G}{R} > \frac{M(C_E - C_0)}{D_f} \quad \text{II-1-3}$$

This equation was obtained by assuming that solidification took place under steady state conditions and that the solid formed was of homogeneous composition. Cline⁹ used a perturbation analysis of the steady state solution for eutectic growth to show that the plane interface would break down when:

$$\frac{G}{R} = \frac{M}{2} \left\{ \frac{K_S}{K_L} + 1 \right\} \frac{C_0 - C_E}{D_f} \quad \text{II-1-4}$$

This criterion agrees well with the experimental data of Mollard and Flemings⁸ for lead-tin eutectic alloys.

II-1-C SOLUTE SEGREGATION PRODUCED DURING SOLIDIFICATION

Pfann¹⁰ derived an equation to link the concentration of solid present at the solid-liquid interface, C_S^* , to the fraction that has solidified:

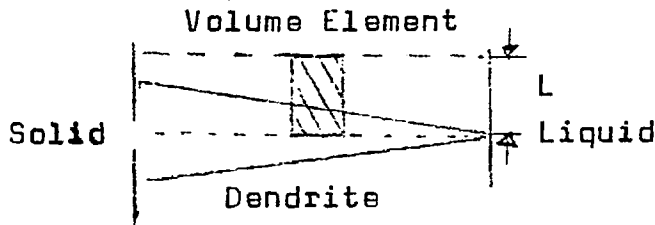
$$C_S^* = k C_0 (1 - f_S)^{k-1} \quad \text{II-1-5}$$

The fraction of the liquid remaining is therefore given by:

$$f_L = \left\{ \frac{C_L^*}{C_0} \right\}^{-\frac{1}{1-k}} \quad \text{II-1-6}$$

where C_L^* is the concentration of liquid phase which is assumed to be completely mixed by diffusion. This expression was derived by assuming that negligible diffusion took place in the solid, that the partition coefficient, 'k', was constant and that equilibrium existed at the solid/liquid interface.

Recently Bordy and Flemings¹¹ considered the distribution of solute during dendritic solidification and showed that equation II-1-5 cannot be applied directly because the value of the partition coefficient is not constant throughout the solidification process, and because diffusion in the solid has an appreciable effect. They assumed that no mass flows in or out of the volume element shown below



that solute is transported in the solid phase by diffusion and that the rate at which the dendrite thickens is constant. They found that the composition of the solid is given by:

$$C_S^* = k C_0 \left\{ 1 - \frac{f_S}{1 + \alpha_f k} \right\}^{k-1} \quad \text{II-1-7}$$

where $\alpha_f = \frac{D_f \tau_f}{L^2}$ and τ_f is the local time for

solidification to be completed and L is half the dendritic spacing. The factor α_f determines the extent

of segregation. If $\alpha_f k \gg 1$, the composition of the primary solid phase approaches uniformity. Moreover, for a particular alloy, the severity of microsegregation depends only on the ratio τ_f/L^2 and not on the dendritic arm spacing or the solidification time. ~~■~~ Where ~~the~~ the value of $\alpha_f k$ is very small the equation II-1-7 reduces to the Pfann's equation II-1-5.

II-2 PREVIOUS METHOD OF PREDICTING PROGRESS OF SOLIDIFICATION OF ALLOYS

The mathematical prediction of the rates at which metals and alloys solidify involves the solution of the unsteady state heat conduction^{equation}. Solutions have been obtained by one of the following methods:

(a) exact solution, (b) approximate solution using the finite difference method, (c) approximate solution using the integral profile method.

II-2-A Exact solutions

Very few formal solutions exist for the unsteady state heat conduction during metal solidification, and, until recently, no formal solution was available for alloy solidification. Goodman¹², while discussing the paper presented by Tien¹³ gave a solution for the case when the surface is held at a constant temperature below the solidus. The boundary conditions are such that all the variables that are functions of position, x , and time, τ , can be described in terms of a dimensionless time, ξ , where:

$$\xi = \frac{x}{\left(\frac{\tau k}{\gamma_a}\right)^{1/2}} \quad \text{II-2-1}$$

The heat conduction equation in the partial zone is:

$$\frac{\partial^2 \theta}{\partial x^2} + \frac{\rho H_p}{k_p} = \frac{\gamma_a}{k_p} \frac{\partial \theta}{\partial \tau} \quad \text{II-2-2}$$

where H_p is the latent heat released in the partial layer and γ_a is the thermal capacity of the alloy. This equation can be in terms of the dimensionless time as:

$$\frac{d^2\theta}{d\zeta^2} + \frac{\zeta}{2} \frac{d\theta}{d\zeta} = \frac{-\rho H f_{SU} \zeta}{4 t_p^* \gamma_a^*} \quad \text{II-2-3}$$

and the general solution is:

$$\theta = \frac{-H^* f_{SU} \zeta}{2 t_p^* \gamma_a^*} + C_1 \exp\left(\frac{\zeta}{2}\right) + C_2 \quad \text{II-2-4}$$

Where C_1 & C_2 are constants

This equation has little practical validity since it only applies when the surface temperature is kept constant, and the alloy occupies a semi-infinite region.

II-2-B Finite difference method

The method consists of reducing the partial difference equations to suitable finite difference equations. The reduction of heat conduction equation of the type:

$$K \frac{\partial^2 \theta}{\partial x^2} = \gamma_a \frac{\partial \theta}{\partial \tau} \quad \text{II-2-5}$$

to finite difference approximation can be effected by means of the Taylor series. If $\Delta \tau$ is small and terms of the order of $\Delta \tau^2$ are neglected then

$$\frac{\partial \theta}{\partial \tau} = \frac{\theta(x, \tau + \Delta \tau) - \theta(x, \tau)}{\Delta \tau} = \frac{\theta_{m,n+1} - \theta_{mn}}{\Delta \tau} \quad \text{II-2-6}$$

where subscript m denotes the temperature at plane m , and subscript n denotes the temperature at time τ .

The subscript $n+1$ denotes the temperature at time $\tau + \Delta \tau$. where x -differential can be treated in a similar manner. Eyres et al. were among the first to apply numerical methods to solve solidification problems. They

assumed that the latent heat of fusion of each slice of the finite difference net was concentrated at the corresponding net point. The solidification front was only assumed to move, once the latent heat has been conducted away so that the solidification front moved in a step-wise fashion. Later Dusenberre¹⁵ and others have used the method to solve solidification problems. A short account of these attempts is given by Ruddle¹⁶. Schniewind¹⁷ modified the method and assumed that latent heat of fusion is distributed throughout the material as a piecewise constant function. It was suggested that this method can be used to study the interaction of solidification with segregation in alloys for unidirectional solidification by solving simultaneously the diffusion and heat conduction equations.

Recently, Mizikar¹⁸, Adennis¹⁹, Peel and Pengally²⁰, have used the finite difference method to predict the progress of unidirectional solidification of alloys by assuming that the latent heat of fusion is liberated uniformly over the interval between liquidus and solidus temperatures. The effective specific heat of the metal in the partially solidified zone is thus adjusted to a constant value to take into consideration the latent heat of fusion. The finite difference method suffers from the disadvantage that it is very lengthy and time consuming.

II-2-C Integral profile method

This method is a general method for obtaining approximate solutions to the unsteady state heat conduction equation when heat flows only in one direction:

$$\frac{\partial}{\partial \theta} \left(k \frac{\partial \theta}{\partial x} \right) = \gamma \frac{\partial \theta}{\partial \tau}$$

II-2-9

Integrating this equation across the region of interest gives:

$$\int_a^b \frac{\partial}{\partial \theta} \left(K \frac{\partial \theta}{\partial x} \right) dx = \int_a^b \gamma \frac{\partial \theta}{\partial x}$$

whence the Leibnitz integral formula can be applied to the R.H.S. to give:

$$K \left(\frac{\partial \theta}{\partial x} \right)_b - K \left(\frac{\partial \theta}{\partial x} \right)_a = \frac{d}{d\tau} \left\{ \int_a^b \gamma \theta dx \right\} - \gamma \theta_b \frac{db}{d\tau} + \gamma \theta_a \frac{da}{d\tau}$$

II-2-10

The temperature integral appearing in this equation is unknown, but it can be determined approximately by fitting an auxiliary temperature function to certain known temperature conditions at the boundaries $x = a$ and $x = b$.

The method has been used by many authors to solve solidification problems involving pure metals and skin forming alloys cooling under certain restricted conditions.

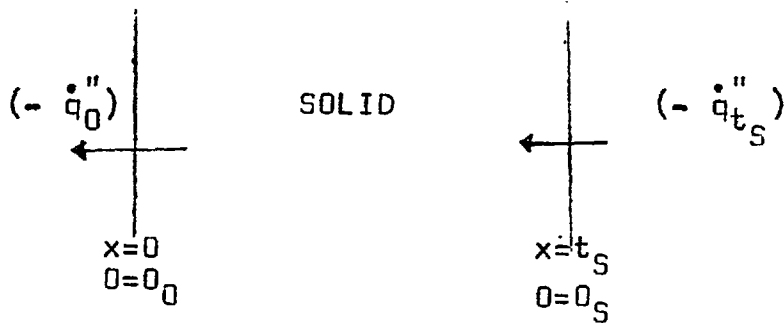
The most flexible treatment, the generalised method developed by Hills¹, is described below, since it forms the basis of the treatment developed later for binary alloys.

Tien & Geiger^{13, 21} have developed ^{the} method to treat binary alloys at zero-superheat and ^{the} method is described subsequently. It can only be used for a restricted set of unrealistic conditions.

II-2-C(i) Hills' solution for the growth of a layer of solid metal

Hills' solution is presented in terms of two parameters, the temperature of the cooled surface and

the thickness of the solid layer. Two simultaneous ordinary differential equations are derived for these parameters. The derivation is discussed here in some detail because it provides a general illustration of the integral profile method and, more important, because the equations apply to the growth of solid metal during the solidification of binary alloys. Thus they form the basis of the theoretical methods developed later in this work.



The above figure illustrates the growing solid layer, cooled at surface $x=0$. Heat crosses the moving boundary, $x=t_s$, from liquid metal or from partially solidified metal. This boundary is at the solidification temperature of the pure metal, or at the non-equilibrium solidus temperature of the alloy.

Thus we can write:

Boundary conditions:

$$\tau > 0, \quad x = 0, \quad \theta = \theta_0$$

$$\tau > 0, \quad x = t_s, \quad \theta = \theta_s$$

Thus equation II-2-5 gives:

$$k_s \left[\frac{\partial \theta}{\partial x} \right]_{t_s} - k_s \left[\frac{\partial \theta}{\partial x} \right]_0 = \frac{d}{d\tau} \left\{ \int_0^{t_s} \rho c_s \theta dx \right\} - \rho c_s [\theta]_{t_s} \frac{dt_s}{d\tau}$$

II-2-11

Applying the heat conservation principle at the boundaries:

$$-k_s \left[\frac{\partial \theta}{\partial x} \right]_0 = \dot{q}_0''$$

II-2-12

and

$$- K_S \left[\frac{\partial \theta}{\partial x} \right]_t = \ddot{q}_{t_S} - \rho_{H_S} \frac{dt_S}{d\tau} \quad \text{II-2-13}$$

The most convenient auxilliary function to use in evaluating the integral in equation II-2-11 is a quadratic polynomial:

$$\theta = a_0 + a_1 \left(\frac{x}{t_S} \right) + a_2 \left(\frac{x}{t_S} \right)^2 \quad \text{II-2-14}$$

The coefficients can be evaluated using the boundary conditions and equation II-2-12, which gives:

$$\theta = \theta_0 - \frac{\ddot{q}_0 t_S}{K_S} \left(\frac{x}{t_S} \right) + \left(\theta_S - \theta_0 + \frac{\ddot{q}_0 t_S}{K_S} \right) \left(\frac{x}{t_S} \right)^2 \quad \text{II-2-15}$$

so that the integral becomes:

$$\int_0^{t_S} \theta dx = \left\{ \frac{1}{3} \theta_S + \frac{2}{3} \theta_0 - \frac{1}{6} \frac{\ddot{q}_0}{K_S} t_S \right\} t_S \quad \text{II-2-16}$$

As integral of an approximate function is more accurate than the function itself, so the approximate integral can be substituted in equation without great error.

After rearrangement we get:

$$\left[\rho_{H_S} + \frac{1}{3} \rho_{C_S} \left\{ 2(\theta_S - \theta_0) + \frac{\ddot{q}_0 t_S}{K_S} \right\} \right] \frac{dt_S}{d\tau} - \frac{2}{3} t_S \rho_{C_S} \frac{d\theta_0}{d\tau} + \frac{1}{6} \frac{t_S^2}{K_S} \rho_{C_S} \frac{d\ddot{q}_0}{d\tau} = -(\ddot{q}_0 - \ddot{q}_{t_S}) \quad \text{II-2-17}$$

Expressing the variables in dimensionless forms ^(a) as:

(a) Full list of dimensionless forms is given in list of symbols.

$$t_S^* = \frac{- [\dot{q}_0'']_0 t_S}{\theta_S k_S}$$

$$\xi = \frac{[\dot{q}_0'']_0^2}{\theta_S^2 \rho c_S k_S}$$

$$\theta^* = \frac{\theta_0}{\theta_S}$$

$$H_S^* = \frac{H_S}{c_S \theta_S}$$

$$q_{t_S}^* = \frac{\dot{q}_{t_S}''}{[\dot{q}_0'']_0}$$

$[\dot{q}_0'']_0$ represents the heat flux from the surface when the surface temperature is equal to the solidification temperature θ_S .

Thus equation II-2-17 reduces to:

$$\left\{ H_S^* + \frac{2}{3}(1-\theta_0^*) - \frac{1}{3}t_S^* q_0^* \right\} \frac{dt_S^*}{d\xi} - \frac{2}{3}t_S^* \frac{d\theta_0^*}{d\xi} - \frac{1}{6}t_S^* \frac{dq_0^*}{d\xi} = q_0^* - q_{t_S}^*$$

II-2-18

In general, heat flux from the surface is a function of surface temperature or time or both. Thus we can write:

$$q_0^* = f(\theta_0^*, \xi)$$

and

$$\frac{dq_0^*}{d\xi} = \frac{\partial f}{\partial \theta_0^*} \frac{d\theta_0^*}{d\xi} + \frac{\partial f}{\partial \xi} = f'_\theta \frac{d\theta_0^*}{d\xi} + f'_\xi \quad \text{II-2-19}$$

Substituting equation II-2-19 in equation II-2-18, we get:

$$\left\{ H_S^* + \frac{2}{3}(1-\theta_0^*) - \frac{1}{3} t_S^* q_0^* \right\} \frac{dt_S^*}{d\bar{x}} - \frac{1}{6} t_S^* (4 + f'_\theta t_S^*) \frac{d\theta_0^*}{d\bar{x}}$$

$$= q_0^* - q_t^* + \frac{1}{6} t_S^{*2} f'_\theta \quad \text{II-2-20}$$

Equation II-2-20 provides one equation for the dimensionless thickness of the solid layer and for its dimensionless surface temperature. Hills,¹ method differs from previous integral profile methods in characterising the solid layer in terms of two parameters in this way. Therefore a second equation is required in the solution. The second equation is derived by considering the variation of $\frac{\partial \theta}{\partial \tau}$ across the solid metal layer.

$$\text{At } x = 0 \quad \left[\frac{\partial \theta}{\partial \tau} \right]_0 = \frac{d\theta_0}{d\tau} \quad \text{II-2-21}$$

At $x = t_S \quad \theta = \theta_S = \text{constant}$

$$\frac{d}{d\tau} \left\{ \theta(t_S, \tau) \right\} = \left[\frac{\partial \theta}{\partial x} \right]_{t_S} \frac{dt_S}{d\tau} + \left[\frac{\partial \theta}{\partial \tau} \right]_{t_S} = 0 \quad \text{II-2-22}$$

Substituting equation II-2-13 in equation II-2-22 and rearranging we get:

$$\left(\frac{d\theta}{d\tau} \right)_{t_S} = \frac{dt_S}{d\tau} \left\{ \frac{\rho H_S}{K_S} \frac{dt_S}{d\tau} - \frac{\ddot{q}_{t_S}''}{K_S} \right\} \quad \text{II-2-23}$$

Differentiating heat conduction equation II-2-5 across the solid layer gives:

$$\left[\frac{\partial \theta}{\partial \tau} \right]_{t_S} - \left[\frac{\partial \theta}{\partial \tau} \right]_0 = \frac{K_S}{\rho c_S} \left\{ \left(\frac{\partial^2 \theta}{\partial x^2} \right)_{t_S} - \left(\frac{\partial^2 \theta}{\partial x^2} \right)_0 \right\} = \frac{K_S}{\rho c_S} \int_0^{t_S} \frac{\partial^3 \theta}{\partial x^3} dx$$

II-2-24

Substituting II-2-23 and II-2-21 in equation II-2-24 we get:

$$-\frac{dt_s}{d\tau} \left\{ \frac{\rho H_s}{K_s} \frac{dt_s}{d\tau} - \frac{\dot{q}_t''}{K_s} \right\} - \frac{d\theta_0}{d\zeta} = \frac{K_s}{\rho c_s} \int_0^{t_s} \frac{\partial^3 \theta}{\partial x^3} dx \quad \text{II-2-25}$$

As long as there is no sudden change in cooling conditions during cooling, we will not expect the value of $\frac{\partial \theta}{\partial x}$ to change very much within solid metal and assuming this to be linear, the value of $\frac{\partial^3 \theta}{\partial x^3}$ will not alter within solid and integral appearing on the right hand side of equation II-2-25, is given by:

$$\int_0^{t_s} \left(\frac{\partial^3 \theta}{\partial x^3} \right) dx = \left[\frac{\partial^3 \theta}{\partial x^3} \right]_0 \int_0^{t_s} dx = t_s \left[\frac{\partial^3 \theta}{\partial x^3} \right]_0 \quad \text{II-2-26}$$

Differentiating heat conduction equation II-2-5 with respect to x, gives:

$$K_s \left(\frac{\partial^3 \theta}{\partial x^3} \right) = \rho c_s \frac{\partial}{\partial x} \left(\frac{\partial \theta}{\partial \tau} \right) = \rho c_s \frac{\partial}{\partial \tau} \left(\frac{\partial \theta}{\partial x} \right) \quad \text{II-2-27}$$

Substituting equation II-2-12 and II-2-27 in equation II-2-26 and writing this equation for $x = 0$,

$$K_s \left(\frac{\partial^3 \theta}{\partial x^3} \right)_0 = \frac{-c_s \rho}{K_s} \left(\frac{dq_0''}{d\tau} \right) \quad \text{II-2-28}$$

Substituting in equation II-2-25 we get:

$$\frac{dt_s}{d\tau} \left\{ \frac{H_s}{K_s} \frac{dt_s}{d\tau} - \frac{\dot{q}_t''}{K_s} \right\} + \frac{d\theta_0}{d\tau} = \frac{t_s}{K_s} \frac{dq_0''}{d\tau} \quad \text{II-2-29}$$

In dimensionless terms, after substituting equation II-2-19 we get:

$$\frac{d\theta_0^*}{d\zeta} = \frac{H_s^* \left\{ \frac{dt_s^*}{d\zeta} \right\}^2 + q_t^* \frac{dt_s^*}{d\zeta} + t_s^* f_\zeta'}{1 + t_s^* f_\theta'} \quad \text{II-2-30}$$

Substituting this equation in II-2-20 we get a quadratic equation in $\frac{dt_S^*}{d\zeta}$ as:

$$\Omega \left[\frac{dt_S^*}{d\zeta} \right]^2 + \Gamma \left[\frac{dt_S^*}{d\zeta} \right] - \Lambda = 0 \quad \text{II-2-31}$$

where

$$\Omega = H_S^* t_S (4 + t_S^* f_\theta')$$

$$\Gamma = \left\{ 6H_S^* + 4(1-\theta_0^*) - 2t_S^* q_0^* \right\} (1+t_S^* f_\theta') + q_t^* t_S^* (4+t_S^* f_\theta')$$

$$\Lambda = 6(q_0^* - q_t^*) (1+t_S^* f_\theta') - 3t_S^{*2} f_\zeta'$$

we can write

$$\frac{dt_S^*}{d\zeta} = \frac{-\Gamma \pm \sqrt{\Gamma^2 + 4\Lambda\Omega}}{2\Omega} \quad \text{II-2-32}$$

As q_t^* is less than q_0^* both will be positive, the positive root of the equation II-2-32 is valid. We can write the final equation for the rate of change of solid thickness, by using theory of quadratic equations.

$$\frac{dt_S^*}{d\zeta} = \frac{2\Lambda}{\Gamma + \sqrt{\Gamma^2 + 4\Lambda\Omega}} \quad \text{II-2-33}$$

Equations II-2-33 and II-2-30 constitute the solution. They can be solved by using standard numerical techniques, like the Runge-Kutta method, to predict how t_S^* varies with θ_0^* once the values of f_θ' , f_ζ' and q_t^* are known in terms of θ_0^* and t_S^* .

II-2-C(ii) Other solutions for the growth of the solid layer

Single parameter integral profile methods have been used by Goodman²², Hills²³, Hills and Moore²⁴ and

V. Koump²⁵, et al, for predicting the progress of solidification of metals at zero-superheat.

Goodman and Shea²⁶ have presented a solution for the melting of a solid with a constant liquid surface heat flux using a double integral profile method. The problem has been solved for the two cases where the solid surface is either adiabatic or isothermal. Their theory can be used to predict the growth of a solid layer, solidifying in the presence of superheat, provided the constant surface heat flux condition is met.

Hrycak²⁷ presented an integral profile solution for the freezing of an isotropic semi-infinite region at superheat, where Newton's law of cooling applies at the surface and the heat transfer coefficient remains constant. He assumed a linear temperature profile in the solid layer and a parabolic temperature profile in the thermal layer, and compared his solution with the exact solution obtained when the heat transfer coefficient is infinite, i.e. the temperature of the surface becomes equal to that of the cooling media. He found good agreement between the two solutions and concluded that it was practical to use the integral profile method.

II-2-C(iii) Previous solutions for the solidification of freezing range alloys

Tien and Geiger¹³ have presented an integral profile solution for alloy solidification at zero-superheat for the case where the mould/metal surface temperature, θ_0 , is kept constant below the solidus temperature. The unsteady state heat conduction equation in the partial layer can be represented as:-

$$\frac{\partial}{\partial x} \left(K_p \frac{\partial \theta}{\partial x} \right) + \frac{\rho L_f}{\tau} = \gamma_a \frac{\partial \theta}{\partial \tau}$$

Tien and Geiger assumed that the fraction of metal solidified at any point, f_S , could be represented as a function of distance by the equation:

$$f_S = f_{SU} \left(1 - \sum_{i=1}^n C_i X_i \right)$$

where f_{SU} is the fraction of solid present at the solidus temperature. The value of f_{SU} was taken as constant and calculated from the Pfann equation II-1-5. They also assumed that K_p was constant.

The temperature distributions and thickness of each region were calculated as functions of time using the error function solution. They compared their predicted values with the exact solution presented by Goodman¹⁸ and found good agreement.

They later modified their theory to treat the solidification of alloys when the surface temperature is a function of time^{21,28}. Recently, Koump et al²⁹ compared theoretical values predicted by Tien's theory with experimental results obtained for the uni-directional solidification of aluminium-copper alloys. They only found qualitative agreement and attributed this to some of the assumptions that they had made.

II-3 EXPERIMENTAL TECHNIQUES

Experimental techniques used to determine the position of the solid/liquid front during solidification can be divided into two broad classifications: techniques in which its position is determined in situ and techniques in which it is determined after solidification has been completed (post mortem techniques). These techniques are reviewed in section II-3-A and II-3-B. Section II-3-C mentions the method selected for the experimental study.

In order to compare the experimental results with the results predicted by the theory developed in

Chapter III, information is required concerning the morphology of the alloys and the distribution of solute. Experimental techniques used to determine the distribution of solute will be dealt with briefly in section II-3-D.

II-3-A IN SITU TECHNIQUES FOR DETERMINING THE POSITION OF THE SOLIDIFICATION FRONT

II-3-A(i) Thermal analysis:

Basically the method involves recording the cooling curves of thermocouples placed at various points in the ingot. The temperature at any point will not fall below the solidification temperature till the solid front reaches that point. Thus the progress of the solidification can be followed from these curves. The method has been used by several workers to determine the start and end of solidification. Ruddle¹⁶ has reviewed some of these attempts and has discussed the relative merits and disadvantages of the method. The usefulness of this method depends upon the correct positioning of the thermocouples, upon accurate temperature measurement and upon the rapidity with which the thermocouples respond to the temperature that they are measuring. In order to measure the temperature accurately, the conduction of heat along the thermocouple wires should be minimised by ensuring that they lie along isothermal surfaces.

The method has the advantage that it gives the temperature history at any point throughout the entire solidification process, but doubts have been expressed about the method by Ruddle¹⁶ and a number of other authors, since the thermocouples may influence the solidification process and the resulting morphology. Moreover, experience has shown that measurement of solidus temperatures in alloys is difficult if the

composition of solute is much less than the maximum solid solubility.

II-3-A(ii) Dip stick:

The method consists of dipping a rod into the molten metal until it contacts the solidification front. This method, though very simple, can yield rather misleading results, particularly in the case of alloys. Moreover, the motion of the dip stick may interfere with the solidification process. Peel and Pengally²⁰ have recently used the method to follow the progress of solidification of aluminium alloys.

II-3-A(iii) Ultrasonic method:

This method consists of using the difference in the velocity of sound in the solid and liquid phases. Kurz and Lux³⁰ found that echoes from the solidification front can be used to determine its position by using an ultrasonic tester. Only a small portion of the transmitted impulses, in fact, reached the receiver due to the influence of inclination and roughness of the solid/liquid interface. This suggests that it will be very difficult to use this method for alloys having dendritic morphology. Moreover, Southin³¹ found that low frequency impulses modify the morphology and leads to grain refinement. This precludes the use of the method for determining the progress of alloy solidification.

II-3-A(iv) X-ray:

Forssten and Miekko-oja³² have used X-rays for the direct and continuous observation of the solid/liquid front in the solidification of aluminium and aluminium-gold alloys. However, this method is expensive to operate and can be used only for metals and alloys that have a low coefficient of absorption for X-rays.

II-3-A(v) Direct Visual Techniques:

A number of authors have observed the growth of organic and inorganic liquids directly. The method can only be used to study the solidification process on the surface of metals.

II-3-B POST MORTEM TECHNIQUES

II-3-B(i) Pour Out Method

The method consists of rapidly decanting the liquid metal that remains after a certain time and then measuring the thickness of the solid left. This method can give a fair estimate of the solidified thickness at any particular time for pure metals and for dilute alloys having a planar interface. For alloys, Chadwick³³ and Weinberg³⁴ have shown that a thin (10-20 μ) skin of liquid remains behind after decantation, covering the original solid/liquid interface. Thus no definite conclusion can be drawn about the shape and position of the interface. Muscon and Hellawal³⁵ observed that the solid/liquid front that is uncovered by decantation does not even approximate to the true solid/liquid interface. In the case of alloys the method is not suitable because liquid remains in the interdendritic channels where it solidifies to give a false picture of the solid/liquid interface. Thus the thickness of solid formed cannot be measured in this way.

II-3-B(ii) Radio-isotopic:

This technique consists of adding a radio-active isotope at a particular time and the ingot sectioned and examined after solidification has been completed. The position and distribution of the radio-isotope is determined by using auto-radiographic techniques which allow the position and the shape of the solid/liquid interface to be determined. The method has been used

by a number of authors to study the solidification of ferrous alloys. This technique is quite useful, but requires that melt be well stirred and that facilities are available to handle the isotopes.

II-3-B(iii) Addition of another metal

This technique involves adding another metal during the solidification process which has either a different colour or structure, higher density, and a higher melting point than the metal being studied. The ingot is sectioned after solidification is completed and the position and the shape of the solidification front is determined from the position of the added metal. This method has been used by a number of authors; for example Peel and Pengally²⁰ have recently used copper to determine the shape of the solidification front during the continuous casting of aluminium. This method is rather laborious and only gives qualitative information. Moreover, the addition of another metal during the solidification process may alter the morphology of the solidified metal.

II-3-C SELECTION OF METHOD FOR EXPERIMENTAL STUDY

From the above review, it can be seen that the most satisfactory technique for studying the progress of alloy solidification is thermal analysis. It is an in-situ technique and provides information about the thermal history at any point as well as showing how the solidus and liquidus fronts progress. Thus thermal analysis was used as the main technique in this work, but a few experiments were performed using the pour out technique and these confirmed that the method is of limited use. A short description of the apparatus and the procedure used in this investigation is given in Chapter IV.

II-3-D SOLUTE DISTRIBUTION

Classical chemical analysis can give only the average composition of a sample, so it is macroscopic in character providing only a qualitative picture of solute segregation. Microscopic and other optical techniques can also be used to determine the solute distribution qualitatively, in steel for example, phosphorous and sulphur distribution has been studied by polishing and etching sectioned specimens after solidification. Methods that have been used for the quantitative study of solute distribution are discussed below.

II-3-D(i) Radio-isotopic method

An alloy is solidified containing a radioactive solute. Segregation can then be studied by sectioning the ingot and using auto-radiography to determine solute distribution. This method has been used by a number of authors, but it requires radioactive facilities

II-3-D(ii) Electron probe micro-analyser

A beam of high energy electrons is focused on to an area on the surface of the specimen about 1 micron in diameter. The bombarding electrons are back scattered from the very thin surface layer in a manner roughly analogous to the reflection of a beam of light from a similar surface. The remaining electrons penetrate to a depth of 1 micron and excite the atoms to give characteristic X-rays. The intensity of these X-rays will give the composition of the element present. This method has the advantage that it gives the solute distribution at any point so that the coring effect can be detected. The method has been used for the study of solute segregation by Doherty and Melford³⁶ and Subramanian et al.³⁷ However, the method has the disadvantage that by far the greater part of the energy

of the incident electrons is converted to the heat, and care should be taken to ensure that this does not alter the solute distribution. This method seems to be ideal for the study of solute segregation produced during the dendritic solidification of alloys.

II-3-0(iii) Spectroscopic

Spot spectroscopic analysis can be used to determine the distribution of solute in a sample, but the method is limited because it gives the average composition over a relatively large area. Thus it is not suitable for the study of coring or dendritic solidification.

II-3-0(iv) Selection of method for determining solute distribution

In the present investigation conventional metallographic techniques have been used to study the morphology of the metal solidified and the electron probe microanalyser has been used to study the segregation of the solute in the different solid phases.

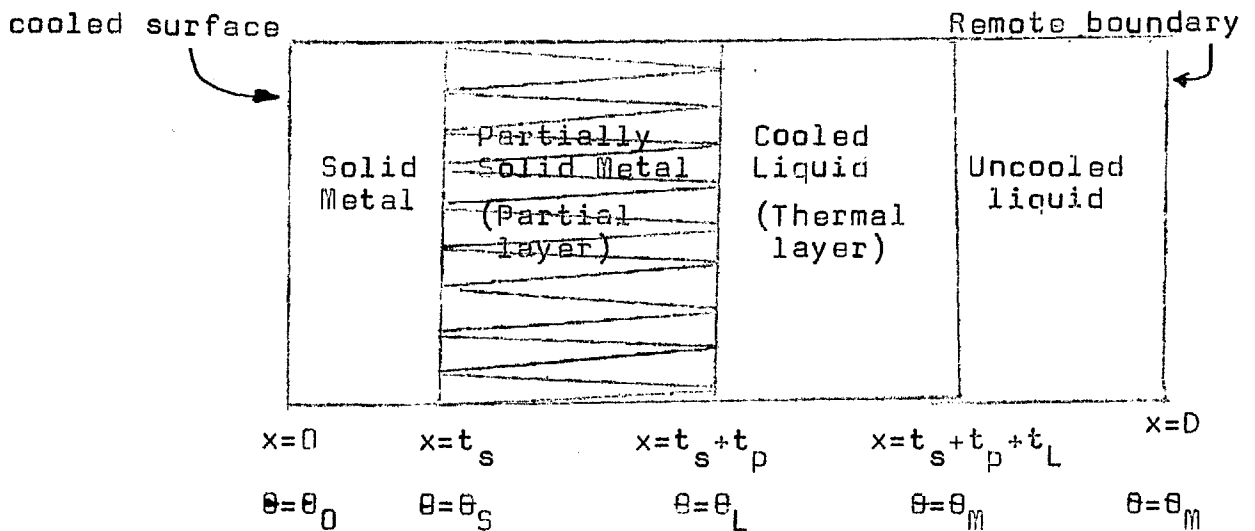
CHAPTER III
THEORETICAL TREATMENT
OF
UNIDIRECTIONAL SOLIDIFICATION
OF BINARY ALLOYS

III THEORETICAL TREATMENT

III-1 STATEMENT OF THE PROBLEM

A formal statement of the problem is given to provide a complete picture and no attempt has been made to solve the equations at this stage. The treatment assumes that liquidus and solidus temperature are unique for an alloy of a particular composition. Only binary alloys forming a eutectic with or without partial solid solubility are considered. The effect of volume contraction on solidification and convection in the liquid alloy has been neglected. Other assumptions, which are not essential to the theoretical treatment, are discussed along with the solution. The assumption that the liquidus and solidus temperature of the alloy are unique enables us to represent the solidification process in terms of various layers.

A typical situation for a semi-infinite liquid, once solid has been formed can be represented as



Thus the solidification process can be described, in simple terms, by the growth of these different layers. As the solidification proceeds, one by one boundaries of various layers will reach the remote boundary. The remote boundary can be either insulated or it can be a

plane of symmetry in a liquid metal region cooled from both sides.

This simple picture hardly ever occurs, but is replaced by several alternative modes of cooling, depending upon actual conditions. Thus if cooling occurs slowly, the entire liquid region might be cooled before any solid has formed. It is then possible that the layer of partially solidified metal could grow to occupy the entire region before any fully solidified metal forms.

Thus solidification process can take different routes starting from the complete region of uncooled liquid to the region of completely solidified material. The actual route depends upon the cooling conditions, the initial temperature, the thickness of liquid region and the nature of the alloy. We can classify the process of solidification in various cooling modes, depending upon the relative position of various layers. The various cooling modes are explained in the Table V-1. The solidification algorithm, which shows the various routes that solidification process can take through the different cooling modes, is illustrated in Fig. V-1 (p.82).

III-2 INTEGRAL PROFILE SOLUTION

Using the integral profile method described earlier, general equations are developed for the growth of the different layers in terms of the heat fluxes interchanged between them. The heat flux equations are then derived for each mode to express how the various layers interact with each other. The general equations for solid metal layer have already been derived (Hills' solution) in section II-2-C(i). This chapter describes the development of general equations for the cooled liquid (thermal) layer and for the partially solidified metal layer (partial layer).




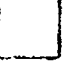
The different boundary conditions that apply during the different modes change the form of these general equations. It is most convenient if different

TABLE V-1

COOLING MODES

Mode Number	Alloy of Metal	Solid Layer	Partial Layer	Thermal Layer	Schematical Representation**
P	Metal	Growing	-	-	
1	"	-	-	Growing	
1F	"	-	-	Cooling	
2	"	Growing	-	Growing	
2F	"	Growing	-	Shrinking	
Z2	Alloy	-	Growing	-	
Z2F	"	-	Cooling	-	
Z3	"	Growing	Growing	-	
Z3F	"	Growing	Shrinking	-	
S1	"	-	-	Growing	
S1F	"	-	-	Cooling	
S2	"	-	Growing	Growing	
S2F	"	-	Growing	Shrinking	
S3	"	Growing	Growing	Growing	
S3F	"	Growing	Growing	Shrinking	

**Different layers are represented as:-

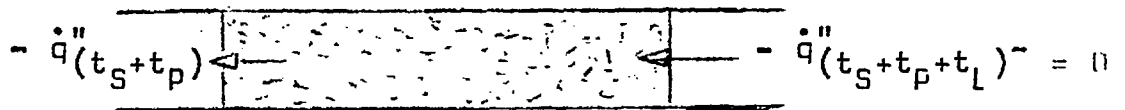
-  Solid layer
-  Partial layer
-  Cooled liquid (thermal layer)
-  Uncooled liquid

characteristic parameters are used to describe the two layers during the different cooling modes, so that both the form of the differential equation, and the characteristic parameter used, can change from mode to mode. The different forms of the differential equations are derived in the second part of this chapter. In the final sections all the differential equations that apply during each mode are listed together with the linking heat transfer equations.

III-3 THERMAL LAYER (COOLED LAYER)

III-3-A GENERAL EQUATIONS:

The thermal layer can be represented schematically as:-



Boundary conditions:

$$x = t_s + t_p; \quad \theta = \theta(t_s+t_p) \quad \text{III-3-1}$$

$$x = t_s + t_p + t_L; \quad \theta = \theta(t_s+t_p+t_L) \quad \text{III-3-2}$$

$$K_L \left(\frac{\partial \theta}{\partial x} \right)_{(t_s+t_p)^+} = - \dot{q}''(t_s+t_p) \quad \text{III-3-3}$$

$$K_L \left(\frac{\partial \theta}{\partial x} \right)_{(t_s+t_p+t_L)^-} = 0 \quad \text{III-3-4}$$

The unsteady state heat conduction equation is given by:

$$K_L \left(\frac{\partial^2 \theta}{\partial x^2} \right) = \gamma_L \left(\frac{\partial \theta}{\partial \tau} \right) \quad \text{III-3-5}$$

Integrating this equation across the layer and using the Leibnitz integral formula, we get the heat conservation equation:

$$\begin{aligned}
 K_L \left(\frac{\partial \theta}{\partial x} \right)_{(t_S+t_P+t_L)} - K_L \left(\frac{\partial \theta}{\partial x} \right)_{(t_S+t_P)} &= \gamma_L \left\{ \frac{d}{d\tau} \int_{t_S+t_P}^{t_S+t_P+t_L} \theta dx \right. \\
 &- \theta(t_S+t_P+t_L) \left[\frac{dt_S}{d\tau} + \frac{dt_P}{d\tau} + \frac{dt_L}{d\tau} \right] \\
 &\left. + \theta(t_S+t_P) \left[\frac{dt_S}{d\tau} + \frac{dt_P}{d\tau} \right] \right\} \quad \text{III-3-6}
 \end{aligned}$$

Auxilliary function for the temperature in the partial layer can be represented by quadratic polynomial:

$$\theta = a_0 + a_1 \left(\frac{x-t_S-t_P}{t_L} \right) + a_2 \left(\frac{x-t_S-t_P}{t_L} \right)^2 \quad \text{III-3-7}$$

The constants in this equation can be evaluated from equations III-3-1, III-3-2 and III-3-4, and we get:

$$\begin{aligned}
 \theta &= \theta(t_S+t_P+t_L) - \left\{ \left[\theta(t_S+t_P+t_L) - \theta(t_S+t_P) \right] \right. \\
 &\left. \left(1 - \frac{x-t_S-t_P}{t_L} \right)^2 \right\} \quad \text{III-3-8}
 \end{aligned}$$

and the integral across the layer is given by:

$$\int_{t_S-t_P}^{t_S+t_P+t_L} \theta dx = \left\{ \frac{2}{3} \theta(t_S+t_P+t_L) + \frac{1}{3} \theta(t_S+t_P) \right\} t_L \quad \text{III-3-9}$$

Substituting heat conservation equations III-3-3, III-3-4 and this integral III-3-9 into III-3-9, we get:

$$\begin{aligned}
 \dot{q}''(t_S+t_P) &= \gamma_L \left\{ \frac{d}{d\tau} \left[\left(\frac{2}{3} \theta(t_S+t_P+t_L) + \frac{1}{3} \theta(t_S+t_P) \right) t_L \right] \right. \\
 &- \left(\theta(t_S+t_P+t_L) - \theta(t_S+t_P) \right) \left[\frac{dt_S}{d\tau} + \frac{dt_P}{d\tau} \right] \\
 &\left. - \left(\theta(t_S+t_P+t_L) \frac{dt_L}{d\tau} \right) \right\} \quad \text{III-3-10}
 \end{aligned}$$

The heat flux equation is derived by differentiating the auxiliary function, III-3-8, with respect to x , and using heat conservation equation at the boundary ($x = t_S + t_P$), as

$$\frac{-\dot{q}''(t_S + t_P)}{K_L} = \frac{2(\theta(t_S + t_P + t_L) - \theta(t_S + t_P))}{t_L} \quad \text{III-3-11}$$

Expressing the heat conservation equation in dimensionless terms*:

$$\begin{aligned} q^*(t_S + t_P) = \gamma_L^* \left\{ \frac{d}{d\zeta} \left[-\left(\frac{2}{3}\theta^*(t_S + t_P + t_L) + \frac{1}{3}\theta^*(t_S + t_P)\right)t_L^* \right] \right. \\ \left. + \theta^*(t_S + t_P + t_L) \left[\frac{dt_S^*}{d\zeta} + \frac{dt_P^*}{d\zeta} + \frac{dt_L^*}{d\zeta} \right] \right. \\ \left. - \theta^*(t_S + t_P) \left[\frac{dt_S^*}{d\zeta} + \frac{dt_P^*}{d\zeta} \right] \right\} \quad \text{III-3-12} \end{aligned}$$

and the heat flux equation:

$$q^*(t_S + t_P) = \frac{2K_L^*(\theta^*(t_S + t_P + t_L) - \theta^*(t_S + t_P))}{t_L^*} \quad \text{III-3-13}$$

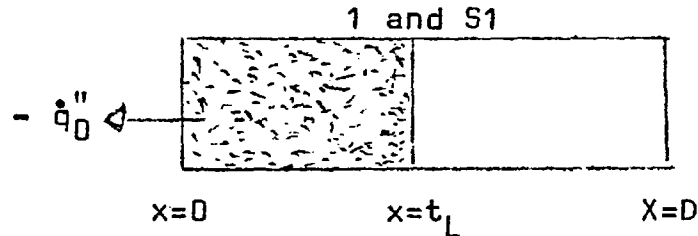
III-3-B CONVENIENT FORMS

Depending upon the mode of cooling in operation at any time, the temperature of the two bounds of the thermal layer can be constant or variable. In order to use the general equations derived above, it is necessary to transcribe the heat conservation equation into its most convenient form for the particular mode in operation. There are four different forms, and these are derived below.

*A full list of the dimensionless variables is given in the list of symbols.

III-3-B(i) Far bound moving at constant temperature, near bound stationary and cooling, and at variable temperature

occurs during modes:



characteristic parameter - surface temperature (θ_0^*)

Boundary conditions:

$$\theta_0^*(t_S+t_P) = \theta_0^* \neq \text{constant}; \quad \theta_m^*(t_S+t_P+t_L) = \theta_m^* = \text{constant}$$

$$t_S = t_P = 0; \quad q_0^*(t_S+t_P) = q_0^*$$

The heat conservation equation, III-3-12, reduces to:

$$q_0^* = \gamma_L^* \left\{ \frac{d}{d\bar{\zeta}} \left[\frac{2}{3} \theta_m^* + \frac{1}{3} \theta_0^* \right] t_L^* + \theta_m^* \frac{dt_L^*}{d\bar{\zeta}} \right\} \quad \text{III-3-14}$$

and heat flux equation becomes:

$$q_0^* = \frac{2K_L^*(\theta_m^* - \theta_0^*)}{t_L^*} \quad \text{III-3-15}$$

Differentiate equation III-3-15 with respect to time:

$$\begin{aligned} \frac{dq_0^*}{d\bar{\zeta}} &= - \frac{2K_L^*}{t_L^*} \frac{d\theta_0^*}{d\bar{\zeta}} - \frac{2K_L^*(\theta_m^* - \theta_0^*)}{t_L^{*2}} \frac{dt_L^*}{d\bar{\zeta}} \\ &= - \frac{q_0^*}{(\theta_m^* - \theta_0^*)} \frac{d\theta_0^*}{d\bar{\zeta}} - \frac{q_0^*}{t_L^*} \frac{dt_L^*}{d\bar{\zeta}} \end{aligned} \quad \text{III-3-16}$$

But

$$\frac{dq_0^*}{d\bar{\zeta}} = f_{\theta} \frac{d\theta_0^*}{d\bar{\zeta}} + f_{t_L} \frac{dt_L^*}{d\bar{\zeta}}$$

since

$$q_0^* = f(\theta_0^*, \xi)$$

Therefore

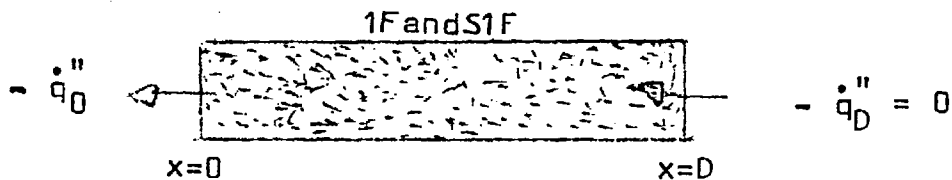
$$\frac{dt_L^*}{d\xi} = - \frac{\frac{d\theta_0^*}{d\xi} f'_\theta + \frac{q_0^*}{(\theta_m^* - \theta_0^*)} + f'_\xi}{\frac{q_0^*}{t_L^*}} \quad \text{III-3-17}$$

Substituting into the heat conservation equation, III-3-14, eliminating t_L^* using equation III-3-15, and rearranging gives:

$$\frac{d\theta_0^*}{d\xi} = - \frac{3q_0^* + 2\gamma_L^* K_L^* (\theta_m^* - \theta_0^*)^2 f'_\xi}{2\gamma_L^* K_L^* (\theta_m^* - \theta_0^*) \{ (\theta_m^* - \theta_0^*) f'_\theta + 2q_0^* \}} \quad \text{III-3-18}$$

III-3-8(ii) Both bound stationary and cooling at variable temperatures

occurs during modes:



Characteristic parameter - surface temperature (θ_0^*)

Boundary conditions:

$$\theta^*(t_S + t_p) = \theta_0^* \neq \text{constant}, \quad \theta^*(t_S + t_p + t_L) = \theta_D^* \neq \text{constant}$$

$$t_S = t_p = 0, \quad t_L^* = D^*$$

$$q^*(t_S + t_p) = q_0^*, \quad q^*(t_S + t_p + t_L) = 0$$

The heat conservation equation, III-3-12, reduces to:

$$q_0^* = \gamma_L^* \left\{ \frac{d}{d\zeta} \left[- \left(\frac{2}{3} \theta_D^* + \frac{1}{3} \theta_0^* \right) D^* \right] \right\}$$

$$= - \gamma_L^* D^* \left[\frac{1}{3} \frac{d\theta_0^*}{d\zeta} + \frac{2}{3} \frac{d\theta_D^*}{d\zeta} \right] \quad \text{III-3-19}$$

and heat flux equation becomes:

$$q_0^* = \frac{2 K_L^* (\theta_D^* - \theta_0^*)}{D^*} \quad \text{III-3-20}$$

Differentiate equation III-3-20 with respect to dimensionless time :

$$\frac{dq_0^*}{d\zeta} = \frac{2K_L^*}{D^*} \left\{ \frac{d\theta_D^*}{d\zeta} - \frac{d\theta_0^*}{d\zeta} \right\}$$

But

$$\frac{dq_0^*}{d\zeta} = f_0' \frac{d\theta_0^*}{d\zeta} + f_{\zeta}' \quad \text{III-3-21}$$

Therefore :

$$\frac{d\theta_D^*}{d\zeta} = \left\{ 1 + \frac{f_0' D^*}{2K_L^*} \right\} \frac{d\theta_0^*}{d\zeta} + \frac{D^*}{2K_L^*} f_{\zeta}' \quad \text{III-3-22}$$

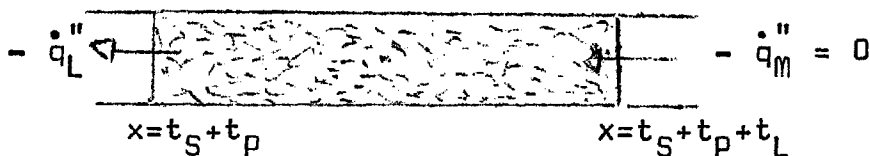
Substituting into the conservation equation, III-3-19, and rearranging it we get:

$$\frac{d\theta_0^*}{d\zeta} = \frac{\frac{-3q_0^*}{\gamma_L^* D^*} - \frac{D^*}{K_L^*} f_{\zeta}'}{3 + \frac{f_0' D^*}{K_L^*}} \quad \text{III-3-23}$$

III-3-8(iii) Both bounds moving at constant temperature

Occurs during modes:

2, S2, S3



Characteristic parameters - Thermal layer thickness (t_L^*)

Boundary conditions:

$$\theta^*(t_S+t_p) = \theta_L^* = \text{constant}; \quad \theta^*(t_S+t_p+t_L) = \theta_S^* = 1.0$$

$$q^*(t_S+t_p) = q_L^*$$

The conservation equation, III-3-12, becomes:

$$\begin{aligned} q_L^* &= \gamma_L^* \left\{ \frac{d}{d\zeta} \left[-\left(\frac{2}{3} \theta_M^* + \frac{1}{3} \theta_L^*\right) t_L^* \right] + \theta_M^* \left[\frac{dt_S^*}{d\zeta} \right. \right. \\ &+ \left. \left. \frac{dt_P^*}{d\zeta} + \frac{dt_L^*}{d\zeta} \right] - \theta_L^* \left[\frac{dt_S^*}{d\zeta} + \frac{dt_P^*}{d\zeta} \right] \right\} \\ &= \gamma_L^* \left\{ \frac{(\theta_M^* - \theta_L^*)}{3} \frac{dt_L^*}{d\zeta} + (\theta_M^* - \theta_L^*) \right. \\ &\quad \left. \left(\frac{dt_S^*}{d\zeta} + \frac{dt_P^*}{d\zeta} \right) \right\} \end{aligned}$$

Therefore :

$$\frac{dt_L^*}{d\zeta} = \frac{1}{3} \left\{ \frac{q_L^*}{\gamma_L^* (\theta_M^* - \theta_L^*)} - \left(\frac{dt_S^*}{d\zeta} + \frac{dt_P^*}{d\zeta} \right) \right\} \quad \text{III-3-24}$$

and the heat flux equation becomes:

$$q_L^* = \frac{2K_L^* (\theta_M^* - \theta_L^*)}{t_L^*} \quad \text{III-3-25}$$

Differentiating this equation with respect to dimensionless time we get :

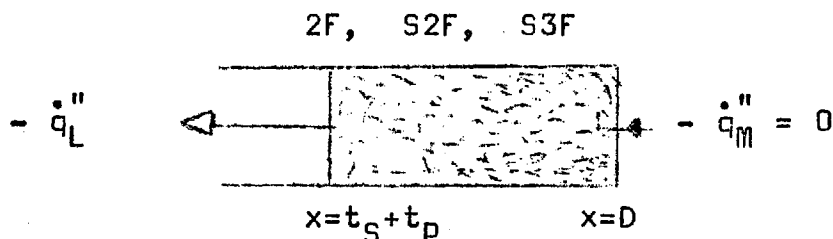
$$\frac{dq_L^*}{d\zeta} = \frac{2K_L^* (\theta_M^* - \theta_L^*)}{t_L^{*2}} \frac{dt_L^*}{d\zeta}$$

on substituting equation III-3-24 and III-3-25 we get:

$$\frac{dq_L^*}{d\zeta} = -\frac{q_L^*}{3t_L^*} \left\{ \frac{q_L^*}{\gamma_L^* (\theta_M^* - \theta_L^*)} - \left[\frac{dt_S^*}{d\zeta} + \frac{dt_P^*}{d\zeta} \right] \right\} \quad \text{III-3-26}$$

III-3-B(iv) Far bound stationary, insulating and cooling; near bound moving

Occurs during modes



Characteristic parameter - temperature of remote boundary (θ_D^*)

Boundary conditions:

$$\theta^*(t_S + t_P) = \theta_L^* = \text{constant}; \quad \theta^*(t_S + t_P + t_L) = \theta_D^* \neq \text{constant}$$

$$t_S^* + t_P^* + t_L^* = D^*$$

$$q^*(t_S + t_P) = q_L^*; \quad q^*(t_S + t_P + t_L) = 0$$

The heat conservation equation III-3-12 becomes:

$$\begin{aligned} q_L^* &= \gamma_L^* \left\{ \frac{d}{d\xi^*} \left[\left(-\frac{2}{3} \theta_D^* + \frac{1}{3} \theta_L^* \right) (D^* - t_S^* - t_P^*) \right] \right. \\ &\quad \left. - \theta_L^* \left(\frac{dt_S^*}{d\xi^*} + \frac{dt_P^*}{d\xi^*} \right) \right\} \\ &= \gamma_L^* \left\{ \frac{2}{3} (\theta_D^* - \theta_L^*) \left(\frac{dt_S^*}{d\xi^*} + \frac{dt_P^*}{d\xi^*} \right) - \left[2(D^* - t_S^* - t_P^*) \frac{d\theta_D^*}{d\xi^*} \right] \right\} \end{aligned}$$

Therefore

$$\frac{d\theta_D^*}{d\xi^*} = \frac{(\theta_D^* - \theta_L^*) \left(\frac{dt_S^*}{d\xi^*} + \frac{dt_P^*}{d\xi^*} \right) - \frac{3}{2} \frac{q_L^*}{\gamma_L^*}}{(D^* - t_S^* - t_P^*)} \quad \text{III-3-27}$$

and the heat flux equation gives:

$$q_L^* = \frac{2 K_L^* (\theta_D^* - \theta_L^*)}{(D^* - t_S^* - t_P^*)} \quad \text{III-3-28}$$

Differentiating this equation with respect to dimensionless time:

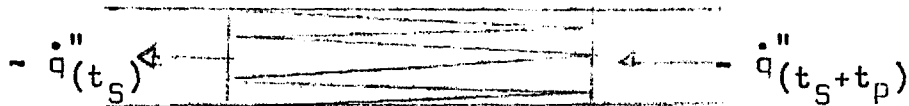
$$\frac{dq_L^*}{d\bar{\zeta}} = \frac{2K_L^*}{(D^* - t_S^* - t_P^*)} \frac{d\theta_D^*}{d\bar{\zeta}} + \frac{2K_L^*(\theta_D^* - \theta_L^*)}{(D^* - t_S^* - t_P^*)^2} \left\{ \frac{dt_S^*}{d\bar{\zeta}} + \frac{dt_P^*}{d\bar{\zeta}} \right\}$$

Substituting equations III-3-27 and III-3-28 we get:

$$\frac{dq_L^*}{d\bar{\zeta}} = - \frac{3q_L^* K_L^*}{\gamma_L^* (D^* - t_S^* - t_P^*)^2} + \frac{2q_L^*}{(D^* - t_S^* - t_P^*)} \left\{ \frac{dt_S^*}{d\bar{\zeta}} + \frac{dt_P^*}{d\bar{\zeta}} \right\} \quad \text{III-3-29}$$

III-4 PARTIAL LAYER (LAYER OF PARTIALLY SOLIDIFIED METAL)

The partial layer is shown schematically as:



The main differences between the partial solidified layer and the other layers considered so far arise because latent heat is liberated within the layer itself and because the thermal conductivity can no longer be taken as constant throughout the layer. Thus the unsteady state heat conduction equation within the layer is:-

$$\frac{\partial}{\partial x} \left(K_P \frac{\partial \theta}{\partial x} \right) = \rho c \frac{\partial \theta}{\partial \tau} - \rho H \frac{\partial f_S}{\partial \tau} \quad \text{III-4-1}$$

where f_S is the fraction of solid present and K_P is the thermal conductivity of the partial layer.

III-4-A LIBERATION OF LATENT HEAT

From the heat conduction equation III-4-1, it can be seen that the liberation of latent at any point is given by:

$$\rho H \frac{\partial f_S}{\partial \tau}$$

Thus equation III-4-1 can most conveniently be solved if

a relation is known between the temperature and the fraction of solid present at any point. Let us assume that the fraction of solid present at any point in the partial layer is a linear function of the temperature at that point.

$$f_S = a + b\theta \quad \text{III-4-2}$$

The value of the constants can be determined from the known conditions at the liquidus and solid temperatures:

$$\text{at } \theta = \theta_L ; f_S = 0 \quad \text{III-4-3}$$

$$\text{at } \theta = \theta_S ; f_S = f_{SU} = \text{constant} \quad \text{III-4-4}$$

where f_{SU} is the fraction solid present at solidus temperature. Thus we get:

$$f_S = f_{SU} \left(\frac{\theta_L - \theta}{\theta_L - \theta_S} \right) \quad \text{III-4-5}$$

and

$$\frac{\partial f_S}{\partial \tau} = - \frac{f_{SU}}{(\theta_L - \theta_S)} \frac{\partial \theta}{\partial \tau} \quad \text{III-4-6}$$

The value of f_{SU} can be calculated from the Pfann equation II-1-5 :

$$\text{Since } f_S = 1 - \left(\frac{C_L^*}{C_0} \right)^{\frac{1}{k-1}} \quad \text{III-4-7}$$

Therefore

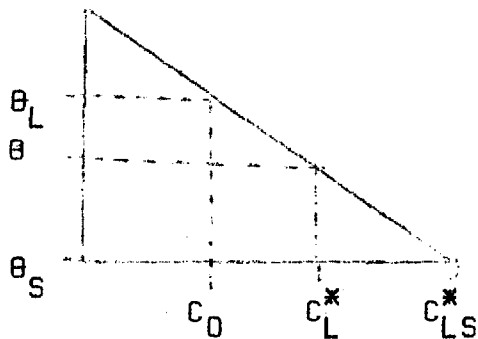
$$f_{SU} = 1 - \left(\frac{C_{LS}^*}{C_0} \right)^{\frac{1}{k-1}} \quad \text{III-4-8}$$

where C_{LS}^* is the concentration in the liquid at the solidus temperature and C_L^* is the concentration in the liquid at temperature, θ^* . Equation III-4-5 can be derived from Pfann's equation, III-4-7.

Dividing equation III-4-7 ~~by~~ ^{by} III-4-8 we get; when $k \ll 1$:

$$\frac{f_S}{f_{SU}} = \left(\frac{C_{LS}^* - C_0}{C_L^* - C_0} \right) \quad \text{III-4-9}$$

Assuming that the liquidus is a straight line, we get from similar triangles:-



$$\frac{\theta_L - \theta_S}{\theta - \theta_S} = \frac{C_{LS}^* - C_0}{C_L^* - C_0}$$

or

$$\frac{\theta_L - \theta}{\theta - \theta_S} = \frac{C_L^* - C_0}{C_{LS}^* - C_L^*}$$

Dividing gives:

$$\frac{C_{LS}^* - C_0}{C_L^* - C_0} = \frac{\theta_L - \theta_S}{\theta_L - \theta}$$

Therefore substituting this equation in equation III-4-9 and rearranging, we get:

$$f_S = f_{SU} \left(\frac{\theta_L - \theta}{\theta_L - \theta_S} \right) \quad \text{III-4-10}$$

when the value of partition coefficient, k , is very small equation, III-4-~~7~~^{7 & 8} reduces to equation III-4-5.

Equation III-4-5 can also be derived from the equation II-1-7 that Flemings developed for micro-segregation, assuming the linear growth of dendrite.

$$C_S^* = kC_0 \left(1 - \frac{f_S}{1 + \alpha_f k}\right)^{k-1} = kC_L^*$$

Rearranging we get

$$f_S = \left[1 - \left(\frac{C_L^*}{C_0}\right)^{\frac{1}{k-1}}\right] (1 + \alpha_f k)$$

and

$$f_{SU} = \left[1 - \left(\frac{C_{LS}^*}{C_0}\right)^{\frac{1}{k-1}}\right] (1 + \alpha_f k)$$

Dividing and rearranging we get; when $k \ll 1$:

$$f_S = f_{SU} \left(\frac{C_{LS}^* - C_0}{C_L^* - C_0}\right)$$

This equation is the same as equation III-4-9. Thus we can see that it is quite valid to assume that the fraction of solid metal is a linear function of temperature, as long as the partition coefficient, k , is small.

III-4-B VARIATION OF THERMAL CONDUCTIVITY

The thermal conductivity at any point in the partial layer depends upon the fraction of solidified metal at the point. This in turn depends upon the temperature at the point, so that the thermal conductivity is a function of temperature. Since we do not know how the volume fraction of solidified metal affects the conductivity in the partial layer and the temperature, we can assume it to be a linear function of temperature.

In dimensionless form this can be represented by:

$$K_p^* = a + b\theta^* \quad \text{III-4-11}$$

At the liquidus temperature the conductivity of the partial layer is equal to that of the liquid, since

the volume fraction solid is close to zero. Thus:-

$$\text{when } \theta^* = \theta_L^* ; \quad K_p^* = K_L^* \quad \text{III-4-12}$$

The conductivity of a two phase region is a complicated function of the volume fractions occupied by two phases and of their specific surface areas. The exact form of that function that applies to solid dendrite/liquid metal region is not known. Since the conductivities of the two phases are not very different, little error can be introduced if we assume that the conductivity of the partial layer at the solidus temperature is given by:-

$$[K_p]_S = K_S f_{SU} + (1-f_{SU})K_L \quad \text{III-4-13}$$

or, in dimensionless terms:

$$[K_p^*]_S = f_{SU} + (1-f_{SU}) K_L^* \quad \text{III-4-14}$$

Equation III-4-12 and 14 can be used to determine the constant a and b, so that

$$a = K_L^* + \frac{f_{SU}(1-K_L^*)}{(\theta_L^*-1)} \theta_L^* \quad \text{III-4-15}$$

$$\text{and } b = - \frac{f_{SU}(1-K_L^*)}{(\theta_L^*-1)} \quad \text{III-4-16}$$

For convenience we will rearrange III-4-11 after substituting these values of a and b, and obtain:

$$K_p^* = 1 - \mathcal{K}(\theta^* - \theta_F^*) \quad \text{III-4-17}$$

where

$$\mathcal{K} = \frac{1-K_L^*}{(\theta_L^* - \theta_F^*)} \quad \text{III-4-18}$$

$$\text{and } \theta_F^* = \frac{(1-\theta_L^* + f_{SU}\theta_L^*)}{f_{SU}} \quad \text{III-4-19}$$

III-4-C DERIVATION OF THE GENERAL EQUATIONS

Substituting equation III-4-6 into the unsteady state heat conduction equation within the partial layer (III-4-1) we get:

$$\frac{\partial}{\partial x} \left(k_p \frac{\partial \theta}{\partial x} \right) = \rho \left(c_p + \frac{H f_{SU}}{\theta_L - \theta_S} \right) \frac{\partial \theta}{\partial \tau} = \gamma_p \frac{\partial \theta}{\partial \tau} \quad \text{III-4-20}$$

where γ_p is a modified volume specific heat for the partial layer and is given by:

$$\gamma_p = \rho \left[c_p + \frac{H f_{SU}}{\theta_L - \theta_S} \right] \quad \text{III-4-21}$$

Integrating equation III-4-20 across the partial layer gives:

$$\left[k_p \frac{\partial \theta}{\partial x} \right]_{(t_S+t_p)^-} - \left[k_p \frac{\partial \theta}{\partial x} \right]_{(t_S)^+} = \gamma_p \left\{ \frac{d}{d\tau} \int_{t_S}^{(t_S+t_p)} \theta \, dx - \theta_{(t_S+t_p)} \left[\frac{dt_S}{d\tau} + \frac{dt_p}{d\tau} \right] + \theta_{t_S} \frac{dt_S}{d\tau} \right\} \quad \text{III-4-22}$$

But the heat transfer at the boundaries is given by:

$$\left[k_p \frac{\partial \theta}{\partial x} \right]_{(t_S)^+} = - \dot{q}''(t_S) \quad \text{III-4-23}$$

and

$$\left[k_p \frac{\partial \theta}{\partial x} \right]_{(t_S+t_p)^-} = - \dot{q}''(t_S+t_p) \quad \text{III-4-24}$$

Substituting these equations into equation III-4-22, and expressing in dimensionless terms the equation gives:

$$q^*(t_S) - q^*(t_S+t_p) = \gamma_p^* \left\{ \frac{d}{d\bar{\tau}} \int_{t_S}^{(t_S+t_p)} \theta^* \, d\left(\frac{x}{t_p}\right) + \theta^*(t_S+t_p) \left[\frac{dt_S^*}{d\bar{\tau}} + \frac{dt_p^*}{d\bar{\tau}} \right] - \theta^*(t_S) \frac{dt_S^*}{d\bar{\tau}} \right\} \quad \text{III-4-25}$$

Let us assume that auxiliary function for the temperature in the partial layer is a quadratic polynomial:-

$$\theta = a_0 + a_1 \left(\frac{x - t_S}{t_p} \right) + a_2 \left(\frac{x - t_S}{t_p} \right)^2 \quad \text{III-4-26}$$

We can evaluate the coefficients a_0 , a_1 and a_2 from the boundary conditions and heat transfer equation III-4-24, when we get:

$$\theta^* = \theta^*(t_S) + \left\{ 2\theta^*(t_S+t_p) - 2\theta^*(t_S) - \frac{q^*(t_S+t_p)t_p^*}{[K_p^*](t_S+t_p)} \right\} \left(\frac{x-t_S}{t_p} \right) - \left\{ \theta^*(t_S+t_p) - \theta^*(t_S) - \frac{q^*(t_S+t_p)t_p^*}{[K_p^*](t_S+t_p)} \right\} \left(\frac{x-t_S}{t_p} \right)^2 \quad \text{III-4-27}$$

and the integral of ^{the} auxiliary function becomes:

$$\int_{t_S}^{t_S+t_p} \theta^* d\left(\frac{x}{t_p} \right) = - \left[\frac{2}{3} \theta^*(t_S+t_p) + \frac{1}{3} \theta^*(t_S) - \frac{q^*(t_S+t_p)t_p^*}{[K_p^*](t_S+t_p)} \right] t_p^* \quad \text{III-4-28}$$

Substituting the integral of this auxiliary function into equation III-4-22 gives:

$$q^*(t_S) - q^*(t_S+t_p) = (\theta^*(t_S+t_p) - \theta^*(t_S)) \gamma_p^* \frac{dt_S^*}{d\zeta} + \theta^*(t_S+t_p) \gamma_p^* \frac{dt_p^*}{d\zeta} + \frac{d}{d\zeta} \left\{ \gamma_p^* t_p^* \left[\frac{2}{3} \theta^*(t_S+t_p) + \frac{1}{3} \theta^*(t_S) - \frac{q^*(t_S+t_p)t_p^*}{[K_p^*](t_S+t_p)} \right] \right\} \quad \text{III-4-29}$$

The heat flux equation is derived by differentiating auxilliary function III-4-27 with respect to x and substituting it into the heat transfer equation at the near boundary:

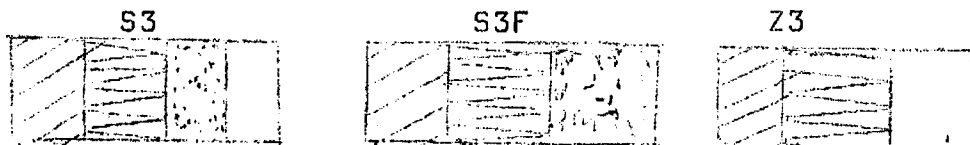
$$\frac{q^*(t_S)}{[K_p^*](t_S)} + \frac{q^*(t_S+t_p)}{[K_p^*](t_S+t_p)} = \frac{2(\theta^*(t_S+t_p) - \theta^*(t_S))}{t_p^*} \quad \text{III-4-30}$$

III-4-C CONVENIENT FORMS

Depending upon the mode of cooling in operation at any time, the temperature of the two bounds of the partial layer can be constant or variable; moreover the two bounds may be stationary or moving. In order to use the general equations derived above, it is necessary to transcribe the heat conservation equation, III-4-29, into convenient forms for ^{the} particular mode in operation. There are five different [^]forms and these are derived below.

III-4-C(i) Both bounds moving at fixed temperatures

Occurs during modes:



Characteristic parameter - Thickness of partial layer, t_p^*

Boundary conditions:

$$\theta^*(t_S) = 1, \quad \theta^*(t_S+t_p) = \theta_L^* = \text{constant}$$

$$[K_p^*](t_S) = [K_p^*], \quad [K_p^*](t_S+t_p) = K_L^*$$

$$q^*(t_S+t_p) = q_L^*$$

The heat flux equation III-4-30 becomes:

$$q_{t_S}^* = \frac{2 K_p^* \theta_L^* (\theta_L^* - 1)}{t_p^*} - \frac{[K_p^*]_S q_L^*}{K_L^*} \quad \text{III-4-31}$$

The heat conservation equation III-4-29 reduces to:

$$\frac{2 [K_p^*]_S (\theta_L^* - 1)}{t_p^*} - \left(1 + \frac{K_p^* \cdot S}{K_L^*}\right) q_L^* = (\theta_L^* - 1) \gamma_p^* \frac{dt_S^*}{d\zeta^*}$$

$$+ \theta_L^* \gamma_p^* \frac{dt_p^*}{d\zeta^*} - \frac{d}{d\zeta^*} \left\{ \gamma_p^* t_p^* \left(\frac{2}{3} \theta_L^* + \frac{1}{3} - \frac{q_L^* t_p^*}{6 K_L^*} \right) \right\}$$

and

$$\frac{2 [K_p^*]_S (\theta_L^* - 1)}{t_p^*} - \left(1 + \frac{K_p^* \cdot S}{K_L^*}\right) q_L^* = (\theta_L^* - 1) \gamma_p^* \frac{dt_S^*}{d\zeta^*}$$

$$+ \theta_L^* \gamma_p^* \frac{dt_p^*}{d\zeta^*} - \frac{\gamma_p^*}{3} \left\{ 2 \theta_L^* + 1 - \frac{q_L^* t_p^*}{K_L^*} \right\} \frac{dt_p^*}{d\zeta^*} + \frac{t_p^{*2}}{6 K_L^*} \frac{dq_L^*}{d\zeta^*}$$

III-4-32

Let us represent heat flux at $x = t_S + t_p$, as:

$$q_L^* = g(t_p^*, \zeta^*) \quad \text{III-4-33}$$

then,

$$g_t^* = \frac{\partial q_L^*}{\partial t_p^*} \quad \text{III-4-34}$$

and

$$g_\zeta^* = \frac{\partial q_L^*}{\partial \zeta^*} \quad \text{III-4-35}$$

so that

$$\frac{dq_L^*}{d\zeta^*} = g_t^* \frac{dt_p^*}{d\zeta^*} + g_\zeta^* \quad \text{III-4-36}$$

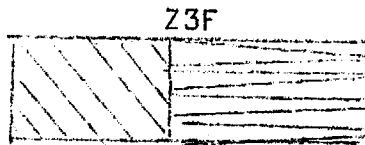
Substituting into the heat conservation equation III-4-32 and rearranging gives:

$$\frac{dt_p^*}{d\zeta} = \frac{(\theta_L^* - 1) \left\{ \frac{2 [K_P^*]_S}{t_p^*} - \gamma_P^* \frac{dt_S^*}{d\zeta} \right\} - \left(1 + \frac{[K_P^*]_S}{K_L^*} \right) q_L^* \frac{t_p^{*2} \gamma_P^* g_{\zeta}'}{6 K_L^*}}{\gamma_P^* \left[\frac{\theta_L^* - 1}{3} + \frac{q_L^* t_p^*}{3 K_L^*} + \frac{g_{\zeta}' t_p^{*2}}{6 K_L^*} \right]}$$

III-4-37

III-4-C(ii) Far bound stationary, insulating and cooling; near bound at fixed temperatures and moving

Occurs during mode



Characteristic parameter - Temperature of remote boundary, θ_D^*

Boundary conditions:

$$\theta^*(t_S + t_p) = \theta_D^* \neq \text{constant}; \quad \theta^*(t_S) = 1$$

$$t_p^* + t_S^* = D^*$$

$$[K_P^*]_{(t_S)} = [K_P]_S; \quad q^*(t_S + t_p) = 0$$

The heat flux equation III-4-30 reduces to:

$$q^*(t_S) = \frac{2 [K_P^*]_S (\theta_D^* - 1)}{t_p^*} \tag{III-4-38}$$

and heat conservation equation III-4-29 reduces to:

$$\frac{2 [K_P^*]_S (\theta_D^* - 1)}{t_p^*} = (\theta_D^* - 1) \gamma_P^* \frac{dt_S^*}{d\zeta} + \theta_D^* \gamma_P^* \left(- \frac{dt_S^*}{d\zeta} \right) - \frac{d}{d\zeta} \left[\gamma_P^* (D^* - t_S^*) \left(\frac{2}{3} \theta_D^* + 1 \right) \right]$$

and

$$\frac{2 \left[K_{pS}^* (\theta_D^* - 1) \right]}{t_p^*} = (\theta_D^* - 1) \gamma_p^* \frac{dt_S^*}{d\bar{x}} + \theta_D^* \gamma_p^* \left(- \frac{dt_S^*}{d\bar{x}} \right) - \frac{2\gamma_p^* (D - t_S^*)}{3} \frac{d\theta_0^*}{d\bar{x}} + \gamma_p^* \left(\frac{2}{3} \theta_D^* + 1 \right) \frac{dt_S^*}{d\bar{x}}$$

Rearranging we get:

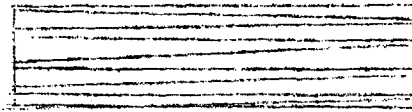
$$\frac{d\theta_0^*}{d\bar{x}} = \frac{\frac{3 \left[K_{pS}^* (\theta_D^* - 1) \right]}{(D^* - t_S^*)} - (\theta_D^* - 1) \gamma_p^* \frac{dt_S^*}{d\bar{x}}}{\gamma_p^* (D^* - t_S^*)}$$

III-4-39

III-4-C(iii) Both bounds stationary; far bound insulated

Occurs during mode

Z2F



Characteristic parameter - Temperature of cooled surface, θ_0^*

Boundary conditions:

$$\theta^*(t_S) = \theta_0^* \neq \text{constant}; \quad \theta^*(t_S + t_p) = \theta_D^* \neq \text{constant}$$

$$t_p^* = D^*$$

$$K_{pS}^* = K_0^* = 1 - \mathcal{K}(\theta_0^* - \theta_F^*)$$

$$q^*(t_S) = q_0^* = f(\theta_0^*, \bar{x}); \quad q^*(t_S + t_p) = 0$$

The heat flux equation III-4-30 reduces to:

$$q_0^* = 2 \left[1 - \mathcal{K}(\theta_0^* - \theta_F^*) \right] \frac{\theta_D^* - \theta_0^*}{D^*}$$

III-4-40

and heat conservation equation, III-4-29, reduces to:

$$q_0^* = - \gamma_p^* D^* \left\{ \frac{2}{3} \frac{d\theta_D^*}{d\zeta} + \frac{1}{3} \frac{d\theta_0^*}{d\zeta} \right\} \quad \text{III-4-41}$$

Differentiating heat flux equation III-4-40 gives:

$$\frac{dq_0^*}{d\zeta} = \frac{2(1-K(\theta_D^* - \theta_F^*))}{D^*} \left\{ \frac{d\theta_D^*}{d\zeta} - \frac{d\theta_0^*}{d\zeta} \right\} - \frac{2(\theta_D^* - \theta_0^*)}{D^*} K \frac{d\theta_0^*}{d\zeta} \quad \text{III-4-42}$$

But

$$\frac{dq_0^*}{d\zeta} = f_\theta' \frac{d\theta_0^*}{d\zeta} + f_\zeta'$$

So that after rearranging we get:

$$\frac{d\theta_D^*}{d\zeta} = \frac{\left\{ D^* f_\theta' + 2 - 2K(\theta_0^* - \theta_F^*) + \frac{D^* q_0^* K}{1 - K(\theta_0^* - \theta_F^*)} \right\} \frac{d\theta_0^*}{d\zeta} + f_\zeta' D^*}{2 - 2K(\theta_0^* - \theta_F^*)} \quad \text{III-4-43}$$

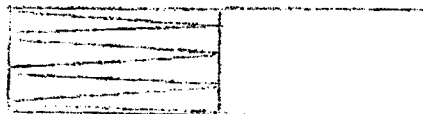
Substituting in the heat conservation equation III-4-41, and rearranging gives:

$$\frac{d\theta_0^*}{d\zeta} = - \frac{\frac{3q_0^*}{\gamma_p^* D^{*2}} - \frac{f_\zeta'}{1 - K(\theta_0^* - \theta_F^*)}}{\frac{f_\theta'}{1 - K(\theta_0^* - \theta_F^*)} + \frac{3}{D^*} + \frac{q_0^* K}{1 - K(\theta_0^* - \theta_F^*)}} \quad \text{III-4-44}$$

III-4-C(iv) Far bound insulated, and moving at constant temperature, near bound stationary at variable temperature

Occurs during mode

Z2



Characteristic parameter - Temperature of cooled surface, θ_0^* .

Boundary conditions:

$$\theta^*(t_S) = \theta_0^* \neq \text{constant}, \quad \theta^*(t_S+t_P) = \theta_D^* \neq \text{constant}$$

$$K_P^*(t_S) = K_0^*; \quad K_P^*(t_S+t_P) = K_L^*$$

$$q^*(t_S) = q_0^* = f'(\theta_0^*, \xi); \quad q^*(t_S+t_P) = 0$$

The thermal conductivity at the cooled surface K_0^* is given by:

$$K_0^* = 1 - K(\theta_0^* - \theta_F^*) \quad \text{III-4-45}$$

The heat flux equation III-4-30 reduces to:

$$q_0^* = \frac{2 K_0^* (\theta_L^* - \theta_0^*)}{t_P^*} \quad \text{III-4-46}$$

and heat conservation equation III-4-29 reduces to:

$$\begin{aligned} q_0^* &= \theta_L^* \gamma_P^* \frac{dt_P^*}{d\xi} - \frac{d}{d\xi} \left\{ \gamma_P^* t_P^* \left(\frac{2}{3} \theta_L^* + \frac{1}{3} \theta_0^* \right) \right\} \\ &= \frac{(\theta_L^* - \theta_0^*) \gamma_P^*}{3} \frac{dt_P^*}{d\xi} - \gamma_P^* t_P^* \frac{d\theta_0^*}{d\xi} \end{aligned} \quad \text{III-4-47}$$

Rearranging the heat flux equation and differentiating gives:

$$\begin{aligned} \frac{dt_P^*}{d\xi} &= - \left\{ \frac{2K_0^*}{q_0^*} + (\theta_L^* - \theta_0^*) \left[\frac{2K}{q_0^*} + \frac{2K_0^* f'(\theta)}{q_0^{*2}} \right] \right\} \frac{d\theta_0^*}{d\xi} \\ &\quad - \frac{2K_0^* f'(\theta_L^* - \theta_0^*)}{q_0^{*2}} \end{aligned} \quad \text{III-4-48}$$

Substituting this equation in heat conservation equation III-4-47 gives:

$$\frac{d\theta_0^*}{d\zeta} = - \frac{\frac{3q_0^{*2}}{2\gamma_p^*(\theta_L^* - \theta_0^*)} + \frac{K_0^{*f}(\theta_L^* - \theta_0^*)}{q_0^*}}{2K_0^* + (\theta_L^* - \theta_0^*) \left(\kappa + \frac{K_0^{*f}}{q_0^*} \right)} \quad \text{III-4-49}$$

III-4-C(v) Far bound uninsulated, moving at fixed temperature; near bound stationary at variable temperature

Occurs during modes:



Characteristic parameter - Thickness of partial layer, t_p^*

Boundary conditions:

$$\theta^*(t_S) = \theta_0^* \neq \text{constant}; \quad \theta^*(t_S + t_p) = \theta_L^*$$

$$K_p^*(t_S) = K_0^*; \quad K_p^*(t_S + t_p) = K_L^*$$

$$q^*(t_S) = q_0^* \quad q^*(t_S + t_p) = q_L^*$$

This is a rather difficult case to cope with as the temperature and thermal conductivity of the cooled surface are not constant. Similar cases treated in sections III-4-C(ii) and C(iii) were solved easily because no heat crossed the moving boundary of the partial layer. In this case, however, the thermal layer growing in front of the partial layer complicates the solution.

The heat flux equation III-4-30 becomes:

$$q_0^* = \frac{2K_0^*(\theta_L^* - \theta_0^*)}{t_p^*} - \frac{K_0^*}{K_L^*} q_L^* \quad \text{III-4-50}$$

where $K_0^* = 1 - K(\theta_0^* - \theta_F^*)$

and heat conservation equation III-4-29 becomes:

$$\begin{aligned} q_0^* - q_L^* &= \theta_L^* \gamma_p^* \frac{dt_p^*}{d\zeta} - \frac{d}{d\zeta} \left[\gamma_p^* t_p^* \left(\frac{2}{3} \theta_L^* + \frac{1}{3} \theta_0^* - \frac{q_L^* t_p^*}{K_L^*} \right) \right] \\ &= \theta_L^* \gamma_p^* \frac{dt_p^*}{d\zeta} - \gamma_p^* \left\{ \left(\frac{2}{3} \theta_L^* + \frac{1}{3} \theta_0^* - \frac{q_L^* t_p^*}{3K_L^*} \right) \right. \\ &\quad \left. \frac{dt_p^*}{d\zeta} + \frac{1}{3} t_p^* \frac{d\theta_0^*}{d\zeta} - \frac{t_p^*}{K_L^*} \left(\frac{dq_L^*}{d\zeta} \right) \right\} \end{aligned} \quad \text{III-4-51}$$

Since:

$$\frac{dq_L^*}{d\zeta} = g_t \frac{dt_p^*}{d\zeta} + g'_{\zeta}$$

The conservation equation becomes:

$$\begin{aligned} q_0^* - q_L^* &= \theta_L^* \gamma_p^* \frac{dt_p^*}{d\zeta} - \gamma_p^* \left\{ \left(\frac{2}{3} \theta_L^* + \frac{1}{3} \theta_0^* - \frac{q_L^* t_p^*}{3K_L^*} \right) \frac{dt_p^*}{d\zeta} \right\} \\ &\quad + \frac{\gamma_p^* t_p^*}{3} \frac{d\theta_0^*}{d\zeta} - \frac{\gamma_p^* t_p^*}{6K_L^*} \left[g_t \frac{dt_p^*}{d\zeta} + g'_{\zeta} \right] \end{aligned} \quad \text{III-4-52}$$

In principle, an expression for $\frac{d\theta_0^*}{d\zeta}$ which appears in this equation can be obtained by differentiating the heat flux equation. However, a very complicated set of equations would result because the thermal conductivity at the cooled surface is a function of temperature. Simpler equations result if $\frac{d\theta_0^*}{d\zeta}$ is evaluated by a method similar to that used by Hills for the layer of solid metal (section II-2-C(1)).

The equation for $\frac{d\theta_0^*}{d\zeta}$ is derived in appendix I and gives:

$$\frac{d\theta_0^*}{d\zeta} = - \frac{\frac{q_L^*}{K_L^*} \frac{dt_p^*}{d\zeta} + \frac{t_p^* f'_{\zeta}}{K_0^*}}{1 + \frac{t_p^*}{K_0^*} F'_{\theta}} \quad \text{III-4-53}$$

where

$$F_{\theta}^i = f_{\theta}^i + \frac{q_0^{*k}}{K_0^*} \quad \text{III-4-54}$$

F_{θ}^i appears in equation III-4-53 because the thermal conductivity varies with temperature.

Equation III-4-53 is not accurate as q_L^* approaches zero and cannot be used as one of two simultaneous equations from which t_p^* and θ_0^* might be determined. It is sufficiently accurate however, to determine the contribution made by $\frac{dq_0^*}{d\bar{x}}$ to equation III-4-52.

Substituting equation III-4-53 in conservation equation III-4-52 gives:

$$\frac{q_0^* - q_L^*}{\gamma_p^*} = \frac{1}{3} \left\{ \theta_L^* - \theta_0^* + \frac{q_L^* t_p^*}{K_L^*} + \frac{t_p^* g_t^*}{2K_L^*} + \frac{t_p^* q_L^* K_0^*}{K_L^* (K_0^* + t_p^* F_{\theta}^i)} \right\} \frac{dt_p^*}{d\bar{x}} + \frac{t_p^{*2}}{3K_L^*} \left[\frac{K_L^* f_{\theta}^i}{K_0^* + t_p^* F_{\theta}^i} + \frac{g_t^i}{2} \right] \quad \text{III-4-55}$$

Finally we get:

$$\frac{dt_p^*}{d\bar{x}} = \frac{\frac{3(q_0^* - q_L^*)}{\gamma_p^*} - \frac{t_p^{*2}}{K_L^*} \left\{ \frac{K_L^* f_{\theta}^i}{K_0^* + t_p^* F_{\theta}^i} + \frac{g_t^i}{2} \right\}}{\theta_L^* - \theta_0^* + \frac{q_L^* t_p^*}{K_L^*} \left[1 + \frac{K_0^*}{(K_0^* + t_p^* F_{\theta}^i)} \right] + \frac{t_p^{*2}}{2K_L^*} g_t^i} \quad \text{III-4-56}$$

and rearranging equation III-4-50, we get:

$$\theta_0^* = \theta_L^* - \frac{1}{2} \left[\frac{q_L^*}{K_L^*} + \frac{q_0^*}{K_0^*} \right] t_p^* \quad \text{III-4-57}$$

* The corresponding equation II-2-30 in Hills' analysis does not suffer from this inaccuracy, because of the dominant effect of the liberation of latent heat at, and above, the solidus temperature.

This equation can be used to relate θ_0^* to t_p^* .

Substituting for thermal conductivity at the cooled surface we get:

$$\theta_0^* = \theta_L^* - \frac{t_p^*}{2} \left[\frac{\theta_0^*}{1 - \kappa(\theta_0^* - \theta_F^*)} \right] + \frac{q_L^*}{K_L^*} \quad \text{III-4-58}$$

Rearranging this equation gives:

$$\theta_0^{*2} - \left[\theta_F^* + \frac{1}{\kappa} + \frac{t_p^*}{2\kappa} + \theta_L^* - \frac{q_L^* t_p^*}{2K_L^*} \right] \theta_0^* + \left(\theta_L^* - \frac{q_L^* t_p^*}{2K_L^*} \right) \left[\frac{1}{\kappa} + \theta_F^* \right] = 0 \quad \text{III-4-59}$$

Let us put:

$$\beta = \theta_F^* + \frac{1}{\kappa} + \frac{t_p^*}{2\kappa} + \theta_L^* - \frac{q_L^* t_p^*}{2K_L^*} \quad \text{III-4-60}$$

and

$$\epsilon = \left(\theta_L^* - \frac{q_L^* t_p^*}{2K_L^*} \right) \left[\frac{1}{\kappa} + \theta_F^* \right] \quad \text{III-4-61}$$

Therefore:

$$\theta_0^{*2} - \beta \theta_0^* + \epsilon = 0$$

So that

$$\theta_0^* = \frac{\beta \pm \sqrt{\beta^2 - 4\epsilon}}{2} \quad \text{III-4-62}$$

The negative root is valid in this case, since θ_0^* will equal to zero as t_p^* approaches infinity.

Therefore:

$$\theta_0^* = \frac{\beta - \sqrt{\beta^2 - 4\epsilon}}{2} \quad \text{III-4-63}$$

where β and ϵ are given by equations III-4-60 and 61 respectively.

This equation shows how θ_0^* is related to t_p^* and can be substituted into the right hand side of equation III-4-56 which is then no longer a function of θ_0^* . The equation can be integrated numerically and the substitution for θ_0^* being made during the numerical procedure. However, the equation is indeterminate when t_p^* is zero, and a limiting value is required for the numerical solution. This limiting value is derived in appendix II and gives:

$$\left[\frac{dt_p}{d\bar{z}} \right]_{t_p^* \rightarrow 0} = \frac{2 K_L^* (f_{\bar{z}}' - g_{\bar{z}}')}{\left([q_L^*]_{f_{\theta}'} + K_L^* g_t' \right) + \sqrt{\left([q_L^*]_{f_{\theta}'} + K_L^* g_t' \right)^2 + 4\gamma_p^* [q_L^*]_{f_{\bar{z}}'} K_L^* (f_{\bar{z}}' - g_{\bar{z}}')}}}$$

III-4-64

where $[q_L^*]_C$ is the dimensionless heat flux at partial layer/thermal layer front when t_p^* is zero and is equal to the dimensionless heat flux leaving the cooled surface when its temperature is equal to the liquidus temperature.

III-5 COOLING MODES FOR SOLIDIFICATION OF PURE METALS AND EUTECTICS IN PRESENCE OF SUPERHEAT

The solidification of pure metals and eutectics can be described in terms of the growth of a solid layer and of a cooled liquid layer. The different modes that can occur are shown in the solidification algorithm (Fig. III-1) and the corresponding calculations algorithm is shown in Fig. III-2. Each 'mode block' in the latter algorithm lists the characteristic parameters required for each layer together with reference number of the corresponding differential equation. The parameters below the dotted line are additional parameters which need to be determined. The parameters are not determined by solving differential equations, but are calculated from equations based on the heat flux equation. The reference numbers to these equations are also listed.

The equations derived in the previous sections have been general equations applicable under any given set of cooling conditions. The cooling conditions used in the experimental part of this investigation correspond to Newton's law of cooling. Thus the heat flux leaving the cooled surface is given by:

$$\dot{q}_0'' = -h A (\theta_0 - \theta_a) \quad \text{III-5-1}$$

Taking ambient temperature θ_a , as zero, we get:

$$\dot{q}_0'' = -h A \theta_0 \quad \text{III-5-2}$$

when $\theta_0 = \theta_s$; then

$$[\dot{q}_0'']_0 = -h A \theta_s \quad \text{III-5-3}$$

In dimensionless terms

$$q_0^* = \theta_0^* \quad \text{III-5-4}$$

and

$$\frac{dq_0^*}{d\zeta} = \frac{d\theta_0^*}{d\zeta} \quad \text{III-5-5}$$

The values of f_θ' and f_ζ' as defined earlier are:

$$f_\theta' = 1.0 \quad \text{III-5-6}$$

$$\text{and } f_\zeta' = 0 \quad \text{III-5-7}$$

The equations given in this section for the various modes have been derived for these cooling conditions.

III-5-A Mode 1 THE THERMAL LAYER GROWING ALONE



Here:

$$t_s^* = t_p^* = 0; \quad D^* > t_L^*$$

$$\theta_0^* > 1.0; \quad \theta_{t_L}^* = \theta_m^*$$

$$q_{t_L}^* = 0$$

The characteristic parameter for the thermal layer in this mode is θ_0^* . Its variation with time is given by equation III-3-18 which, for Newton's law cooling becomes:

$$\frac{d\theta_0^*}{d\bar{z}} = - \frac{3 \theta_0^*}{2 K_L^* \gamma_L^* (\theta_m^{*2} - \theta_0^{*2})} \quad \text{III-5-8}$$

The thickness of the layer is related to the surface temperature by the heat flux equation III-3-15, which becomes:

$$t_L^* = \frac{2 K_L^* (\theta_m^* - \theta_0^*)}{\theta_0^*} \quad \text{III-5-9}$$

Equation III-5-8 and corresponding equation for the next mode, mode 1F, can be integrated analytically. This mode has two limiting conditions, the surface temperature could reach the solidification temperature while the thermal layer is still growing, or the thermal layer could reach the remote boundary while the surface temperature is still above the solidification temperature. Equations III-5-8 and III-5-9 allow us to predict the time when these limiting conditions will occur.

Consider when $\theta_0^* = 1.0$, then from equation III-5-9 we find that the thickness of the thermal layer is

$$t_L^* = 2 K_L^* (\theta_m^* - 1.0) \quad \text{III-5-10}$$

If the value of t_L^* given by this equation is greater than D^* , the thermal layer will reach the remote boundary before the base temperature has reached the solidification temperature. Thus this occurs when:

$$\theta_m^* > \left(1 + \frac{D^*}{2 K_L^*}\right) \quad \text{III-5-11}$$

and the solidification process will proceed from mode 1 to 1F, the entire region being occupied by cooling liquid.

However, when:

$$\theta_m^* < \left(1 + \frac{D^*}{2 K_L^*}\right) \quad \text{III-5-12}$$

the solidification process proceeds from mode 1 to mode 2, and the thermal layer continues to grow ahead of the advancing solidification front. In the latter case the time $\bar{\zeta}_1$, that elapses before metal starts to solidify is given by:

$$\bar{\zeta}_1 = \int_{\theta_m^*}^{1.0} \left(\frac{d\theta_0}{d\bar{\zeta}}\right)^{-1} d\theta_0^* \quad \text{III-5-13}$$

and

$$\bar{\zeta}_1 = \frac{\gamma_L^* K_L^*}{3} \left\{ \theta_m^{*2} - 1.0 - 2 \ln \theta_m^* \right\} \quad \text{III-5-14}$$

In the former case the time that elapses before solidification starts must be calculated in two stages, the first in this mode and the second in mode 1F. The first stage represents the time ██████ for the thermal layer to reach the remote boundary. This occurs when the surface temperature is given by:

$$\theta_0^* = \frac{\theta_m^*}{\left[1 + \frac{D^*}{2 K_L^*}\right]} \quad \text{III-5-15}$$

The time that elapses before this temperature is reached can be calculated from equation III-5-13 where the upper limit of the integral is given by equation III-5-15:

$$\bar{\zeta}'_1 = \frac{\gamma_L^* K_L^*}{3} \left\{ \left(1 + \frac{D^*}{2 K_L^*} \right) - 1.0 - 2 \ln \left[1.0 + \frac{D^*}{2 K_L^*} \right] \right\}$$

III-5-16

III-5-B Mode 1F ENTIRE LIQUID REGION COOLING



Here:

$$t_S^* = t_P^* = 0, \quad t_L^* = D^*$$

$$\theta_0^* > 1.0, \quad \theta_M^* > \theta_D^* > 1$$

$$q_D^* = 0$$

The characteristic parameter for the liquid in this mode is θ_0^* , and its variation is given by equation III-3-23. For Newton's law of cooling we get:

$$\frac{d\theta_0^*}{d\bar{\zeta}} = - \frac{3 \theta_0^*}{\gamma_L^* D^* \left(3.0 + \frac{D^*}{K_L^*} \right)} \quad \text{III-5-17}$$

The temperature of the remote boundary is related to θ_0^* by the equation derived from heat flux equation III-3-20:

$$\theta_D^* = \theta_0^* \left\{ 1 + \frac{D^*}{2 K_L^*} \right\} \quad \text{III-5-18}$$

This mode ends when the surface temperature reaches the solidification temperature, so the time for which it operates $\bar{\zeta}'_{1F}$, can be evaluated from equation III-5-13 where the bottom limit of the integral is

given by equation III-5-15, but where the integral is given by equation III-5-17. Thus we have:

$$\bar{S}'_{1F} = \frac{\gamma_L^* D^*}{3} \left\{ \ln \left(\frac{\theta_m^*}{1 + \frac{D^*}{2 K_L^*}} \right) \right\} \left[3 \cdot 0 + \frac{B^*}{K_L^*} \right] \quad \text{III-5-19}$$

Thus the total time that elapses between the start of cooling and the start of solidification, when this mode operates, can be obtained by adding equations III-5-16 and III-5-19:

$$\begin{aligned} \bar{S} = \bar{S}'_1 + \bar{S}'_{1F} &= \frac{\gamma_L^* K_L^*}{3} \left\{ \left(1 + \frac{D^*}{2 K_L^*} \right)^2 - 1 \cdot 0 - 2 \ln \left[1 + \frac{D^*}{2 K_L^*} \right] \right\} \\ &+ \frac{\gamma_L^* D^*}{3} \left\{ \ln \left(\frac{\theta_m^*}{1 + \frac{D^*}{2 K_L^*}} \right) \right\} \left[3 \cdot 0 + \frac{D^*}{K_L^*} \right] \end{aligned} \quad \text{III-5-20}$$

Equation III-5-18 shows that the top temperature when solidification starts is given by:

$$\theta_D^* = 1 + \frac{D^*}{2 K_L^*} \quad \text{III-5-21}$$

III-5-C Mode 2 THE SOLID AND THERMAL LAYERS GROWING TOGETHER



Here:

$$D^* > (t_S^* + t_L^*) \quad t_p^* = 0$$

$$\theta_0^* < 1 \cdot 0, \quad \theta_{t_S}^* = 1 \cdot 0, \quad \theta_{t_L}^* = \theta_m^*, \quad \theta_D^* = \theta_m^*$$

$$q_{t_S}^* = q_L^* \quad q_{t_S+t_L}^* = 0$$

In this mode the characteristic parameters for the solid layer are its thickness and the temperature of its cooled surface, the corresponding differential equations being II-2-33 and II-2-30 . The characteristic parameter for the thermal layer is its thickness, and it is given by equation III-3-24.

q_L^* , the heat flux from liquid to the solid is given by equation III-3-25.

III-5-D Mode 2F THE SOLID LAYER IS GROWING AFTER THE THERMAL LAYER HAS REACHED THE REMOTE BOUNDARY



Here:

$$D^* = t_S^* + t_L^* ; t_P^* = 0.0$$

$$\theta_0^* < 1.0 ; \theta_{t_S}^* = 1.0 ; \theta_D^* > 1.0$$

$$q_{t_S}^* = q_L^* \quad q_D^* = 0$$

The characteristic parameters for the solid layer, and their equations are the same as in the previous mode. The characteristic parameter for the thermal layer is the temperature of the remote boundary and it is given by equation III-2-27. The heat flux from the liquid to the solid is given by equation III-3-28.

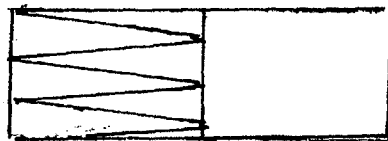
III-6 COOLING MODES FOR THE SOLIDIFICATION OF BINARY ALLOYS

As discussed earlier, the process of binary alloy solidification can be described by the algorithm shown in Fig. III-1. This defines all the cooling modes that can occur depending upon the relative growth rates of the various layers. The differential equations and the relevant equations for the additional parameters required are given here for each mode -

for the Newton's law cooling conditions ($q_0^* = \theta_0^*$, $f_\theta^* = 1.0$, $f_z^* = 0.0$).

The differential equations for variation of the surface temperature can be integrated analytically during modes Z2, Z2F, S1 and S1F. Numerical methods are required during the remaining modes. The calculation algorithm is given in Fig. III-3 which is of the same form as that given in Fig. III-2 for the solidification of pure metals and eutectics in the presence of superheat.

III-6-A Mode Z2 THE PARTIAL LAYER IS GROWING INTO LIQUID AT THE LIQUIDUS TEMPERATURE



Here:

$$t_S^* = 0, D^* > t_p^*, t_L^* = 0$$

$$\theta_L^* > \theta_0^* > 1, \theta_{t_p}^* = \theta_L^*$$

$$q_{t_p}^* = 0$$

The characteristic parameter for the partial layer is θ_0^* , the cooled surface temperature. Its variation is given by equation III-4-49, which, for Newton's law cooling becomes:

$$\frac{d\theta_0^*}{d\zeta} = - \frac{3 \theta_0^{*2}}{2\gamma_p^* (\theta_L^* - \theta_0^*) \left\{ 2K_0^* + (\theta_L^* - \theta_0^*) \left(\kappa + \frac{K_0^*}{\theta_0^*} \right) \right\}} \quad \text{III-6-1}$$

The thickness of the partial layer, t_p^* , is given by equation III-4-46, which becomes:

$$t_p^* = \frac{2K_0^*(\theta_L^* - \theta_0^*)}{\theta_0^*} \quad \text{III-6-2}$$

K_0^* in these equations is given by:

$$K_0^* = 1 - \kappa(\theta_0^* - \theta_F^*)$$

This mode will end when the temperature of the cooled surface falls to the solidus temperature, or when the partial layer reaches the remote boundary, whichever occurs first.

Equation III-6-2 shows that the first condition will be met first if:

$$D^* > 2 \left[K_p^* \right]_S (\theta_L^* - 1)$$

that is if

$$\theta_L^* < \left(1 + \frac{D^*}{2 \left[K_p^* \right]_S} \right) \quad \text{III-6-3}$$

Under these conditions, the solidification process will proceed from this mode to mode Z3 after dimensionless time period $\bar{\zeta}_1$, given by:

$$\begin{aligned} \bar{\zeta}_1 &= \int_{\theta_L^*}^{1.0} \left\{ \frac{d\theta_0^*}{d\bar{\zeta}} \right\}^{-1} d\theta_0^* \\ &= \frac{4}{3} \gamma_p^* \left\{ \kappa(\theta_L^* - 1) - \left(\frac{1 + \kappa\theta_F^* + 2K_0^*}{2} \right) \ln \theta_L^* + \left(\frac{1 + \kappa\theta_F^*}{4} \right) (\theta_L^{*2} - 1) \right\} \end{aligned} \quad \text{III-6-4}$$

The partial layer thickness at this time is given by:

$$t_p^* = 2.0 \left[K_p^* \right]_S (\theta_L^* - 1) \quad \text{III-6-5}$$

If $\theta_L^* > \left(1 + \frac{D^*}{2[K_p^*]_S}\right)$, the solidification process will

proceed to mode Z2F, when $t_p^* = D^*$. The temperature of cooled surface at this time is given by:

$$[\theta_0^*]_1 = \frac{\theta_L^*}{1 + \frac{D^*}{2K_0^*}} = \frac{\theta_L^*}{1 + \frac{D^*}{2[1 - \kappa([\theta_0^*]_1 - \theta_F^*)]}} \quad \text{III-6-7}$$

Rearranging this quadratic equation gives:

$$\kappa[\theta_0^*]_1^2 - (\kappa\theta_L^* + 1 + \kappa\theta_F^* + \frac{D^*}{2})[\theta_0^*]_1 + (1 + \kappa\theta_F^*)\theta_L^* = 0$$

so that:

$$[\theta_0^*]_1 = \frac{(\kappa\theta_L^* + \kappa\theta_F^* + 1 + \frac{D^*}{2}) \pm \sqrt{(\kappa\theta_L^* + \kappa\theta_F^* + 1 + \frac{D^*}{2})^2 - 4(1 + \kappa\theta_F^*)\theta_L^*}}{2\kappa}$$

As θ_0^* is less than θ_L^* it is the minus sign that is valid in this equation. Therefore:

$$[\theta_0^*]_1 = \frac{(\kappa\theta_L^* + \kappa\theta_F^* + 1 + \frac{D^*}{2}) - \sqrt{(\kappa\theta_L^* + \kappa\theta_F^* + 1 + \frac{D^*}{2})^2 - 4(1 + \kappa\theta_F^*)\theta_L^*}}{2\kappa}$$

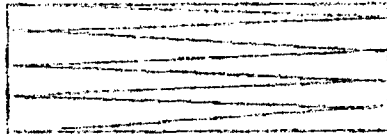
III-6-8

Thus the dimensionless time, ξ'_{1A} , taken for the partial layer to reach remote boundary is given by:

$$\begin{aligned} \xi'_{1A} &= \int_{\theta_L^*}^{[\theta_0^*]_1} \left(\frac{d\theta_0^*}{d\xi}\right)^{-1} d\theta_0^* \\ &= \frac{4}{3}\gamma_p^* \left\{ \kappa(\theta_L^* - [\theta_0^*]_1) - \left(\frac{1 + \kappa\theta_F^* + 2\kappa\theta_L^*}{2}\right) \ln\left(\frac{\theta_L^*}{[\theta_0^*]_1}\right) + \left(\frac{1 + \kappa\theta_F^*}{4}\right) \left(\frac{\theta_L^*}{[\theta_0^*]_1}\right)^2 - 1 \right\} \end{aligned}$$

III-6-9

III-6-B Mode Z2F PARTIAL LAYER OCCUPIES ENTIRE REGION



Here:

$$t_S^* = 0 \quad t_P^* = D^*$$

$$\theta_L^* > \theta_0^* > 1$$

$$q_D^* = 0$$

The characteristic parameter in this mode is the temperature of the cooled surface and it is given by equation III-4-44 which for Newton's law cooling becomes:

$$\frac{d\theta_0^*}{d\zeta^*} = - \frac{3 \theta_0^*}{\gamma_P^* D^{*2} \left[\frac{1}{K_0^*} + \frac{3}{D^*} + \frac{\theta_0^*}{K_0^{*2}} \right]} \quad \text{III-6-10}$$

The temperature of the remote boundary is then given by equation III-4-40. This mode persists for a period of time, ζ'_{1F} , during which the surface temperature drops from the value given by equation III-6-8 to the solidus. ζ'_{1F} is given by:

$$\zeta'_{1F} = \int_{\left[\theta_0^* \right]_1}^{1.0} \left(\frac{d\theta_0^*}{d\zeta^*} \right)^{-1} d\theta_0^* = \frac{\gamma_P^* D^{*2}}{3} \left\{ \frac{1}{(1 + \theta_F^*)} \ln \left[\frac{[K_P^*]_S [\theta_0^*]_1}{[K_0^*]_1} \right] + \frac{3}{D^*} \ln [\theta_0^*]_1 - \frac{1}{[K_P^*]_S} + \frac{1}{[K_0^*]_1} \right\} \quad \text{III-6-11}$$

where $\left[\theta_0^* \right]_1 = 1 - K(\theta_0^* - \theta_F^*) \quad \text{III-6-12}$

III-6-C Mode Z3 PARTIAL LAYER IS GROWING
AHEAD OF SOLID LAYER



Here:-

$$D^* > t_S^* + t_p^* \quad t_L^* = 0; \quad q^*(t_S+t_p) = q_L^* = 0$$

$$D_0^* < 1.0; \quad \theta_{t_S}^* = 1.0 \quad \theta_{t_S+t_p}^* = \theta_L^*$$

The characteristic parameters for the solid layer are the temperature of cooled surface, given by equation II-2-30, and the thickness of the solid layer, given by equation II-2-33. The partial layer is characterised by its thickness, given by equation III-4-37.

Since $q_L^* = 0$, the equation becomes:

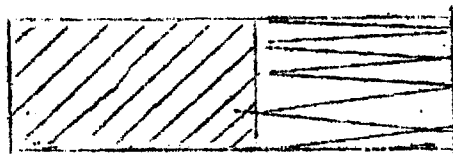
$$\frac{dt_p^*}{d\bar{z}} = \frac{3(\theta_L^* - 1) \left\{ \frac{2[K_p^*]_S}{t_p^*} - \gamma_p^* \frac{dt_S^*}{d\bar{z}} \right\}}{\gamma_p^* (\theta_L^* - 1)}$$

$$= \frac{6[K_p^*]_S}{\gamma_p^* t_p^*} - 3.0 \frac{dt_S^*}{d\bar{z}} \quad \text{III-6-13}$$

$q_{t_S}^*$, the heat flux crossing the solid boundary is given by equation III-4-31 which becomes:

$$q_{t_S}^* = \frac{2[K_p^*]_S (\theta_L^* - 1)}{t_p^*} \quad \text{III-6-14}$$

III-6-D Mode Z3F PARTIAL LAYER IS SHRINKING IN FRONT OF GROWING SOLID LAYER



Here:-

$$D^* = t_S^* + t_P^*$$

$$\theta_0^* < 1.0, \quad \theta_{t_S}^* = 1.0 \quad \theta_L^* > \theta_D^* > 1.0$$

$$K_{t_S}^* = [K_{P_S}^*] \quad q_D^* = 0$$

The solid layer is characterised by the variables used for the previous mode and the partial layer is characterised by the temperature of the remote boundary. This temperature is given by equation III-4-39. $q_{t_S}^*$, the heat flux crossing the solidus boundary is given by equation III-4-38.

III-6-E, F Mode S1 THERMAL LAYER GROWING
and
Mode S1F ENTIRE LIQUID REGION COOLING



These modes are identical to the modes 1 and 1F treated earlier except that the end condition involved the liquidus temperature of the alloy rather than the solidification temperature of pure metal.

The thickness of thermal layer when cooled surface reaches the liquidus temperature, therefore would be given by equation III-5-2 as:

$$t_L^* = \frac{2K_L^*(\theta_m^* - \theta_L^*)}{\theta_0^*} \quad \text{III-6-15}$$

Thus if $\theta_m^* > \theta_L^* \left(1 + \frac{D^*}{2K_L^*}\right)$, the thermal layer will reach

the remote boundary before the base temperature has reached the liquidus temperature. Under these conditions the solidification process will proceed from mode S1 to S1F when the base temperature is:

$$\theta_0^* = \frac{\theta_m^*}{1 + \frac{D^*}{2K_L^*}} \quad \text{III-6-16}$$

This will occur after a dimensionless period $\bar{\zeta}_{1A}^*$ given by:

$$\bar{\zeta}_{1A}^* = \frac{\gamma_L^* K_L^*}{3} \left\{ \left(1 + \frac{D^*}{2K_L^*}\right)^2 - 1.0 - 2 \ln \left(1 + \frac{D^*}{2K_L^*}\right) \right\} \quad \text{III-6-17}$$

Mode 1F will then persist for a time period, $\bar{\zeta}_{1F}^*$, given by:

$$\bar{\zeta}_{1F}^* = \frac{\gamma_L^* D^*}{3} \left\{ \left(3 + \frac{D^*}{K_L^*}\right) \left(\ln \left(\frac{\theta_m^*}{1 + \frac{D^*}{2K_L^*}} \right) \right) - \ln \theta_L^* \right\} \quad \text{III-6-18}$$

after which the partial layer will start to grow. The temperature of the remote boundary when this occurs is given by III-3-18 as:

$$\theta_D^* = \theta_L^* \left(1 + \frac{D^*}{2K_L^*}\right) \quad \text{III-6-19}$$

However, if $\theta_m^* < \theta_L^* \left(1 + \frac{D^*}{2K_L^*}\right)$ solidification will proceed

directly from mode S1 to mode S2 after the dimensionless time period $\bar{\zeta}_1$, given by:

$$\xi_1 = \frac{\gamma_L^* K_L^*}{3} \left\{ \left(\frac{\theta_m^*}{\theta_L^*} \right)^2 - 1.0 - 21n \left(\frac{\theta_m^*}{\theta_L^*} \right) \right\} \quad \text{III-6-20}$$

The thickness of the thermal layer when this occurs is given by equation III-5-2 as:

$$t_L^* = \frac{2.0 K_L^* (\theta_m^* - \theta_L^*)}{\theta_L^*} \quad \text{III-6-21}$$

III-6-G Mode S2 PARTIAL AND THERMAL LAYERS ARE GROWING TOGETHER



Here:

$$t_S^* = 0 \quad D^* > (t_p^* + t_L^*)$$

$$\theta_0^* > 1; \quad \theta_{t_p}^* = \theta_L^*; \quad \theta_{(t_p+t_L)}^* = \theta_m^*$$

$$q_{(t_p+t_L)}^* \equiv 0$$

In this mode the characteristic parameters for the partial layer and the thermal layer are their thicknesses t_p^* and t_L^* , given by equations III-4-56 and III-4-24 respectively.

q_L^* the heat flux from liquid to the partial layer is given by equation III-3-25. Equation III-3-56 which describes the growth of the partial layer contains the variables θ_0^* , g_{ξ}^* and g_t^* . The temperature of cooled surface θ_0^* is given by equation III-4-61 and rearranging equation III-3-26 we get:

$$\frac{\partial q_L^*}{\partial t_p^*} = g_t^* = \frac{q_L^*}{3 t_L^*} \quad \text{III-6-22}$$

and

$$\frac{\partial q_L^*}{\partial \xi} = g_{\xi}^* = - \frac{q_L^{*2}}{3 t_L^* \gamma_L^* (\theta_m^* - \theta_L^*)} \quad \text{III-6-23}$$

As discussed earlier equation III-4-56 for the growth of the partial layer becomes indeterminate when t_p^* is zero. The limiting value is given by equation III-4-64.

III-6-H Mode S2F THE PARTIAL LAYER IS GROWING AFTER THE THERMAL LAYER HAS REACHED THE REMOTE BOUNDARY



Here:

$$t_S^* = 0 ; D^* = t_p^* + t_L^*$$

$$\theta_0^* > 1 ; \theta_{t_p}^* = \theta_L^*$$

$$q_D^* = 0$$

The characteristic parameter for the partial layer and its differential equation are the same as in the previous mode. The characteristic parameter for the thermal layer is the temperature of the remote boundary θ_D^* , and it is given by equation III-3-27. The heat flux from the liquid to the partial layer, q_L^* , is given by equation III-4-28. The equation for the surface temperature, θ_0^* and the limiting form of the equation for the thickness of the partial layer are the same as in the previous mode. The variables describing the rate of change q_L^* are given by rearranging equation III-3-29, whence we get:

$$\frac{\partial q_L^*}{\partial t_p^*} = g_t' = \frac{2 q_L^*}{D^* - t_S^* - t_p^*} \quad \text{III-6-24}$$

$$\frac{\partial q_L^*}{\partial \xi} = g_\xi' = - \frac{3 q_L^* K_L^*}{\gamma_L^* (D^* - t_S^* - t_p^*)^2} \quad \text{III-6-25}$$

III-6-I Mode S3 THE SOLID, PARTIAL AND THERMAL LAYERS ARE GROWING TOGETHER



Here:

$$D^* > t_S^* + t_P^* + t_L^*$$

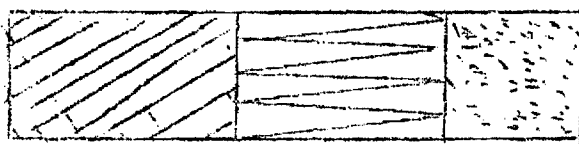
$$\theta_{t_S}^* = 1.0 ; \quad \theta^*(t_S + t_P) = \theta_m^*$$

$$q^*(t_S + t_P + t_L) = 0$$

The characteristic parameters for the solid layer are temperatures of the cooled surface and the layer thickness, the corresponding differential equations being II-2-30 and II-2-33. The characteristic parameters for the partial layer and thermal layers are the layer thicknesses and the corresponding differential equations are III-4-37 and III-3-24 respectively. The heat flux from liquid to the partial layer is given by equation III-3-25 and the heat flux from partial layer to the solid is given by equation III-4-31.

Equations for the variables (g_t^i and g_z^i), defining the differential of heat flux q_L^* are given by III-6-22 and 23 respectively.

III-6-J Mode S3F THE SOLID AND PARTIAL LAYERS ARE GROWING AFTER THE THERMAL LAYER HAS REACHED THE REMOTE BOUNDARY

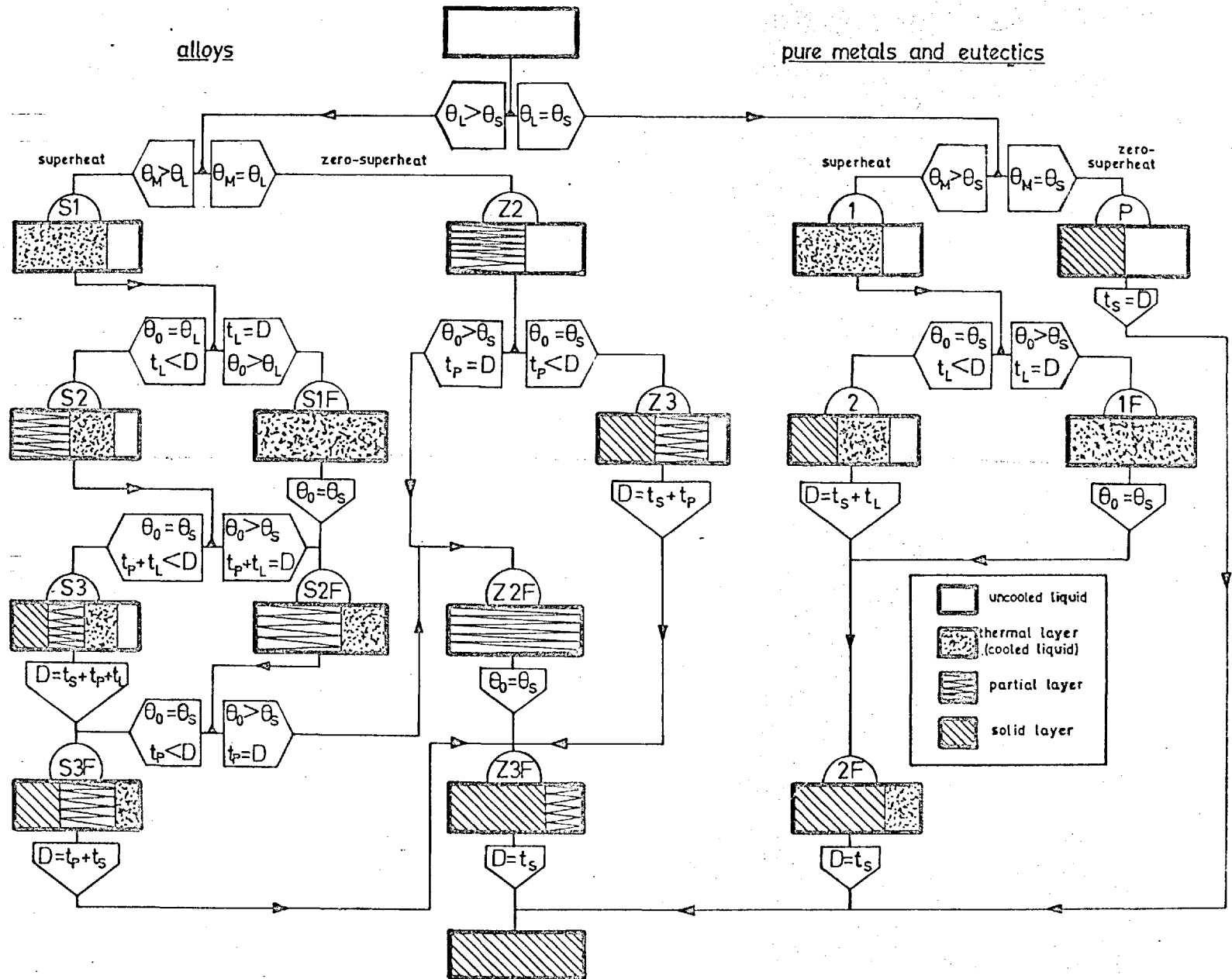


Here:

$$D^* = t_S^* + t_P^* + t_L^*$$

$$\theta_{t_S}^* = 1.0 ; \quad \theta^*(t_S + t_P) = \theta_L^* , \quad \theta_D^* \neq \text{constant}$$

$$q_D^* = 0$$



FIII-1 SOLIDIFICATION ALGORITHM FOR PURE METALS AND BINARY ALLOYS

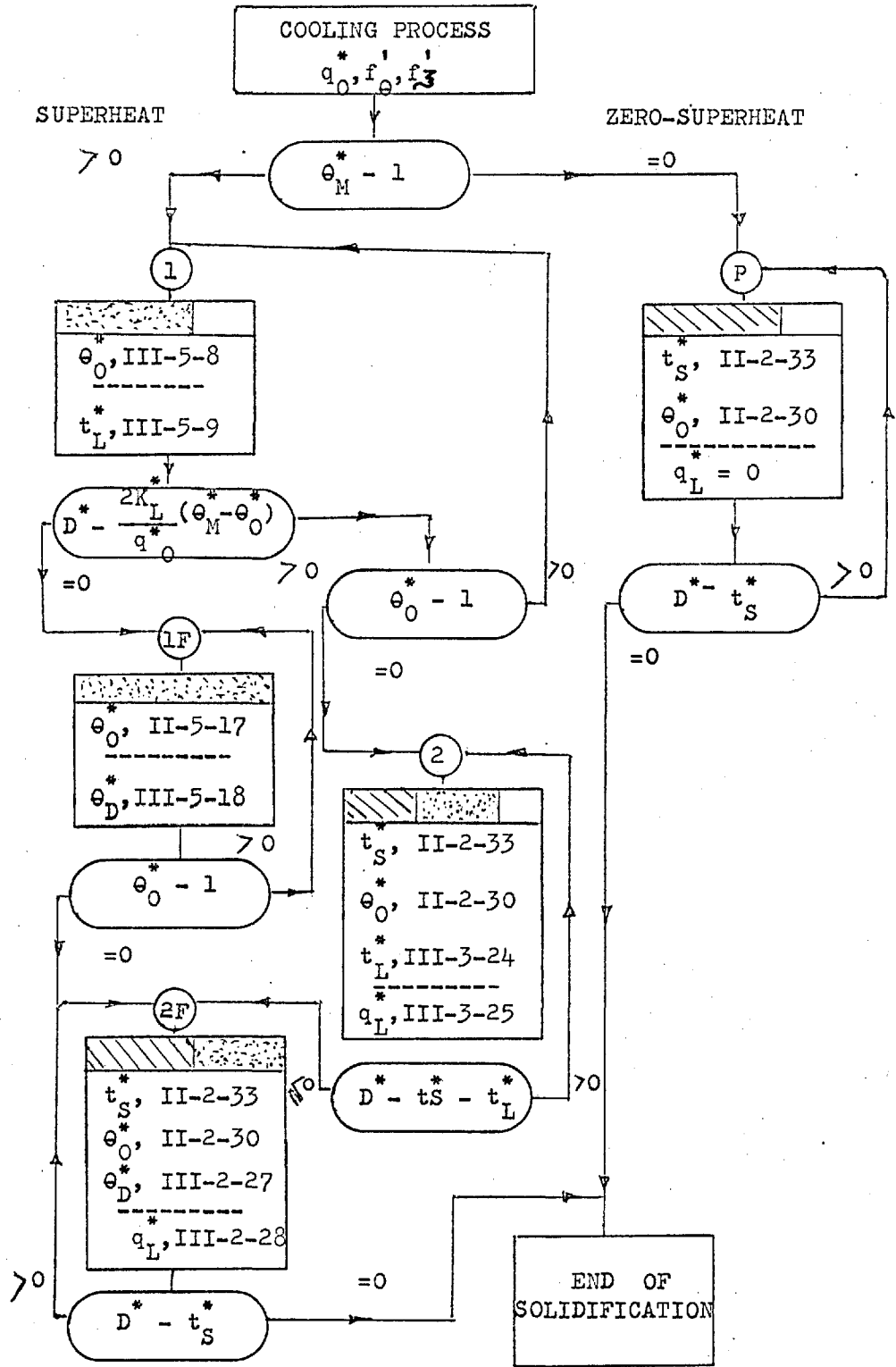


Fig. III-2. CALCULATION ALGORITHM OF PURE METALS AND EUTECTIC SOLIDIFICATION

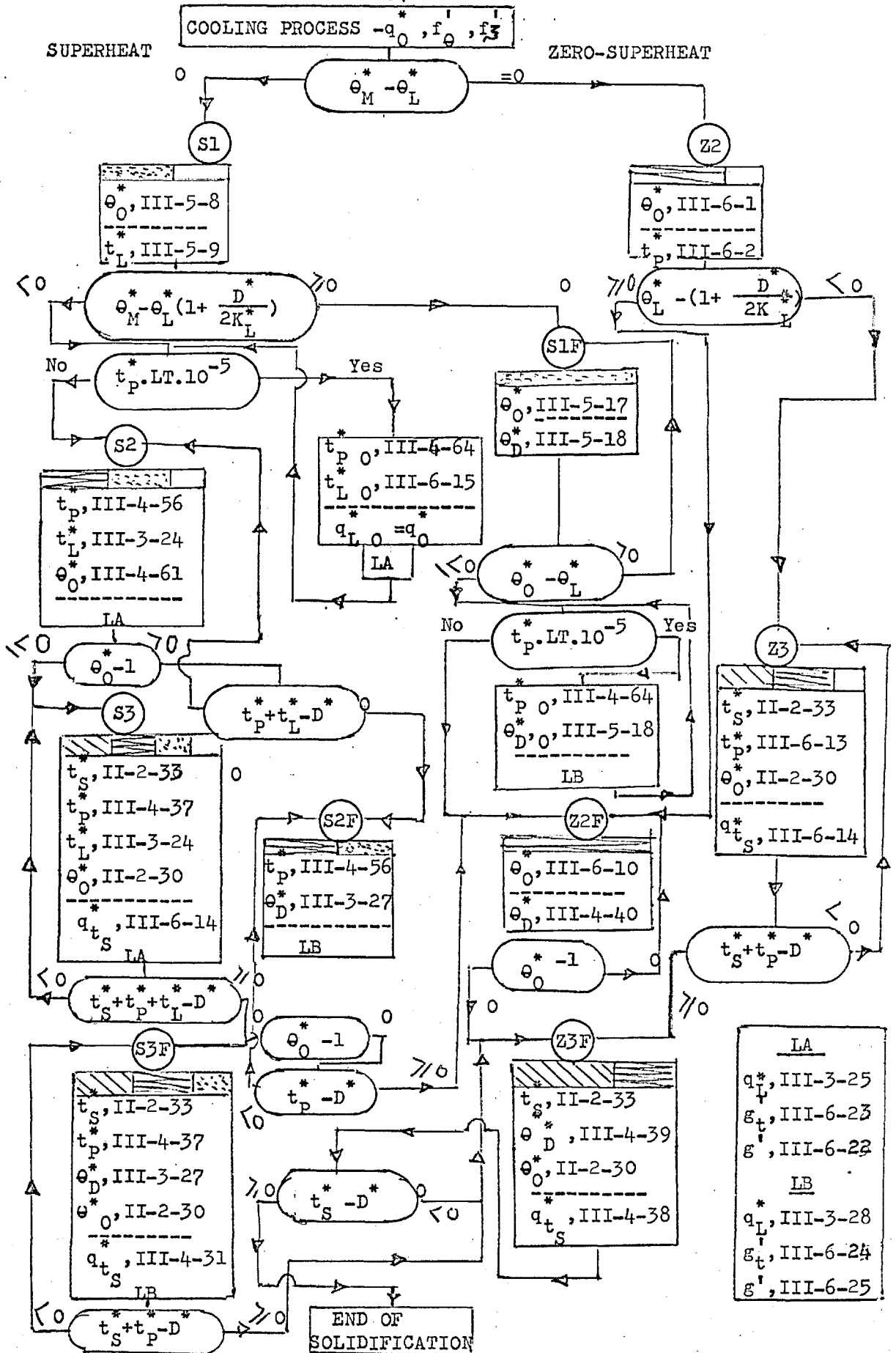


Fig. III-3. CALCULATION ALGORITHM OF ALLOY SOLIDIFICATION

The characteristic parameters for the solid and partial layers and their differential equation are the same as in the previous mode. The characteristic parameter for the thermal layer is the temperature of the remote boundary and is given by equation III-4-27. The heat flux crossing the liquidus front is given by equation III-3-28, while the heat flux from the partial layer to the solid is given by equation III-4-31. The variables g_t' and g_3' describing the differential of heat flux g_L^* are given by equations III-6-24 and 25.

III-7 VALUES OF THE PHYSICAL PROPERTIES AND OTHER VALUES USED IN THE THEORETICAL PREDICTIONS

The values of the physical properties of pure lead, tin and antimony that have been used in this work are given in Table III-2, together with the relevant references. The values of the physical properties for the alloys are given in Tables III-3 to III-6 and the methods whereby these were calculated are discussed below.

III-7-A DENSITY, THERMAL CONDUCTIVITY AND SPECIFIC HEAT

The values of the density and thermal conductivity of the solid and liquid alloy phases have been calculated by assuming additive behaviour on a volumetric basis, while the specific heats of the solid and liquid alloy phases have been calculated by assuming additive behaviour on weight basis.

Typical calculation for the lead-tin eutectic:

Alloy compositions: (wt. %) Tin = 61.9, Lead = 38.1
(Vol. %) Tin = 71.6, Lead = 28.4

$$\text{Density of the solid} = \frac{100}{\frac{61.9}{448} + \frac{38.1}{696}} = 518.4 \text{ lb/ft}^3$$

$$\begin{aligned} \text{Thermal conductivity of the solid} &= 34.4 \times .716 + 17.9 \times .284 \\ &= 29.7 \text{ Btu/ft.hr.}^\circ\text{F} \end{aligned}$$

$$\begin{aligned}\text{Specific heat of the solid} &= 0.063 \times .619 + 0.033 \times .381 \\ &= 0.0516 \text{ Btu/lb.}^\circ\text{F}\end{aligned}$$

III-7-B LATENT HEAT

III-7-B(i) Eutectic metals

The heat released when a eutectic alloy is solidified to produce a mixture of two solid alloys depends upon the latent heats of the constituent pure metals at the eutectic temperature and upon the heat of formation of the solid and liquid alloys. Thus the latent heat of solidification of a mass of unit eutectic alloy is given by:-

$$\Delta H_{S,E} = C_A \Delta H_{S,A} + C_B \Delta H_{S,B} - \Delta H_{F,L:E} + C_\alpha \Delta H_{F,\alpha} + C_\beta \Delta H_{F,\beta}$$

The latent heats of the pure metals can be determined from the data presented by Hultgren et alia³⁸, extrapolated by subtracting the heat content of the liquid metal to the eutectic temperature from that of the solid metal. Very little data is available concerning the heats of formation of solid and liquid alloys.

III-7-B(i)(a) Lead antimony

Hultgren et alia³⁸ report that the heat of formation of liquid lead-antimony alloys of eutectic composition is zero. No measured value is available for the heats of formation of the solid alloys, so they, also, have been taken as zero. Thus the latent heat of the lead-antimony eutectic, at its eutectic temperature is:

$$\Delta H_{S,Pb/Sb:E} = -15.9 \text{ Btu/lb}$$

III-7-B(i)(b) Lead-tin eutectic

Kleppa³⁹ has measured the heat of formation of liquid lead-tin alloys at 350°C and 450°C and found, for alloys of eutectic compositions, values in the range 3.1 ± 0.5 Btu/lb. Taylor⁴⁰ has measured the total heat of formation of solid eutectic lead-tin alloy, $C_\alpha \Delta H_{F,\alpha} + C_\beta \Delta H_{F,\beta}$, reporting a value of 3.4 Btu/lb. Thus the value of

the latent heat of eutectic lead-tin alloy calculated from data in the literature is:-

$$\Delta H_{S,PbSn:E} = -19.0 \text{ Btu/lb}$$

This value did not agree with the overall heat balances made on the solidification experiments, since it indicated that about 20% more heat was liberated from the solidifying metal than was removed by the cooling air (see Tables V-4 and V-5). However, similar heat balances made on the authors' experiments involving pure metals and lead-antimony eutectic alloys were accurate to about 5% (see Tables V-3 and V-4). Similar results have been obtained by Moore⁴¹ for pure lead and pure tin using the same apparatus.

The literature on latent heat values thus seemed far too high, and the calorimetric experiments reported in section IV-9 were therefore carried out. These experiments measured the heat liberated when liquid lead-tin eutectic alloy was cooled from just above its melting point to about 97°F, at which temperature the solid solutions formed just below the eutectic temperature are no longer stable. Borelius⁴² has studied the kinetics of the precipitation reaction by which supercooled metal solid solutions decompose. He found that the precipitation reaction in the lead-tin system was extremely rapid, the maximum rate occurring at 122°F and decreases only slightly at lower temperatures. His results show that this precipitation reaction will be about 90% complete after 1 minute at 87°F. Thus, at the end of the calorimetric experiments which take about 2 minutes, the eutectic alloy will consist of a mixture of virtually pure lead and pure tin. The experiments therefore measure the heat involved in decomposing the liquid eutectic alloy, solidifying the constituent pure metals and cooling them to the final temperature. Thus the results in Table V show that

$$C_{Pb,E} \Delta H_{S,Pb} + C_{Sn,E} \Delta H_{S,Sn} - \Delta H_{F,L:E} \\ = -18.6 \pm 0.97 \text{ Btu/lb}$$

Since the data reported by Hultgren et alia³⁸ shows that

$$C_{Pb,E} \Delta H_{S,Pb} + C_{Sn,E} \Delta H_{S,Sn} = -19.3 \text{ Btu/lb}$$

the calorimetric values show that the heat of the formation of the liquid alloy at the liquidus temperature is either zero or very small. We have assumed it to be zero, which gives

$$\Delta H_{S,Pb/Sn:E} = -15.9 \text{ Btu/lb}$$

III-7-B(ii) Alloys

When a non-eutectic alloy solidifies latent heat is liberated in the partial layer, and at the eutectic temperature if the initial alloy composition is high enough. The latent heat liberated at the eutectic temperature, per unit mass of alloy, is equal to $(1-f_{SU}) \Delta H_{S,E}$ where $\Delta H_{S,E}$ is to be determined as described above, and the value of f_{SU} is determined as described in section III-7-C. The latent heat liberated in the partial layer, per unit mass of alloy, is:-

$$f_{SU} (C_A \overline{\Delta H}_{S,A} + C_B \overline{\Delta H}_{S,B} - \Delta H_{F,L} + \Delta H_{F,\alpha:C_B})$$

where $\overline{\Delta H}_S$ represents the average difference between the heat contents of the solid and liquid pure metals between the liquidus and eutectic temperature. C_A and C_B are the mean concentrations in the solid alloy formed in the partial layer, and $\Delta H_{F,\alpha:C_B}$ is the heat of formation of this alloy.

C_A and C_B can be calculated from a mass balance on the solidification process:-

$$\begin{aligned} \text{Fraction of A solidifying at the eutectic temperature} \\ = (1-f_{SU})C_E \end{aligned}$$

$$\begin{aligned} \text{Fraction of B solidifying in the partial layer} \\ = C_0 - (1-f_{SU})C_E \end{aligned}$$

But the total fraction of A and B solidifying in the partial layer = f_{SU} .

Therefore

$$C_B = \frac{C_0 - (1-f_{SU})C_E}{f_{SU}}$$

and $C_A = 1 - C_B$

III-7-B(ii)(a) Typical calculation for the lead tin system - Pb20Sn

$$C_0 = 0.2, \quad f_{SU} = 0.804$$

$$\therefore C_{Sn} = 0.098 \text{ and } C_{Pb} = 0.902$$

No information is available in the literature about how the heat of formation of solid lead-tin alloys varies with composition. The quantity of β phase formed in this system is extremely small, so that this phase can be considered to make a negligible contribution to the heat effect measured by Taylor for eutectic alloys. Since this alloy contains 46 wt. % of the α phase, his figure of 3.4 Btu/lb corresponds to a figure

$$\Delta H_{F,\alpha:0.19} = 7.4 \text{ Btu/lb } (\alpha \text{ phase})$$

The heats of precipitation measured by Borelius suggest that ΔH varies approximately linearly with composition so that:-

$$\Delta H_{F,\alpha:0.098} = 3.82 \text{ Btu/lb } (\alpha \text{ phase})$$

$$\begin{aligned} \therefore \text{ the latent heat effect in the partial zone} \\ = 0.804(0.902 \times (-9.5) + 0.098 \times (-25.3) + 3.82 \text{ Btu/lb}) \\ = - 5.8 \text{ Btu/lb.} \end{aligned}$$

The value of f_{SU} calculated as described below shows that the latent heat effect at the eutectic temperature is 3.1 Btu/lb.

III-7-C FRACTION SOLID PRESENT AT SOLIDUS TEMPERATURES (f_{SU})

As discussed in section III-4, the fraction of solid present at any temperature is given by the

Pfann equation II-1-5,

$$f_{SU} = 1 - \left(\frac{C_L}{C_0} \right)^{1/(1-k)} \quad \text{III-4-7}$$

so that f_{SU} , the fraction of solid present at the solidus temperature, is given by:-

$$f_{SU} = 1 - \left(\frac{C_{LS}}{C_0} \right)^{1/(1-k)} \quad \text{III-4-8}$$

When the solidus temperature is the eutectic temperature C_{LS} is equal to the eutectic composition and we get:

$$f_{SU} = 1 - \left(\frac{C_E}{C_0} \right)^{1/(1-k)} \quad \text{III-4-9}$$

In calculating f_{SU} from this equation, the value of the partition coefficient 'k' is assumed to equal its value at the eutectic temperature (liquidus and solidus curves are straight lines).

III-7-C(i) Typical calculations for the tin rich side of the lead-tin system

Eutectic composition = 0.381 (Pb)

∴ limit of solid solubility = 0.015 (Pb)

∴ $k = \frac{0.015}{0.381} = 0.0394$

For Sn 10 Pb, $C_0 = 0.10$ (Pb) so that $f_{SU} =$

$$1 - \left(\frac{0.381}{0.10} \right)^{-1/0.9606} = 0.751$$

III-7-D LIQUIDUS AND SOLIDUS TEMPERATURE

The value of the liquidus temperature observed in the experiments for each alloy as discussed in section IV-6 was used in the theoretical treatment. The solidus temperature has been taken as the eutectic temperature.

III-8 NUMERICAL SOLUTION

The relevant differential equations and link equations for each cooling mode have been listed in section III-6. In each case, they represent a set of simultaneous ordinary differential equations that can be solved using standard numerical techniques, the Runge-Kutta method having been used in this work. The computations have been performed using the Imperial College I.B.M. 7094 computer, as discussed in Appendix A-III. The values of the physical properties that have been used in the computations have already been presented in section III-7 and specimen numerical results are presented in Appendix IV.

TABLE III-2

THERMAL PROPERTIES OF METALS USED IN CALCULATIONS

Property	Phase	Unit	Lead	Tin	Antimony
Specific heat ⁴³	Solid	BTU/lb°F	0.033 ¹⁶	0.063 ¹⁶	0.051 ⁴³
	Liquid		0.0364 ⁴³	0.0615 ⁴³	0.0587 ⁴³
Density ⁴³	Solid	lb/ft ³	696 ¹⁶	448 ¹⁶	418.6 ⁴³
	Liquid		662.3 ⁴³	434.7 ⁴³	406.2 ⁴³
Thermal conductivity	Solid	BTU/ft ² hr.°F	17.9 ¹⁶	34.4 ¹⁶	12.56 ⁴³
	Liquid		9.44 ⁴³	19.37 ⁴³	9.68 ⁴³
Latent heat		BTU/lb	10.6 ¹⁶	26.1 ¹⁶	69.4 ⁴³
Melting point ³⁸		°C	327.6	232	630
		°F	621.1	449.6	1166
Atomic weight ³⁸			207.2	118.7	121.76

The reference from which the data has been taken is represented as: value number of reference

TABLE III-3

CALCULATED VALUES OF THERMAL PROPERTIES
OF
LEAD ANTIMONY EUTECTIC

Property/ Phase	Units	Method of Calculations	Calculated Value
Specific heat	BTU/lb°F	Additive	
solid		"	0.0350
liquid		"	0.0389
Density	lb/ft. ³		
solid		"	648.3
liquid		"	644.9
Thermal capacity	BTU/ft. ³ .°F		
solid		"	22.7
liquid		"	25.1
Thermal conductivity	BTU/ft.hr.°F		
solid		"	16.4
liquid		"	19.5
Latent heat	BTU/lb	"	15.9

Melting Point = 485.6°F (252°C) (Phase diagram)⁴⁴
 484.0 ████°F (251°C) Experimentally observed

Composition = 11.1 wt. % Antimony (Phase diagram)⁴⁴
 11.4 wt. % (average from analysis)

TABLE III-4

CALCULATED VALUES OF THERMAL PROPERTIES
OF
LEAD TIN EUTECTIC

Property	Phase	Units	Calculated Values	Remarks
Specific heat	Solid	BTU/lb°F	.0516	Additive
	Liquid		.052	"
Density	Solid	lb/ft ³	518.4	"
	Liquid		500.2	"
Thermal Capacity	Solid	BTU/ft. ³ °F	26.8	"
	Liquid		26.0	"
Thermal Conductivity	Solid	BTU/ft.hr°F	29.7	"
	Liquid		16.5	"
Latent heat		BTU/lb	15.9	

Melting Point = 361.4°F (183°C) (Phase diagram)⁴⁴
 = 359.6°F (182°C) (using commercial metals)
 = 361.4°F (183°C) (using pure metals)

Composition = 61.9 wt. % Tin (Phase diagram)⁴⁴
 = 61.0 wt. % (average from analysis)
 commercial alloy
 = 64.9 wt. % (pure metal
 prepared in situ)

TABLE III-5

CALCULATED VALUES OF THERMAL PROPERTIES OF LEAD TIN ALLOYS

Identification Symbols	Composition (wt.)	Specific Heat		Density		Thermal Capacity		Thermal Conductivity		Latent heat of Alloy in Partial Layer (Btu/lb.)
		S	L	S	L	S	L	S	L	
		Btu/lb.°F		lb/ft ³		Btu/ft ³ .°F		Btu/ft.hr.°F		
Pb-10-Sn	10% Tin	0.0359	0.0389	659.5	629.3	23.7	24.5	20.3	10.9	8.6
Pb-20-Sn	20% Tin	.0388	.0414	626.6	599.5	24.4	24.8	22.5	12.2	7.2
Pb-40-Sn	40% Tin	.045	.0464	569.8	547.6	25.6	25.4	26.3	14.5	8.4
Sn-20-Pb	80% Tin	.057	.0565	482.4	466.8	27.5	26.4	32.1	18.0	25.5
Sn-10-Pb	90% Tin	.060	.059	464.6	450.2	27.9	27.0	33.3	18.7	25.5

TABLE III-6

SOME VALUES USED FOR LEAD TIN ALLOYS

Identification symbol	Composition	Liquidus Temp. (°F)		Solidus Temp. (°F)		Fraction ⁺⁺ solid at solidus (fsu)	Modified thermal capacity ⁺⁺⁺	Latent heat liberated at solidus temp.
		from phase diagram	observed	phase	observed			
Pb-10-Sn	10% Tin	570.2	565.	361.4	-	0.92	40.4	1.3
Pb-20-Sn	20% Tin	536	519.8	361.	361.4	0.804	49.0	3.1
Pb-40-Sn	40% Tin	472	455.0	361.4	361.4	0.467	48.9	8.5
Sn-20-Pb	80% Tin	401	393.8	361.4	361.4	0.489	210.2	8.1
Sn-10-Pb	90% Tin	428	420.6	361.4	361.4	0.751	175.	4.0

⁺⁺ Calculated from Pfann equation

⁺⁺⁺ Modified thermal capacity = $c \left\{ c + \frac{H \text{ fsu}}{\theta_L - \theta_S} \right\}$

CHAPTER IV
EXPERIMENTAL APPARATUS
AND
PROCEDURE

IV EXPERIMENTAL APPARATUS AND PROCEDURE

IV-1 DESCRIPTION OF THE APPARATUS

A line diagram of the apparatus used in the solidification experiments is given in Fig. IV-1. The apparatus consists of three main parts; the casting unit, cooling system and the thermocouple rig used to measure the progress of solidification. A short description of these is given below.

IV-1-A THE CASTING UNIT

The casting unit (Fig. IV-2) consists of a thin walled ($\frac{1}{16}$ ") stainless steel crucible, 4 inches diameter and six inches high. The crucible rests on a steel ring supported by a refractory insulating block. The crucible is heated by a 900 watts thermocord heater (supplied by Electrothermal Limited) and the rate of heating is controlled by connecting this heater to the main supply via a 15 amps variac. The crucible is surrounded by a mild steel cylinder 10 inches diameter and $\frac{1}{16}$ inch thick. The spacing between the two being loosely filled with $\frac{1}{4}$ inch vermicullite aggregate. Above this crucible the vermicullite was contained by a mild steel cylinder of the same diameter as the crucible counter-levered from the outer cylinder.

IV-1-A(i) The Crucible: An unlined stainless steel crucible was successfully used during the study of metals and alloys of commercial purity. In order to find out whether this crucible could be used to contain high purity alloys used in subsequent experiments, high purity lead (99.999% lead) was melted in a graphite crucible and a stainless steel strip was kept immersed in the lead for 4 hours. The strip was removed and the lead was analysed for iron by X-ray fluorescence and was found to contain about 0.05 wt. % iron. This experiment showed that an unlined stainless crucible could not be used in

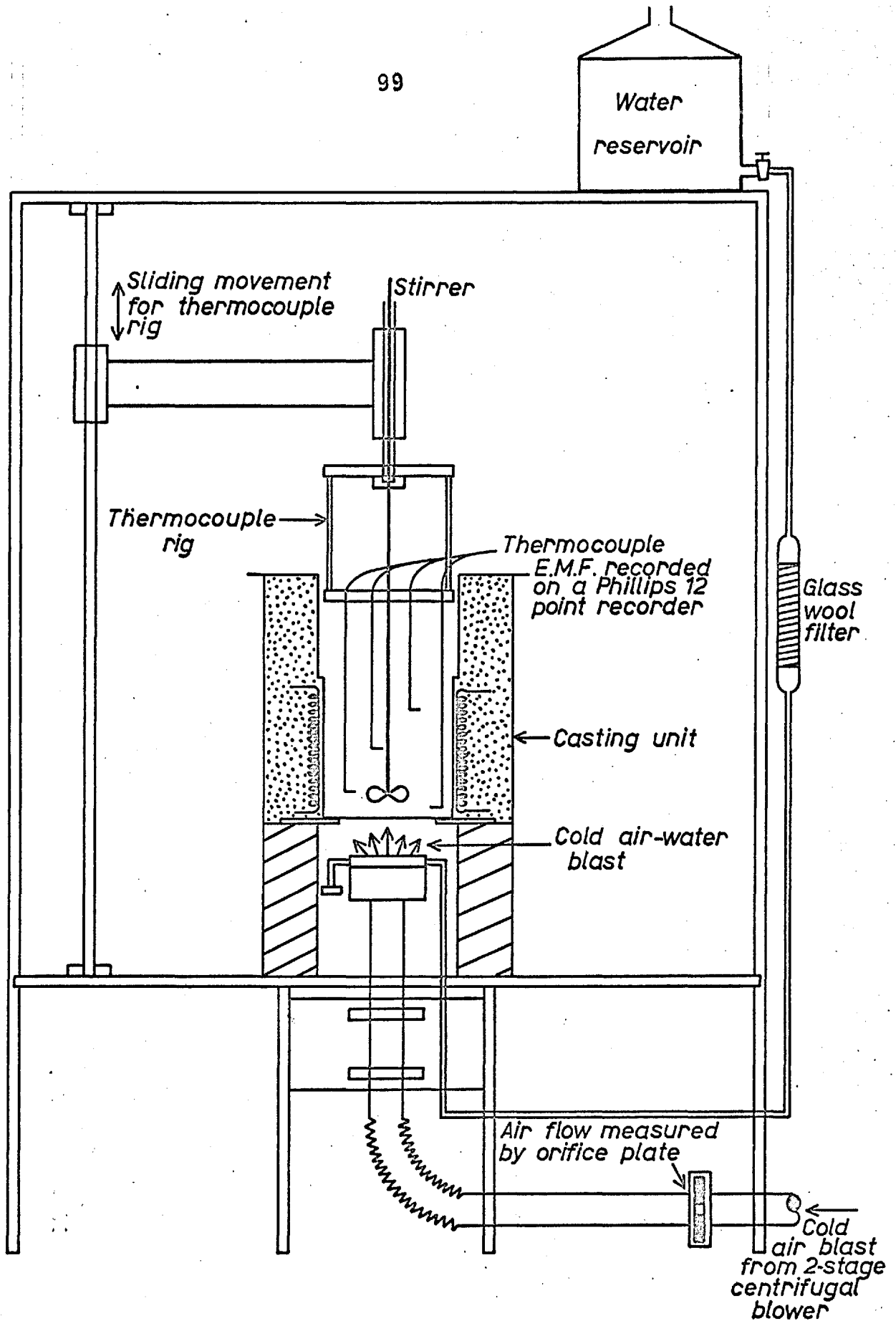


Fig. IV-1 LINE DIAGRAM OF THE APPARATUS

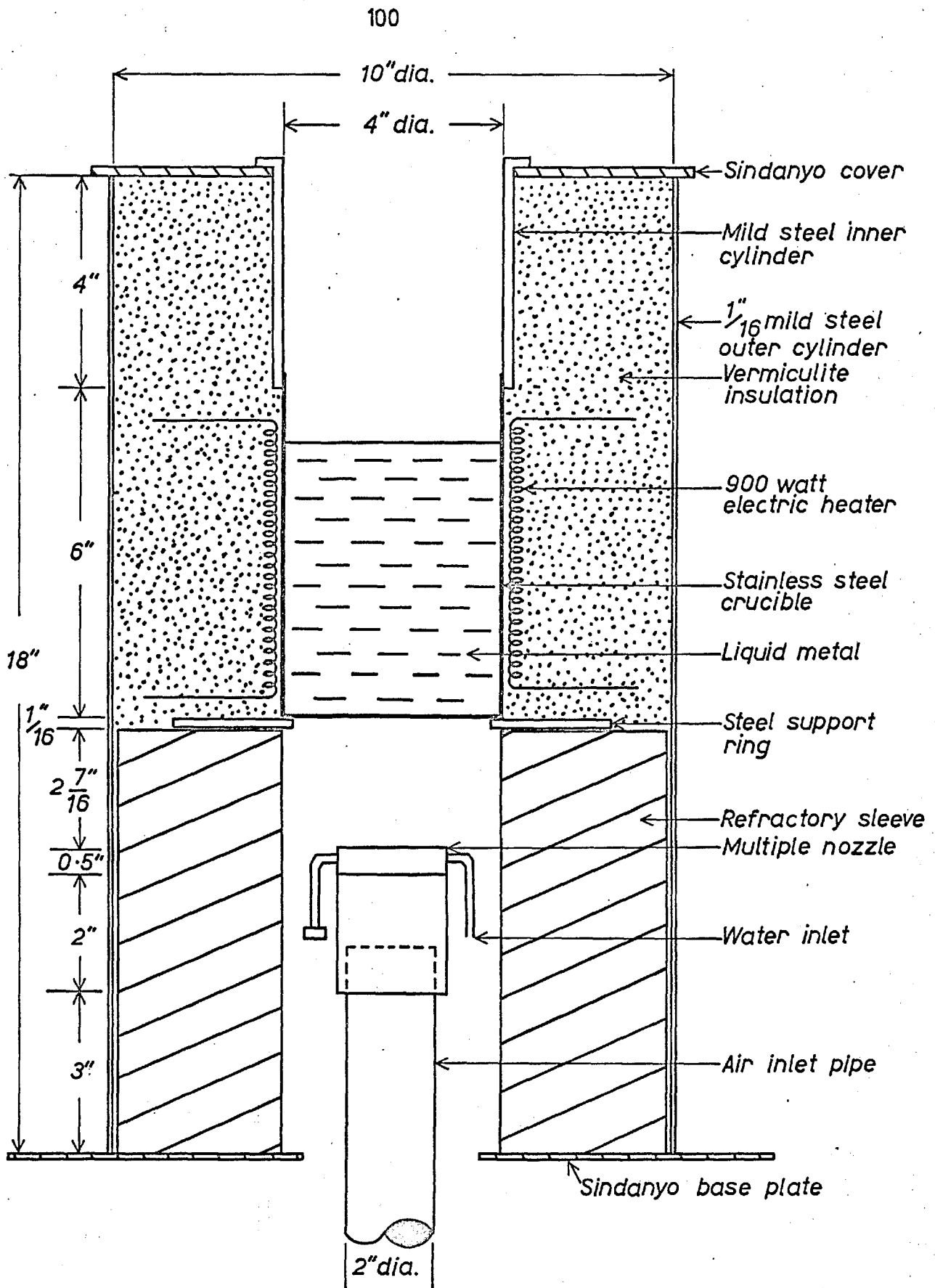


Fig. 1V-2 CASTING UNIT

the study of high purity lead and its alloys and a series of different crucibles were tried.

IV-1-A(ii) Graphite Crucibles: A graphite crucible with a $\frac{1}{4}$ " wall was machined from an electrode grade graphite block so that it would just fit the inside of a stainless steel crucible. The base of this latter was cut to leave a rim $\frac{1}{16}$ inch wide to support the graphite crucible but to allow the cooling air direct access to its base.

The crucible was found to be very porous and lead seeped through it. The seepage could be greatly reduced by using a crucible made of EY95 grade graphite block manufactured by Morgan Graphite Ltd. However, heat balances conducted on preliminary experiments showed that the thermal mass of the crucible was too large for linear heat flow conditions to be set up, and that the thermal resistance of its base could not be neglected.

IV-1-A(iii) Lined Crucibles: The work with graphite crucibles suggested that the low thermal mass required could only be achieved if metal crucibles were used, but that these crucibles would have to be lined to stop the contamination.

Vitreous enamel crucibles were tried first, but could not withstand the thermal shock involved - the enamel cracked after two heats and the iron content of the lead was found to be about 0.1 wt. %. Various methods of coating stainless steel crucibles were then investigated. Autostick and Milk of magnesia coatings were found to be suitable from the point of view of corrosion, but the coatings were friable and floated on the molten metal. Silicone resin SR 84 and SR 125 (supplied by General Electric Co.) were tried, but they burned off at about 200°C. Mixtures of either titanium dioxide or milk of magnesia with silicone resin gave friable coatings. A coherent coating was obtained by using fiberfax refractory cement (marketed by Carborundum Co. Ltd.),

but it would flake off after few heats. A composite coating of fiberfrax and silicone resin gave good results. After about twenty heats, however, the coating left the top of the crucible. This problem was solved by coating the top with silicone resin and graphite powder slurry over the composite coating. A sample of lead was taken after about twenty heats in a stainless steel crucible lined in this way and analysed by X-ray fluorescence and spectroscopic analysis. Iron, nickel and chromium were found to be below the limit of detection (about 40 parts per million). The coating was very adherent and could withstand thermal and mechanical shocks.

Thus stainless steel crucibles were used in the study of high purity alloys and were prepared in the following manner. Each new crucible, $\frac{1}{16}$ inch thick, was roughened with emery paper, cleaned and dried. A coating of fiberfrax cement about one millimeter thick was applied to the inside surface with a paint brush, and crucible dried in a muffle furnace. The dried crucible was then coated with silicone resin SR 125, and the top half inch of the inside surface was coated with silicone resin/graphite slurry. Crushed and graded ($\frac{1}{16}$ inch) alumina brick was sprinkled over the inside surface of the crucible base, and the crucible was cured at 250°C for four to five hours. The thermocouples described later were also coated with fiberfrax cement, and dried and then coated with the silicone resin/graphite slurry. After curing for four to five hours the coated thermocouples were fixed to the rig described below.

IV-1-B MEASUREMENT OF SOLIDIFICATION FRONT

As discussed in section II-3, thermal analysis is the most suitable method for following the solidification of alloys. However, an apparatus was designed to pour the liquid metal out during a solidification experiment and to withdraw the cooling nozzle at the same time. In the few experiments that were conducted it was realized that residual liquid remains and will render the results unreliable. Thus thermal analysis was used throughout this work to study the progress of solidification.

The thermal analysis arrangement is shown in Fig. IV-2. The thermocouples used in this work were stainless steel sheathed chromel-alumel thermocouples manufactured by Pyrotenax Co., 0.062 inches diameter with the bead bonded to the sheath. The thermocouples were fixed to the support rig so that they could be easily withdrawn for coating. The rig could be moved up and down and rotated around the fixed rod. The thermocouples themselves were bent at right angles so that the last 2 cm. of their length lay normal to heat flow direction. The thermocouples were arranged axis symmetrically at $1\frac{1}{2}$ inches from the centre to allow room for a stirrer of stainless steel for commercial alloys and of glass for the high purity alloys. The thermocouple rig was positioned by lowering it until the bottom thermocouple just touched the base of the crucible.

An additional thermocouple was silver soldered to the lower side of the crucible base in order to check on the formation of an air gap. The temperature of the cold air was measured by a thermocouple in the air pipe just below the nozzle.

All the thermocouples were connected, via an ice box cold junction, to a Phillips 12 point temperature recorder, or to a Dynamco data logger. The Phillips recorder has a chart speed of 600 mm/hr and ranges of

0 - 10 or 0 - 20 mV, and its response time is 24 seconds per channel. The data logger recorded the thermal E.M.F.'s on punched tape at rates up to 10 channels per second. It offered little advantage over the recorder, especially as the latter presented 'temperature graphs' directly so that arrest points etc. were seen immediately. Moreover, since most of the alloys solidified in about 20 - 40 minutes, the response time of the recorder was adequate.

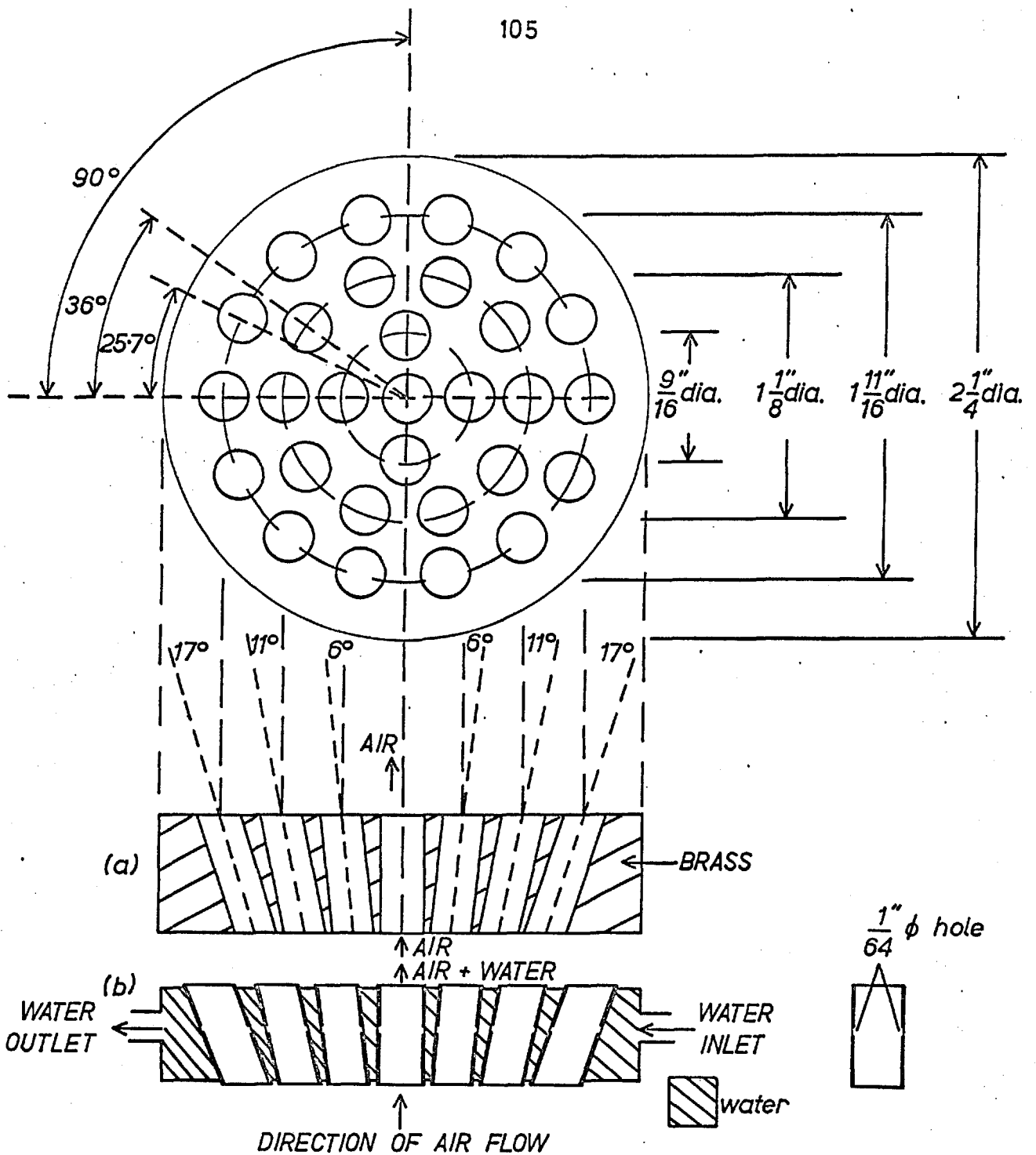
IV-1-C COOLING SYSTEM

The cooling system consists of a five horse power two-stage centrifugal blower connected through the pipe work to a multiple nozzle below the crucible. The blower delivered a maximum air flow rate of 85 cfm. The air flow was controlled by a gate valve and measured by an orifice plate designed to British standard code 1042. The orifice plate was one and half inch in diameter with pressure tapings one pipe diameter upstream and half pipe diameter downstream. The pressure drop across the orifice was measured by a water manometer and the air flow rate calculated according to the standard formula.

The multiple air nozzle was designed by Moore⁴¹ to give a uniform distribution of the local heat transfer coefficient over the base of the crucible. The multiple nozzle consisted of 29 3/16 inch diameter holes, which were arranged in the 2 1/4 inch diameter nozzle plate as shown in Fig. IV-3, so as to distribute the cooling air uniformly over the base of the crucible.

Moore⁴¹ carried out experiments using the sublimation of Naphthalene and showed that local heat transfer coefficient values were distributed evenly over the base of the crucible, when the nozzle was 2 1/2 inches from it.

The mean value of the heat transfer coefficient obtained with this nozzle could be varied between 15 and



RADIUS FROM CENTRE OF NOZZLE PLATE (")	FRACTIONAL RADIUS $R=1.125$	NO. OF $\frac{3}{16}$ DIA. HOLES	ANGULAR SPACING OF $\frac{3}{16}$ " DIA. HOLES	INCLINATION OF HOLES TO VERTICAL
0	CENTRE	1		0°
$\frac{9}{32}$	$R/4$	4	90°	6°
$\frac{9}{16}$	$R/2$	10	36°	11°
$\frac{27}{32}$	$3R/4$	14	25.7°	17°

Fig. 1V-3 MULTIPLE NOZZLE

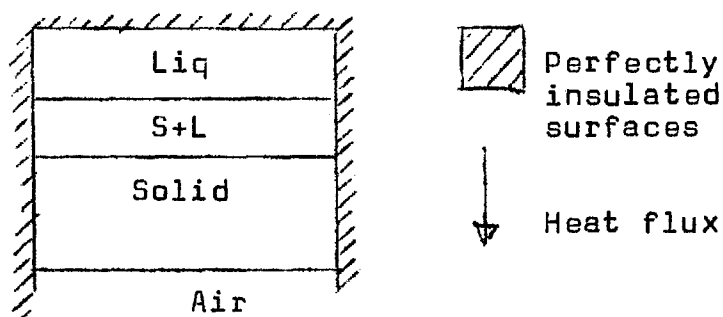
(a). SECTION OF AIR NOZZLE

(b). SECTION OF AIR - WATER NOZZLE

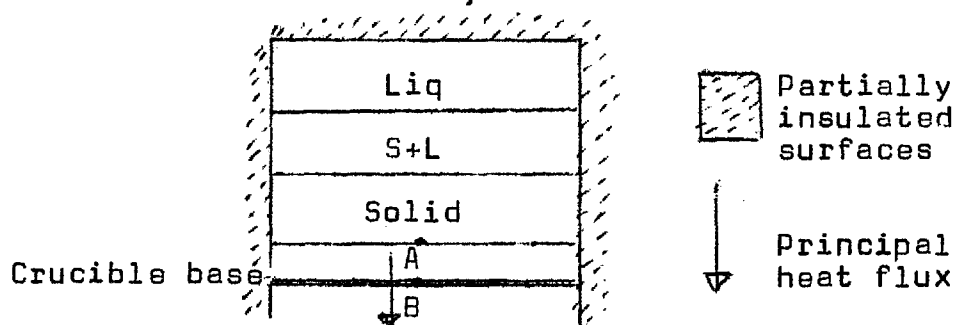
45 Btu/ft².hr.°F. as the air flow rate was changed from 15 to 90 cfm. In order to study the progress of solidification at higher heat transfer coefficients, the multiple nozzle was modified to give an air-water spray (Fig. IV-3). The air-water nozzle consisted of 29 brass tubes (3/16 inch I.D.) mounted between two circular brass plates in the same spatial arrangement as the holes in Moore's original nozzle. The plates themselves were mounted in a 1/2 inch length of brass pipe (2 inch I.D.) and filtered water was circulated through the enclosed space. Two 1/64 inch holes had previously been drilled through the wall of each tube, so that the water could flow through these holes and be atomised by cooling air flow through the tubes. The value of the overall heat transfer coefficient from the lower side of the solidifying metal that was obtained when this nozzle was used was 167 Btu/ft².hr.°F.

IV-2 HEAT FLOW CONDITION

In the theoretical treatment given in Chapter III, we have assumed unidirectional heat flow as illustrated below.



However, during the experiments the actual cooling conditions are affected by the crucible base and sides:



The cooling condition from the lower surface of the solid metal can be represented in terms of an overall thermal resistance ($1/h$) which is ~~the sum of~~ the sum of three separate resistances: the thermal resistance from the lower surface of the crucible base to the cooling air ($1/h_A$), the thermal resistance through the crucible base (r_c) and the thermal resistance from the solid surface to the crucible base (r_g), i.e.

$$\frac{1}{h} = \frac{1}{h_A} + r_c + r_g$$

IV- 2-1

Let us consider a typical case when $h = 40 \text{ Btu/ft}^2 \cdot \text{hr.}^\circ\text{F.}$ so that the rate of heat removal is about 1500 Btu/hr. If a metal crucible is used, the wall thickness of which is 1/16 inch, the thermal resistance, r_c , is about 1% of the overall thermal resistance,* so that this resistance can be neglected. In order to determine the relative magnitude of the thermal resistance from the lower surface of the solid metal to the crucible base, a thermocouple was placed inside the crucible so that it touched the inside of the crucible at point A. Another thermocouple was silver soldered to the lower side of the crucible base at point B. The difference between the temperatures indicated by these two was never more than 35°F, a result similar to that reported⁴¹ by Moore. The temperature difference across the stainless steel crucible was about 10°F, so that the temperature difference between the lower surface of the solid metal and the upper surface of the crucible base was about 25°F. Since the heat flux across this interface was 1500 Btu/hr. under these conditions, the interface heat transfer coefficient must have been about $750 \text{ Btu/ft}^2 \cdot \text{hr.}^\circ\text{F.}$ and the corresponding thermal resistance (r_g) was

* Where an alumina crucible is to be used the value of r_c could be as high as 40% of the overall resistances.

about 5% of the total thermal resistance between the solid metal and the cooling air. The cooling condition in the experimental apparatus could therefore be described in terms of a convective mechanism involving the overall heat transfer coefficient h as the only parameter.

The sides and top of the crucible cannot be perfectly insulated, but the experimental heat flow conditions will be virtually uni-directional if the heat lost by the side and the top of the crucible is kept small relative to the heat extracted by the cooling air. Heat will flow radially from the side wall to the metal during solidification if the metal is cooled more rapidly than the side, and vice versa. In this study of the solidification of commercial purity lead and tin in a similar apparatus to that used here, Moore found that the two heat flows in either direction in the top and bottom parts of the crucible more or less cancelled each other out when the heat transfer coefficient was at its maximum value - $40 \text{ Btu/ft}^2 \cdot \text{hr.}^\circ\text{F}$. At lower values the net heat flow was found to be from the metal to the side walls. These observations were confirmed in this work, and, moreover, it was found that the maximum heat lost from the top of the crucible was about half the maximum radial heat flow. These heat flows are of the same order as those determined by the overall heat balances. Even in the worst case, the heat losses were less than 10% of the total quantity of heat removed during the experiment, so that unidirectional heat flow conditions were maintained fairly accurately.

IV-3 MEASUREMENT OF HEAT TRANSFER COEFFICIENT

41

Moore determined the overall heat transfer coefficient from the lower surface of the solidified metal to the cooling air as a function of air flow rate and base temperature using a direct steady state method

He also measured the heat transfer coefficient from the lower side of the crucible base to the cooling air by studying the evaporation of Naphthalene into the air stream. Thus he could determine the mass transfer coefficient and then the heat transfer coefficient by the Chilton and Coburn analogy between heat and mass transfer.

To carry out the steady state method, 2100 watts stainless steel sheathed electric heater was coiled around the thermocouples and immersed in the bath of molten lead about three inches above the base. The heater leads were removed through the hole in the centre of the thermocouple rig provided for the stirrer, and the lead was allowed to solidify. The lead was then heated by the external thermocord side wall heaters and brought to a steady state temperature below its melting point. The cold air blast and the immersion heaters were then turned on at the same time, the power supplied to the heater being increased until steady state conditions had been reestablished as close as possible to the original steady state conditions. A linear temperature profile was thus set up along the axis of the crucible and from the temperature gradient the value of the heat transfer coefficient ^{could} be calculated. The heat removed by the cold air is given by:

$$\begin{aligned} \dot{q} &= h A (\theta_{\text{base}} - \theta_{\text{ambient}}) \\ &= h A (\theta_0 - \theta_a) \end{aligned} \quad \text{IV-3-1}$$

and heat conducted through the lead is given by:

$$\dot{q} = K_{pb} A \frac{d\theta_{pb}}{dx} \quad \text{IV-3-2}$$

where $\frac{d\theta_{pb}}{dx}$ is the axial temperature gradient in solid lead. Therefore the heat transfer coefficient is given by:

$$K_{pb} A \frac{K_{pb} \frac{d\theta_{pb}}{dx}}{(\theta_0 - \theta_a)} \quad \text{IV-3-3}$$

41

Moore's experiments were repeated with and without the lining so that its effect could be ascertained and with the air/water spray system. The results are reported in section V-1 .

IV-4 CALIBRATION OF THERMOCOUPLES

As discussed in section IV-1-B the thermocouples used in this work were stainless steel sheathed, chromel-alumel thermocouples 0.062 inch in diameter. All the thermocouples were calibrated using pure lead and taking its melting point as the standard. The calibration was found to apply to all thermocouples from the same batch and the calibration remained unchanged with time. Different calibrations applied to thermocouples from different batches so that calibrated thermocouples from the same batch were used in all the solidification experiments.

IV-5 PREPARATION OF ALLOYS

Alloys of commercial purity were prepared by melting lead in a graphite crucible heated by an oil fired furnace. The solute metal was added after the lead was molten and the alloy stirred thoroughly. The alloy was cast in iron molds and the ingots were melted in the solidification apparatus.

Alloys made from the high purity metals (99.999 purity) were prepared in situ. A known quantity of lead was melted in the solidification apparatus and the correct quantity of tin was added to give the desired alloy composition. The alloy was stirred thoroughly after it was completely molten using a glass stirrer. The alloy was solidified and remelted several times to give a homogeneous composition.

The complete analyses of the commercial and high purity metals used are given in section IV-10.

IV-6 SOLIDIFICATION OF LEAD-TIN ALLOYS AT ZERO SUPERHEAT

Homogenised alloys were solidified at positive superheat so that the liquidus temperature could be determined from the thermal analysis curves. The liquidus was clearly marked by an arrest point which was shown by thermocouples placed at some distance from the base. This liquidus arrest point was observed at exactly the same temperature in a series of experiments performed at various superheats and cooling rates and was taken to indicate the start of solidification in all subsequent experiments with the alloy when the composition of the alloy lay between the partial solid solubility limit (solidus temperature) and the eutectic composition. In these cases the end of solidification was observed at 361.4°F (183°C).

In the solidification experiments the alloys were heated to a temperature some 40°F above the liquidus temperature and then the side wall heater was switched off. The alloy was stirred while it cooled, until its temperature was within 10°F of the liquidus temperature. When the stirrer was withdrawn, solidification was started after one minute by opening the air valve, the fan having been run for the previous 30 minutes, so that its temperature could become steady. The point on the recorder chart at which the temperature of each thermocouple fell below the liquidus temperature, was taken as the time at which the liquidus front had reached that couple. When the temperature of each thermocouple fell below the solidus temperature the solidus front was considered to have reached that couple.

No marked solidus arrest point was observed for alloys with less solute than the partial solid solubility limit, although a slight change in gradient was sometimes observed. In these cases the solidus temperature was taken as the eutectic temperature, the justification for the same is discussed in section VI-2-B.

IV-7 SOLIDIFICATION OF LEAD-TIN ALLOYS AT SUPERHEAT

The alloys were heated to some 40°F above the desired superheat temperature of the experiment. The heater was switched off and the alloy was stirred thoroughly to homogenise the temperature and composition of the molten metal. When the temperature was some 10°F above the desired temperature, the stirrer was withdrawn and the flow of the cooling air was started one minute later.

The moment at which solidification started near each couple, i.e. when the liquidus front has reached that couple, was found when its temperature had fallen to the liquidus temperature determined as described before. A small amount of undercooling was observed at the liquidus^{temperature} in those experiments in which the alloy Sn 20 Pb was solidified from about 220°F above its liquidus temperature. The temperature dropped initially about 5°F below the liquidus determined as described above, and then rose rapidly to it before falling slowly once more. In the rare cases where this occurred, the time at which solidification commenced was taken as the second time at which the temperature fell from the experimental liquidus value.

IV-8 MORPHOLOGY AND SOLUTE SEGREGATION STUDIES

The alloys were solidified with the thermocouple rig removed and samples were cut with faces lying along the heat flow direction and normal to it. The samples were polished, etched and studied metallographically.

In order to determine the shape of the dendrites, four 1/32 inch holes were drilled in the surface of one sample about $\frac{1}{4}$ inch apart, and thin copper wires were inserted into the holes to serve as permanent markers. The sample was polished, etched and a microphotograph taken. A thin section of the surface was then filed off and the sample was polished and etched again and another microphotograph taken. The procedure was repeated

several times so that a number of parallel sections were obtained through the dendritic structure. A three dimensional picture of the dendrites was derived from this series of photographs.

Samples were also examined using an electron probe microanalyser so that the segregation of solute could be examined. Compositions of the dendrites and of the matrix were determined along the heat flow direction and normal to it.

IV-9 CALORIMETRIC DETERMINATION OF LATENT HEAT OF LEAD-TIN EUTECTIC

As discussed in section III-7, the latent heat of an alloy can be calculated from published thermodynamic data, provided it is reliable. However, in view of the meagre data available for the lead-tin alloy system, and the discrepancies observed in the experimental thermal balances based on this data, it was decided to determine the latent heat of lead-tin eutectic alloy using a drop calorimeter. The alloy was melted in a $\frac{1}{4}$ inch diameter pyrex tube around which a 'Thermocord' heater had been wound. A 1 mm. bore capillary was fused to the lower end of this tube and plugged with a stainless steel 1 mm. diameter wire inserted from above. The alloy was heated above its melting point and allowed to cool. When its temperature had fallen to within 5°F of the solidification temperature, the plug was withdrawn and the molten alloy allowed to fall into a copper vessel filled with water. The water was continuously stirred by a copper stirrer and its temperature measured with a mercury in glass thermometer. The maximum temperature, which occurred after about 2 minutes was recorded. The results are presented in section V-6.

IV-10 PURITY OF METALS USED

IV-10-A COMMERCIAL METALS

LEAD:

Analysis: Chemical analysis

Pb = 99.97% (by difference)
Bi = 0.02%
Sb = 0.01%

TIN:

Analysis: Chemical analysis

Sn = 99.85% (by difference)
Pb = 0.03%
Cu = 0.03%
As = 0.03%
Fe = 0.01%
Sb = 0.01%

ANTIMONY:

Analysis: X-Ray Fluorescence

Sb = 99.96%
Pb = 200 ppm*
As, Sn, Bi, Cu below 40 ppm.

IV-10-B PURE METALS

LEAD:

Supplied by Associated Lead Manufacturers Ltd.
Analysis: as supplied by the manufacturers

Pb = 99.999% min.
Cu = less than 0.0001%
Cd = " " 0.000005%
Th = " " 0.0001%

No other impurity was detected by spectroscopic analysis

TIN: (S-brand)

Supplied by Copper Pass & Sons Ltd.
Analysis: as supplied by the manufacturers

Sn = 99.999% min.
Cu = 0.5 ppm
Pb = 2.5 ppm
Sb = 2.0 ppm
S = 1.0 ppm

As, Bi, Fe, Ag, Al less than 1 ppm
In, Co, Ni, Ga not detected

*Term ppm refers to part per million.

CHAPTER V

RESULTS

V RESULTS

V-1 HEAT TRANSFER COEFFICIENT

As discussed in section IV-4, the heat transfer coefficient from the crucible was determined from the measured temperature gradient in the lead, and the measured temperatures of the crucible base and of the cooling air, using the equation:

$$h = \frac{K_{Pb} \frac{d\theta_{Pb}}{dx}}{(\theta_0 - \theta_a)} \quad V-3-3$$

The results obtained at various air flow rates and base temperatures are given in Table V-1. The experimental error in these results is ± 1 Btu/ft².hr.°F. The values obtained by Moore⁴¹ are also plotted in Fig. V-1 and it can be seen that the two sets of values agree within the experimental error. Results obtained for the air/water spray system are also given in the table, and it can be seen that very much higher values were obtained.

No results are given in the table for the experiments involving coated crucibles. This was because the temperatures measured in these experiments were identical within the limits of experimental error to the temperatures measured in corresponding experiments with unlined crucibles. It was therefore concluded that coating the crucible made no difference to the heat transfer coefficients between the metal and the cooling air.

V-2 PROGRESS OF SOLIDIFICATION OF PURE METALS AND EUTECTICS

The solidification of pure lead, lead-tin and lead-antimony eutectics was studied by thermal

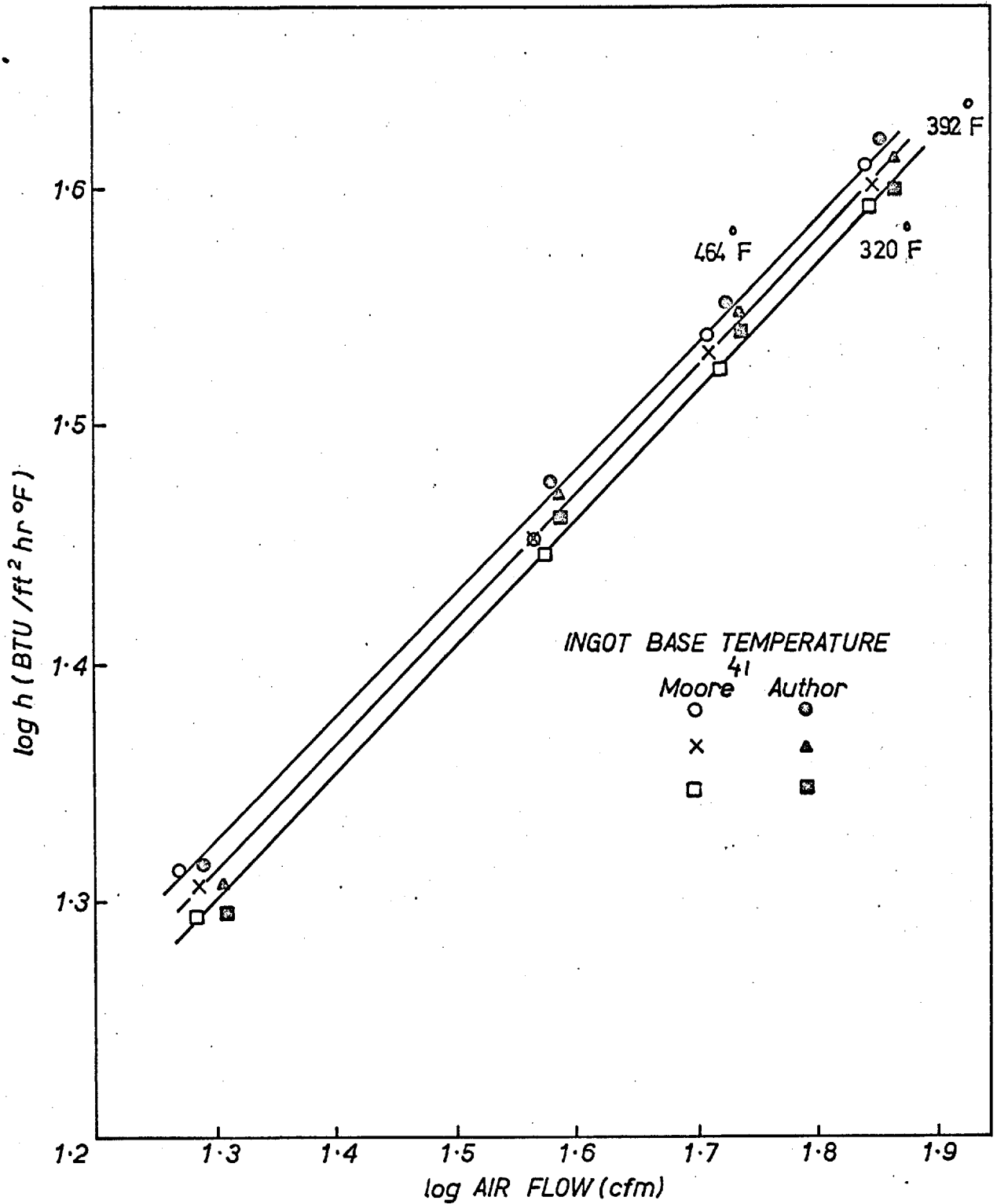


Fig. V-1 STEADY STATE HEAT TRANSFER RESULTS PLOTTED AS $\log h$ (BTU / ft² hr °F) VERSUS \log AIR FLOW RATE FOR DIFFERENT INGOT BASE TEMPERATURES

TABLE V-1.

HEAT TRANSFER COEFFICIENT VALUES
OBTAINED FROM STEADY STATE
HEAT TRANSFER METHOD

Metal used - LEAD

Nozzle Type	Air Flow Cubic ft/min.	Steady State Base Temperature °F	Temp. Gradient °F/in.	Heat Transfer Coefficient BTU/ft ² .hr.°F
Air	69.5	324	39.8	39.4
	69.5	396	54.5	40.7
	69.0	468	68.5	41.0
	56.2	333	36.1	34.4
	55.6	396	47.1	35.2
	53.0	467	60.4	36.3
	38.9	335	29.7	28.0
	38.5	398	38.0	28.2
	38.0	470	48.5	28.9
	20.0	320	19.7	19.9
	19.5	394	27.0	20.3
	18.9	467	34.8	20.9
Air-Water	69.0	230	95.8	165.7
	69.0	225	92.8	167.1
	69.5	234	100.6	168.6

analysis as discussed in Chapter IV at zero-superheat and with various degrees of superheat. The results obtained are presented below.

V-2-A LEAD

The thickness of solid lead measured under zero-superheat conditions are plotted against casting time in Fig. V-2 for experiments in which the heat transfer coefficient was 167, 40.5, 29.5 and 21.0 Btu/ft².hr.°F*. Some results obtained by Moore⁴ are also plotted for comparison. The full lines in the figure have been predicted using Hills'¹ theory.

The experimental results* obtained in the presence of superheat are presented in Fig. V-3, and compared with predictions of the theory developed in Chapter III. Specimen numerical results obtained with this theory are presented in Tables A-IV-1 and A-IV-2. The property values used in the calculations of these values are listed in Table III-2.

V-2-B LEAD-ANTINOMY EUTECTIC

The solidification of the lead-antimony eutectic was studied using commercial purity metals. The experimental results* are compared with the predictions of Hills'¹ theory in Fig. V-4, the computed results being given in Table A-IV-3. Property values used in obtaining these results are listed in Table III-3.

V-2-C LEAD-TIN EUTECTIC

The solidification of lead-tin eutectic was studied at zero and at positive superheats, using both commercial and high purity metals. The experimental results are compared with the theoretical predictions obtained, as discussed in section III-5, in Figs. V-5 and V-6, specimen theoretical results being presented in Tables A-IV-4 and A-IV-5.

* The experimental points plotted are the mean of at least three experiments.

The determination of the thermal properties used in the calculations is described in section III-7 and the values are listed in Table III-4.

V-3 PROGRESS OF SOLIDIFICATION OF LEAD-TIN ALLOYS

The solidification of a range of commercial and high purity lead tin alloy was studied at zero-superheat and at various positive superheats. The compositions used are listed in Table V-2.

Table V-2 COMPOSITION OF LEAD-TIN STUDIED

Composition wt. %	Identification Symbols	Purity
10-Tin 90-Lead	Pb-10-Sn	Commercial
20-Tin 80-Lead	Pb-20-Sn	Commercial and High Purity
40-Tin 60-Lead	Pb-40-Sn	Commercial
80-Tin 20-Lead	Sn-20-Pb	High Purity
90-Tin 10-Lead	Sn-10-Pb	High Purity

Typical sets of cooling curves obtained under superheat conditions for each of these alloys are shown in Figures V-7 to V-11. The liquidus point obtained from the temperature arrest experienced by the thermocouple farthest from the crucible base is plotted on the phase diagram shown in Figure V-12, for each of these alloys.

. These values are also listed in Tables III-5 and III-6.

The progress of these liquidus and solidus fronts determined from the cooling curves as described in section IV-1-B are shown in Figures V-13 to V-21.* The full lines in these graphs refer to the values predicted using the theory described in Chapter III and the property values are listed in Tables III-5 and III-6. Specimen theoretical results are listed in Tables A-IV-6 to A-IV-14.

V-4 VARIATION OF COOLED SURFACE TEMPERATURE

As discussed in Chapter III the theoretical treatment not only predicts the progress of solidus and the liquidus fronts, but also the variation of cooled surface temperature and the temperature of the remote boundary. This latter temperature can only be obtained in the experiments by extrapolation, but the temperature of the cooled surface is given by the thermocouple touching the crucible on the metal side. Figures V-22 and V-23 show comparison between theoretical and experimental results for this temperature, for three typical cases.

V-5 THERMAL BALANCES

In the theoretical treatment given in Chapter III, it has been assumed that heat is only transferred from the casting metal through the base of the crucible and then to the cooling air. If this is true the latent heat produced by the solidifying metal should be equal to the ~~latent~~ heat removed by the cooling air. Thermal balances were drawn from the experimental results to test whether this condition was met. Typical balances are given in Tables V-3 to V-9. The heat balances

*The experimental results in these graphs are plotted as points and are the mean of at least three experiments.

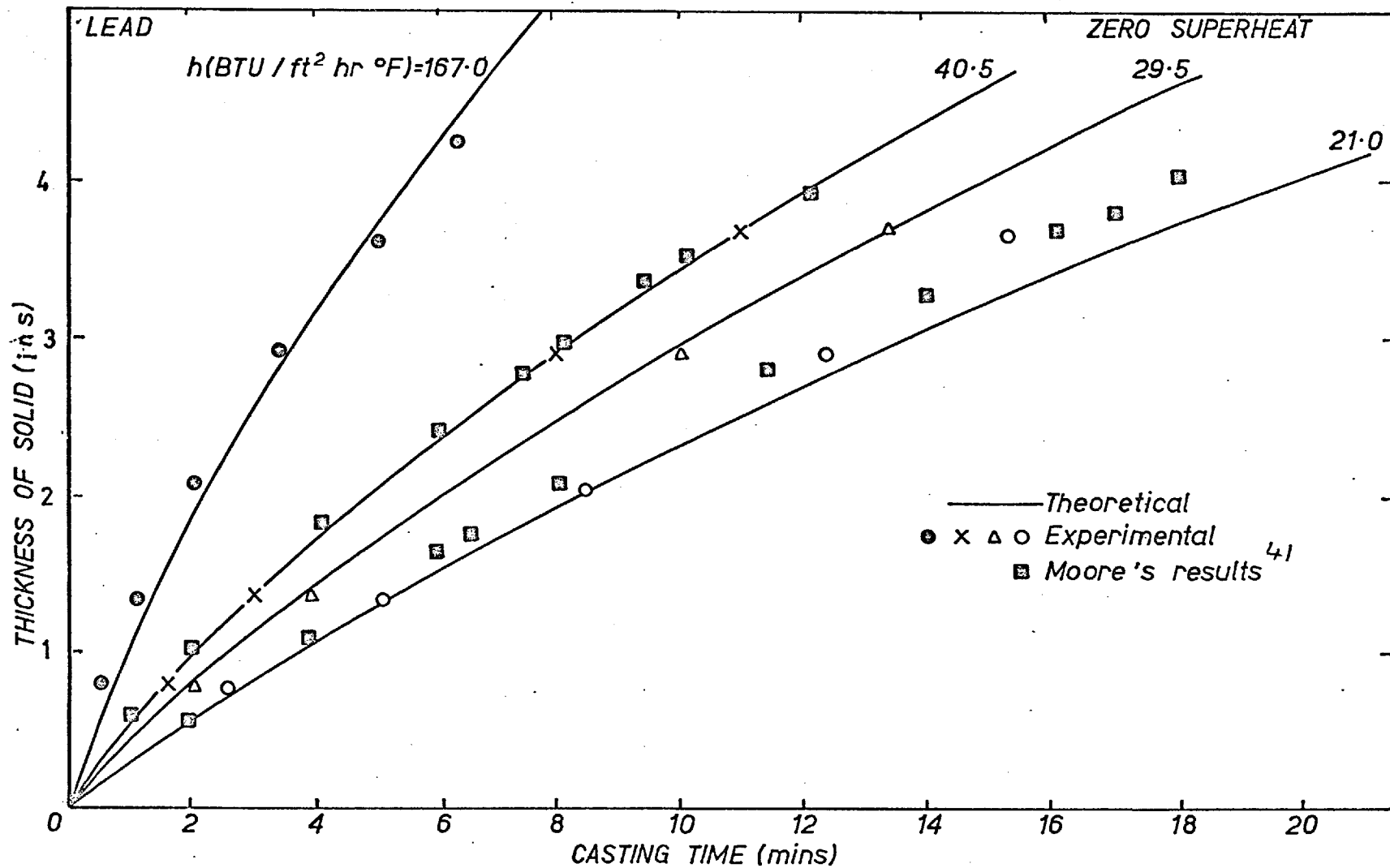


Fig. V-2 SOLIDIFICATION OF LEAD AT ZERO SUPERHEAT
Comparison of theoretical and experimental results using Hills' theory

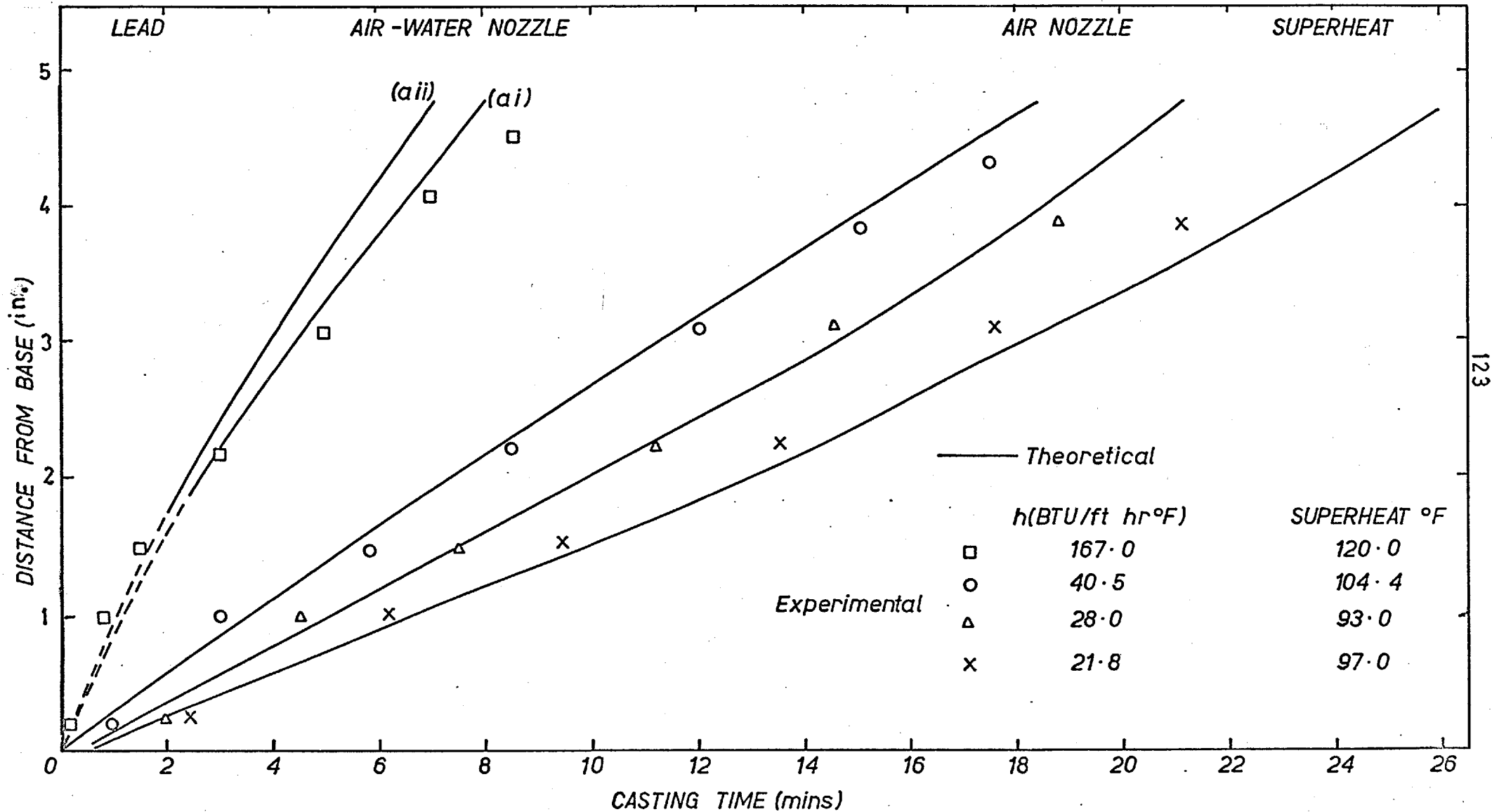


Fig V-3 SOLIDIFICATION OF LEAD AT SUPERHEAT

Comparison of theoretical and experimental results. (a) air nozzle, theoretical results using (ai) 92 $^{\circ}$ F ambient temperature calculated from heat balance (aii) 104 $^{\circ}$ F ambient temperature.

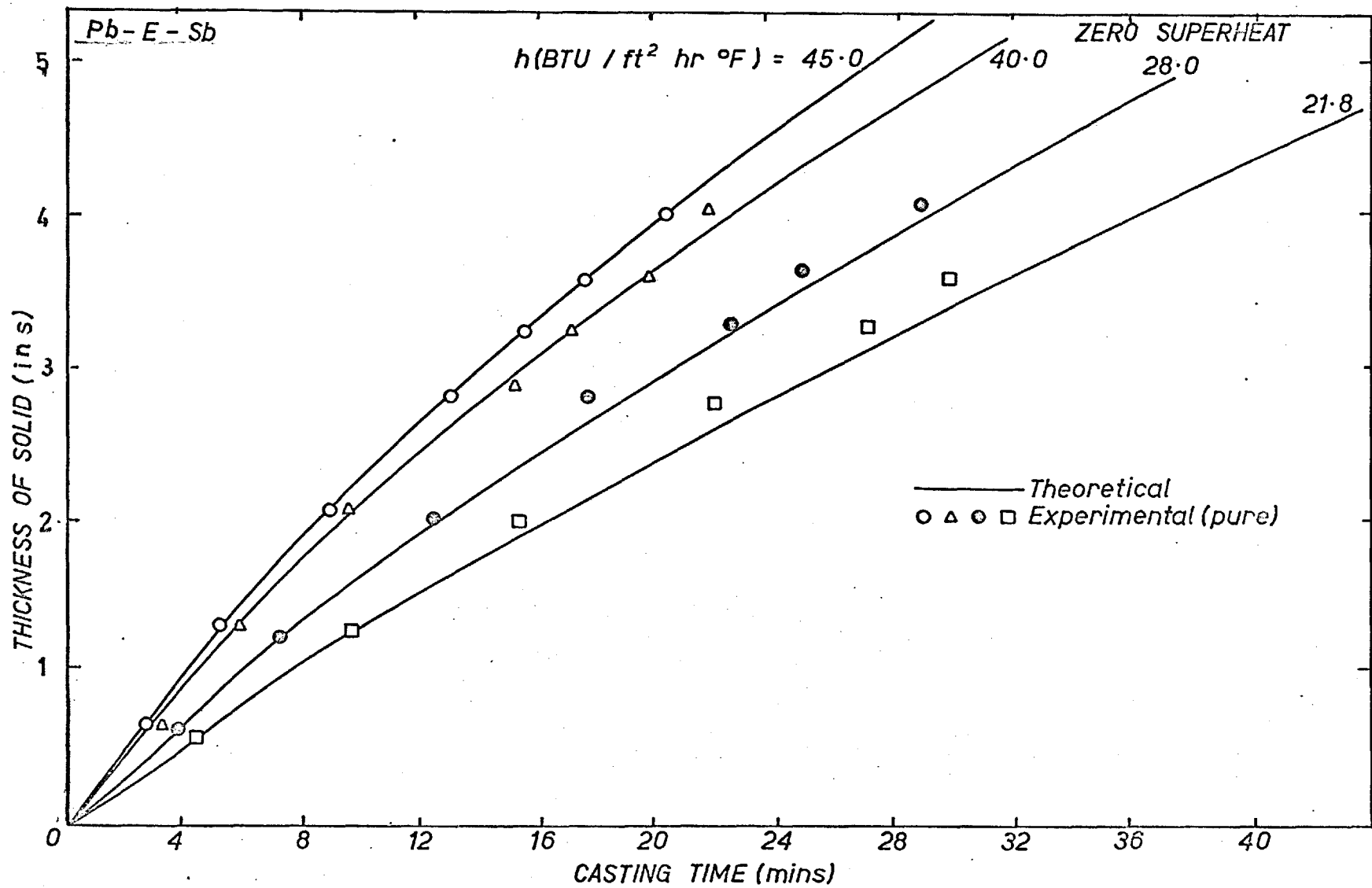


Fig. V-4 SOLIDIFICATION OF LEAD ANTIMONY EUTECTIC AT ZERO SUPERHEAT
Comparison of theoretical and experimental results

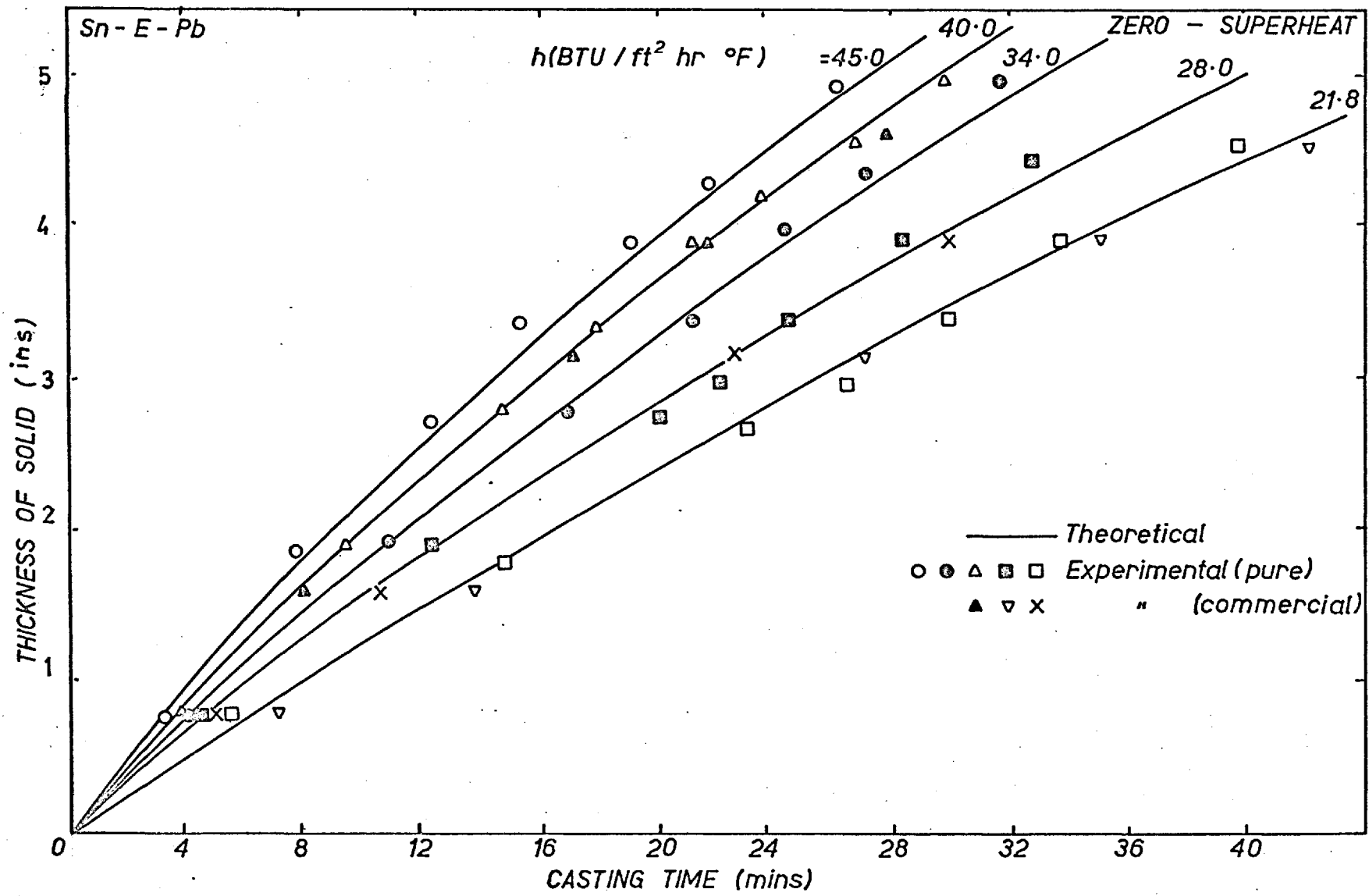


Fig.V-5 SOLIDIFICATION OF LEAD-TIN EUTECTIC AT ZERO SUPERHEAT
Comparison of theoretical and experimental results

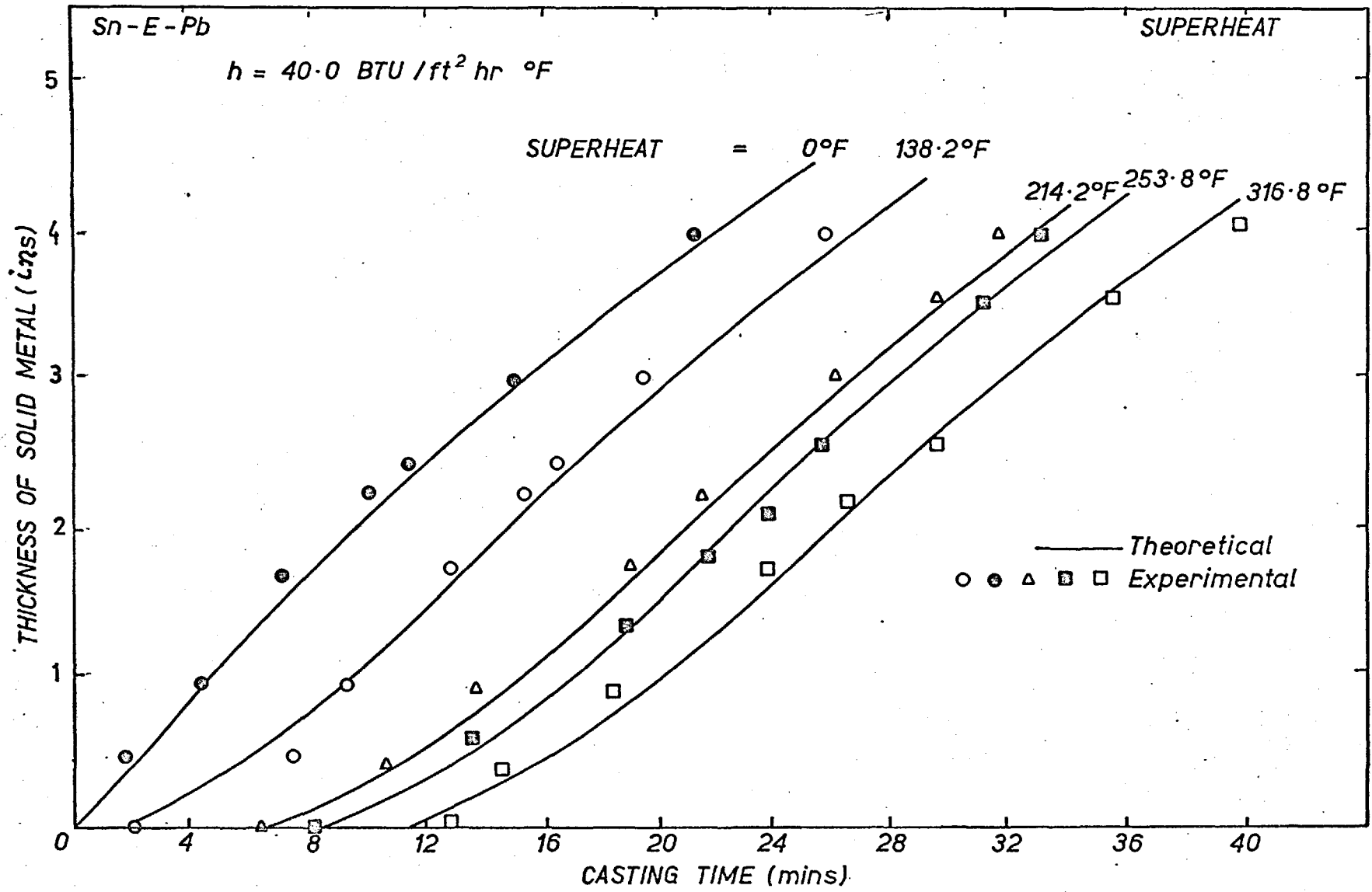


Fig. V-6 SOLIDIFICATION OF LEAD-TIN EUTECTIC AT POSITIVE SUPERHEAT
 Comparison of theoretical and experimental results

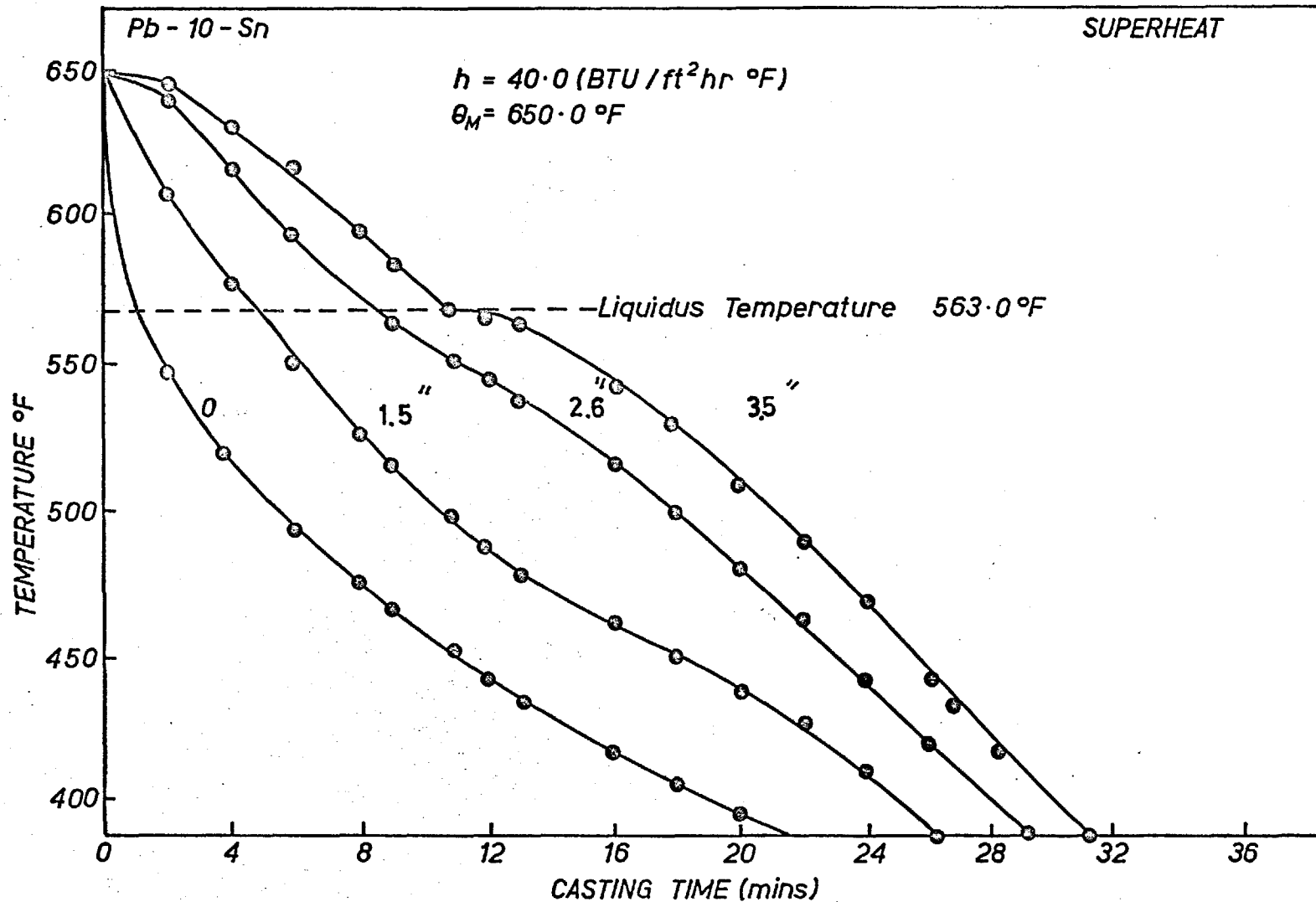


Fig. V-T COOLING CURVES FOR 10wt% TIN, LEAD-TIN ALLOY AT VARIOUS DISTANCES FROM BASE

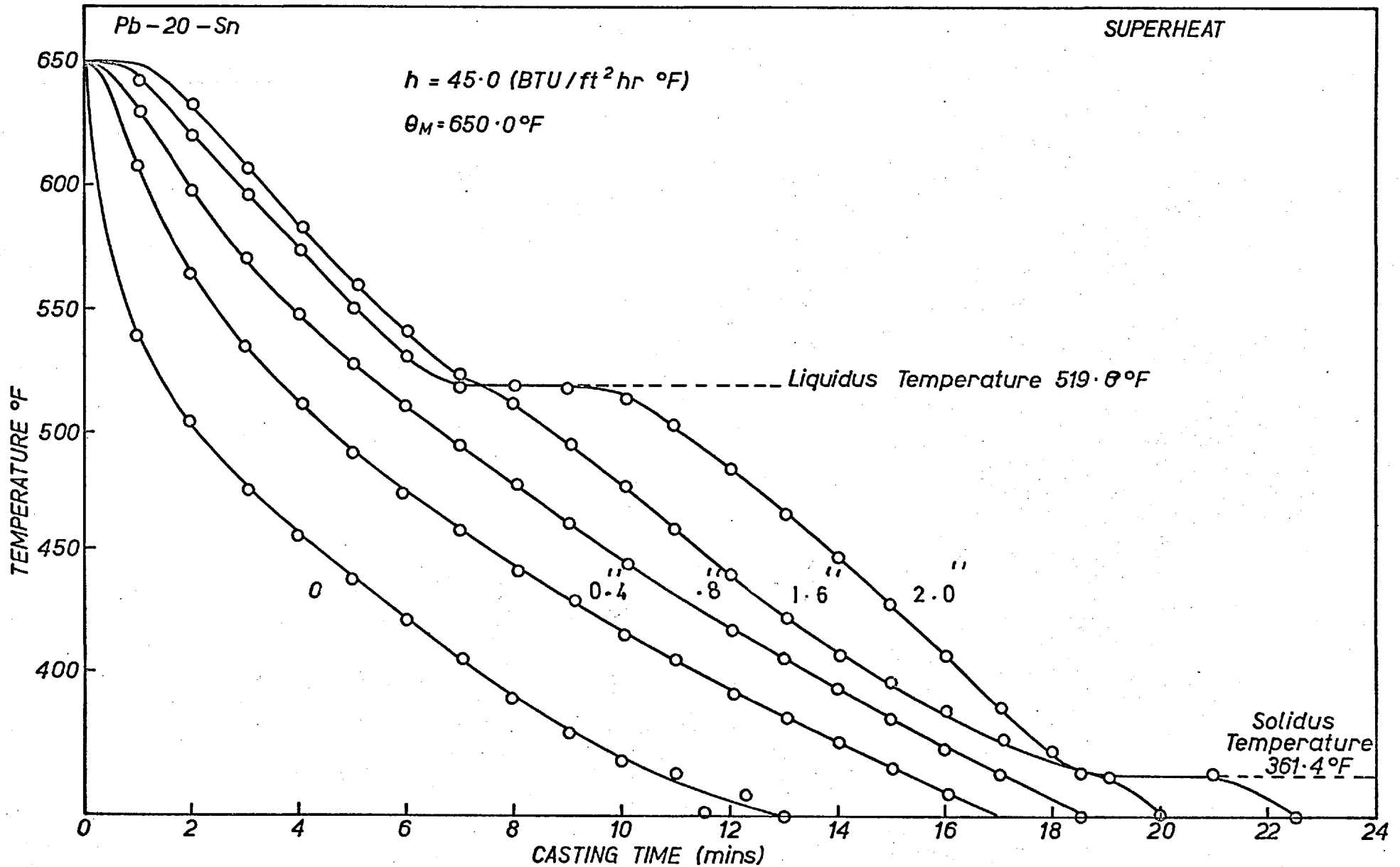


Fig V- 8 COOLING CURVES FOR 20wt% TIN, LEAD-TIN ALLOY AT VARIOUS DISTANCES FROM BASE

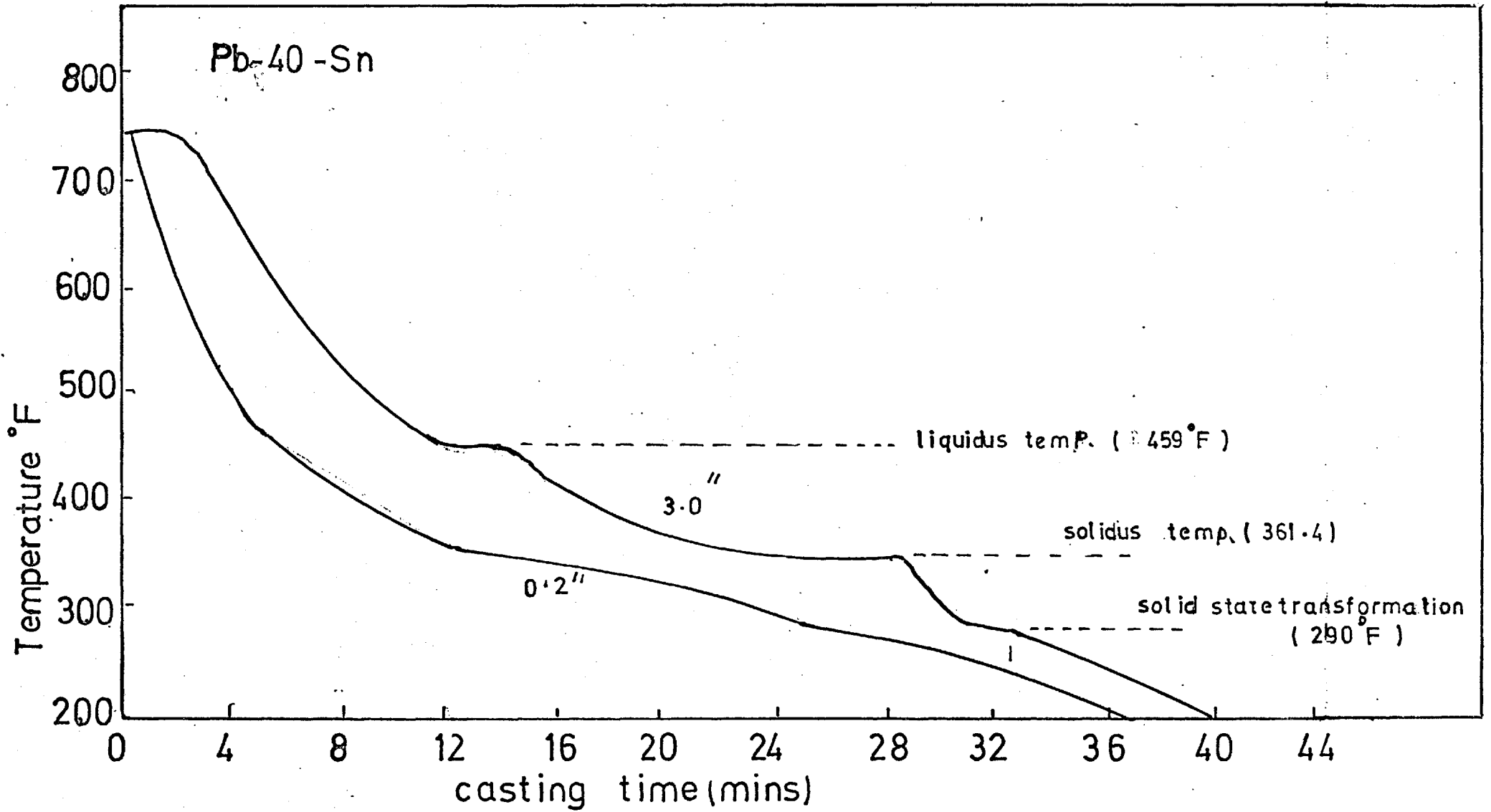
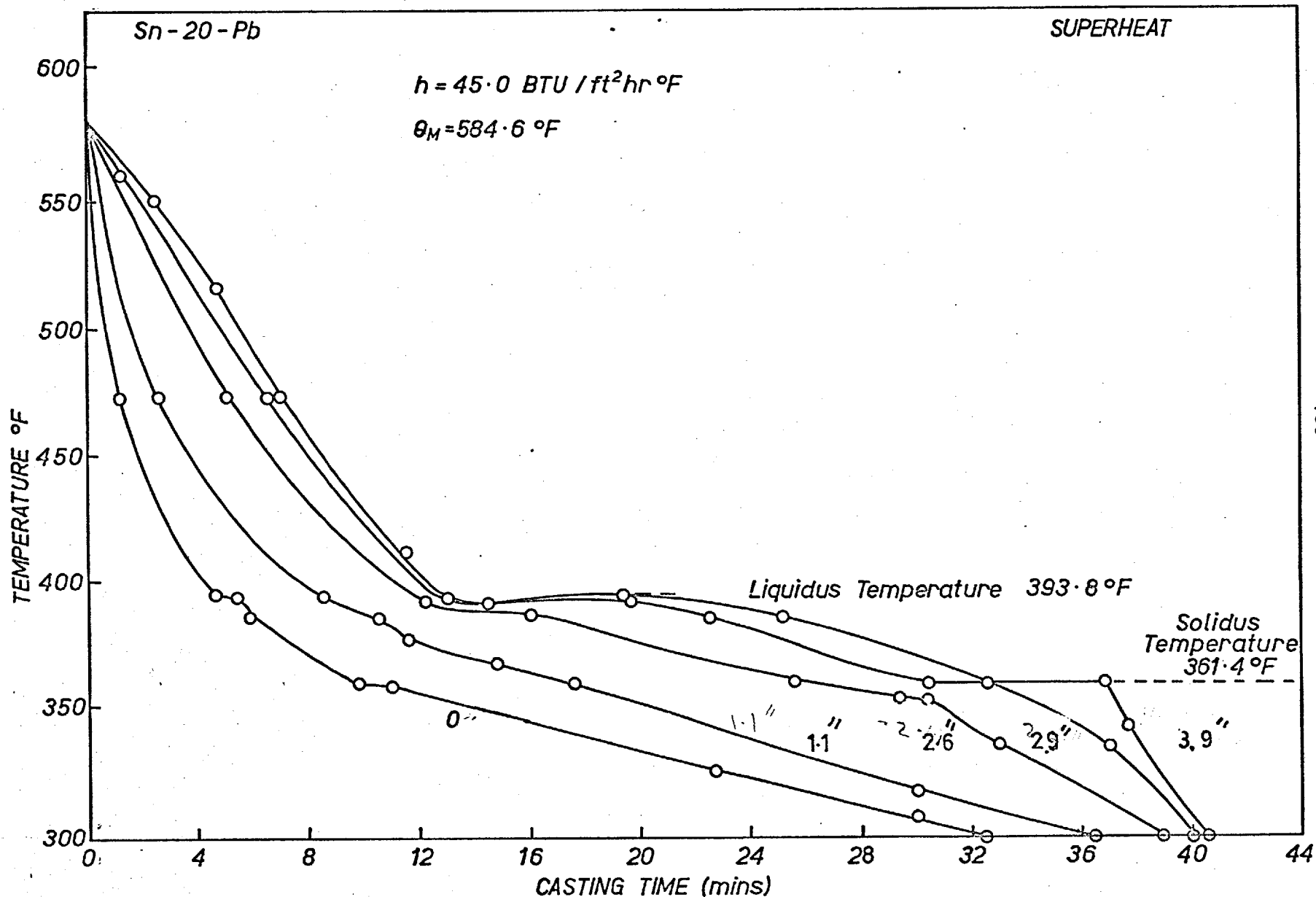


Fig.V-9 Cooling Curves for 40 wt.% Tin, Lead-Tin Alloy



130

Fig. V-10 COOLING CURVES FOR 20wt% LEAD, TIN-LEAD ALLOY AT VARIOUS DISTANCES FROM BASE

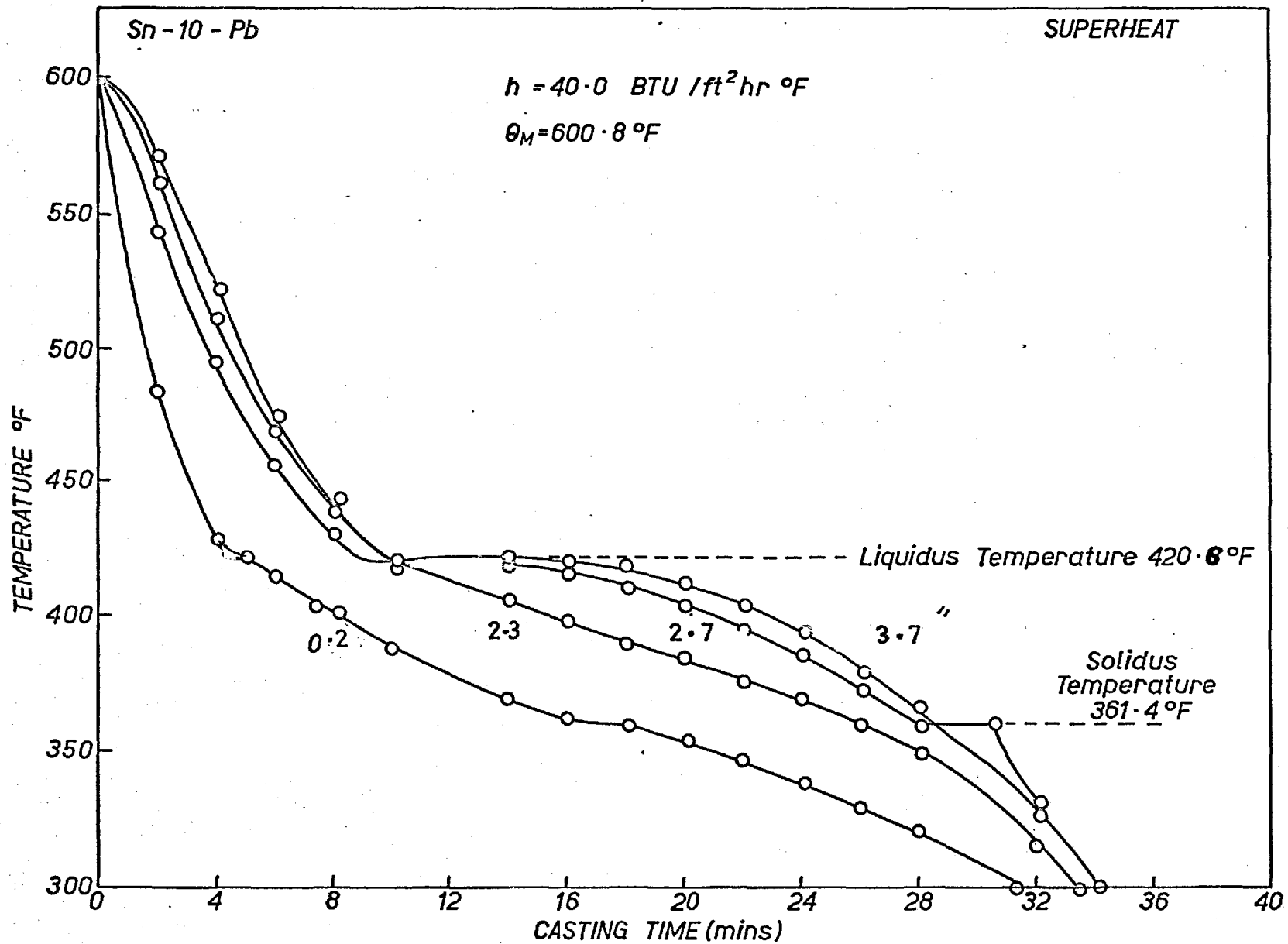


Fig V-11 COOLING CURVES FOR 10wt% LEAD TIN-LEAD ALLOY AT VARIOUS DISTANCES FROM BASE

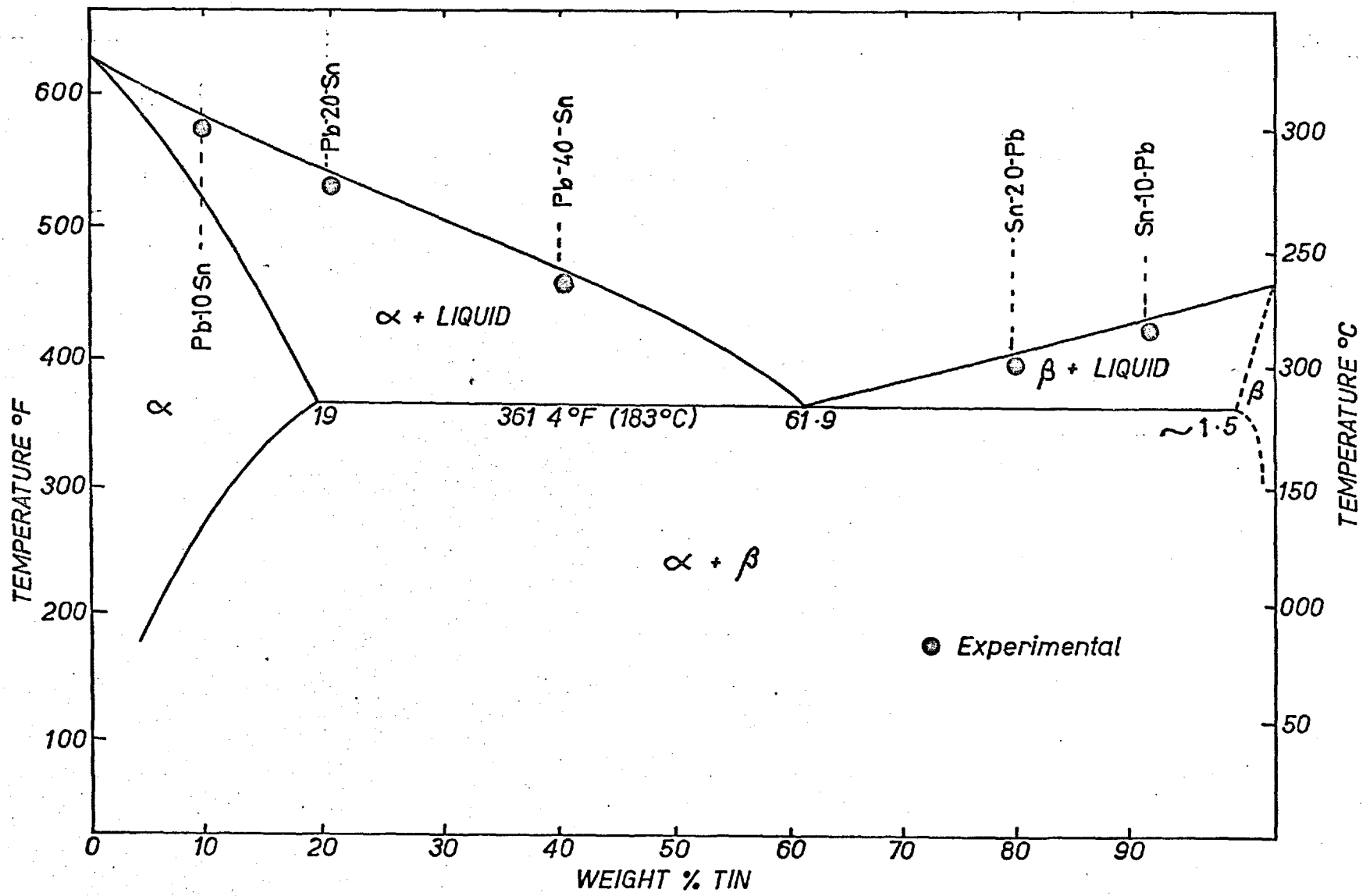


Fig V-12 LEAD-TIN PHASE DIAGRAM

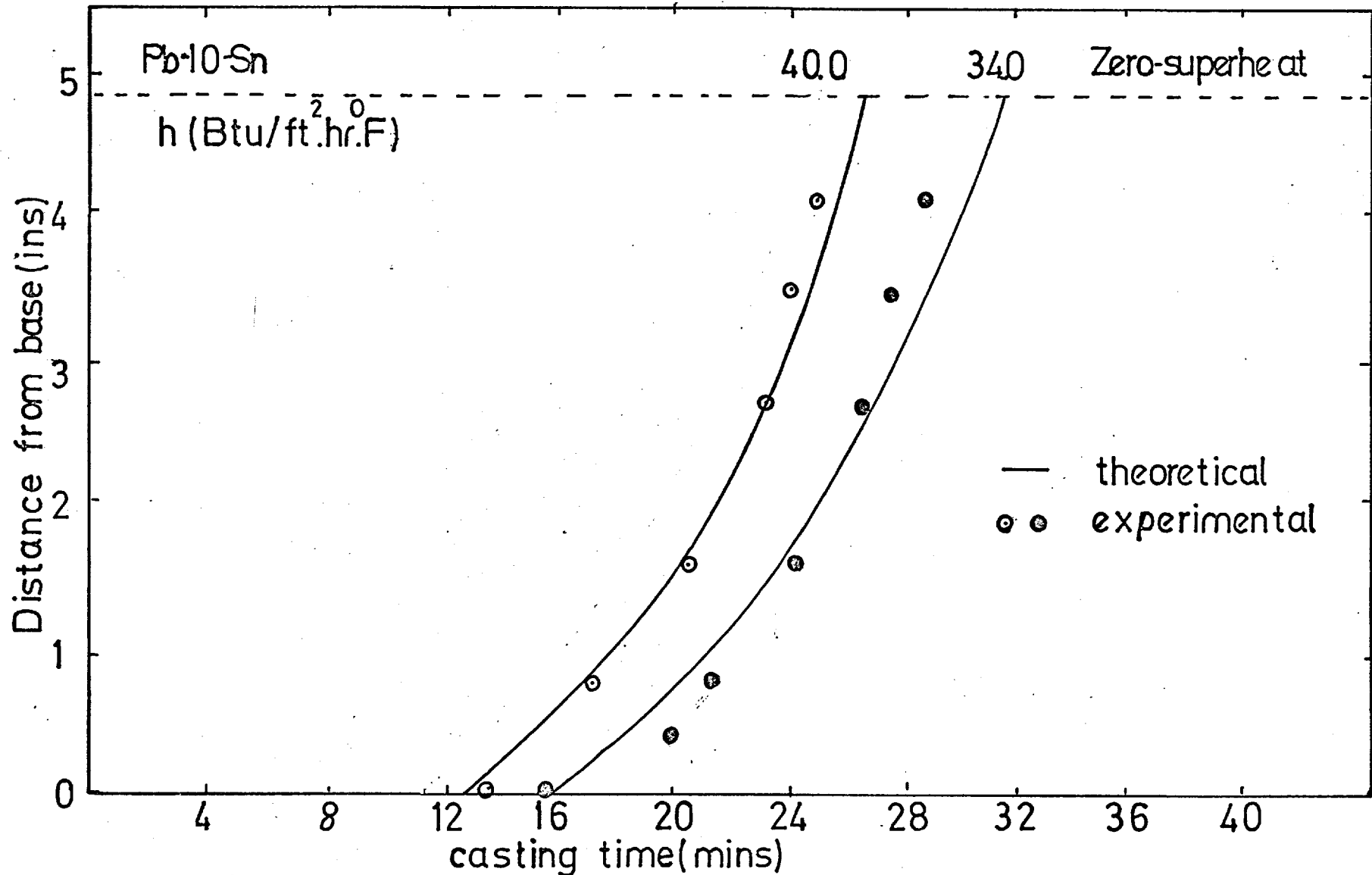


Fig. V-13. Solidification of 10 wt.% Tin, Lead-Tin Alloy
comparison of theoretical and experimental results

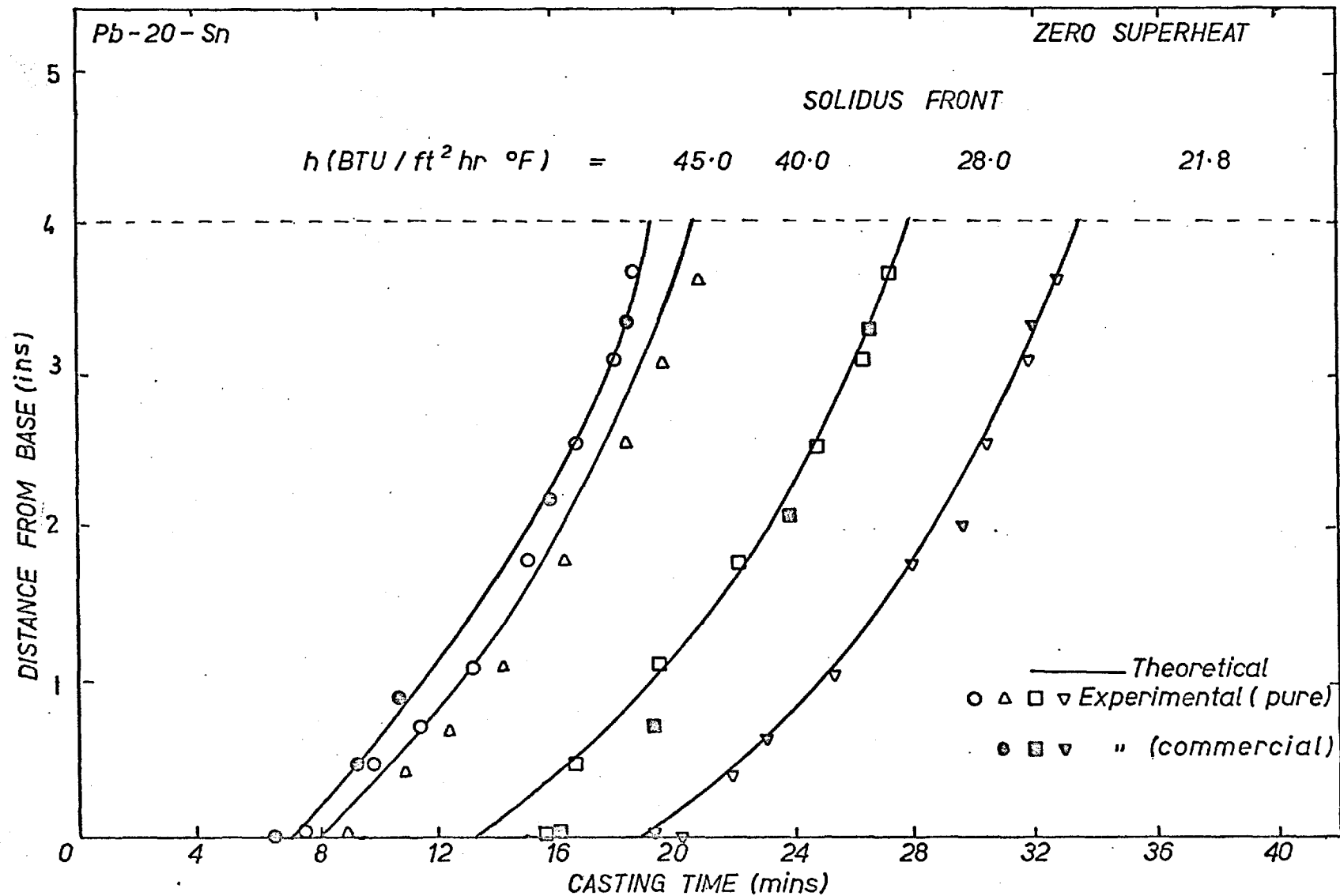


Fig.V-14 SOLIDIFICATION OF 20wt% TIN, LEAD - TIN ALLOY AT ZERO SUPERHEAT
 Comparison of theoretical and experimental results

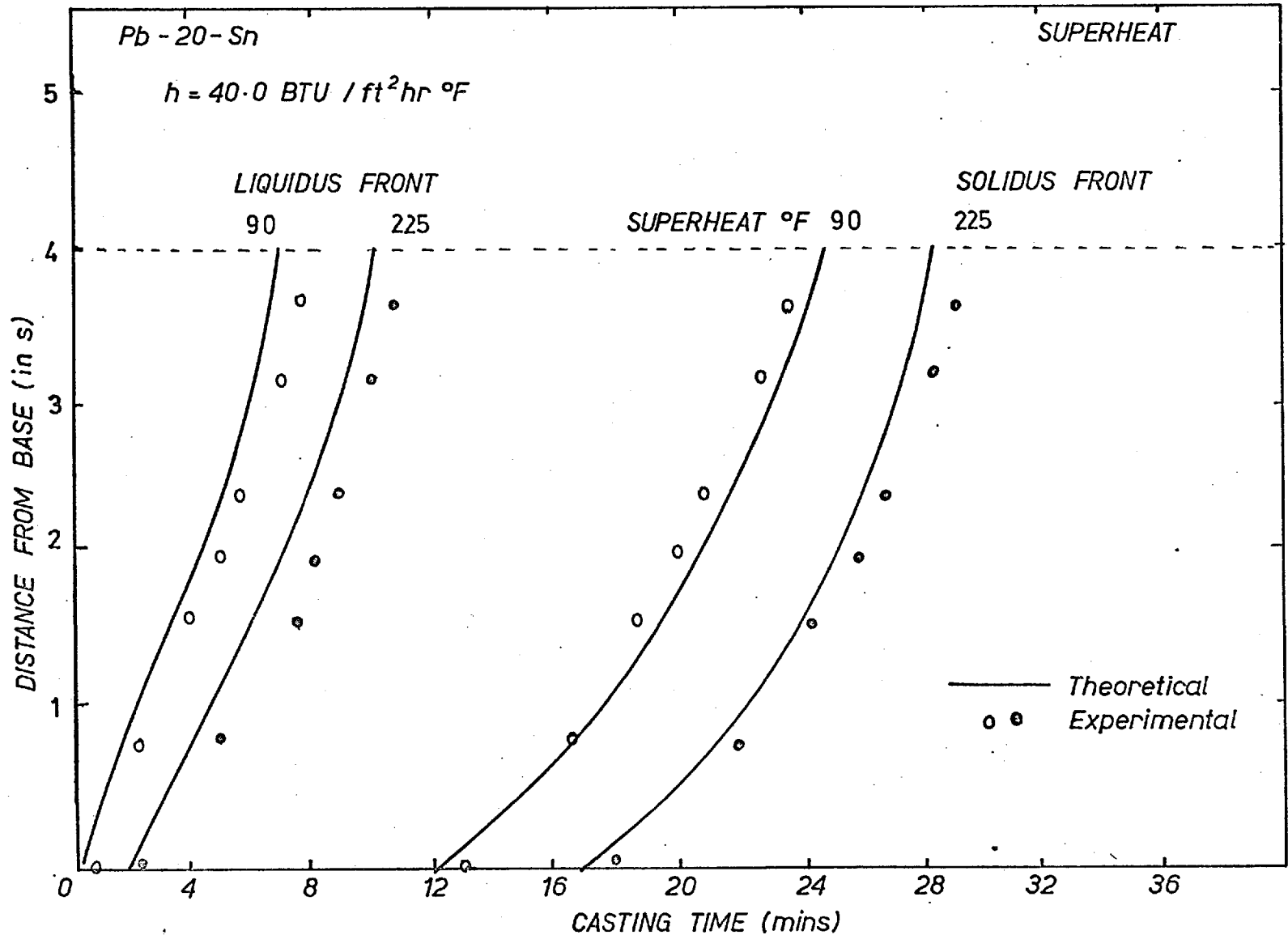


Fig.V-15, SOLIDIFICATION OF 20.0 wt% TIN, LEAD-TIN ALLOY AT POSITIVE SUPERHEAT
 Comparison of theoretical and experimental results

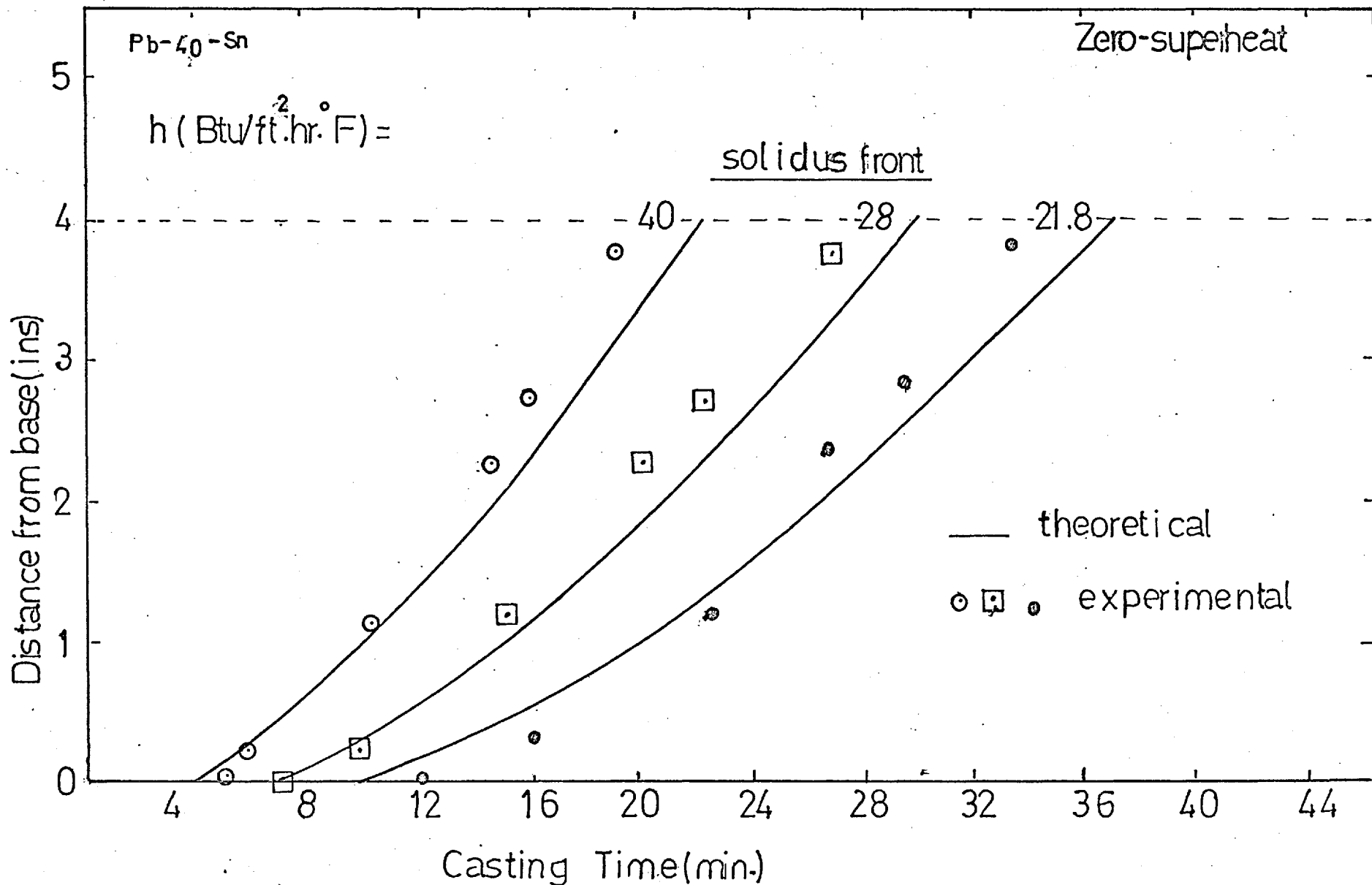


Fig. V-16 SOLIDIFICATION OF 40 wt% TIN LEAD-TIN ALLOY
comparison of theoretical & experimental results.

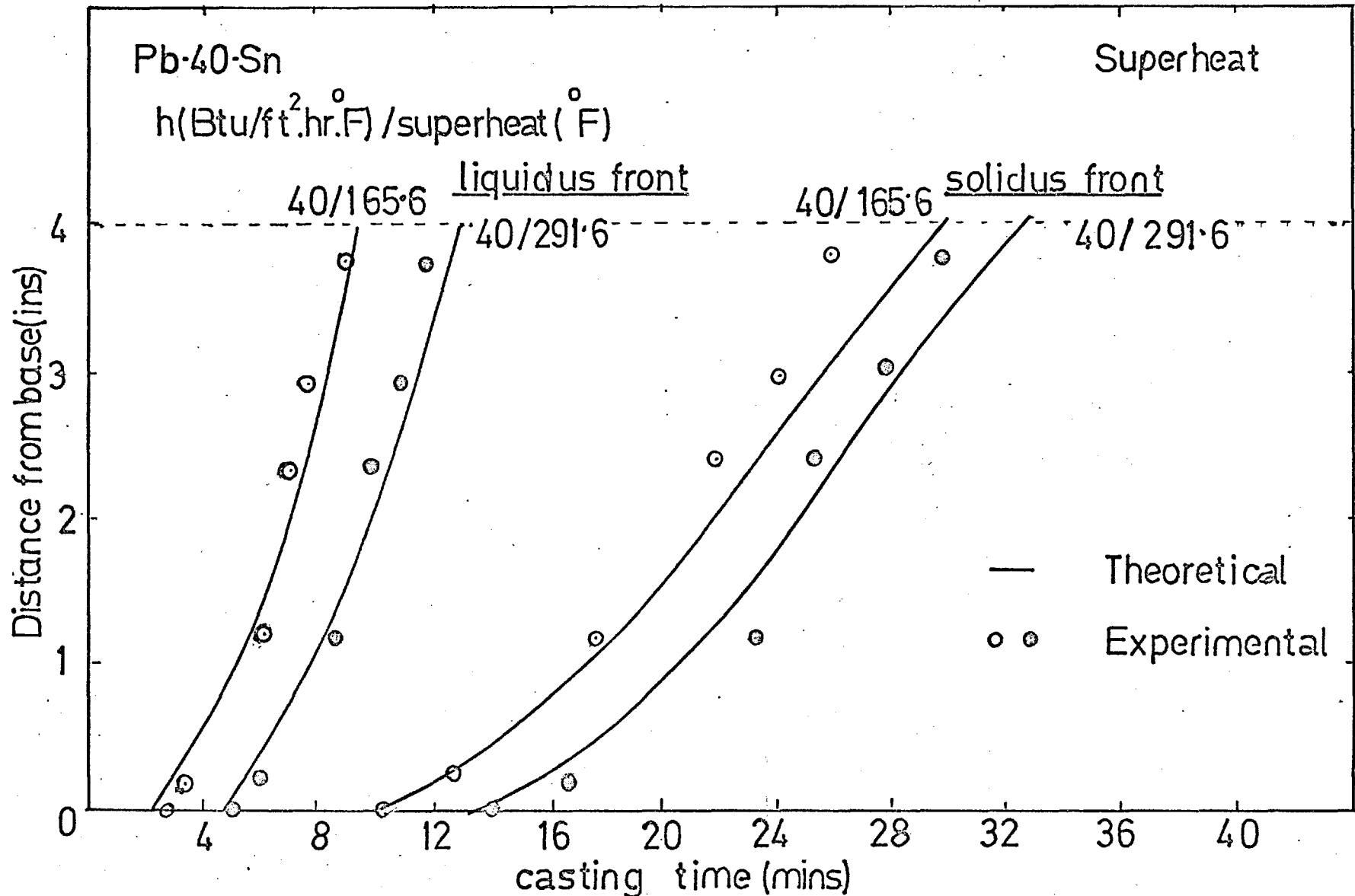


Fig.V 17 Solidification of 40 wt.% Tin, Lead-Tin Alloy
comparison of theoretical and experimental results

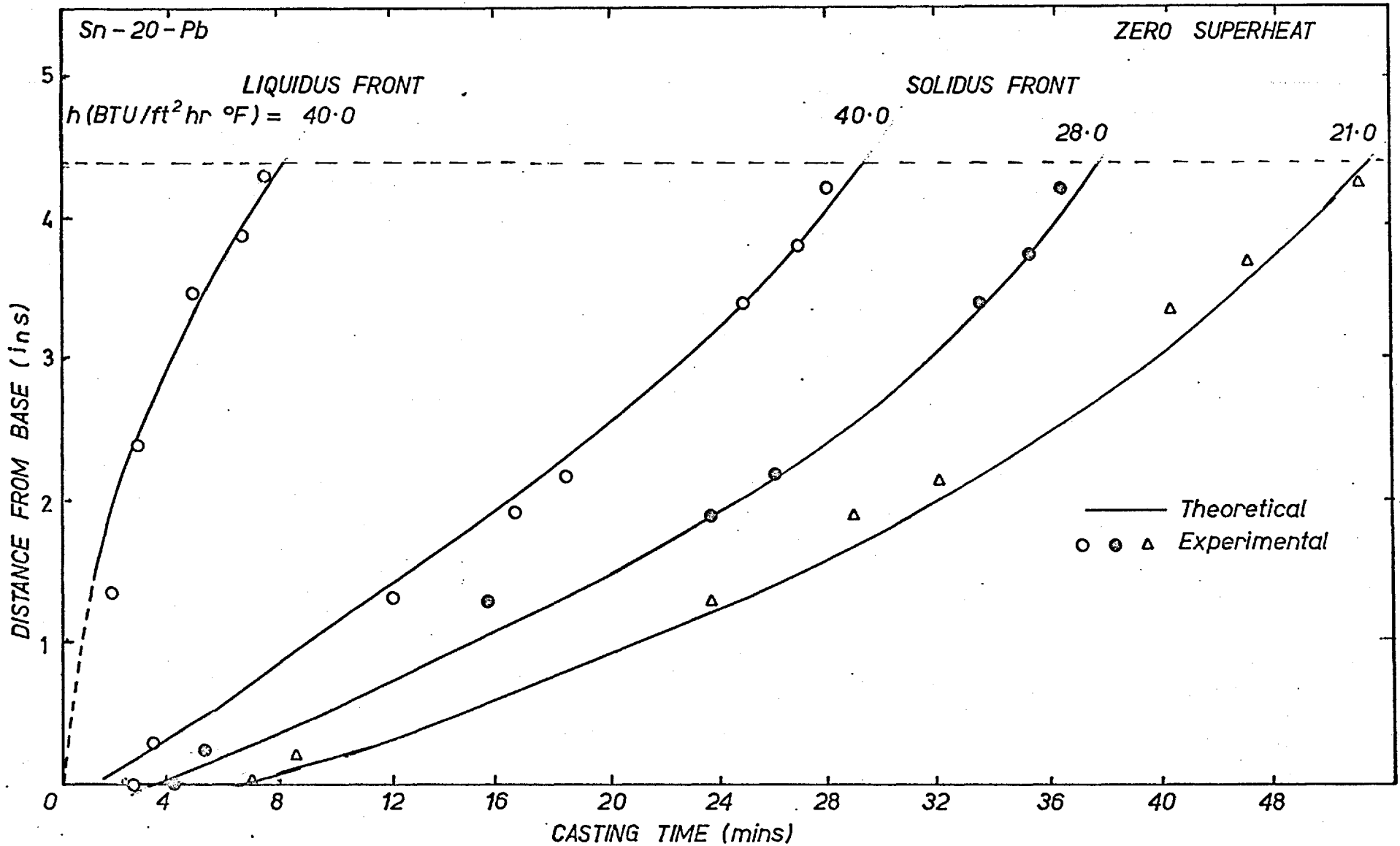


Fig.V-18 SOLIDIFICATION OF 20wt% LEAD, TIN-LEAD ALLOY AT ZERO SUPERHEAT
Comparison of theoretical and experimental results.

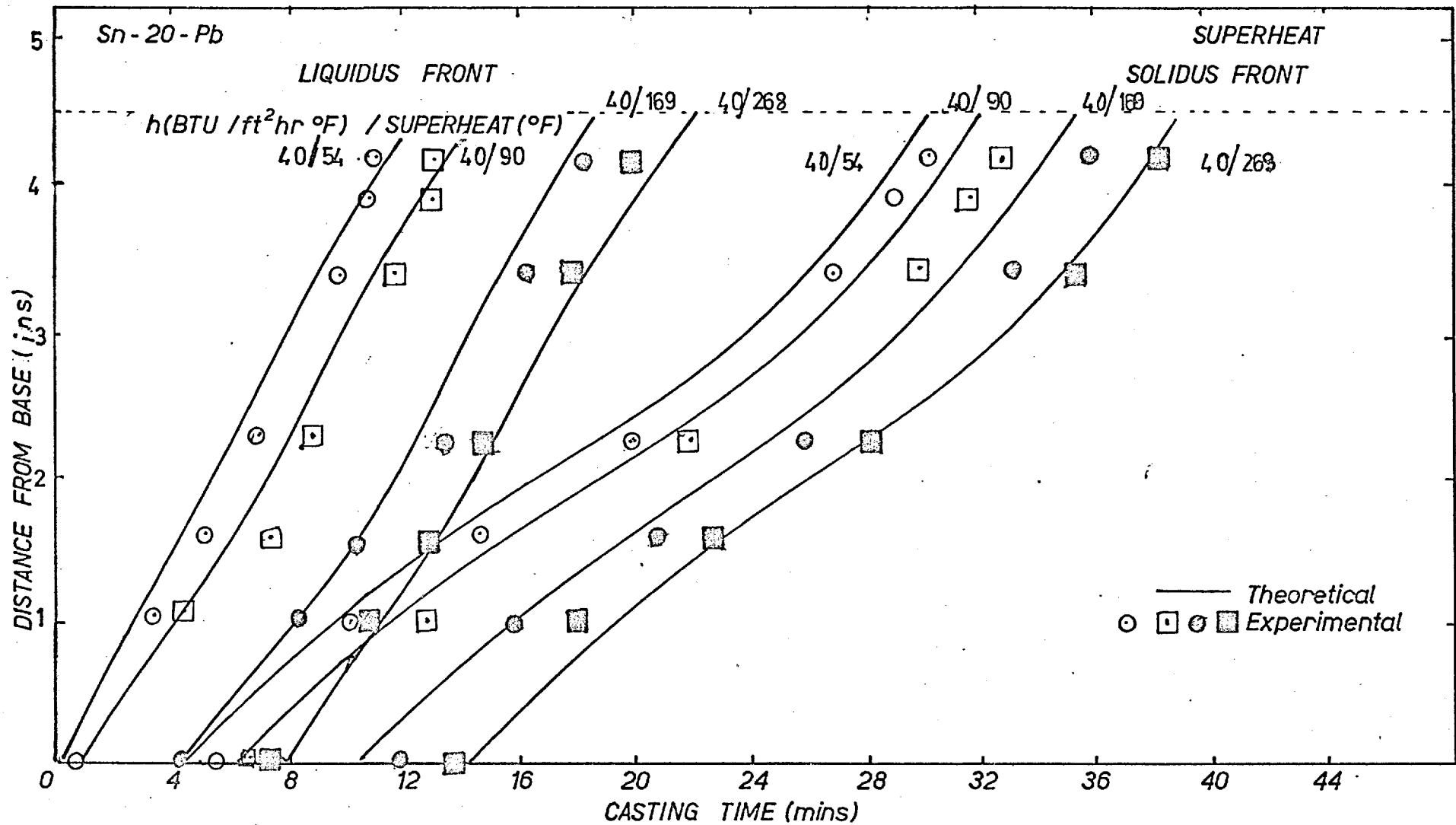
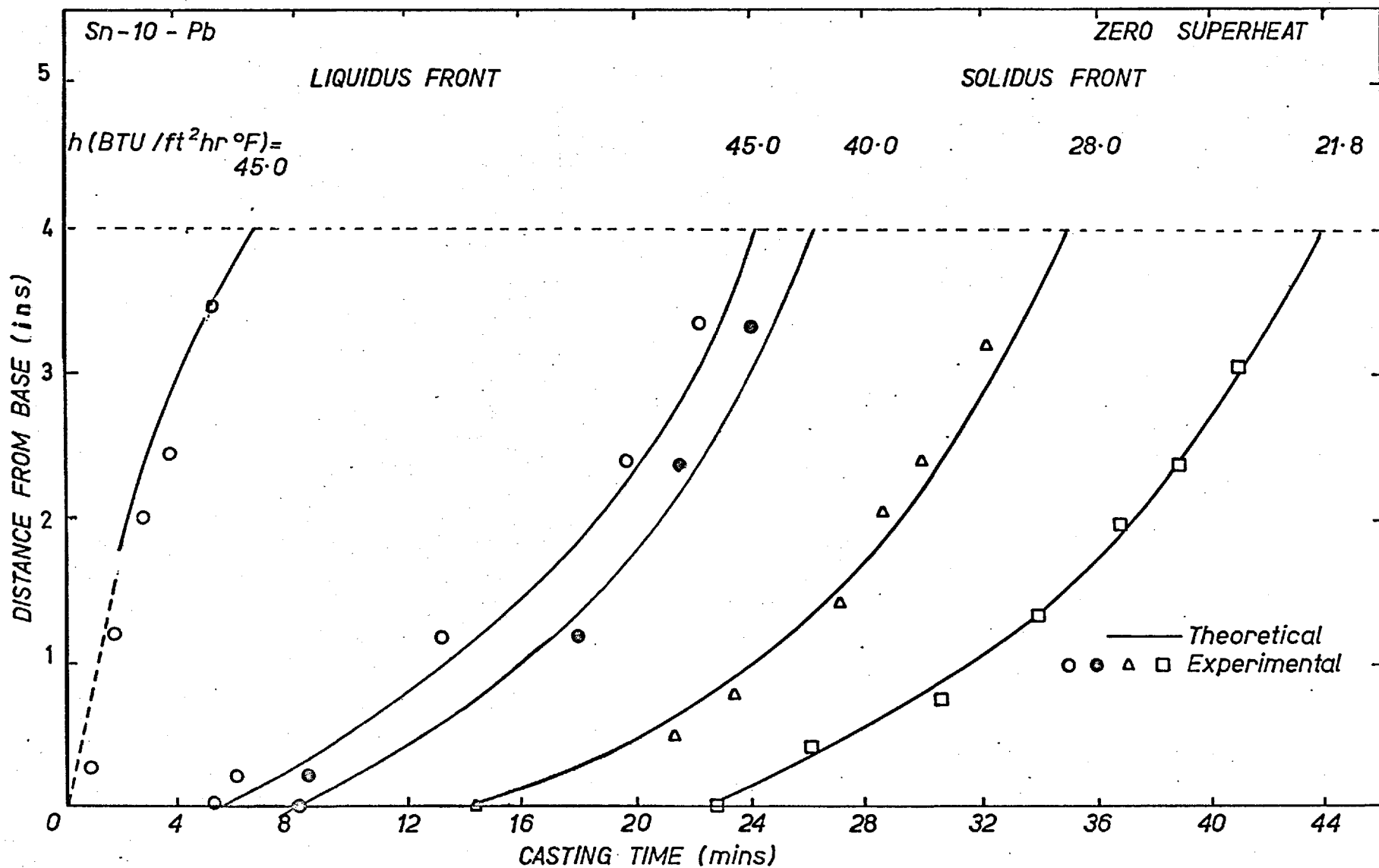


Fig.V-19 SOLIDIFICATION OF 20wt% LEAD, TIN-LEAD ALLOY AT POSITIVE SUPERHEAT
 Comparison of theoretical and experimental results



Figv-20 SOLIDIFICATION OF 10wt% LEAD, TIN-LEAD ALLOY AT ZERO SUPERHEAT
 Comparison of theoretical and experimental results.

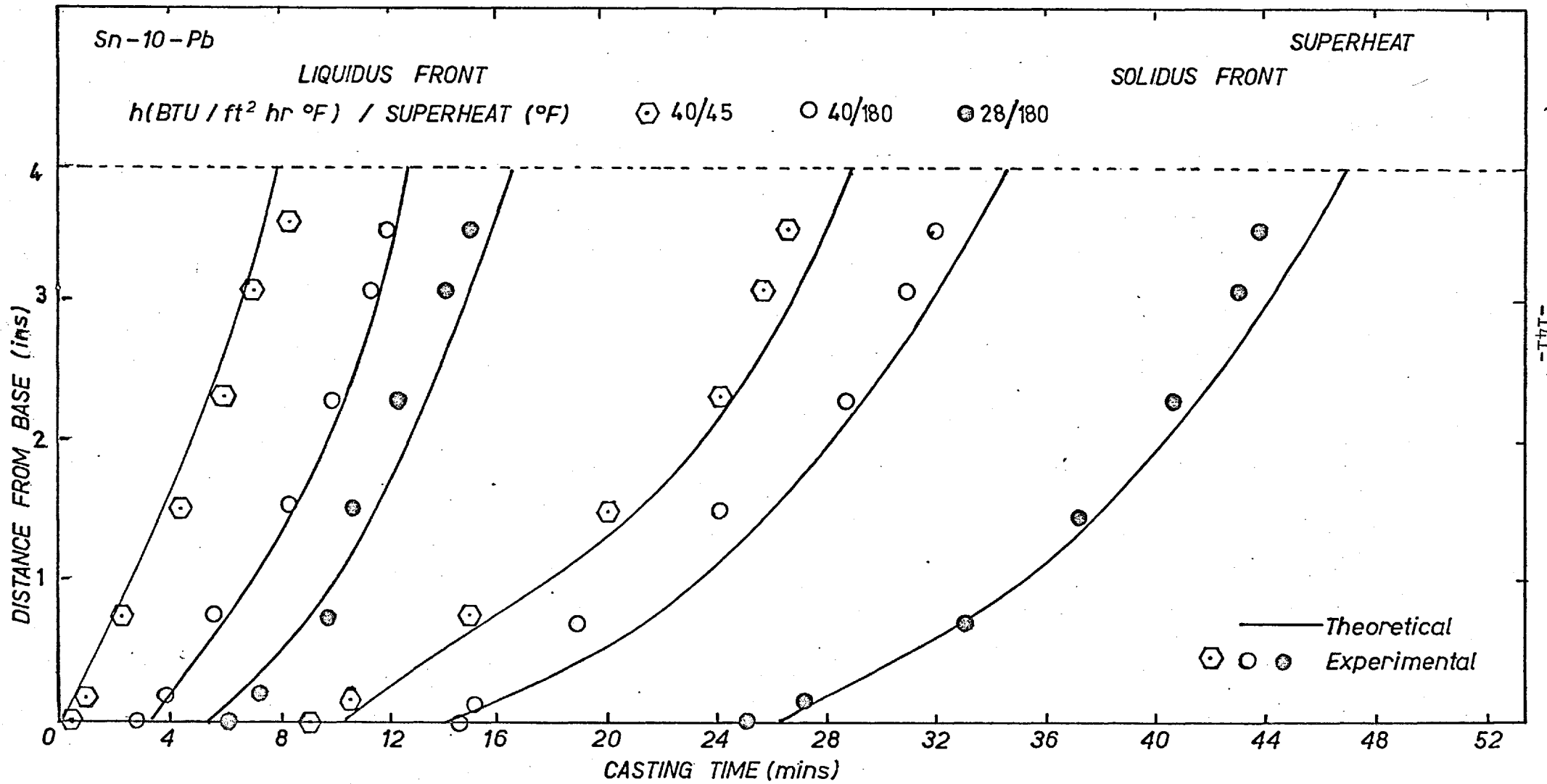


Fig.V-21 SOLIDIFICATION OF 10wt% LEAD, TIN-LEAD ALLOY AT POSITIVE SUPERHEAT
 Comparison of theoretical and experimental results

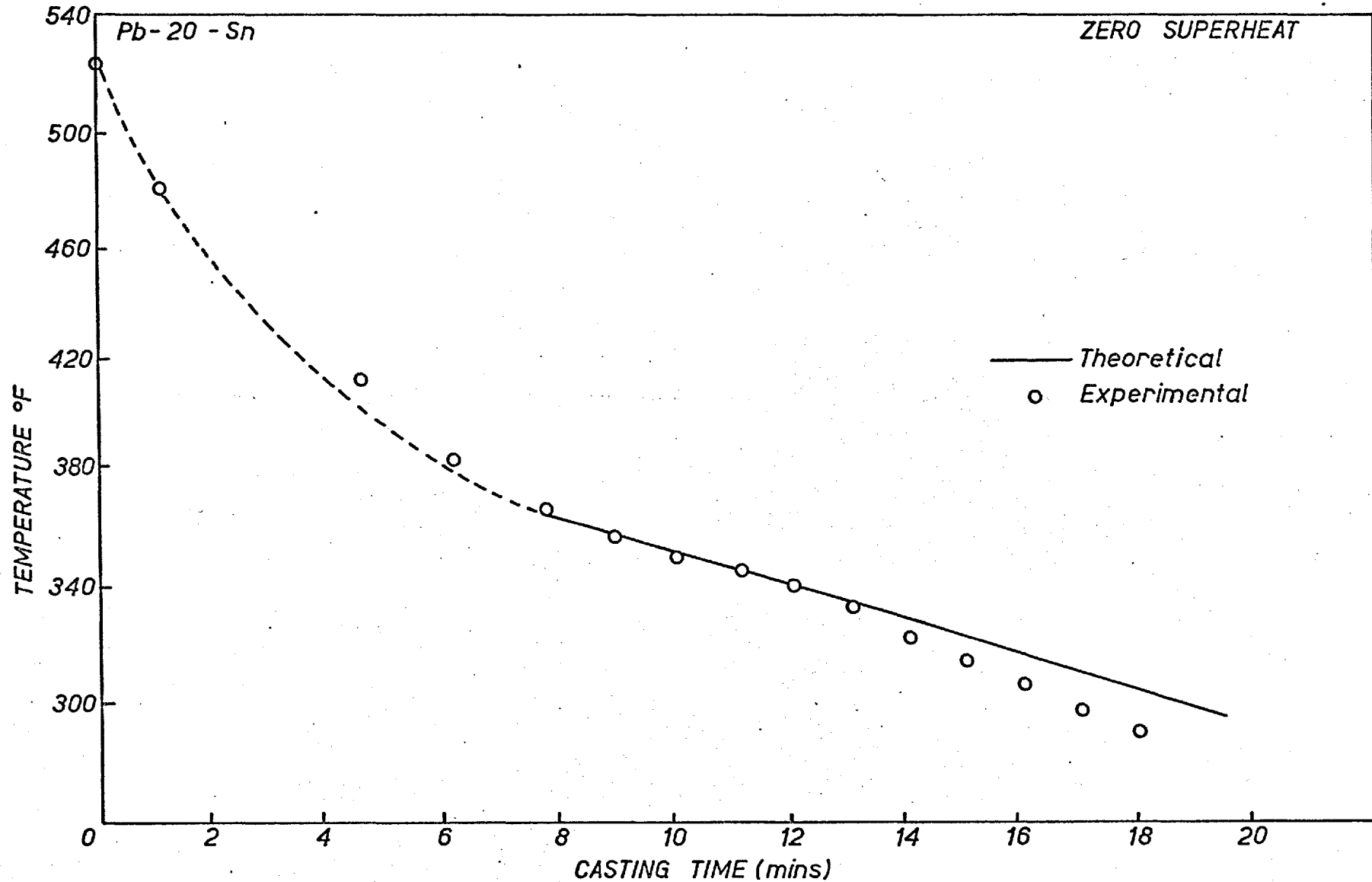


Fig.V-22 SOLIDIFICATION OF 20wt% TIN, LEAD-TIN ALLOY AT ZERO SUPERHEAT
Comparison of theoretical and experimental base temperature.

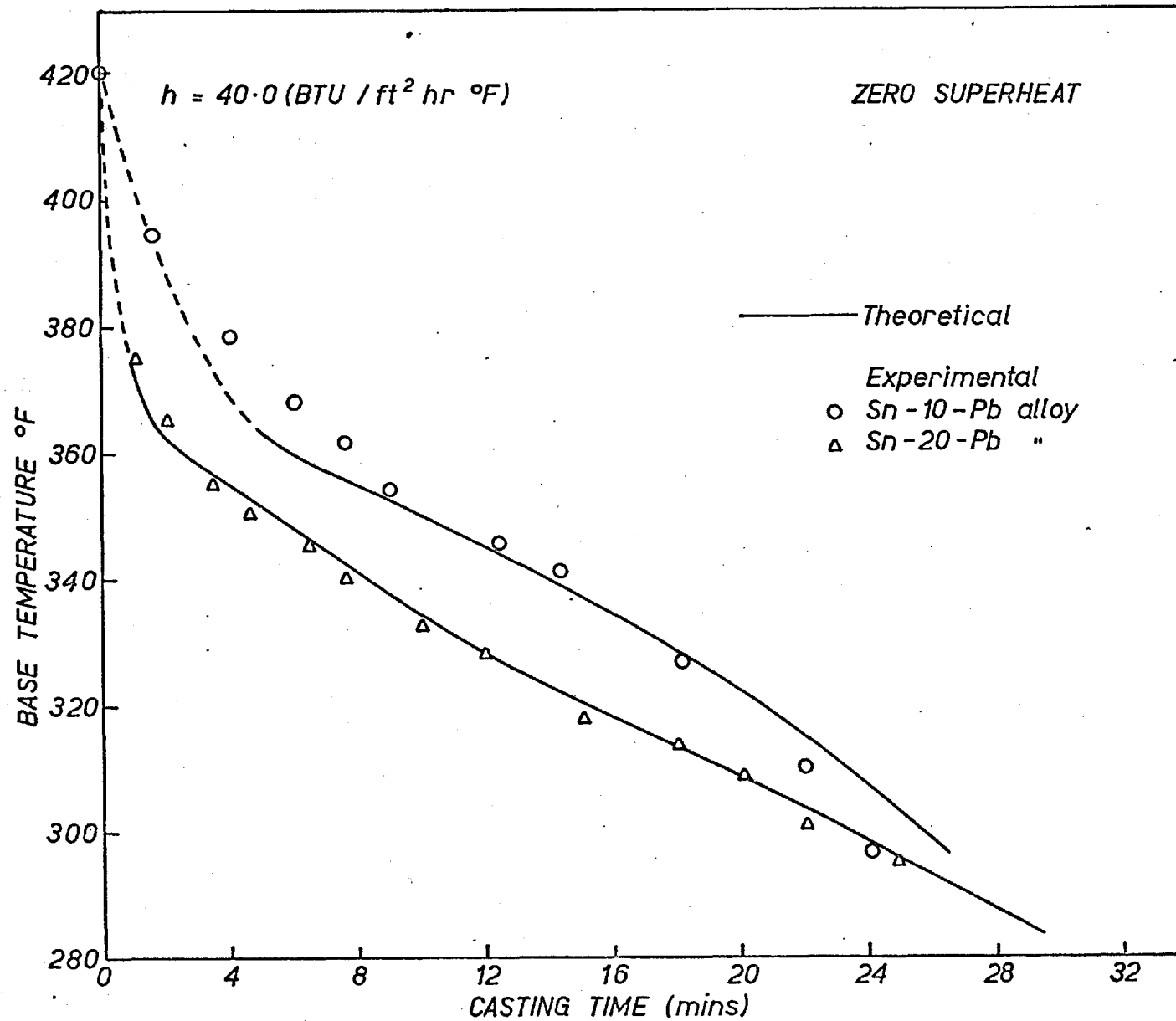


Fig.V-23 SOLIDIFICATION OF TIN RICH ALLOYS
Comparison of theoretical and experimental base temperatures

are calculated as described below.

q_M the total heat liberated from a solidifying alloy is liberated from the liquid, from the partially solidified layer, at the solidus front, and from the completely solid layer.

$$q_M = q_T + q_p + q_{SL} + q_S \quad V-5-1$$

The temperature profile in the thermal layer can be plotted at any time from the thermocouple readings. Taking the mean temperature, θ_{MT} , between any two thermocouple positions, distance 'd' apart, we can calculate the sensible heat given up by the liquid metal, as:

$$q_T = AdC_L(\theta_M - \theta_{MT}) \quad V-5-2$$

and the total heat that has been liberated by the thermal layer (q_T) can be obtained by summation.

The partial layer and solid layer can be treated in the ~~same~~^{same} way to give q_p and q_S , except that the specific heat used in the partial layer is the modified specific heat defined in Chapter III. The quantity of heat that has been liberated at the solidus front is given by:

$$q_{SL} = \frac{\Delta H}{\rho} (1 - f_{SU}) t_S \quad V-5-3$$

The quantity of heat removed by the cooling air is most easily calculated by substituting a time mean value, θ_{OM} , of the temperature of the cooled surface into the equation:

$$q_a = hA (\theta_{OM} - \theta_a) \quad V-5-4$$

⁴¹ Moore has shown that sufficient accuracy can be obtained if θ_{OM} is taken as the indicated temperature of the crucible base half way through the time period.

TABLE V-3

THERMAL BALANCES FOR THE SOLIDIFICATION OF
LEAD
AT ZERO SUPERHEAT

Initial temperature = 621.6°F
Liquidus temperature = 621.6°F
Solidus temperature = 621.6°F
Height of metal = 4 inches

Heat transfer coefficient (Btu/ft ² .hr.°F)	40.5		29.5	
Casting time (min.)	5	10	5	10
Solid layer (in.)	2.0	3.4	1.7	3.0
Latent heat liberated at solidus temperature (Btu)	107.4	182.5	91.2	161.0
Temperature in metal				
0 in.	495	459	536	494
0.8 in.	560	509	567	520
1.4 in.	594	536	599	548
2.2 in.	621.6	572	621.6	581
3.0 in.		606		621
4.0 in.		621.6		
Sensible heat liberated in solid layer (Btu)	18.1	41.7	13.3	33.8
Total heat liberated in metal (Btu)	125.5	224.2	104.5	194.8
Base temperature at mid time (°F)	545	495	567	536
Heat removed by cooling air (Btu)	129.8	230.1	99.3	185.2
Excess heat liberated in metal (Btu)			5.2	9.6
Excess heat supplied by casting unit (Btu)	4.3	5.9		

TABLE V-4

THERMAL BALANCES FOR THE SOLIDIFICATION OF
LEAD-ANTIMONY EUTECTIC
AT ZERO SUPERHEAT

Initial temperature = 484.0°F
Liquidus temperature = 484.0°F
Solidus temperature = 484.0°F
Height of metal = 4.3 inches
Heat transfer coefficient = 40.0 Btu/ft².hr.°F

Casting time (min.)	5	10	15	20
Solid layer (in.)	1.1	2.1	2.9	3.6
Latent heat liberated at solidus temperature (Btu)	82.4	157.3	217.2	269.7
Temperature in metal				
0 in.	401	356	295	275
0.7 in.	417	369	313	311
1.3 in.	484	414	351	414
2.0 in.		482	426	453
3.1 in.		484	484	
3.7 in.				
Sensible heat liberated in solid layer (Btu)	10.8	27.6	40.9	51.4
Total heat liberated in metal (Btu)	93.2	184.9	258.1	321.1
Base temperature at mid time (°F)	432.0	401	371	356
Heat removed by cooling air (Btu)	95.4	172.7	232.0	293.0
Excess heat liberated in metal (Btu)		12.2	26.1	28.0
Excess heat supplied by casting unit (Btu)	2.2			

TABLE V-5

THERMAL BALANCES FOR THE SOLIDIFICATION OF
LEAD-TIN EUTECTIC
AT ZERO SUPERHEAT

Initial temperature = 361.4°F
Liquidus temperature = 361.4°F
Solidus temperature = 361.4°F
Height of metal = 4 inches

Heat transfer coefficient (Btu/ft ² .hr.°F)	40.0			28.0			21.8		
Casting time (min.)	5	10	20	5	10	20	10	20	30
Solid layer (in.)	1.1	2.1	3.7	0.8	1.5	2.9	1.3	2.5	3.5
Latent heat liberated at solidus temperature (Btu)	(a) 65.9	125.8	221.6	47.9	89.9	173.7	77.9	149.8	209.7
	(b) 78.7	150.3	264.8	57.3	107.4	207.6	93.0	178.9	250.6
Temperature in metal									
0 in.	333	315	291	343	329	311	346	325	316
1.7 in.		342	315			336		347	338
3.1 in.			243						
4.0 in.									
Sensible heat liberated in solid layer (Btu)	3.0	11.0	28.2	1.2	4.5	13.5	2.4	8.5	15.1
Total heat liberated in metal (Btu)	(a) 68.9	136.8	249.8	49.1	94.4	187.2	80.3	158.3	234.6
	(b) 81.7	161.3	293.0	58.5	111.9	221.1	95.4	187.4	275.6
Base temperature at mid time (°F)	345	333	315	352	343	329	349	340	334
Heat removed by cooling air (Btu)	70.0	133.1	245.3	50.5	97.3	183.1	77.6	149.5	218.6
Excess heat liberated in metal (Btu)	(a)	3.7	4.5			4.1	2.7	8.8	16.0
	(b) 11.7	28.2	47.7	8.0	14.6	38.0	17.8	37.9	57.0
Excess heat supplied by casting unit (Btu)	(a) 1.1			1.4	2.9				
	(b)								

(a) using latent heat value 15.9 Btu/lb
(b) using latent heat value 19.3 Btu/lb

TABLE V-6

THERMAL BALANCES FOR THE SOLIDIFICATION OF
LEAD-TIN EUTECTIC
AT POSITIVE SUPERHEAT

Initial temperature = 449.6°F
 Liquidus temperature = 361.4°F
 Solidus temperature = 361.4°F
 Heat transfer coefficient = 40.0 BTU/ft²·hr.°F
 Height of metal = 4.3 inches

Casting time (min.)	10.5	16.5	21	24
Solid layer (in.)	1.3	2.4	3.1	3.6
Partial layer (in.)	-	-	-	-
Thermal layer (in.)	3.0	1.9	1.2	0.7
Latent heat liberated at solidus temperature (Btu)	77.9	143.8	185.7	215.6
Temperature in metal				
0 in.	327	309	299	291
0.4 in.	334	323	311	306
0.9 in.	345	336	325	318
1.8 in.	356	352	336	330
2.5 in.	367	361.4	350	349
3.5 in.	-	-	361.4	359
4.3 in.	368.7	361.4	361.4	361.4
Sensible heat liberated in solid layer (Btu)	81.4	87.4	95.2	99.0
Total heat liberated in metal (Btu) (a)	159.3	231.2	280.9	314.6
Base temperature at mid time (°F) (a)	351	338	327	324
Heat removed by cooling air (Btu)	150.8	224.5	272.2	306.9
Excess heat liberated (a) in metal (Btu)	8.5	6.7	8.7	7.7
(b)	23.6	34.7	44.9	49.8
Excess heat supplied by casting unit (Btu)	-	-	-	-

(a) using latent heat value 15.9 Btu/lb.
 (b) using latent heat value 19.3 Btu/lb.

TABLE V-7

THERMAL BALANCES FOR THE SOLIDIFICATION OF
20.0 wt. % TIN, LEAD-TIN ALLOY
AT POSITIVE SUPERHEAT

Initial temperature = 700°F
Liquidus temperature = 519.8°F
Solidus temperature = 361.4°F
Heat transfer coefficient = 40.0 BTU/ft².hr.°F
Height of metal = 4 inches

Casting time (min.)	4.5	9.5	14.5	20	25
Solid layer (in.)	0	0	0	1.2	3.6
Partial layer (in.)	1.5	3.0	4.0	2.8	0.4
Thermal layer (in.)	2.5	1.0	-	-	-
Latent heat liberated at solidus temperature (Btu)	-	-	-	17.8	53.5
Temperature in metal					
0 in.	484	417	369	333	291
0.7 in.	-	666	396	351	300
1.9 in.	565	469	430	378	322
2.6 in.	600	520	457	390	336
3.6 in.	615	-	-	-	-
4.0 in.	622.4	519.8	458.6	392	361.4
Heat liberated in partial layer (Btu)	9.8	54.9	150.1	210.0	222.6
Sensible heat liberated in solid layer (Btu)	-	-	-	3.0	22.0
Sensible heat liberated in thermal layer (Btu)	103	131	131	131	131
Total heat liberated in metal (Btu)	112.6	185.0	283.1	361.8	429.1
Base temperature at mid time (°F)	533	455	445	417	396
Heat removed by cooling air (Btu)	112.7	193.8	287.4	364.0	424.0
Excess heat liberated in metal (Btu)					5.0
Excess heat supplied by casting unit (Btu)	0.1	8.8	4.3	2.2	

TABLE V-8

THERMAL BALANCES FOR THE SOLIDIFICATION OF
80.0 wt. % TIN, TIN-LEAD ALLOY
AT ZERO SUPERHEAT

Initial temperature = 393.8°F
 Liquidus temperature = 393.8°F
 Solidus temperature = 361.4°F
 Heat transfer coefficient = 40.0 BTU/ft²·hr.°F
 Height of metal = 4.3 inches

Casting time (min.)	11.0	16	20	25
Solid layer (in.)	1.1	1.8	2.5	3.4
Partial layer (in.)	3.3	2.6	1.9	1.0
Latent heat liberated at solidus temperature (Btu)	31.2	51.1	71.0	96.5
Temperature in metal				
0 in.	337	318	309	297
1.2 in.	363	352	336	324
2.1 in.	385	372	358	343
3.4 in.	387	380	370	360
4.2 in.	392	380	373	363
4.8 in.	393.2	380.3	372.7	366.0
Heat liberated in partial layer (Btu)	134.3	174.7	193.7	203.9
Sensible heat liberated in solid layer (Btu)	3.3	7.5	13.4	20.6
Total heat liberated in metal (Btu)	168.8	233.3	278.1	321.0
Base temperature at mid time (°F)	354	347	335	325
Heat removed by cooling air (Btu)	159.9	226.0	268.6	321.2
Excess heat liberated in metal (Btu)	8.9	7.3	9.5	0.2
Excess heat supplied by casting unit (Btu)				

TABLE V-9

THERMAL BALANCES FOR THE SOLIDIFICATION OF
90.0 wt. % TIN, TIN-LEAD ALLOY
AT ZERO SUPERHEAT

Initial temperature = 420.6°F
Liquidus temperature = 420.6°F
Solidus temperature = 361.4°F
Heat transfer coefficient = 40.0 BTU/ft.².hr.°F
Height of metal = 4.0 inches

Casting time (min.)	11.5	15.5	20.5
Solid layer (in.)	0.5	0.9	1.8
Partial layer (in.)	3.5	3.1	2.2
Latent heat liberated at solidus temperature (Btu)	6.8	12.2	24.3
Temperature in metal			
0 in.	351	338	319
0.8 in.		361	342
2.0 in.	405	387	364
2.4 in.			
4.0 in.	411.8	398.5	378.0
Heat liberated in partial layer (Btu)	177.0	229.1	279.0
Sensible heat liberated in solid layer (Btu)	0.1	0.2	0.4
Total heat liberated in metal (Btu)	183.9	241.5	303.7
Base temperature at mid time (°F)	369	362	351.0
Heat removed by cooling air (Btu)	177.2	232.5	294.4
Excess heat liberated in metal (Btu)	6.7	9.0	9.3
Excess heat supplied by casting unit (Btu)			

V-6 LATENT HEAT OF LEAD-TIN EUTECTIC

The latent heat of lead-tin eutectic was determined as discussed in section IV-9. The results obtained are listed in Table V-10

TABLE V-10 LATENT HEAT OF LEAD-TIN EUTECTIC

Initial temperature of the liquid metal:
183°C ±2°C

Weight of the copper calorimeter and stirrer: 125.14 gm.

Water equivalent of the calorimeter:
11.38

Exp. No.	Weights (gm)		Temperature(°C)		Heat (cal/gm)		
	Water	Metal	Initial	Final	Total*	Sensible	Net
1	60.32	8.24	25.8	27.8	17.4	8.1	9.3
2	68.68	7.44	23.8	25.5	18.3	8.2	10.1
3	65.25	6.60	23.8	25.5	19.74	8.2	11.54
4	59.22	7.07	24.0	25.8	17.98	8.2	9.78
5	60.23	6.86	23.7	25.2	18.8	8.2	10.60
6	63.45	6.74	25.0	26.7	18.87	8.1	10.77

Mean Value = 10.35 cal/gm = 18.6 Btu/lb.

Standard deviation (S) = $\sqrt{\frac{1}{N} (x-x_1)^2}$ = 0.97 Btu/lb.

Therefore

Heat released by the metal = 18.6 ±0.97 Btu/lb.

Latent heat of lead-tin eutectic = 18.6 Btu/lb $-\Delta H_{f,E}$

V-7 SOLID STATE TRANSFORMATION

As discussed in section III-7 the lead-tin system showed an evolution of heat as the solid was cooled from about 295° - 275°F. This has been attributed to the precipitation reaction which occurs when the α solid solution breaks down. Table V-11 gives brief details of the temperatures at which this reaction was observed to occur.

*No cooling correction was applied to these results, since the experiments were of such short duration.

TABLE V-11

Alloy	(Btu/ft ² .h. ^h .°F)	Super-heat °F	Arrest or Change of Gradient	Precipitation Temperature °F
Pb-10-Sn	34.0	0	change of gradient	295
	45.0	230	"	295
	45.0	0	"	295
Pb-20-Sn (Commercial)	34.0	240	arrest	275
	34.0	0	"	280
Pb-20-Sn (Pure)	34.0	0	"	284
	34.0	180	"	284
	45.0	0	"	280
	21.8	0	"	284
	45.0	0	"	284
Pb-40-Sn (Commercial)	34.0	0	"	284
	34.0	155	"	288
	21.8	0	"	293
Pb-E-Sn	45.0	0	change of gradient near base T.C. only	280

In the case of the alloy Pb-40-Sn (40 wt. %) the arrest point was observed to occur for about one minute and was very distinct. In the case of eutectic alloy the arrest point was not sharp, a change in gradient being observed in the temperature record of thermocouples near the base plate only.

V-8 MORPHOLOGY AND SOLUTE SEGREGATION STUDIES IN LEAD ALLOYS

V-8-A LEAD-ANTIMONY EUTECTIC

The alloy was solidified at a heat transfer coefficient of 40 Btu/ft².h.^h.F^o as discussed in section IV-8. The structures obtained are shown in Fig. V-24 and Fig. V-25.

The microphotographs show that some lead rich dendrites are present in a matrix of lead-antimony eutectic. When the structure was examined at higher magnification it was found that the nucleating phase for the lead rich dendrite is a light etching phase marked 'A' in Fig. V-25. The sample was examined by electron probe microanalyser, which clearly showed that the dendrite is a lead rich phase of uniform composition (Fig. V-26) and the regular shaped white area marked 'A' is nearly pure antimony.

V-8-B LEAD-TIN EUTECTIC

The alloy was solidified at a heat transfer coefficient of $26 \text{ Btu/ft}^2 \cdot \text{hr.} \cdot \text{°F}$, after 5 minutes the value of the heat transfer coefficient was increased to $40.0 \text{ Btu/ft}^2 \cdot \text{hr.} \cdot \text{°F}$. The structure near the base showed some lead rich dendrites in a matrix of lead-tin eutectic (Fig. V-27). The change in structure produced by changing from slow cooling to fast cooling conditions is also shown in Fig. V-27.

Near the top of the ingot a lamellar eutectic was observed with no lead rich dendrites (Fig. V-28).

In the case of the eutectic prepared from high purity metals, no dendritic structure was observed (Fig. V-29). The grains were observed to lie in the heat flow direction, though the size of the grains increased from 0.1 inches at the base to 0.5 inches at the top of the ingot. The lamelle width was determined from microprobe analysis and was found to be about 2-3 micron. In view of the oriented structure produced, the standard tensile strength specimen were prepared along and across the heat flow direction. The results obtained are given in Appendix V. To study the effect of orientation on the progress of solidification and the strength of the alloy, the apparatus was vibrated by using an eccentric motor. The randomly oriented structure was produced in the first $1\frac{1}{4}$ inches from the base (Fig. V-29), while beyond this the structure was oriented along heat flow direction. No effect on

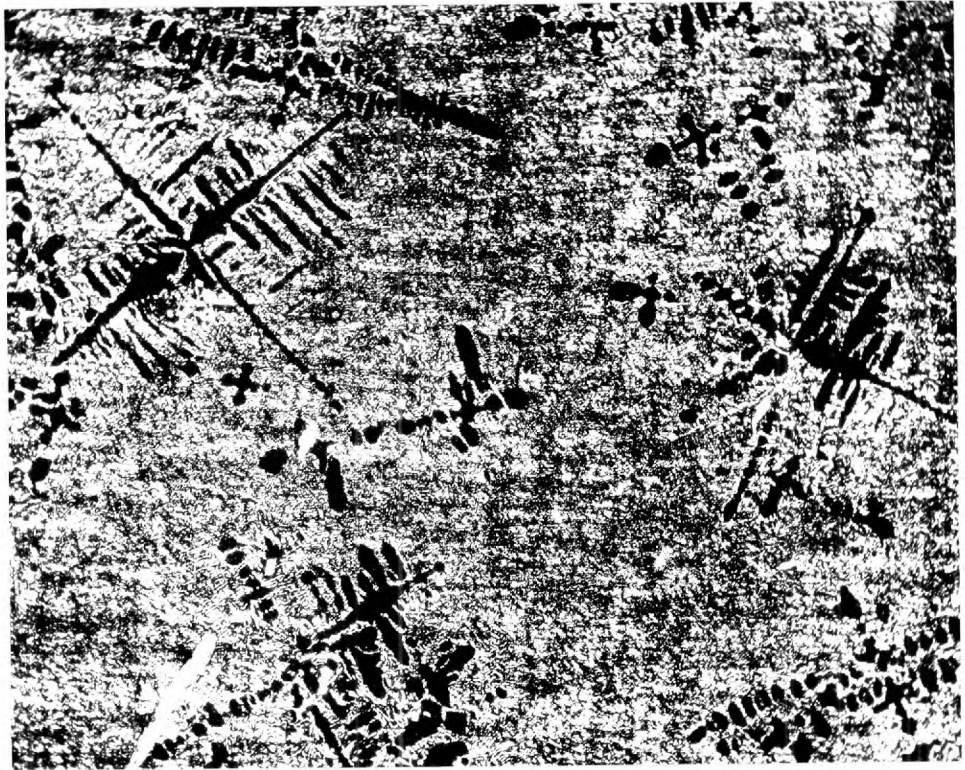


Fig. V-24 MICROPHOTOGRAPH OF LEAD-ANTIMONY EUTECTIC

Alloy:- Lead-Antimony Eutectic (commercial purity)

Distance from base: 0.5 inch

Cooling conditions: Zero-superheat
 $h = 40 \text{ Btu/ft}^2 \cdot \text{hr} \cdot ^\circ\text{F}.$

Plane of the section: Normal to heat flow

Phases: Dendritic: Lead rich solid solution of lead and antimony

Matrix: Lead-Antimony Eutectic.

Etchant: 5% Nital

Magnification: 64

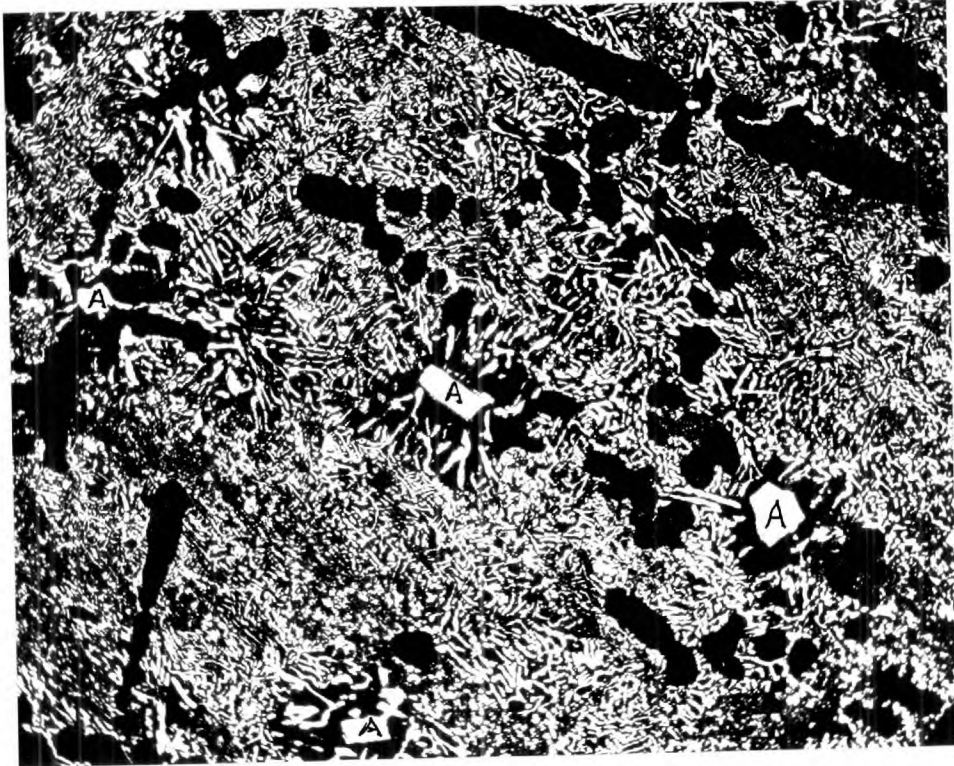


Fig. V- 25 MICROPHOTOGRAPH OF LEAD ANTIMONY EUTECTIC

Alloy: Lead-Antimony Eutectic (commercial)

Distance from base: $1\frac{1}{2}$ inches

Cooling Conditions: Zero-superheat
 $h=40 \text{ Btu/ft}^2 \cdot \text{hr.}^\circ\text{F.}$

Plane of the section: Normal to heat flow

Phases: Dendrite: lead rich solid solution of
lead and antimony

Matrix: Lead-antimony eutectic

Region 'A' - Antimony rich phase

Etchant: 5% Nital

Magnification: 180

Area Marked 'A' in Fig.V-25

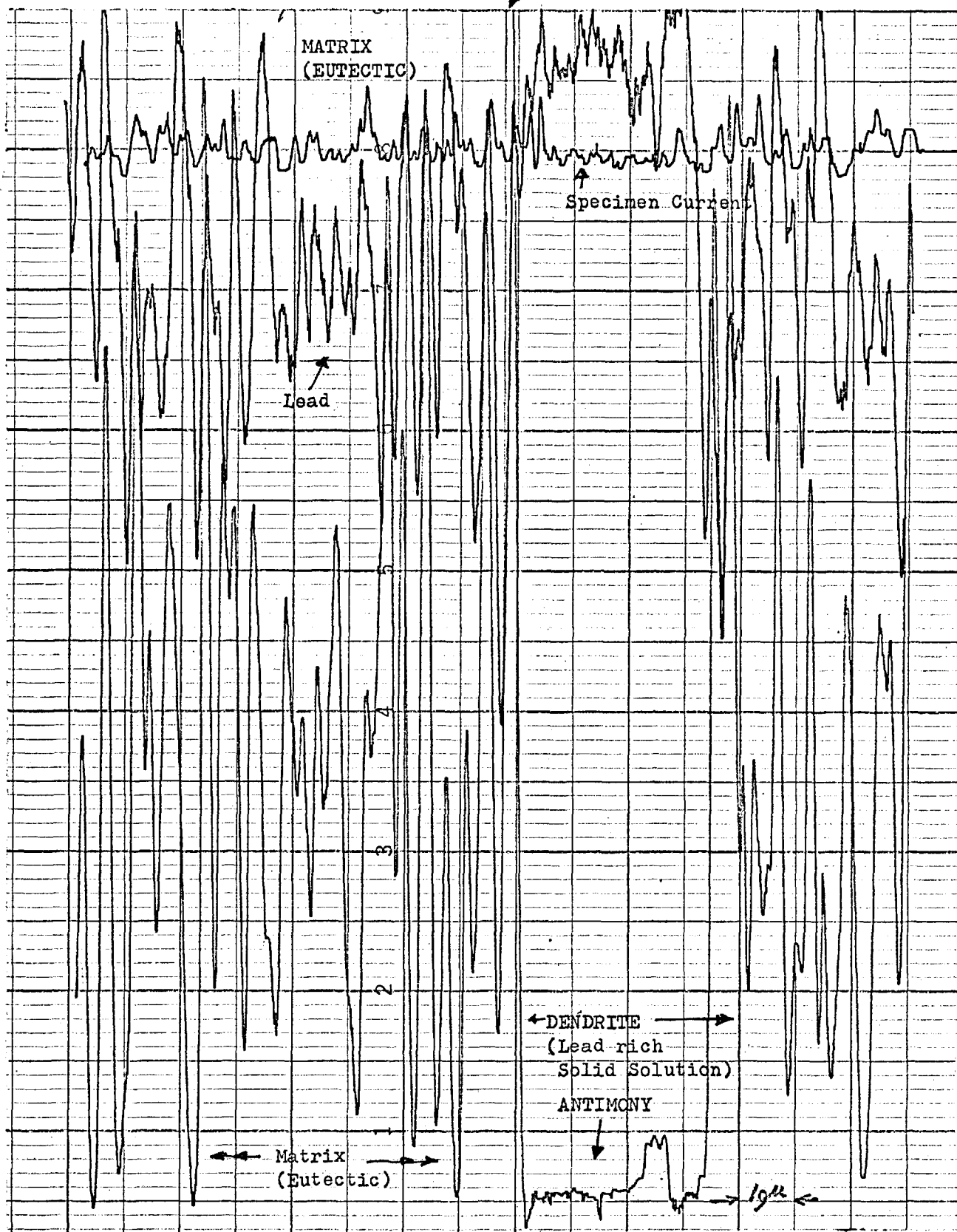


Fig.V-26 ,ELECTRONE PROBE MICROANALYSER CHART SHOWING DISTRIBUTION OF LEAD AND ANTIMONY IN LEAD-ANTIMONY EUTECTIC

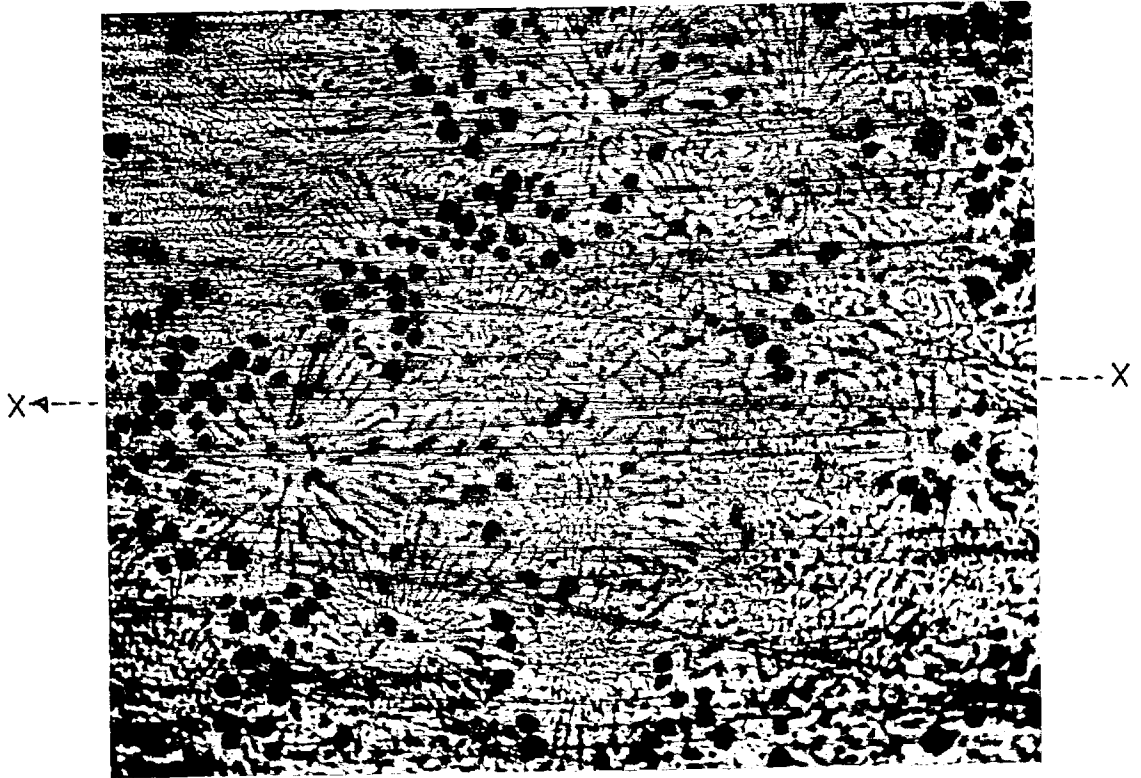


Fig. V- 27 MICROPHOTOGRAPH OF LEAD-TIN EUTECTIC

Alloy: Lead-Tin Eutectic (commercial purity)

Distance from base: 2.5 inches

Cooling Conditions: Zero-superheat
heat transfer coefficient
changed from 28 to 40
Btu/ft².hr.°F.

Plane of the section: Along heat flow X --->X

Phases: Dendrites-Lead rich solid solution

Matrix: Eutectic .

Etchant: 1 part acetic acid, 1 part nitric acid
4 parts glycerol.

Magnification: 60

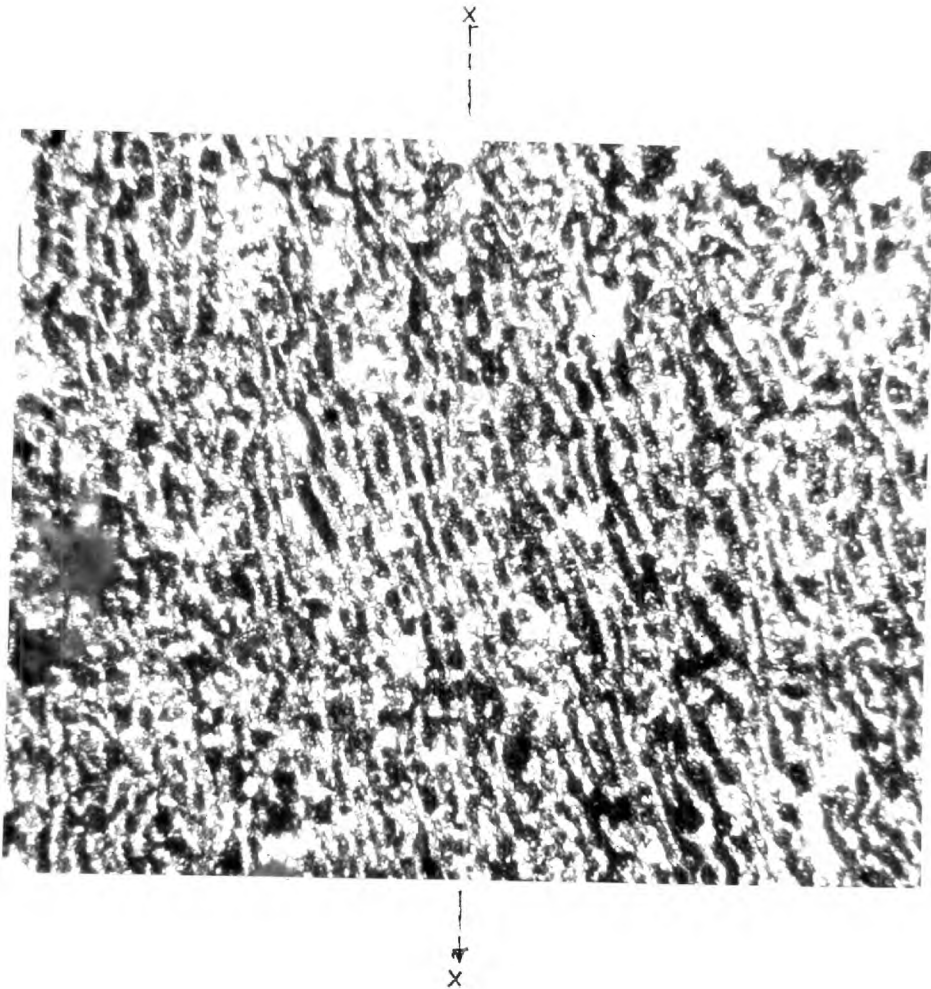


Fig. V-28 MICROPHOTOGRAPH OF LEAD-TIN EUTECTIC

Alloy: Lead-Tin eutectic (commercial)

Distance from base: $3 \frac{3}{4}$ inches

Cooling Conditions: Zero-superheat
 $h = 40 \text{ Btu/ft}^2 \cdot \text{hr.}^\circ\text{F}$

Plane of the section: Along heat flow $x \dashrightarrow x$

Phase: Eutectic

Etchant: 1 part acetic acid, 1 part nitric acid,
4 parts glycerol

Magnification: 320

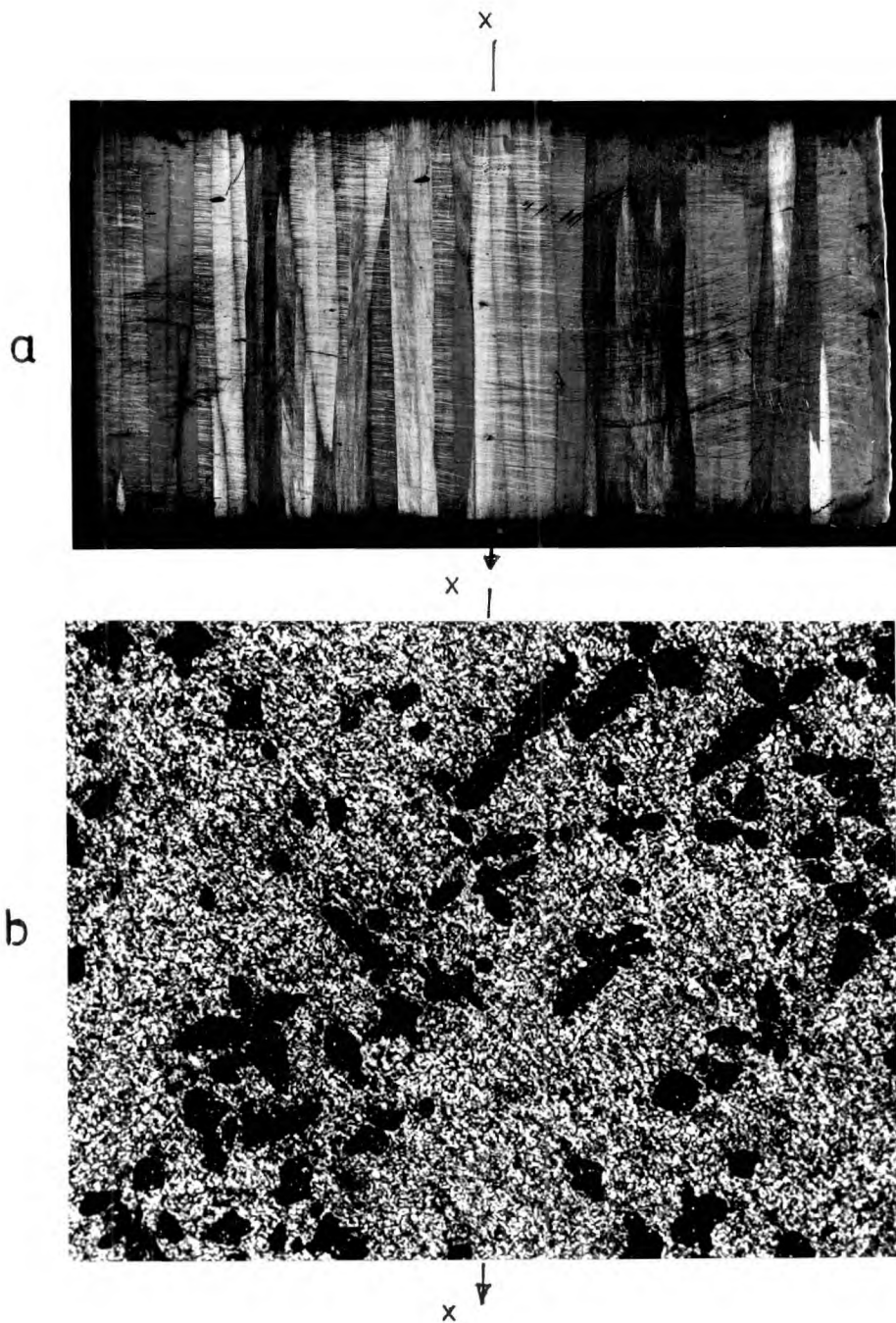


Fig. V-29 MICROPHOTOGRAPH OF LEAD-TIN EUTECTIC

Alloy: Lead-Tin eutectic (pure)

Cooling conditions: Zero-superheat,
 $h = 40 \text{ Btu/ft.}^2 \text{ hr.}^\circ\text{F}$

Plane of section: Along heat flow $x \rightarrow$

Etchant: 1 part acetic acid, 1 part nitric acid,
4 parts glycerol

(a) $1\frac{1}{2}$ inches from base. Grains oriented in heat flow direction. Magnification-4

(b) 1 inch from base. Vibrator was used during solidification. Matrix eutectic and lead dendrites. Magnification-120

the progress of solidification was noticed. The tensile strength of the specimen is given in Appendix V.

V-8-C LEAD-TIN ALLOY 20 WT. % IN (Pb-20-Sn)

Commercial purity lead-tin alloys containing 20 wt. % were solidified in the stainless steel crucible at zero superheat as discussed in section V-8. The structures obtained are shown in Fig. V-30 and Fig. V-31. The structure shows the oriented dendrites of primary lead rich solid solution (dark etching) and the matrix of lead-tin eutectic (light etching). The experiments were repeated with alloys prepared from high purity metals, using fiberfrax-resin coated stainless steel crucible. On polishing the samples it was found that the first $\frac{3}{4}$ inches of the sample consisted of a dark etching constituent, while the rest of the sample was a light etching ~~phase~~^{area}. The relative position of the two ~~phases~~^{areas} in the ingot is shown schematically in Fig. V-32. The microphotographs of the two ~~phases~~^{area} are shown in Fig. V-33 and Fig. V-34. The light etching ~~phase~~^{are} consists of random oriented lead rich dendrites and a eutectic matrix. The dark etching ~~phase~~^{area} could not be resolved. By taking an electron probe trace along x-x axis marked in Fig. V-33, it was established that the dark etching ~~phase~~^{area} is of uniform composition (Fig. V-35). When the experiment was repeated using a fiberfrax-resin and graphite coated crucible as discussed in section IV-1-A(i) only some areas showed the dark etching ~~phase~~^{area} (Fig. V-34(b)). When the experiment was performed using fiberfrax-resin-alumina coated stainless crucible no such dark etching ~~phase~~^{area} was observed. Oriented dendrites up to one inch from the base of the crucible ^{were observed} but higher up the dendrites were oriented at random. Fig. V-36 showed the growth of dendrites from the base onwards and it can be seen that oriented structure has broken (Fig. V-36⁽³⁾) and Fig. V-36⁽⁴⁾ shows complete random oriented structure.

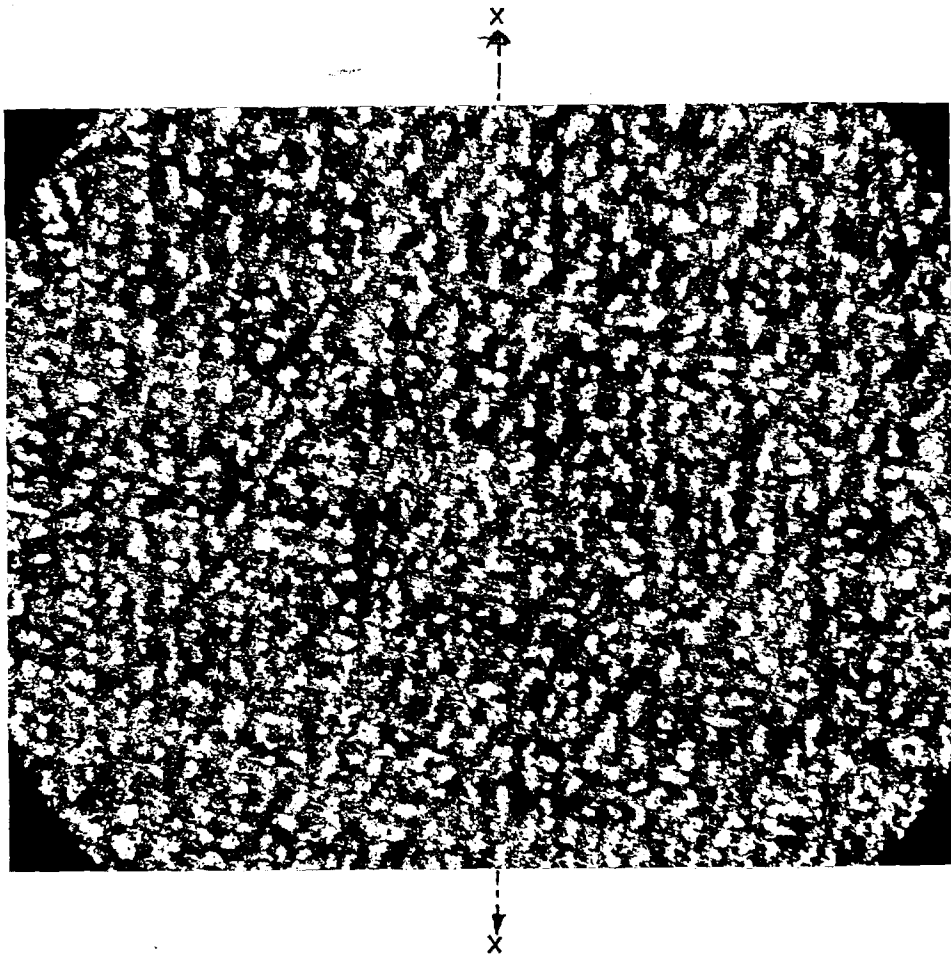


Fig. V-30 MICROPHOTOGRAPH OF 20 WT. % TIN LEAD-TIN ALLOY

Alloy: 20 Wt. % Tin Lead-Tin alloy (commercial)

Distance from base: 1 inch

Cooling Conditions: Zero-superheat
 $h = 40 \text{ Btu/ft}^2 \cdot \text{hr.}^\circ\text{F}$

Plane of the section: Along heat flow $x \rightarrow x$

Phases: White - tin rich phase
Dark - lead rich phase

Etchant: 2% Nital

Magnification: 60

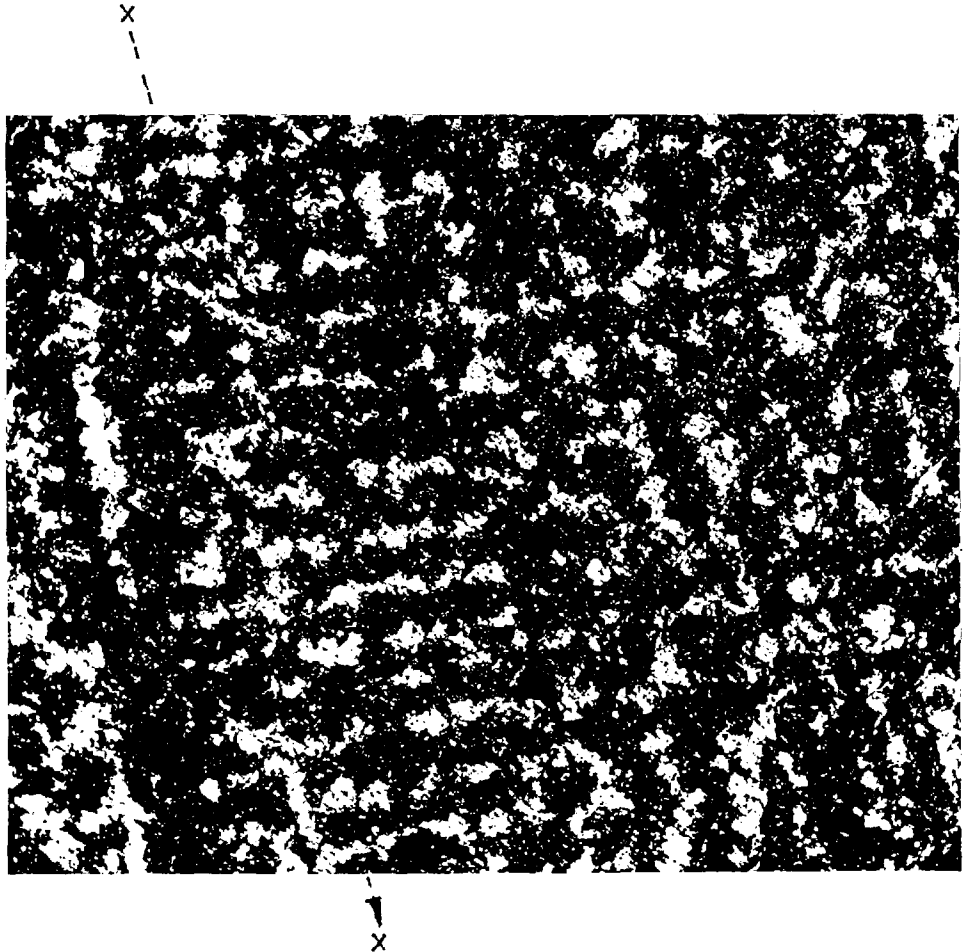


Fig. V-31 MICROPHOTOGRAPH OF 20 WT. % TIN LEAD-TIN ALLOY

Alloy: 20 Wt. % Tin Lead-Tin (Commercial)

Distance from base: $2\frac{1}{2}$ inches

Cooling Conditions: Zero-superheat
 $h = 40 \text{ Btu/ft}^2 \cdot \text{hr.}^\circ\text{F.}$

Plane of the section: Along heat flow $x \rightarrow x$

Phases: White - tin rich
Dark - lead rich

Etchant: 5% Nital

Magnification: 180

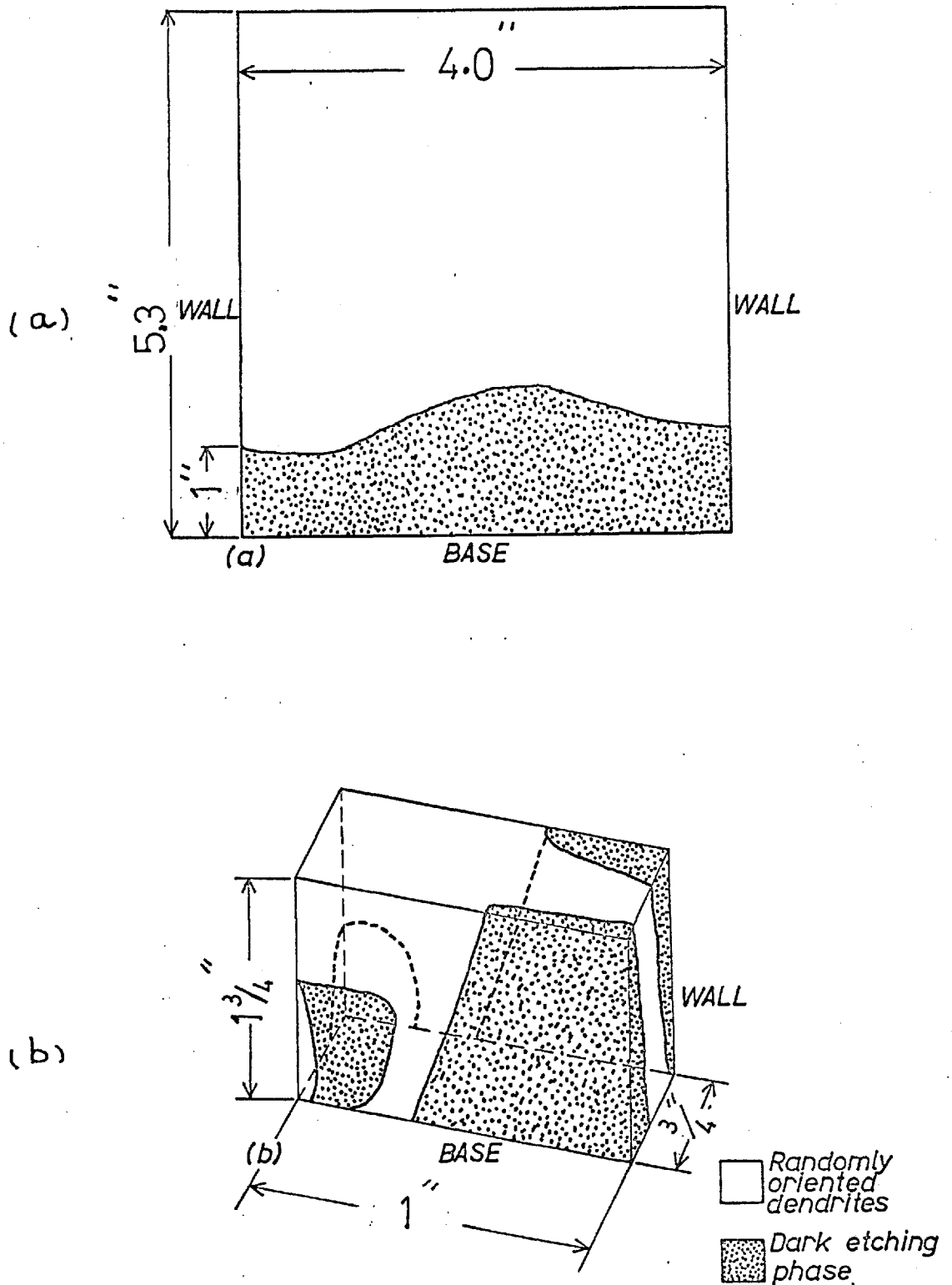


Fig.V-32 DIAGRAMATIC REPRESENTATION OF TWO PHASE STRUCTURES OBTAINED

(a) using fiberfrax and resin coated crucible
 (b) using fiberfrax - resin and graphite coated crucible

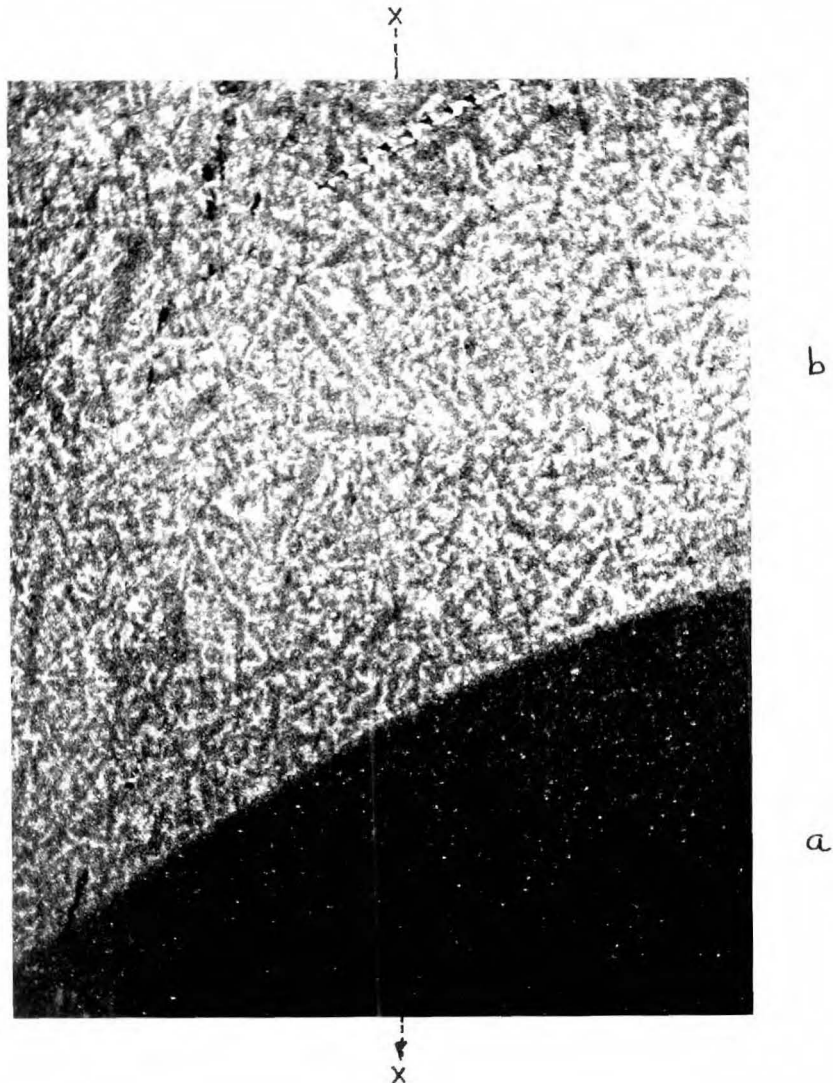


Fig. V-33 MICROPHOTOGRAPH OF 20 WT. % TIN LEAD-TIN ALLOY

Alloy: 20 Wt. % Tin Lead-Tin Alloy (pure)

Distance from base: $\frac{1}{2}$ inch

Cooling conditions: Zero-superheat
 $h = 40 \text{ Btu/ft}^2 \cdot \text{hr.}^\circ\text{F.}$

Crucible: Fiberfrax-resin stainless steel

Plane of the Section: Along the heat flow $x \cdots \rightarrow x$

Phases: Dark ~~phase~~^{area} (a) lead rich solid solution
Light: Random oriented
(b) dendrites of lead rich phase
in a matrix of eutectic

Etchant: 5% Nital

Magnification: 80

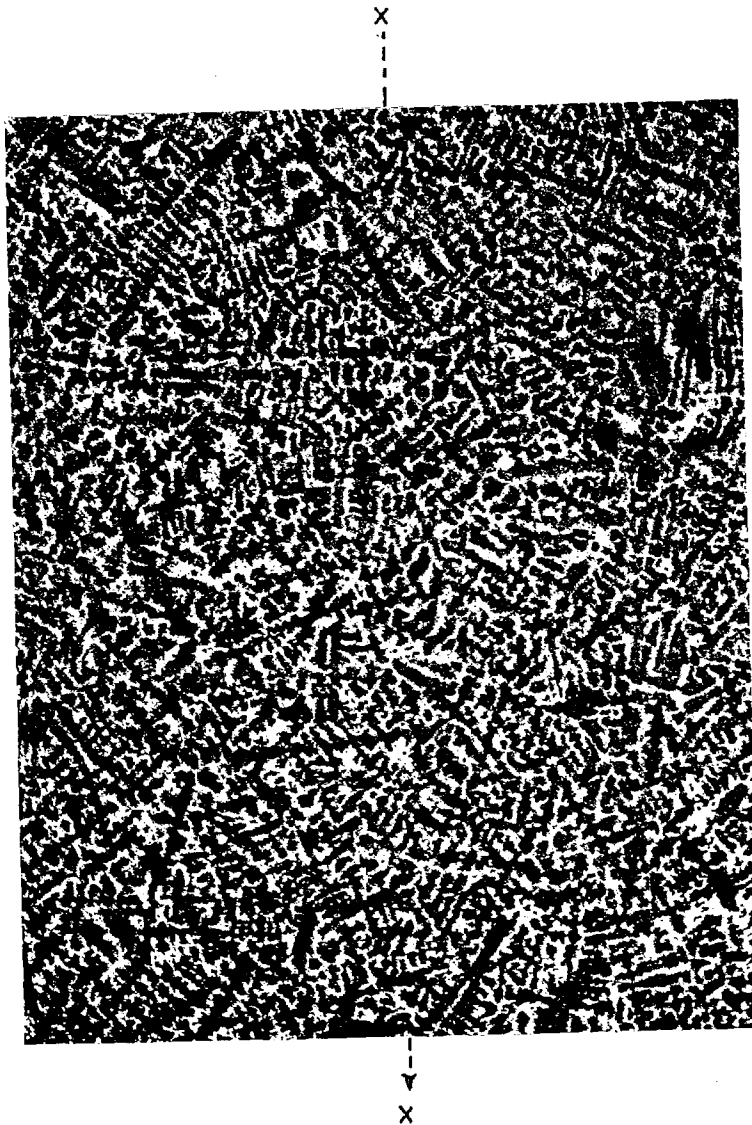


Fig. V-34 MICROPHOTOGRAPH OF 20 WT. % TIN LEAD-TIN ALLOY
Alloy: 20 wt. % Tin Lead-Tin (pure)
Distance from base: $2\frac{1}{2}$ inches
Cooling conditions: Zero-superheat
 $h = 40 \text{ Btu/ft}^2 \cdot \text{hr.}^\circ\text{F}$
Crucible: Fiberfrax-resin coated stainless steel
Plane of the section: Along the heat flow $x \rightarrow x$
Phases: Random oriented dendrites (dark phase)
in a matrix of eutectic
Etchant: 5% Nital
Magnification: 80

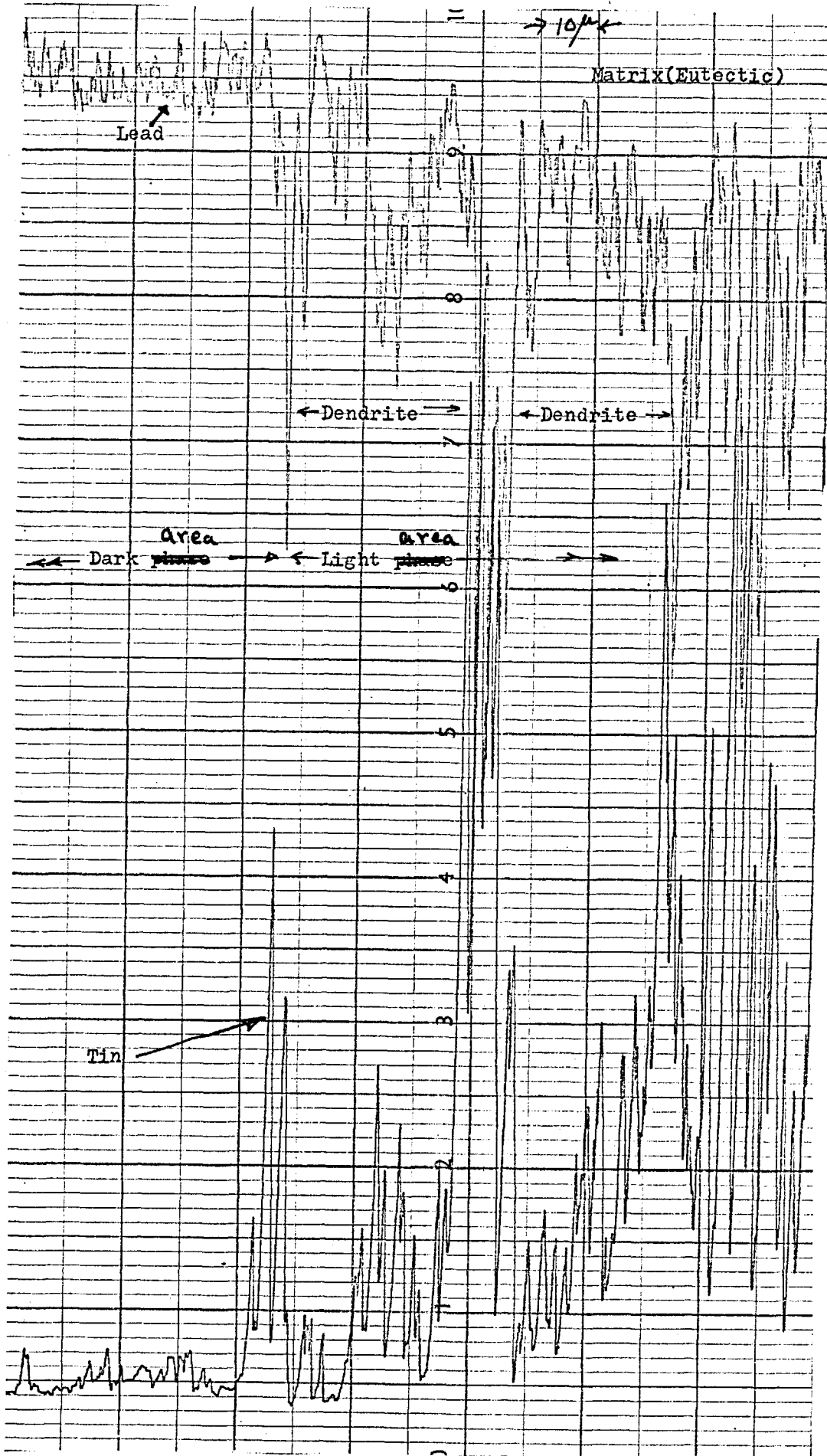
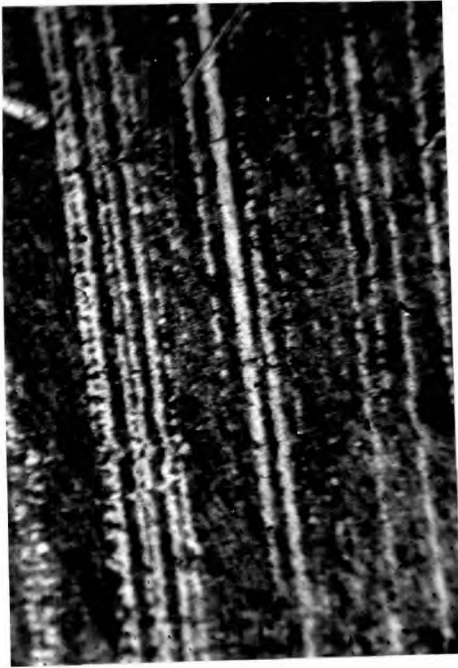
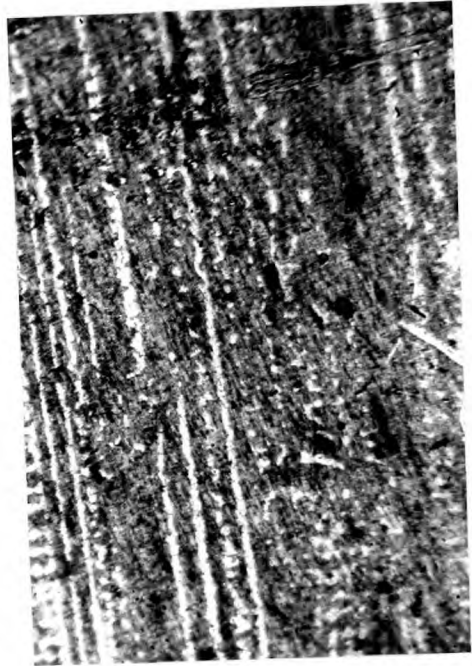


Fig.V-35 ELECTONE PROBE CHART SHOWING DISTRIBUTION OF LEAD AND TIN
IN LIGHT & DARK ~~PHASES~~ ^{AREAS} OF FIG. V-34)

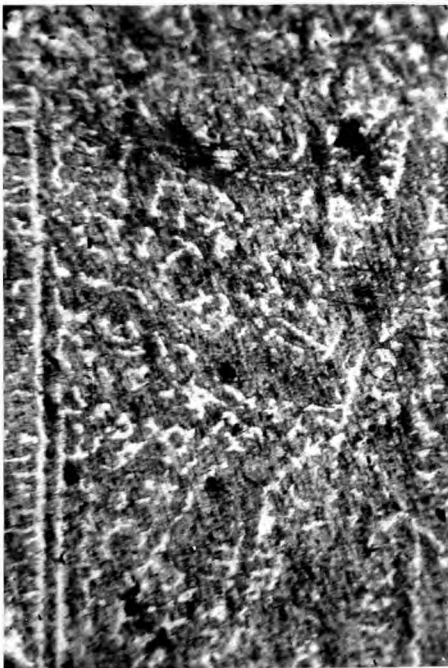
(a)



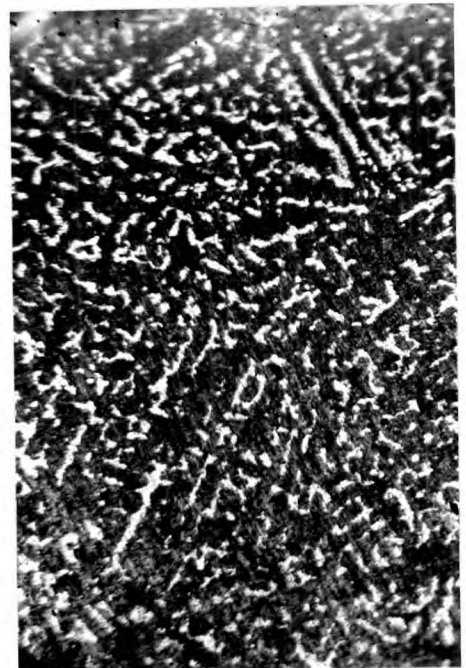
(b)



1. Base
(c)



2. (a)
(d)



3. (b)

4. (c)

Fig. V-36 MICROPHOTOGRAPHS OF 20 WT. % TIN LEAD-TIN ALLOY (pure) Showing the breakdown of dendrites with distance. Dendrites grow from base (a)-(b)-(c) to (d). Heat flow along the length of the section. Fiberfrax-resin alumina coated stainless steel crucible $h = 40 \text{ Btu/ft}^2 \cdot \text{hr.}^\circ\text{F}$. 5% Nital. Etched. Magnification = 80

V-8-D TIN-LEAD ALLUOY - 20 wt. % LEAD (Sn-20-P)

As discussed in section V-8-C oriented dendrites were obtained by using fiberfrax-resin-alumina coated stainless steel crucible. The alloy was solidified at zero superheat, at a heat transfer coefficient value of 40 and the structures obtained are shown in Fig. V-37 to V-39. Fig. V-37 shows that a small proportion of the metal at the base is of eutectic composition later giving rise to a random oriented dendritic structure. After a short distance an oriented structure grows out of the random structure, and then extends to the top of the crucible. The dendrites are of a tin rich phase and the matrix is of eutectic composition. Fig V-38 and Fig V-39 clearly show the oriented dendrites and the matrix. The solute segregation was studied by electron probe microanalyser. A typical count chart obtained is shown in Fig V-40. The dendrites were found to be of uniform composition both along and normal to heat flow direction. The dendritic composition near the base and the top of the ingot was nearly the same. An attempt was made to determine the fraction of matrix (eutectic) at various distances from the base by using the Qantimet image analyser. The fraction of matrix was found to be within $40\% \pm 10$ and no correlation with distance was observed.

To determine the shape of the dendrite, as discussed in section IV-8, four holes were drilled and the sample polished and photographed after every successive polishing. The starting structures are shown in Figs. V-41 and 42 and some of the structures obtained after polishings are shown in Fig V-43. The possible shape of the dendrites was determined from these sections and it is shown in Fig. V-44.

After the pour out study of the alloy, the surface was photographed (Fig V-45) and the microphotograph is shown in Fig V-46. The surface of the sample was found

to be plain. When the sample was examined using a Stereoscan microscope, the suggested shape of the dendrite seemed to be confirmed. A typical picture is given in Fig. V-47.

V-8-E TIN-LEAD ALLOY - 10 WT. % LEAD (Sn-10-Pb)

Using the fiberfrax-resin coated crucible, a 10 wt. % lead alloy was solidified at zero superheat. The structures obtained are shown in Fig. 50-51. The structures are randomly oriented and are of irregular shape. When the samples were examined by electron probe microanalyser the dendrites were found to be of uniform composition (1.5 wt. % lead) both along and normal to heat flow direction. The matrix is of eutectic composition. Fig. V-52 shows the count chart obtained. An attempt was made, using the Quantimet micro image analyser, to determine the fraction of matrix as a function of distance from the crucible base. The volume of the matrix was found to be 20% \pm 10%.

V-9 EFFECT OF MORPHOLOGY ON THE PROGRESS OF SOLIDIFICATION

As reported in section V-8-C, 20 wt. % lead, tin-lead alloy solidifies in an oriented dendritic morphology (Fig. V-37-39). In order to study the effect of morphology on the progress of solidification this alloy was solidified while the apparatus was vibrated, an eccentric motor being fitted to the crucible support. The resulting microstructures are shown in Fig. V-48 and V-49. They indicate that the vibrations were enough to break down the orientated structure and, in fact, the whole ingot consisted of randomly oriented dendrites. The corresponding results in the case of lead-tin eutectic alloy have been described in section V-8-B. In both cases, it was found that thermal analysis curves obtained under specific heat transfer conditions were unaffected by the vibrations.

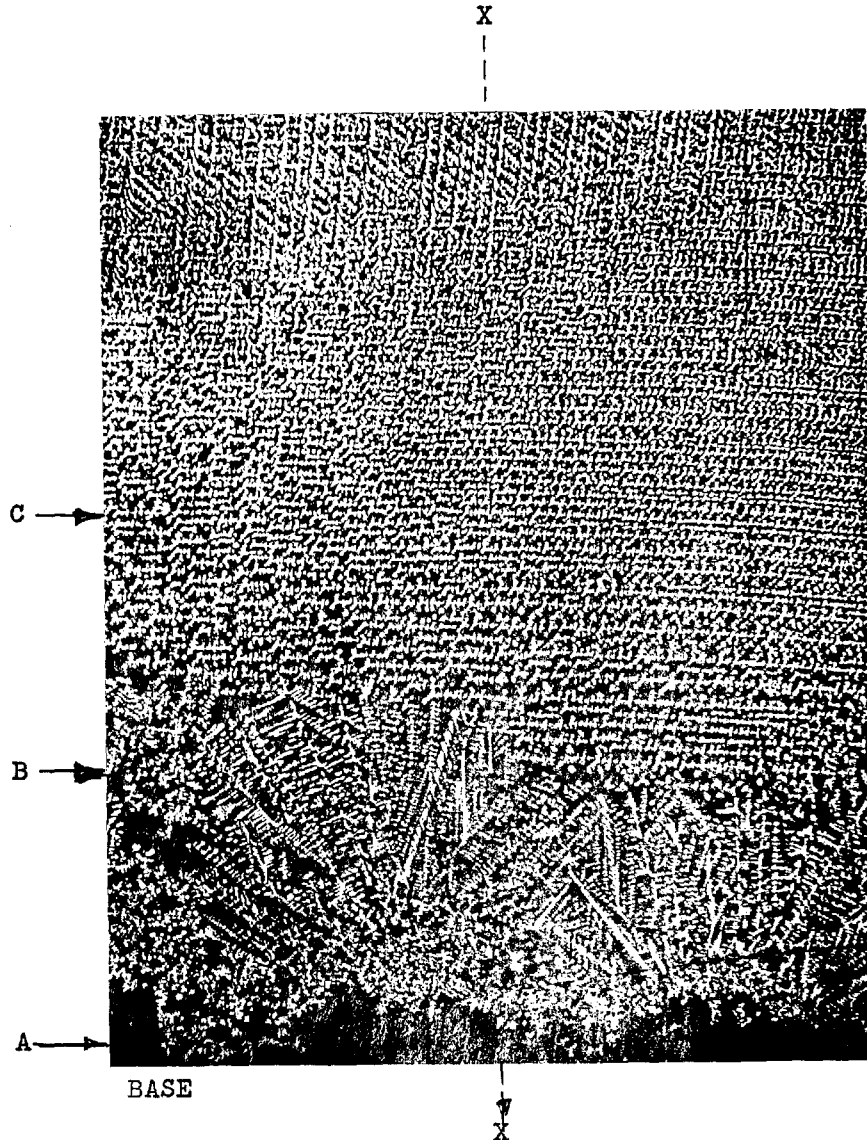


Fig. V-37 MICROPHOTOGRAPH OF 20 WT. % LEAD TIN-LEAD ALLOY
Alloy: 20 wt. % Lead Tin-Lead (Pure) (Pure)
Cooling conditions: Zero-superheat
 $h = 40 \text{ Btu/ft}^2 \cdot \text{hr.}^\circ\text{F}$
Plane of the section: Along heat flow $x \text{---} \rightarrow x$
Phases: Region 'A' - Eutectic
Region 'B' Random oriented dendrites
of tin
Region 'C' Oriented dendrites of tin
Matrix: Eutectic
Etchant: Electrolytic, 1 part orthophosphoric
acid, 3 parts methyl alcohol
Magnification: 20

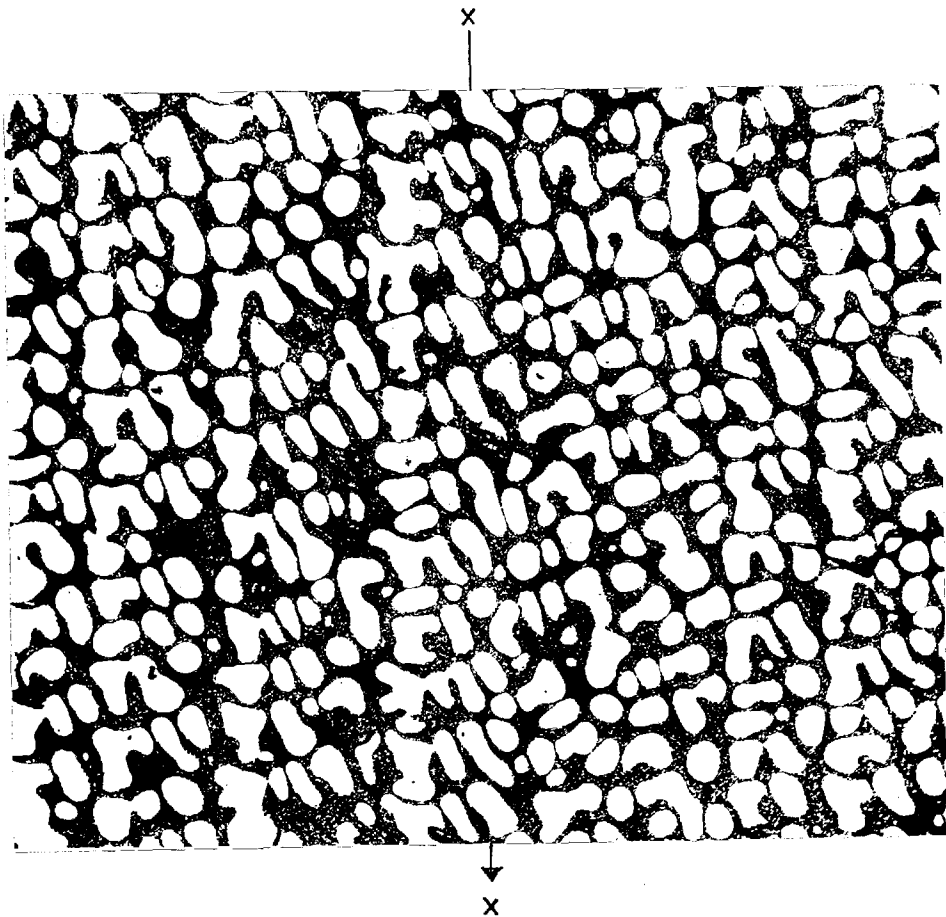


Fig. V-38 MICROPHOTOGRAPH OF 20 WT. % LEAD TIN-LEAD ALLOY
Alloy: 20 wt. % lead tin-lead alloy (pure)
Distance from base: $\frac{1}{2}$ inch
Cooling Conditions: Zero-superheat
40 Btu/ft².hr.°F.
Crucible: Fiberfrax-resin-alumina coated
Plane of the section: Along heat flow x→x
Phases: Tin dendrites oriented along the heat flow
direction
Matrix: Eutectic
Etchant: Electrolytic etching
Magnification: 120

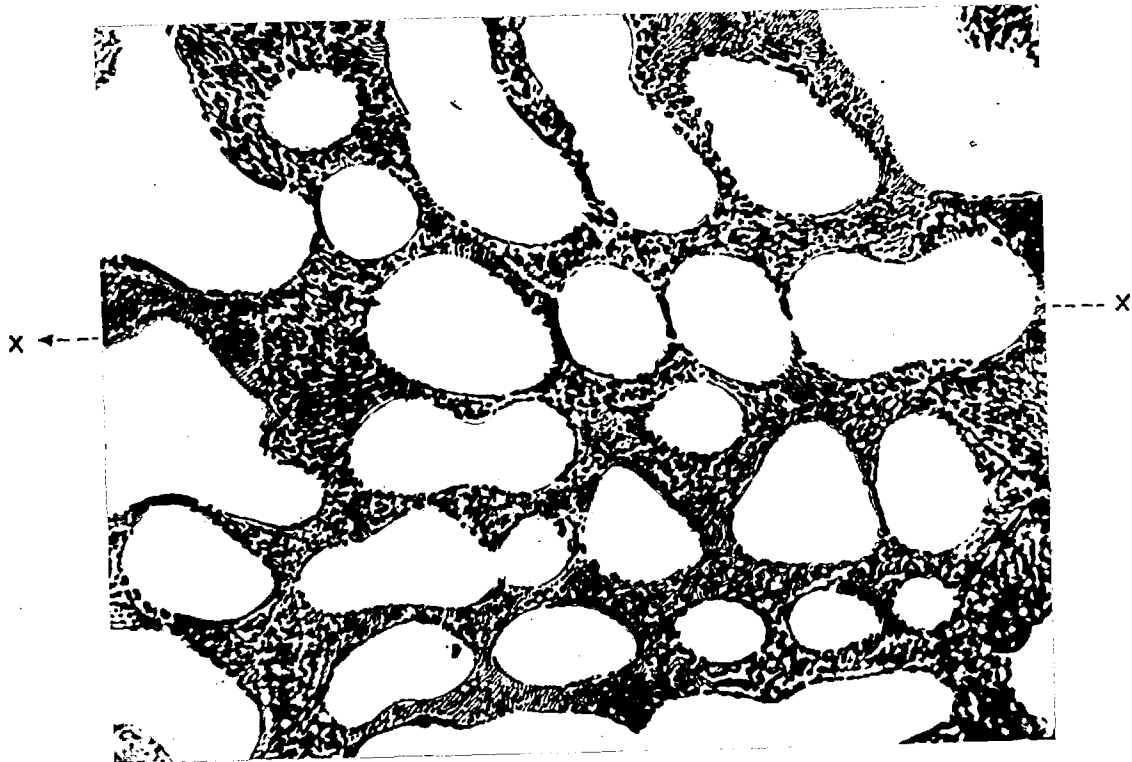


Fig. V-39 MICROPHOTOGRAPH OF 20 WT. % LEAD TIN-LEAD ALLOY

Alloy: 20 wt. % lead tin-lead alloy (pure)

Distance from base: $\frac{1}{2}$ inch

Cooling conditions: Zero-superheat
 $h = 40 \text{ Btu/ft}^2 \cdot \text{hr.} \cdot ^\circ\text{F.}$

Crucible: Fiberfrax-resin-alumina coated

Plane of the section: Along heat flow x ---> x

Phases: tin dendrites

Matrix: Eutectic

Etchant: Electrolytic etching

Magnification: ~~320~~ 480

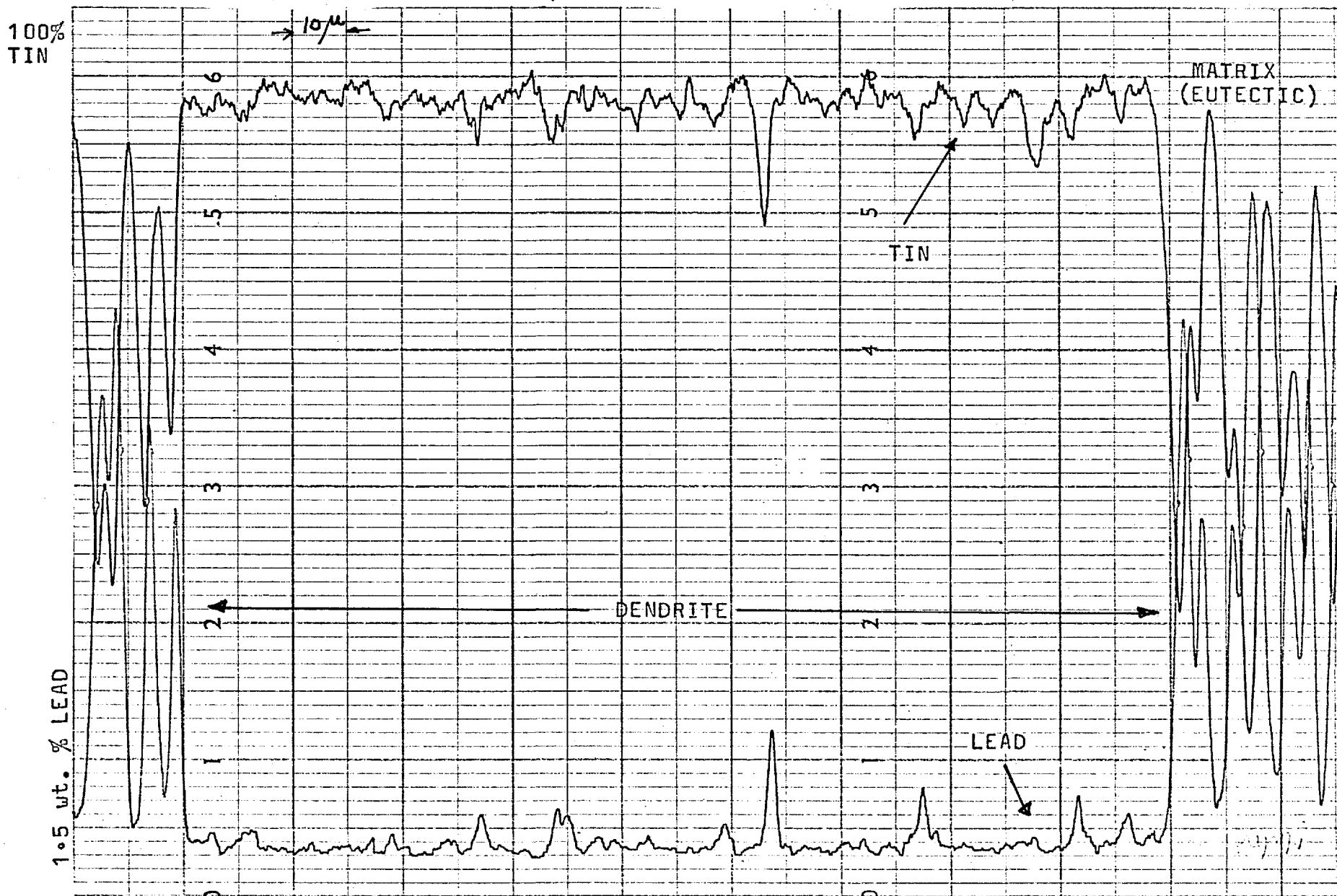


Fig. V-40 ELECTRON PROBE MICROANALYSER CHART, SHOWING DISTRIBUTION OF LEAD AND TIN IN 20 WT. % LEAD, TIN-LEAD ALLOY

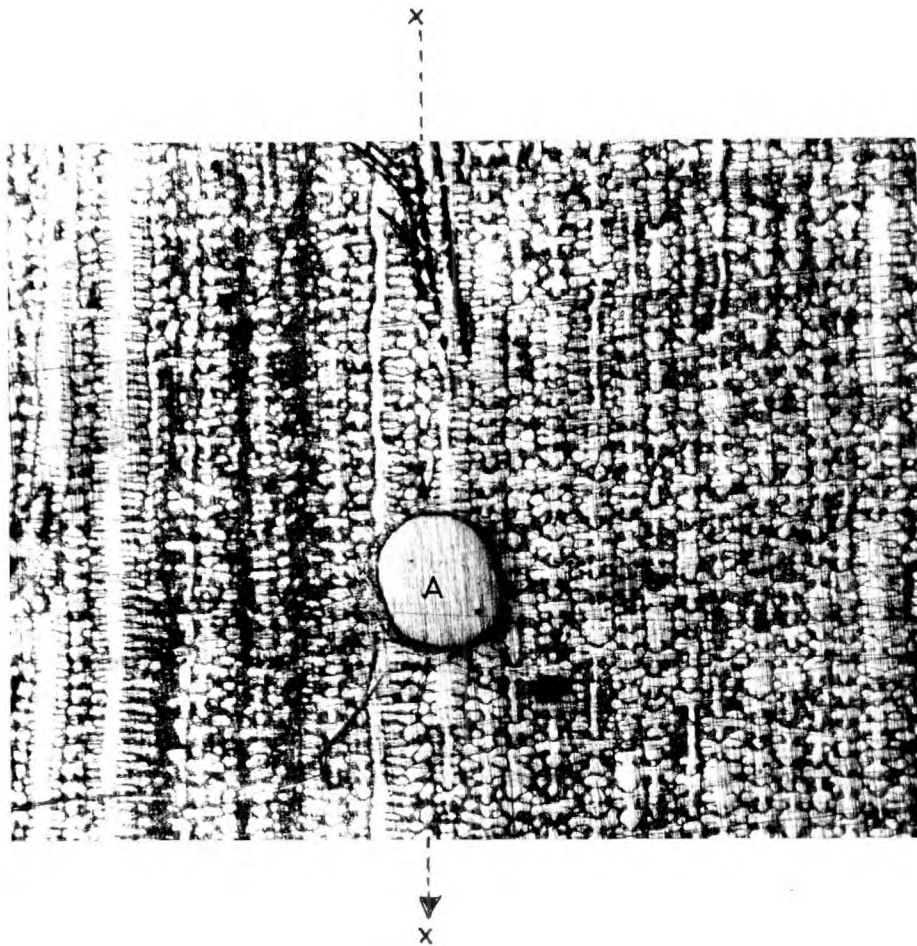


Fig. V-41 MICROPHOTOGRAPH OF 20. WT. % LEAD TIN-LEAD ALLOY

Alloy: 20 wt. % lead, tin-lead alloy (pure)

Distance from base: $\frac{1}{2}$ inch

Cooling conditions: Zero-superheat
 $h=40 \text{ Btu/ft}^2 \cdot \text{hr.}^\circ\text{F.}$

Crucible: Fiberfrax-resin-alumina coated
stainless steel

Plane of the Section: Along heat flow $x \rightarrow x$

Phases: Oriented tin dendrites in a matrix of
lead-tin eutectic. Region marked 'A'
is one of the copper wires introduced as a
marker for locating the dendrites under
study

Etchant: 5% Nital

Magnification: 40

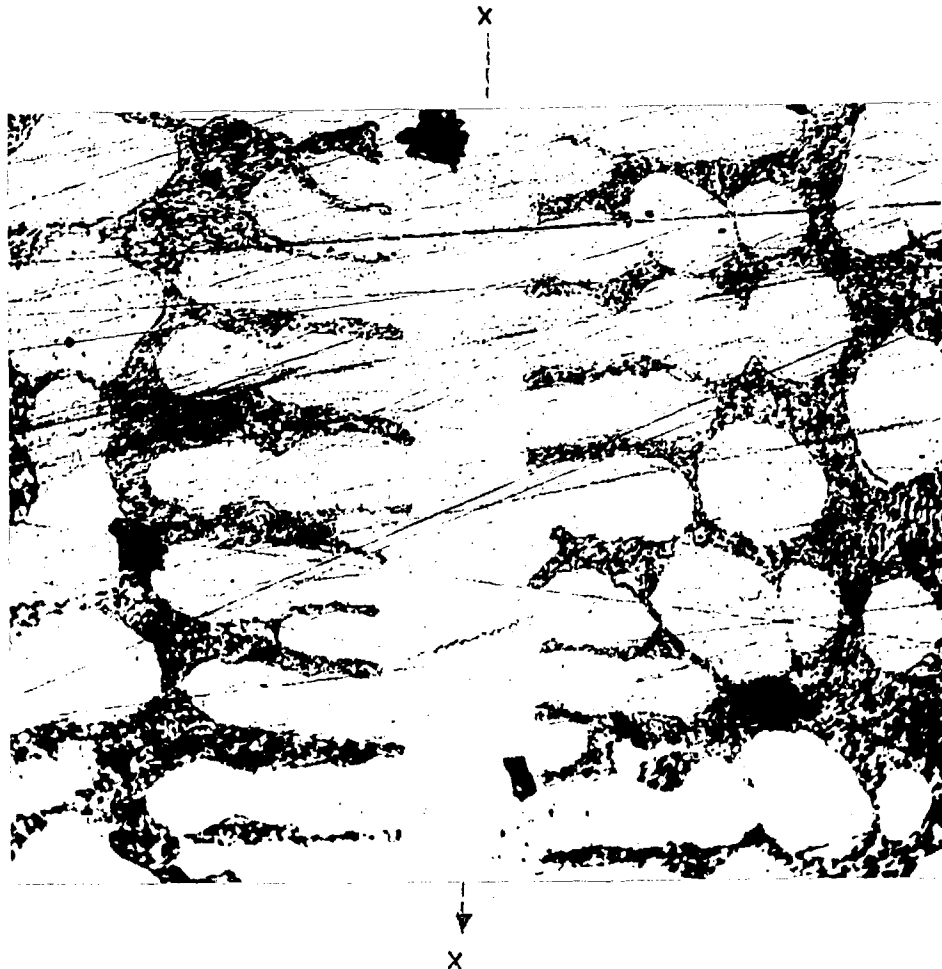


Fig. V- 42 MICROPHOTOGRAPH OF 20. WT. % LEAD TIN-LEAD ALLOY

Alloy: 20 wt. % Lead, tin-lead alloy (pure)

Distance from base: $\frac{1}{2}$ inch

Cooling Conditions: Zero-superheat
 $h=40 \text{ Btu/ft}^2 \cdot \text{hr.}^\circ\text{F.}$

Crucible: Fiberfrax-resin-alumina coated
 stainless steel

Plane of the section: Along heat flow $x \rightarrow x$

Phases: Oriented dendrite of tin in a matrix of
 eutectic. Starting dendrites under study
 for determining the shape of the dendrite

Etchant: 5% Nital

Magnification: ~~525~~ 480

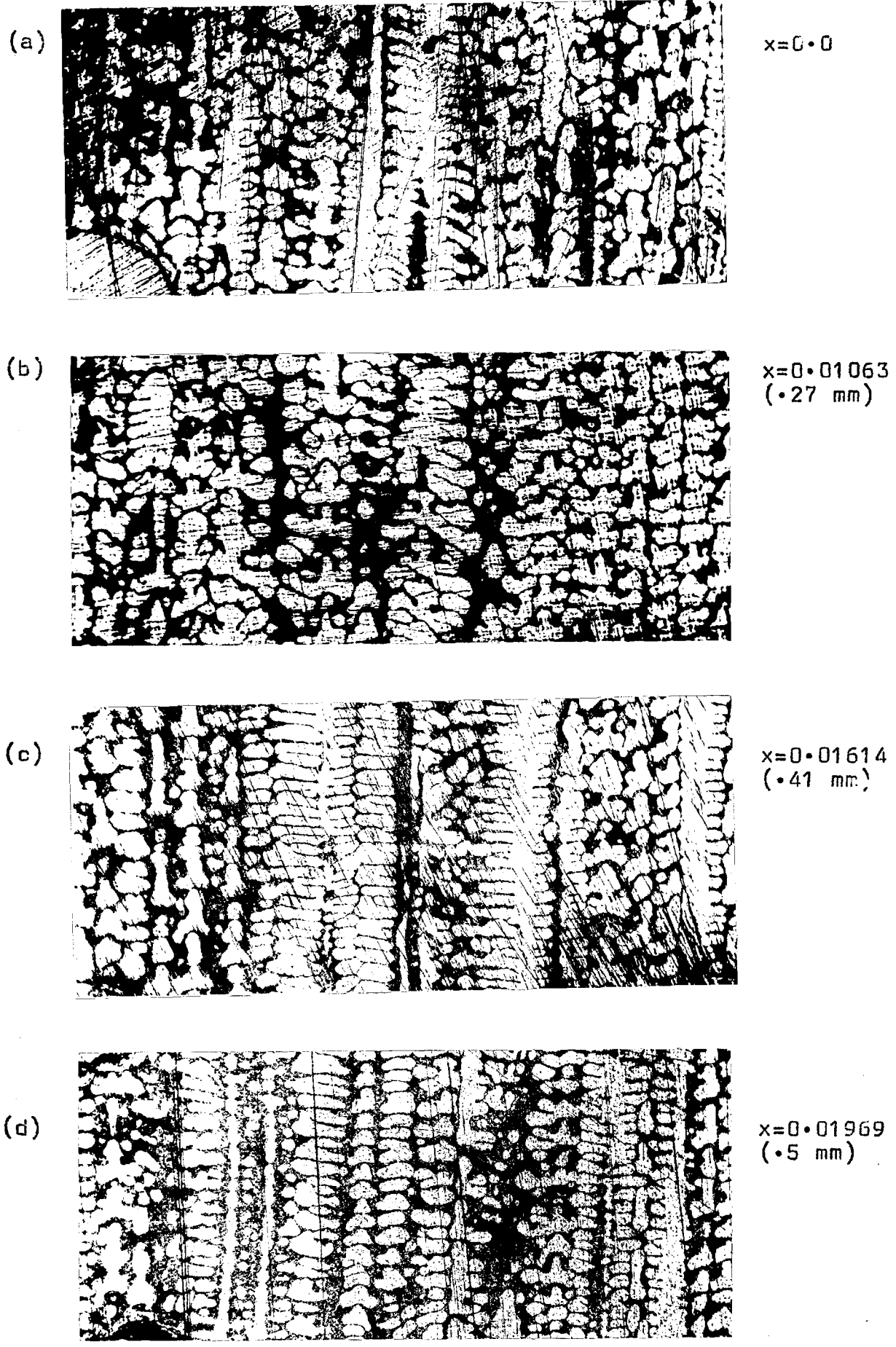


Fig. V-43 MICROPHOTOGRAPH OF 20 WT. % LEAD TIN-LEAD ALLOY
(Pure)
Microstructures obtained after removing x inches of metal.
X120

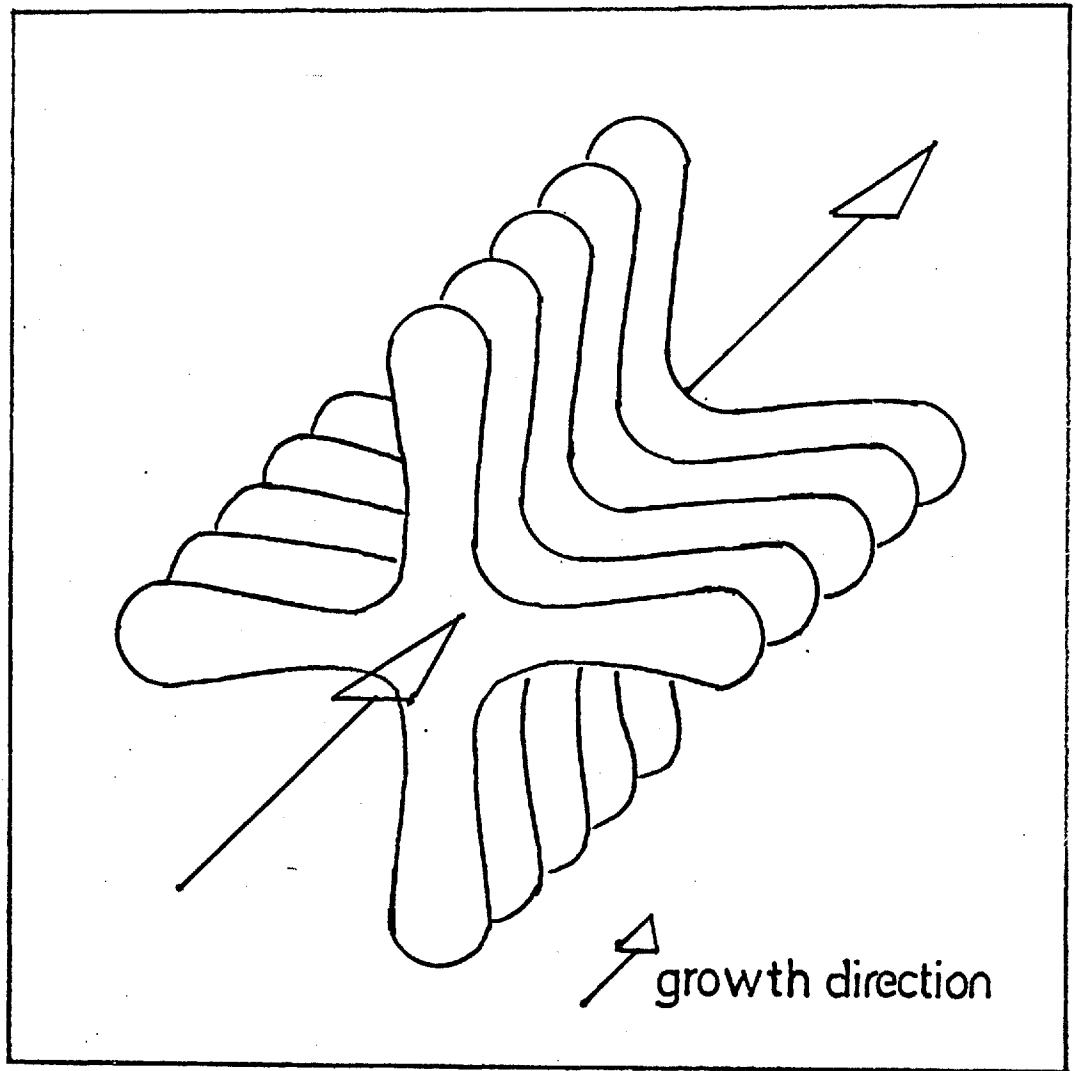


Fig. V-44 SHAPE OF DENDRITES



Fig. V-45 MICROPHOTOGRAPH OF 20 WT. % LEAD, TIN-LEAD ALLOY

Alloy: 20.0 wt. % Lead Tin-lead alloy (pure)

Distance from base: $\frac{1}{4}$ inch

Cooling Conditions: Zero-superheat
 $h=40.0 \text{ Btu/ft}^2 \cdot \text{hr.}^\circ\text{F.}$

Plane of the section: Normal to heat flow

Phases: White - tin dendrite
Dark - pour out liquid

Pour out sample photographed without preparation

Magnification: 60

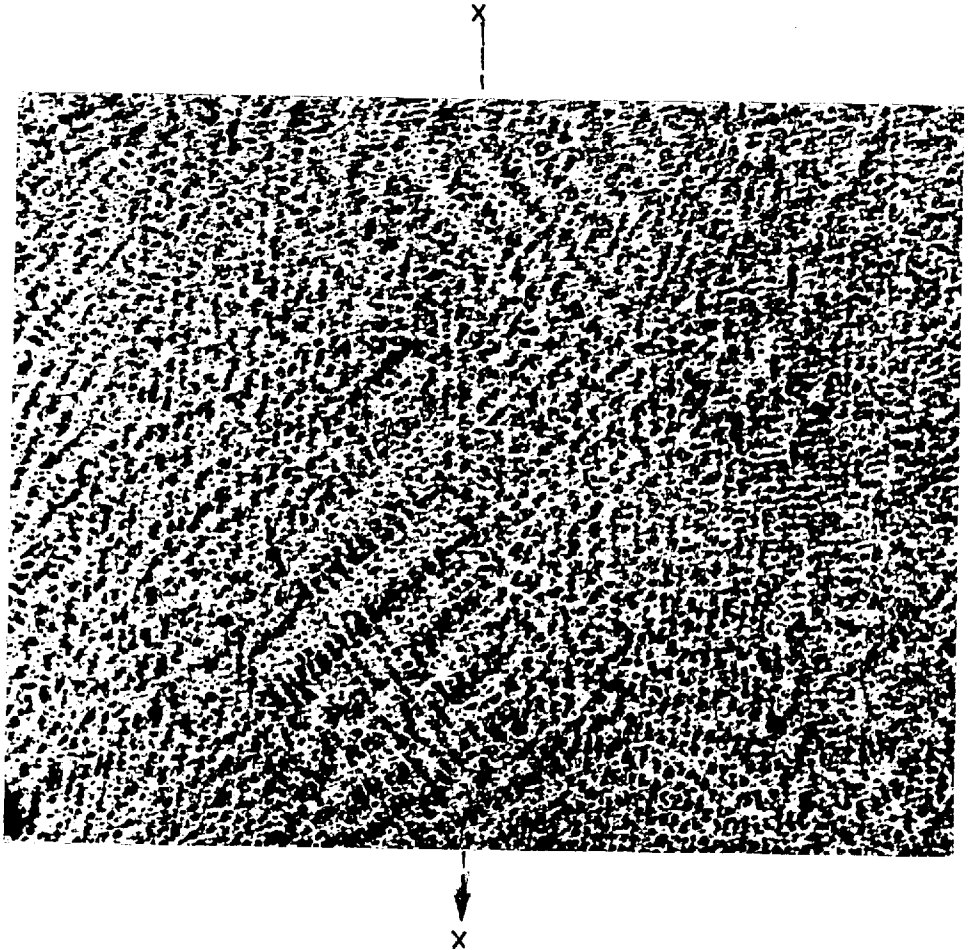


Fig. V-46 MICROPHOTOGRAPH OF 20 WT. % LEAD, TIN-LEAD ALLOY

Alloy: 20 wt. % Lead, Tin-lead alloy (pure)

Distance from base: Base marked 'B'

Cooling Conditions: Zero-superheat
 $h = 40 \text{ Btu/ft}^2 \cdot \text{hr.} \cdot ^\circ\text{F.}$

Plane of the section: Along heat flow $x \text{ --- } \rightarrow x$

Phases: White - Tin dendrites
Dark - Eutectic

Etchant: 2 % Nital

Magnification: 60

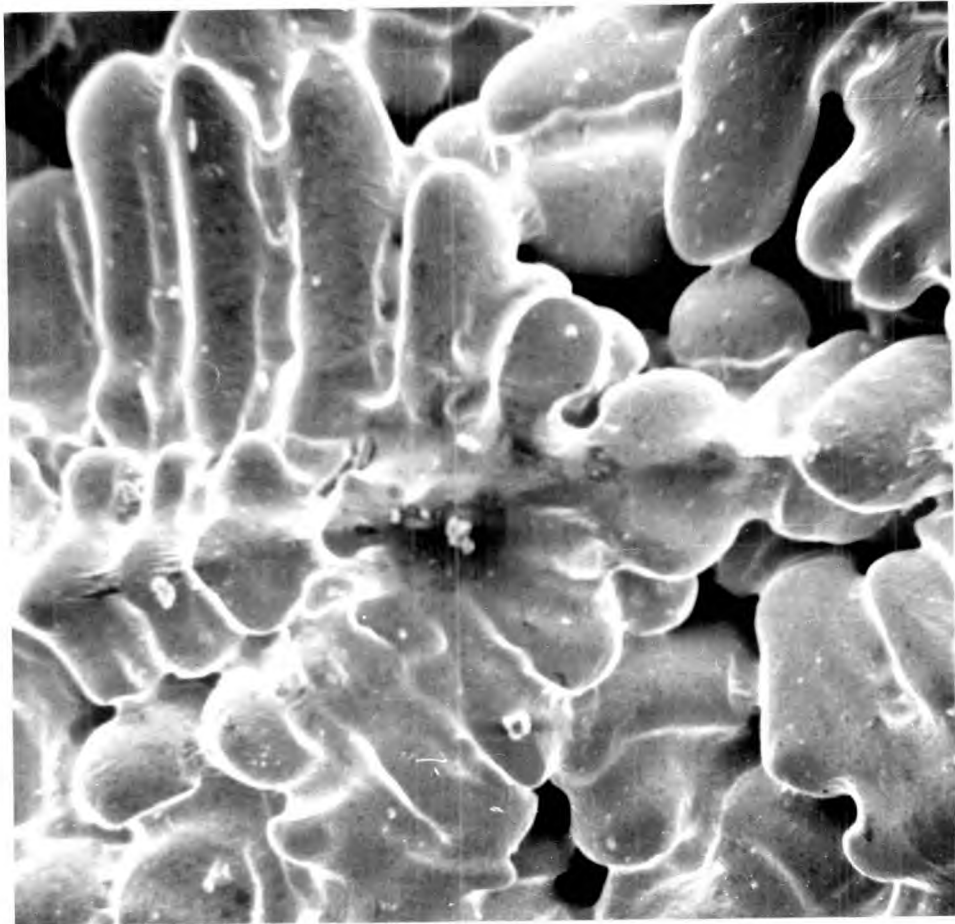


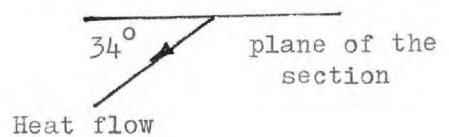
Fig. V-47 STERIO SCAN PHOTOGRAPH OF POUR OUT SAMPLE

Alloy: 20 Wt. % Lead Tin-Lead alloy (pure)

Cooling conditions: Zero-superheat
 $h = 40 \text{ Btu/ft}^2 \cdot \text{hr.} \cdot \text{°F.}$

Plane of the section: 34° to the heat flow

Magnification: 340



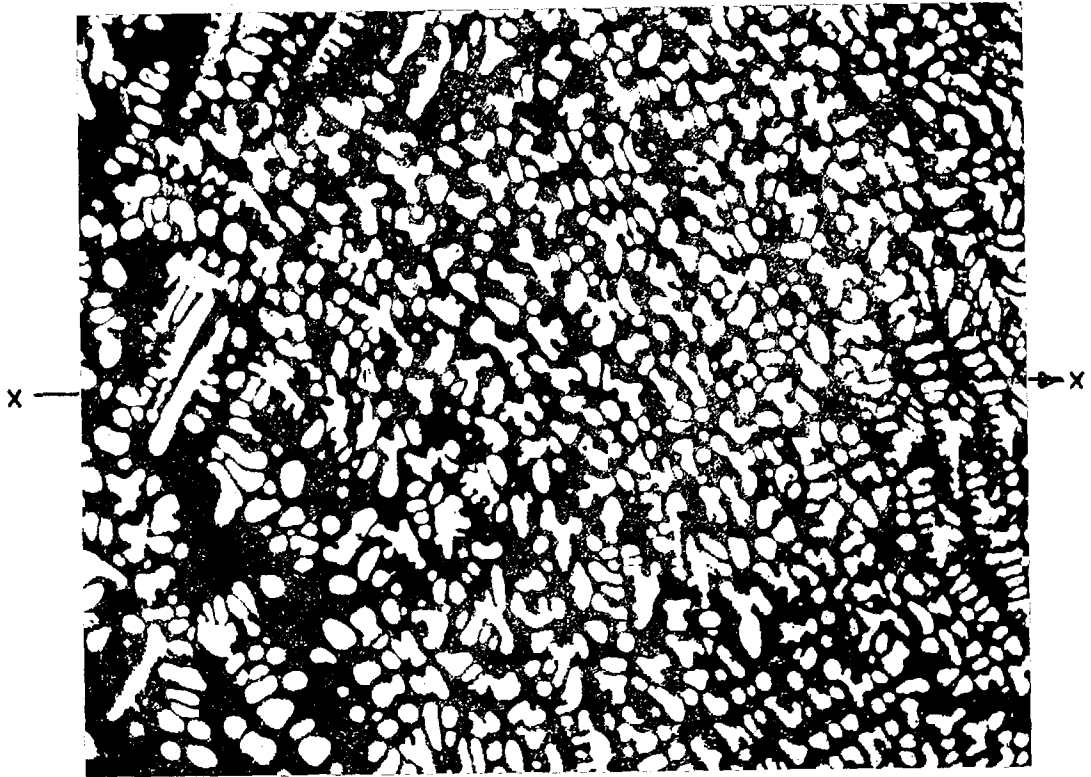


Fig. V-48 MICROPHOTOGRAPH OF 20 WT. % LEAD TIN-LEAD ALLOY

Alloy: 20 wt. % lead, tin-lead alloy (pure)

Distance from base: $\frac{1}{2}$ inch

Cooling conditions: Zero-superheat
 $h = 40.0 \text{ Btu/ft}^2 \cdot \text{hr.}^\circ\text{F.}$

Crucible: Fiberfrax-resin coated

Eccentric motor fitted to apparatus

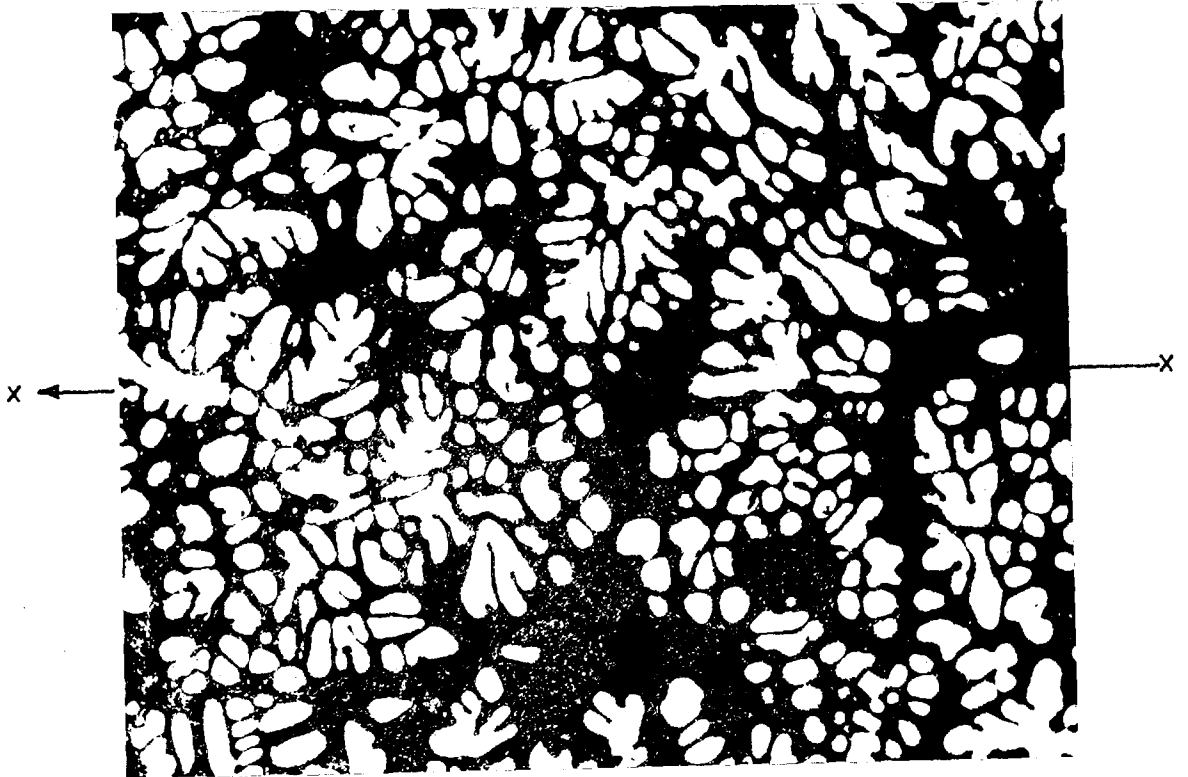
Plane of the section: Along heat flow $x \rightarrow x$

Phases: Randomly oriented tin dendrites.

Matrix: Eutectic

Etchant: 2% Nital

Magnification: 60



49
Fig. V-59 MICROPHOTOGRAPH OF 20. WT. % LEAD, TIN-LEAD ALLOY

Alloy: 20 wt. % Lead, tin-lead alloy (pure)

Distance from base: 1 inch

Cooling Conditions: Zero-superheat
 $h = 40 \text{ Btu/ft}^2 \cdot \text{hr.}^\circ\text{F.}$

Crucible: Fiberfrax-resin coated stainless steel
eccentric motor fitted with apparatus.

Plane of the section: Along heat flow $x \rightarrow x$

Phases: Tin dendrites in a matrix of eutectic
randomly oriented dendrites

Etchant: Electrolytic

Magnification: 60

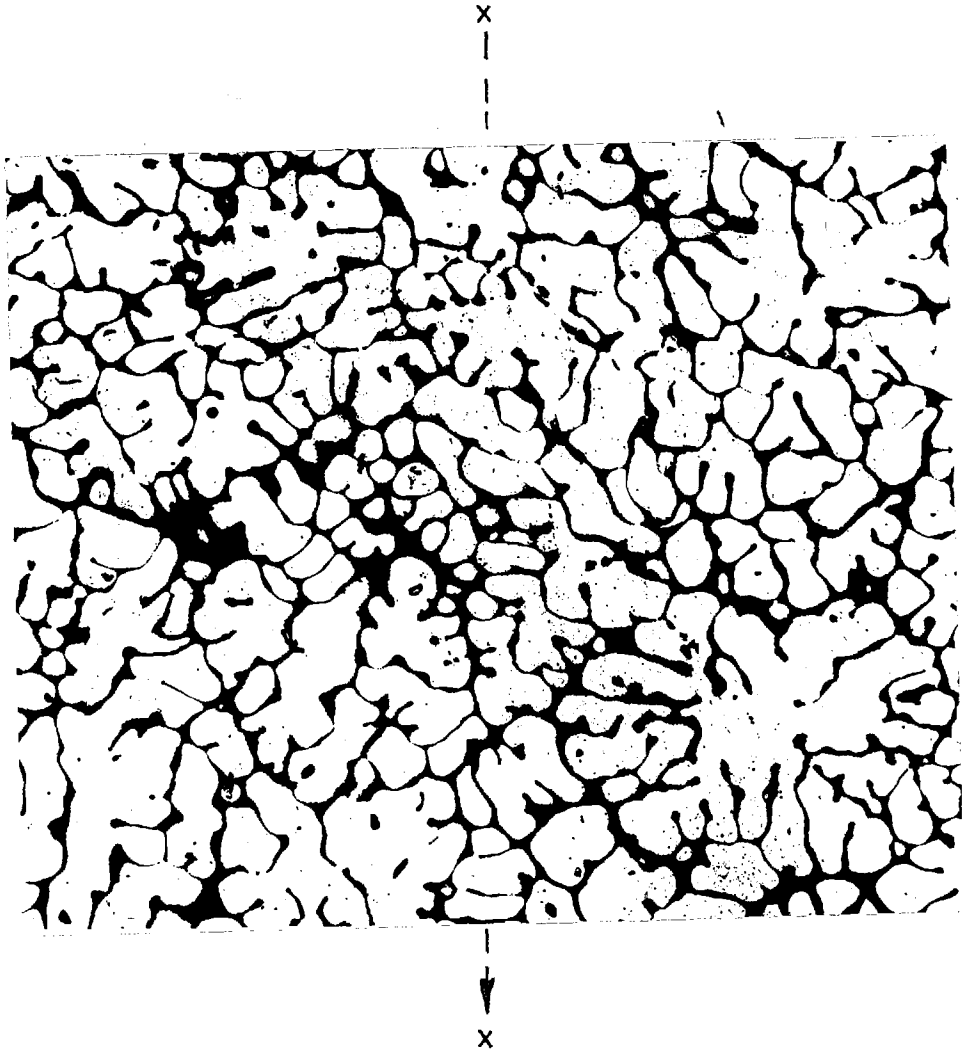


Fig. V-50 MICROPHOTOGRAPH OF 10. WT. % LEAD, TIN-LEAD ALLOY

Alloy: 10 wt. % Lead, tin-lead alloy (pure)

Distance from base: 1 inch

Cooling Conditions: Zero-superheat
 $h = 40 \text{ Btu/ft}^2 \cdot \text{hr.}^\circ\text{F.}$

Crucible: Fiberfrax-resin coated stainless steel

Plane of the section: Along heat flow $x \text{ --- } \rightarrow x$

Phases: Tin dendrites in a matrix of eutectic

Etchant: Electrolytic

Magnification: 60

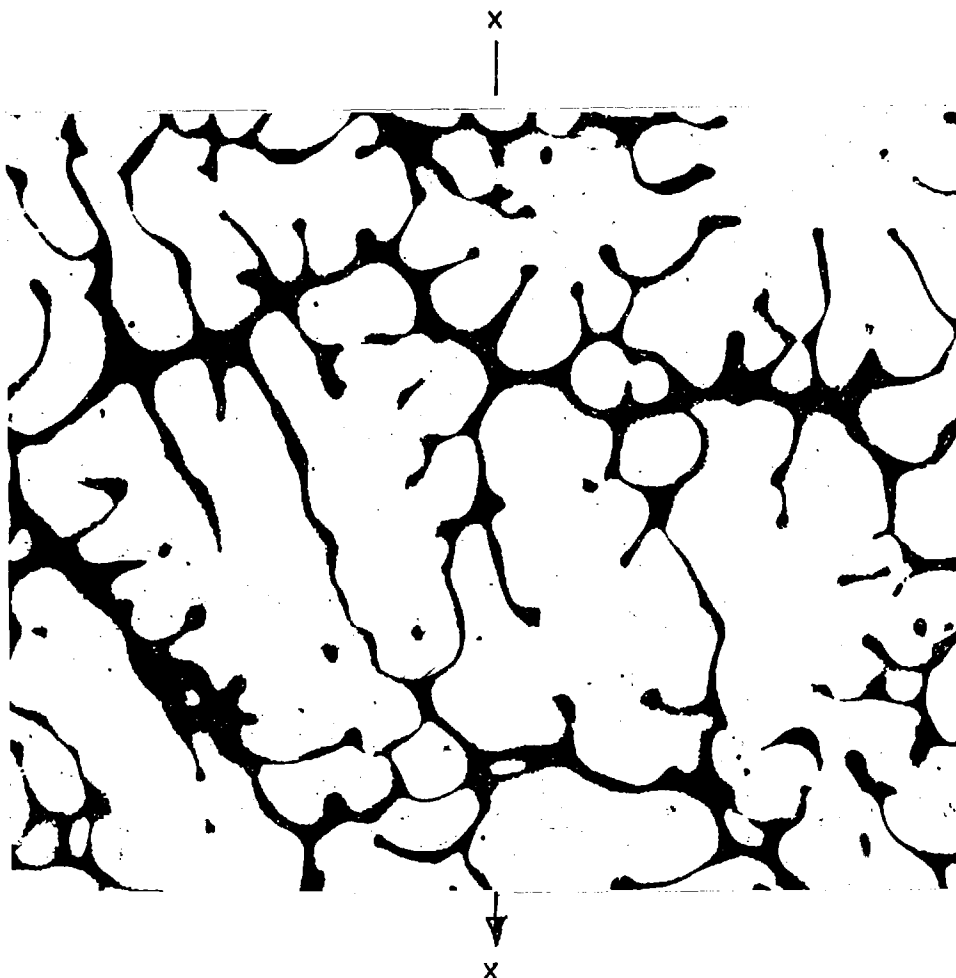


Fig. V-51 MICROPHOTOGRAPH OF 10. WT. % LEAD, TIN-LEAD ALLOY
Alloy: 10 wt. % Lead, tin-lead alloy (pure)
Distance from base: 2 inches
Cooling Conditions: Zero-superheat
 $h = 40 \text{ Btu/ft}^2 \cdot \text{hr.}^\circ\text{F.}$
Crucible: Fiberfrax-resin coated stainless steel
Plane of the section: Along heat flow $x \leftarrow \rightarrow x$
Phases: Tin dendrites in a matrix of eutectic
Etchant: Electrolytic
Magnification: 180

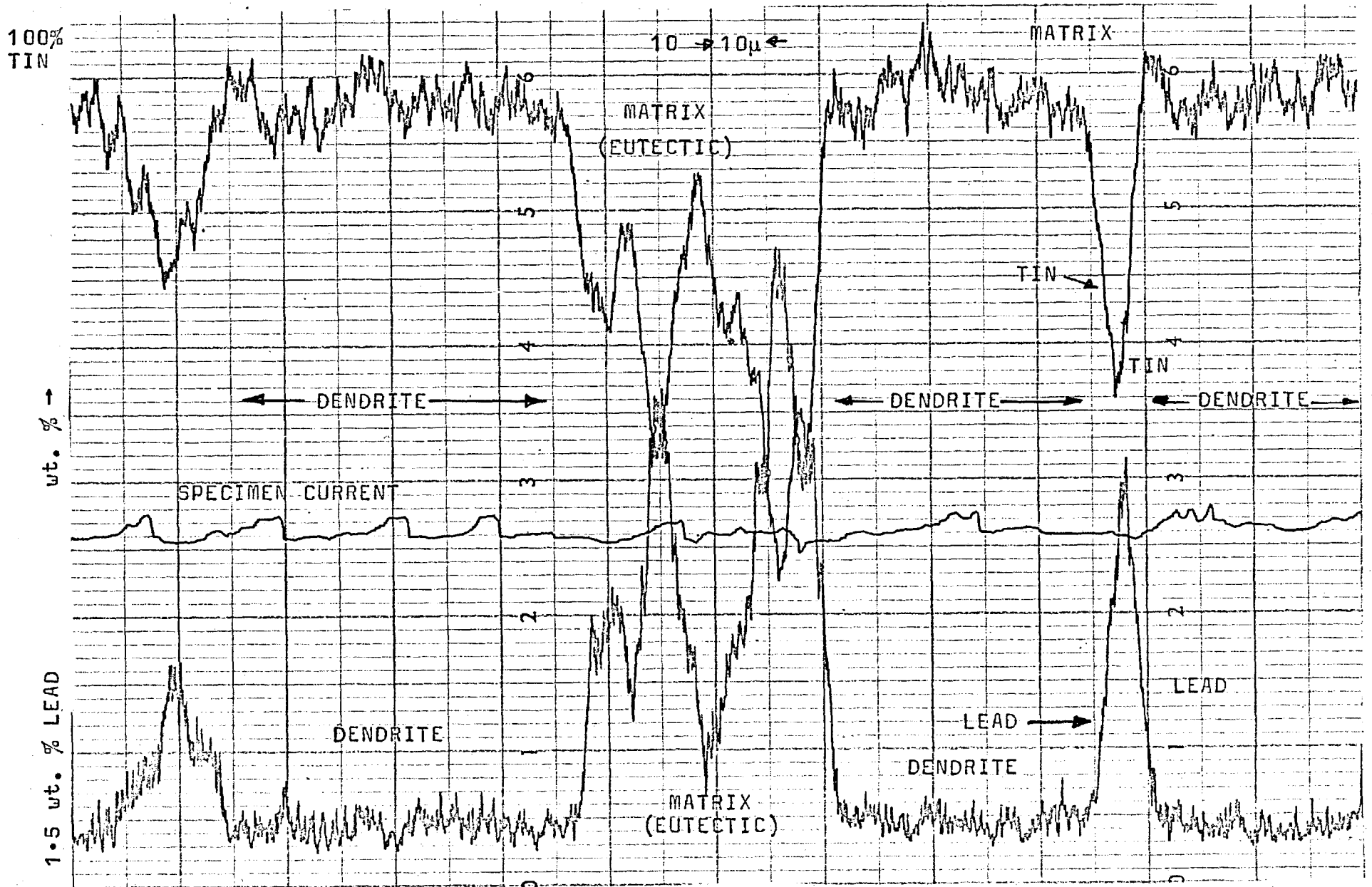


Fig. V-52 ELECTRON PROBE MICROANALYSER CHART, SHOWING DISTRIBUTION OF LEAD AND TIN IN 10 WT.% LEAD, TIN-LEAD ALLOY

CHAPTER VI

DISCUSSION

VI DISCUSSION

In Chapter III a theoretical method has been developed using the integral profile method to predict the progress of the solidification of binary alloys. This chapter discusses the validity of the integral profile method and the assumptions used in the derivation. The theory is then discussed in the light of the experimental observations.

VI-1 INTEGRAL PROFILE METHOD

The integral profile method is an approximate method for solving the one dimensional unsteady heat conduction equation. As section II-2-C shows, the method has been applied by many workers to predict solidification rates under conditions where the formal methods cannot be used. All these workers have examined the accuracy of the method by comparing its predictions for those cases where a formal solution can be obtained with the formal solution itself^{1,22,27}. In all cases they found that the agreement was satisfactory.

Moore⁴¹ compared the predictions of several integral profile methods with the results of his accurate experiments on the solidification of pure lead and pure tin. He found little difference between the predictions of the various methods and concluded that their accuracy was at least as good as the accuracy of his experimental measurements.

VI-2 ASSUMPTION USED IN THE PRESENT THEORETICAL TREATMENT

As discussed in Chapter III, the following assumptions have been made in developing the theory.

1. Unique liquidus and solidus temperatures
2. The fraction of solid present at any point in the partial layer is a linear function of temperature.

3. The fraction of solid present at the eutectic temperature is constant.
4. The effective thermal conductivity in the partial layer is a linear function of temperature.
5. The liquid and solid are assumed to be of the same density, but of different volumetric thermal capacity, and effects due to convection in the liquid are ignored.

The validity of the assumptions and their possible effect on the accuracy of the theory are discussed in this section.

V-2-A LIQUIDUS TEMPERATURE OF THE ALLOY IS UNIQUE

The cooling curves obtained during the experiments on alloy solidification have two important features: the liquidus arrest point was slightly below the equilibrium liquidus temperature (Fig. V-7/6 11) and the thermocouple furthest from the base sometimes showed a small rise in temperature near the liquidus point.

The difference between the equilibrium liquidus temperature and the observed value was small and nearly independent of cooling rate. This result has also been reported by a number of previous authors, recently Doherty and Feest⁴⁵ during a study of the solidification of copper-nickel alloys observed that the arrest point occurred some 10°C below the equilibrium value and that it occurred at the same temperature even though the cooling rate was varied from 10°C/min to 38°C/min. During the present investigation, the arrest point shown by the thermocouple farthest from the crucible base occurred at the same temperature although the heat transfer coefficient was varied from 20 to 45 Btu/ft²,hr.°F, and the degree of superheat from zero to 150°C. Thus it would appear that the liquidus arrest point can indeed be assumed to occur at a constant temperature.

This assumption⁴⁶ is in conflict with the hypothesis of Bolling and Tiller who suggest that the arrest point

in the cooling curves correspond, not to the liquidus arrest point of the alloy, but to the liquidus of the solute enriched layer around the growing dendrites. If this were true the variation in the cooling rates used in our experiments would affect the difference between the equilibrium liquidus temperature and the observed values. The effect on the agreement between the theoretical predictions and the experimental results, however, would be very small since the solidification rate does not vary very much during the experiments.

Rise⁴⁷ in temperature near the liquidus have been observed in cooling curves by a number of workers. Hunt and Chilton found that the degree of undercooling at the solid/liquid interface during the solidification of lead-tin eutectic alloy varied linearly with the solidification rate. In the range of solidification rates that correspond to this investigation, their results show that the degree of undercooling would vary between 1 and 1.5°C. However, Moore and Elliot⁴⁸ have recently reported lower values than those obtained by Hunt and Chilton - about 0.5°C under these conditions. No undercooling was detected in the present investigation during the solidification of lead-tin eutectic alloy because the temperature differences involved were too small to be measured with the apparatus used. In fact, undercooling was only observed during the solidification of one tin-lead alloy that contained 20 wt. % lead, even then, only at very high degrees of superheat (> 220°F).

Such undercooling is presumably due to a nucleation delay, but since the temperature differences involved are so small this undercooling will not invalidate the assumption that the liquidus temperature is unique and the error of 2-3°F will have a negligible effect on the theoretical predictions.

VI-2-B SOLIDUS TEMPERATURE OF THE ALLOY IS UNIQUE

When the solute content of the alloy being solidified is more than the maximum partial solid solubility, the last liquid to solidify will be of eutectic composition, and will solidify at the eutectic temperature. As we have seen in the previous section this temperature will remain effectively constant unless there are intense changes in the solidification rate. In the absence of such changes, then we are quite justified in assuming that the solidus temperature is constant and this assumption is further borne out by the experimental results. In no case was the solidus temperature found to be different from the eutectic temperature by an amount greater than the experimental error ($\pm 1^\circ\text{C}$).

The situation is less clear when the solute content is less than the maximum solid solubility. Brick⁴⁹ has suggested that the solidus temperature will be lower than the equilibrium solidus temperature by an amount that depends upon the cooling conditions. On the other hand, Subramanian and coworkers³⁷ found that the solidus temperature in iron-10% arsenic alloys could be taken as the equilibrium solidus temperature, and Malinocka⁵⁰ has suggested that the equilibrium and non-equilibrium solidus temperature are nearly the same. During this investigation no change in gradient was found near the equilibrium solidus temperature for 10 wt. % tin, lead-tin alloy (Pb-10-Sn), but a change was observed at the eutectic temperature although it was very slight. This observation suggests that some liquid still remains when the eutectic temperature is reached even in the case of this alloy, so that this temperature is still the effective solidus temperature*. Pfann's equation predicts that 8% of this alloy will be liquid at the eutectic temperature, and some eutectic metal was

*In itself, this fact cannot be taken as evidence, since Pfann's equation only predicts the fraction of liquid present once the solidus temperature has been assumed.

certainly observed in the microstructures prepared of the alloy. Thus it can be assumed that the solidus temperature is uniquely defined as the eutectic temperature for all the alloys investigated in this work.

VI-2-C THE FRACTION OF SOLID PRESENT IN THE PARTIAL LAYER IS A FUNCTION OF TEMPERATURE

It is quite evident that rates of heat removal control the rates of normal freezing processes - only when the freezing rate is extremely small will diffusion control the process. Thus it is logical to assume that the fraction of solid present at any point in the partial layer during a normal freezing process will be a function of the temperature. We can represent this function as a polynomial:

$$f_s = a_0 + a_1 \theta + a_2 \theta^2 \quad V-2-1$$

A first order polynomial, i.e. a linear function, has been used in this analysis. A polynomial of higher order could be used, but the derivation would become very much more complex. In any case, the discussion in section III-4-A shows that a linear relation is implied by the equations due to both Pfann¹⁰ and Flemings,^{11,64} provided the value of the k is small. Thus we would expect that any error in the theoretically predicted solidification rates due to the use of this linear function would be more apparent for the lead rich alloys ($k = 0.31$) than for the tin rich alloys ($k = 0.04$). However, the figures presented in section V-3 show that the agreement achieved between theoretical predictions and experimental results for the lead rich alloys is almost as good as that achieved for tin rich alloys.

Thus it can be assumed that errors due to the use of linear function are relatively small, and certainly do not warrant the extra computational effort involved

in the use of a polynomial of higher order.

However, we can assume f_S as a function of distance:

$$f_S = f_{SU} \left(1 - \left(\frac{x - t_S}{t_p} \right)^n \right) \quad \text{VI-2-2}$$

The heat conduction equation within the partial layer for the simple case where k_p is constant can be written in the form:-

$$k_p \left(\frac{\partial^2 \theta}{\partial x^2} \right) = \gamma_a \left(\frac{\partial \theta}{\partial \tau} \right) - \left(\frac{\partial f_S}{\partial \tau} \right) \rho H_p \quad \text{VI-2-3}$$

Integrating across the layer gives:

$$k_p \left(\frac{\partial \theta}{\partial x} \right)_t - k_p \left(\frac{\partial \theta}{\partial x} \right)_{t_S} = \gamma_a \left\{ \frac{d}{d\tau} \int_{t_S}^{t_S+t_p} \theta dx - \theta_L \left(\frac{dt_S}{d\tau} + \frac{dt_p}{d\tau} \right) + \theta_E \frac{dt_S}{d\tau} - H_p \frac{d}{d\tau} \int_{t_S}^{t_S+t_p} f_S dx + f_{SU} \frac{dt_S}{d\tau} \right\} \quad \text{VI-2-4}$$

but using equation VI-2 we have:

$$\int_{t_S}^{t_S+t_p} f_S dx = f_{SU} \left[1 - \frac{1}{n+1} \right] t_p = \frac{n \cdot f_{SU} t_p}{(n+1)}$$

so we can substitute this integral into equation VI-2-4 and solve it in a manner similar to that discussed in Chapter III. Fig. VI-1 shows solidification rates predicted in this way for 10 wt. % lead, tin-lead alloys using various values of n together with the experimental results for this system. Similar curves were obtained from the alloys Pb-20-Sn and Sn-20-Pb.

These curves show that the value of n which corresponds to the best fit between theory and experiment is a function of composition. Moreover, the shape of the curves predicted using constant values of n is not the same as that of the best fit line through the experimental points, and this suggests that n should also be taken to be a function of time. These results show that equation VI-2 does not represent the variation of f_S very closely. Nor could it be expected to, since, for example, it

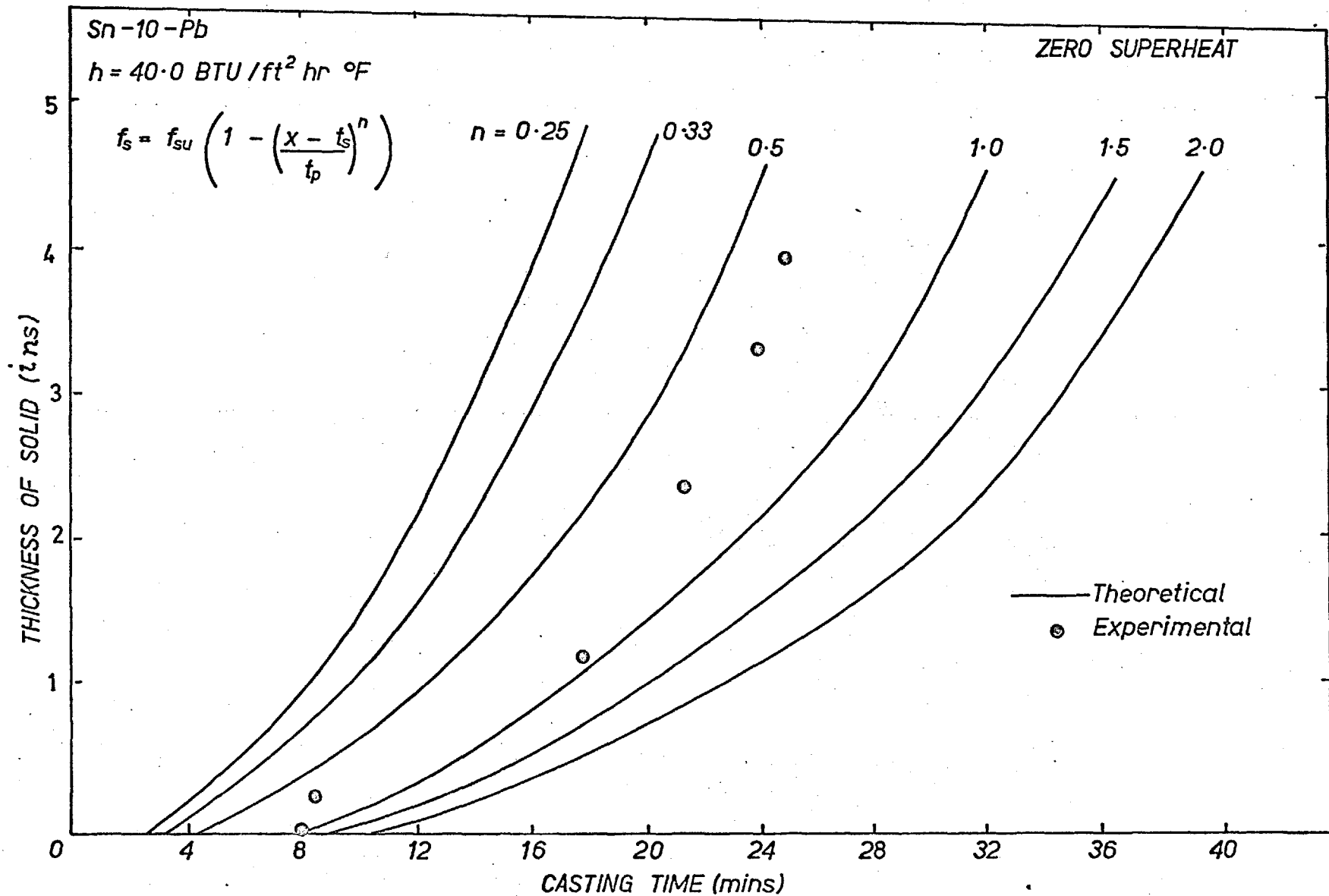


Fig.VI-1 SOLIDIFICATION OF 10wt% LEAD, TIN-LEAD ALLOY, AT ZERO SUPERHEAT. Theoretical results (assuming fraction solidified (f_s) as a function of distance), are compared with experimental results.

suggests that f_S would remain constant at the cooled surface ($x = 0$) while its temperature is falling from the liquidus to the solidus, i.e. when $t_p > 0$ but $t_s = 0$.

VI-2-D FRACTION SOLID PRESENT AT THE SOLIDUS TEMPERATURE IS CONSTANT

As discussed in section IV-2 the solidus temperature is actually the eutectic temperature so that the composition of the liquid present when the solidus temperature is reached will be that of eutectic. The value of f_{SU} can therefore be estimated from the Pfann equation (II-1-5) or from Flemings' equation (II-1-7). Both these equations assume that the equilibrium partition coefficient does not vary between the solidus and liquid temperatures, an assumption that is valid if the solidus and liquidus lines in the phase diagram are similar in shape. This is not strictly true for the lead rich side of the lead-tin system, although the variation in the value of k is insufficient to invalidate either equation.

Pfann's equation, applied to the partial layer, assumes that the interdendritic liquid is perfectly mixed in directions normal to the principal growth direction, but that no mixing takes place within the liquid along the direction of growth, or within the solid dendrites. The first two assumptions are reasonable because the interdendritic spacing is very much smaller than the thickness of the partial layer and very much smaller than the 'diffusion distance' ($\sqrt{D_p \tau_p}$). Pfann's equation gives the value of f_{SU} as:-

$$f_{SU} = 1 - \frac{C_E}{C_0} \frac{1}{k-1} \quad \text{VI-2-5}$$

so that f_{SU} will be constant as long as Pfann's equation applies. However, solid state diffusion can even out the concentration differences that are set up within

the dendrites during the growth of the partial layer. If this occurs, Pfann's equation is no longer strictly applicable, and Flemings' has produced a modified form to take account of solid state diffusion within plate-like dendrites:

$$f_{SU} = \left\{ 1 - \left(\frac{C_E}{C_0} \right)^{\frac{1}{k-1}} \right\} (1 + \alpha_f k) \quad \text{VI-2-6}$$

where

$$\alpha_f = \frac{\tau_f D_f}{L^2}$$

where ' τ_f ' is the total time taken for metal at any point in the partial layer to cool from the liquidus to the solidus, and 'L' is half the interdendritic spacing. Many workers have reported that mean interdendritic spacings in many alloy systems are proportional to the square root of freezing time.⁵¹ Thus the value of α_f does not change with cooling rate, and Flemings' equation shows that the fraction of solidified metal present at the solidus temperature will be unaffected by changes in the cooling rate. This conclusion is borne out by the work reported in section V-8-D since no variation in f_{SU} could be found along the length of the ingot. However, it could be argued that conclusions based on Fleming's equation are only valid for the plate-like dendrites for which it was derived. If this were so we would expect cooling curves and solidification times to be affected by changes in the morphology of the dendrites. The experiments described in section V-9 showed that the cooling curves obtained under otherwise identical conditions were unaffected by the change from an oriented dendritic structure to a random dendritic structure. This result shows that the value of f_{SU} is not changed when the morphology of the dendrites is changed.

VI-2-E LIQUID AND SOLID ASSUMED TO BE OF THE SAME DENSITY

In themselves, density differences will have a very small effect on heat transfer during solidification. Since the solid metal occupies a volume slightly smaller than the liquid from which it has been formed, the remote boundary will move during the process. There will also be small mass flows in the thermal and partial layers relative to the co-ordinate system used in the analysis. However, since the total volume change is between 2 and 3% of the original volume, the effects produced will be very small, and certainly less than the experimental error.

Slightly larger effects will arise due to the change in volumetric specific heat (about 4%), but these have been accounted for in the theoretical treatment.

VI-3 ASSUMPTIONS MADE IN USING THE THEORY TO PREDICT SOLIDIFICATION RATES OF THE ALLOYS USED IN THIS INVESTIGATION

VI-3-A CALCULATION OF DENSITY, THERMAL CONDUCTIVITY AND SPECIFIC HEATS OF THE ALLOYS

As discussed in section III-7, the values of density, thermal conductivity and specific heat of liquid and solid alloy phases used in the theory have been calculated on an additive basis. This seems to be perfectly reasonable since small changes in the values of these parameters produce very little change in the theoretical predictions.

VI-3-B CALCULATION OF THE LATENT HEATS OF THE ALLOYS

As discussed in section III-7-2, the value of latent heat must be known rather more accurately than other parameters, since the accuracy of theoretical prediction depends to a great extent on the latent heat. Unfortunately, the experimental value of

latent heat liberated during solidification is not generally known for binary alloys, however, the heat liberated can be calculated from the thermodynamic data, provided these values are known with sufficient accuracy. The present work on the lead-tin eutectic and on lead-tin alloys has demonstrated that less heat is liberated on solidification than would be calculated on an additive basis or on an additive basis modified to include reported values of the heat of mixing of the liquid alloy and the heat of formation of the solid alloy. The heat released during the solidification of lead-tin eutectic alloy was therefore measured using a drop calorimeter, as discussed in section IV- 9 . These experiments showed that the heat of mixing of the liquid phase is very much smaller than that reported in the literature, and can be considered to be zero. The latent heat value was thus calculated on an additive basis modified to include the heat of formation of the solid alloy measured by Taylor.⁴⁰ This latter value was considered to be reliable since it agreed with the heat of precipitation of solid solution lead-tin alloys, as measured by Borelius.⁴²

The thermal balances made using the value of the latent heat calculated in this way were similar in accuracy to those obtained from the experiments with pure lead both in this investigation and in the investigation carried out by Moore⁴¹ using the same apparatus. This fact indicated that this latent heat value could be used to predict theoretical solidification rates without too great an error.

A similar procedure was adopted for the lead rich lead-tin alloys, the latent heat being calculated taking account of the amount of lead rich solid solution that was formed (section III-7). Once again the thermal balances obtained on the experiments were of sufficient accuracy to justify the calculated latent values.

VI-3-C CALCULATION OF THE FRACTION OF SOLID PRESENT AT SOLIDUS TEMPERATURE

A number of workers have used finite difference methods to predict solidification rates of binary alloys assuming that all the latent heat is released uniformly over the freezing range. This treatment presupposes that the fraction of solid present at the solidus temperature is one. In the case of alloys whose initial composition is greater than the limit of solid solubility so that the solidus temperature is the eutectic temperature, this assumption is invalid. Moreover, Flemings et al¹¹ have shown that, even though the alloy content is less than the partial solid solubility, some eutectic metal will be formed. Even in this case, then, we cannot assume that the fraction of solid present at solidus temperature is one.

We can calculate the fraction solid present at solidus temperature from the Pfann equation as discussed in section III-7. This equation is based on the assumptions that there is complete mixing in the liquid and no diffusion in the solid. If we wished to consider the effect of solid diffusion we should use Flemings' equation (II-2-7), but in order to use this equation we require the value of the local solidification time ' τ_f ' and the width of the dendrites. However, at the present time, these variables are not known, nor are methods available for their calculation, and, indeed, the plate-like dendrites, from which Flemings' equation has been derived, do not form in the systems considered here.

VI-3-D SOLIDUS TEMPERATURE OF LEAD-TIN ALLOY CONTAINING 10 WT. % TIN

In the case of alloys whose initial concentration is less than the maximum solid solubility, a number of workers have reported that some eutectic will be formed during solidification.^{8, 11, 49, 50, 51} This observation

suggests that the equilibrium solidus temperature cannot be taken as the temperature at which solidification has been completed. Moreover, the cooling curves of 10 wt. % tin, lead-tin alloys have shown an arrest point at the eutectic temperature. Therefore, it can be concluded that the eutectic temperature can be taken as the solidus temperature for this alloy.

VI-4 EXTENT TO WHICH EXPERIMENTAL APPARATUS REPRODUCES THEORETICAL CONDITIONS

VI-4-A UNIDIRECTIONAL HEAT FLOW

In section IV-2, it has been shown that the heat flow in the experimental apparatus is unidirectional and the cooling condition can be described in terms of overall heat transfer coefficient. The evidence was further borne by the thermal balances obtained for pure metals.

In order to check that heat loss from the top of the vessel could be ignored, a heater was placed just above the metal and adjusted to keep the top temperature nearly constant when no cooling air was applied. This heater made no noticeable difference to the cooling curves obtained. Thus it can be concluded that heat lost from the top of the vessel in the absence of the heater had no influence on the solidification process.

VI-4-B ABSENCE OF CONVECTION EFFECTS

Convective flows can affect the process of solidification in three ways: it can alter the dendrite morphology by providing more nuclei; it can result in bulk transport of solute metal between partial zone and the bulk liquid; and it can affect the heat transfer processes in the liquid and partial zones.

Since the metal in the experimental apparatus is not stirred during solidification natural convection is the only convective process that can occur.

In this case natural convection could not result from temperature difference, as the heat was extracted from below the metal. Neither could natural convection occur in the case of the tin rich alloys because the solute rejected in the dendritic region is lead, so that the interdendritic liquid is heavier than the bulk liquid. However, in the case of lead rich alloys the concentration difference could give rise to natural convection since tin is rejected, and the interdendritic liquid is less dense than the bulk liquid. The convective flows will be restricted to the partial zone because relatively small vertical distances are involved and the fluid cannot be accelerated appreciably and, therefore will only effect the morphology. This was borne out by the experimental observations since no change in bulk composition was noticed and the liquidus arrest point remained constant. The effect on morphology was observed in the breaking up of oriented dendrites (Fig. V-48). Therefore we can ignore the convection effects for predicting the progress of solidification. However, the experiments in which the vessel was vibrated have already shown that the heat transfer processes are unaffected by the morphology of the **solidification**. Thus the concentration induced natural convection that occurred during the solidification of the lead rich alloys does not invalidate comparisons made between the experimental and theoretical results.

VI-4-C ACCURACY OF THE EXPERIMENTAL RESULTS

The experimental results reported are subject to mainly three sources of error:

- (i) the accuracy in measurement of heat transfer coefficient
- (ii) the accuracy in temperature measurement
- (iii) the accuracy in measurement of distance between the thermocouples.

(i) As discussed in section IV-1 the heat transfer coefficient measurements are accurate to ± 1 Btu/ft².hr.°F.

(ii) The temperatures are measured from the temperature recorder as described in section IV-1-B, the accuracy possible is $\pm 5^\circ\text{F}$, though thermocouple reproducibility is within 2°F .

(iii) The accuracy in measurement of distances between thermocouples is within ± 0.05 inches.

Considering these errors, the results obtained are accurate to $\pm 5\%$.

VI-4-D SOLUTE SEGREGATION STUDIES

Solute segregation was studied by an electron probe microanalyser. However, the solute distributions obtained cannot be attributed to solidification alone, since the alloys remained at a comparatively high temperature for some time after solidification was completed. Solid state diffusion could thus even out the concentration distributions formed during solidification.

VI-5 COMPARISON OF THEORETICAL AND EXPERIMENTAL RESULTS VI-5-A EUTECTICS AND PURE METALS

The predicted theoretical rates of solidification have been compared with those observed experimentally in section V-2. From the comparison it can be seen that Hills' theory can predict the progress the progress of solidification of pure metals at zero-superheat with a fair accuracy. Furthermore, the theory developed in this work can similarly predict the progress of solidification of pure metals at positive superheat. In the case of eutectics, it has been shown that, using a correct value of latent heat released during solidification, the theory could be applied to eutectics also, and the progress of solidification can be predicted with a fair accuracy. The correct value of latent heat can be

determined either by calorimetric investigations corresponding closely to the experimental conditions, or from the thermal balance of the process itself.

The study of the microstructures of lead-tin and lead-antimony eutectics has shown that a small quantity of lead dendrites could be present (Figs. V-24 to 28). These dendrites were thought to be due to the presence of nucleating sites provided by the impurities present. During the study of pure lead-tin eutectic, no such dendrites were observed. However, some dendrites were observed when, during the solidification, the apparatus was vibrated (Fig. V-29), to produce random oriented grains. From the cooling curves obtained in the above mentioned experiments no difference in the rates of solidification was observed. Therefore, it can be concluded that presence of a small amount of dendrites made no difference in the experimental results and that the theory presented in this work can predict the rate of solidification of pure metals and eutectics at zero and positive superheats with fair accuracy.

VI-5-B TIN RICH ALLOYS

In tin rich alloys the theoretical conditions are satisfied to a great extent, since the convection effects are absent. Moreover, the small value of partition coefficient 'k' renders the assumption of fraction solid present at any point is a linear function of the temperature is strictly valid. Therefore it is to be expected that the theoretical predictions should be in close agreement with experimental observations. The theoretically predicted rates of solidification are compared with experimentally observed rates of solidification of tin rich alloys (Sn-20-Pb and Sn-10-Pb) in Figs. V-38 to V-41. From these results it can be concluded that the agreement between theory and experiments is quite good and is within experimental error.

... Furthermore, the experiments conducted to produce oriented and random oriented morphologies in 20 wt. % lead, tin-lead alloy (Sn-20-Pb) have shown that morphology has no measurable effect on the rates of solidification. Therefore it can be concluded that the theory developed in this work is adequate to predict the progress of solidification if alloys have small solid solubility.

VI-5-C LEAD RICH ALLOYS

VI-5-C(i) Alloy Composition More Than Maximum Solid Solubility

In the case of lead rich alloys whose composition is more than the solid solubility limit, the theoretical assumption of negligible convection effect is strictly not valid. However, it has been shown in section VI-4-B that the convection effects are not likely to effect the concentration of the bulk liquid. Therefore the convection effects, though present as shown by the breaking up of oriented dendrites (Fig. V-3(b)) does not invalidate the theory. The comparison between theoretical and experimental rates of solidification (Figs. V-34 to V-37) suggests that the theory predicts the progress of solidification of lead rich alloys with fair accuracy. Moreover it can be concluded that the simple assumption of linear relationship between fraction solid present and temperature is quite adequate.

VI-5-C(ii) Alloy Composition Less Than Maximum Solid Solubility

When the composition of the alloy is less than the maximum solid solubility, the main problem in applying this theory is the choice value of the solidus temperature. As discussed in section VI-2-B the most likely choice is the eutectic temperature. In this work the eutectic temperature has been chosen as the solidus temperature for 10 wt. % tin, lead-tin alloy.

The theoretically predicted and experimentally observed rates of solidification are compared in Fig. V-33. The agreement is quite reasonable and suggests that the theory developed in this work also can be applied to predict the progress of solidification of these alloys. However, this conclusion warrants more experimental verification particularly in low alloy regions.

CHAPTER VII

CONCLUSIONS

VII CONCLUSIONS

In the preceding chapter it has been shown that the theory developed in this work can predict the rates of solidification of pure metals, eutectics and binary alloys, with fair accuracy. The main merits of this theory can be enumerated as:

1. The theory rationalises the effect of positive superheat on the rates of solidification.
2. The theory developed in this work is a generalised theory and can be used to predict the rates at which a wide range of binary alloys solidify under a variety of cooling conditions.
3. This theory provides a simple solution for the solidification of alloys and is economical in the use of computer time. The average time required for the computation is less than 0.1 min. (about 5 seconds).
4. The theory assumes a simple linear relationship between fraction solid present and temperature. This simplifies the mathematics and the comparison between theoretical and experimental results have shown that it is quite an adequate assumption for predicting the growth of solidification fronts.
5. The theory not only predicts the rate of solidification, but it also predicts the temperature of the cooled surface and remote boundary.
6. The theory presented in this work can be used with minor changes in the computer programme given in Appendix III, to predict the temperature profile at any time in the entire length of the ingot or a cooling curve can be obtained at any point in the ingot.
7. The theory can be extended to treat situations where a solid state transformation affects the temperature in the solid layer. The region in which such a reaction would occur can be treated as a separate layer. If the solid state transformation occurs over a range of temperature, the region can be treated in a similar manner

to the partial layer (section III-4) and if the solid state transformation occurs at a fixed temperature the region can be treated in a similar manner to the solid layer (section II-2).

Therefore we can conclude that the theory developed in this work is of a generalised type.

At present the main limitation of the theory developed in this work is the use of calculated values of fraction solid present at the solidus temperature, though it has been shown that Pfann's equation is quite adequate. It is hoped that this limitation can be removed by considering the transfer of solute normal to heat flow direction in the liquid and solid phases in the partial layer. Thus defining the fraction solid present in terms of dendritic spacing parameter. Such a theory will be able to predict the dendritic spacing as a function of distance.

The theory has been developed only for binary alloys that form a eutectic, though it can be used for other types of binary alloys once the boundary temperatures and fraction solid present at these boundaries are known.

Therefore we can conclude that the theory developed in this work is of a generalised type and from the known values of the thermal and physical properties the rates of solidification and the thermal history of the ingot can be predicted. This information could be of use in the design of continuous casting of alloys, and uni-directional solidification of alloys to obtain high strength and ductility. Moreover, this theory helps to rationalise the understanding of the solidification of alloys at positive superheats.

APPENDIX I

DERIVATION OF DIFFERENTIAL EQUATION OF COOLED SURFACE TEMPERATURE IN MODES S2 AND S2F

The treatment is similar to that used by Hills for the growth of the solid metal layer (section II-2-c(i)). Let us consider the variation of $\frac{\partial \theta}{\partial \tau}$ across the layer. At stationary surface, $x = 0$, we can write:

$$\left(\frac{\partial \theta_0}{\partial \tau}\right)(\tau, 0) = \frac{d\theta_0}{d\tau} \quad \text{A-I-1}$$

and at the moving boundary $x = t_p$, the temperature is constant (θ_L^*), so we can write:

$$\frac{d}{d\tau} \left\{ \theta(t_p, \tau) \right\} = \left[\frac{\partial \theta_0}{\partial x} \right]_{t_p} \frac{dt_p}{d\tau} + \left[\frac{\partial \theta}{\partial \tau} \right]_{t_p} = 0 \quad \text{A-I-2}$$

Substituting for the temperature gradient from the heat flux equation III-4-23 we get:

$$\left[\frac{d\theta_0}{d\tau} \right]_{t_p} = \frac{\dot{q}_L''}{K_L^*} \frac{dt_p}{d\tau} \quad \text{A-I-3}$$

since

$$q^*(t_S+t_p) = q_L^* \text{ and } [K_P^*]_{(t_S+t_p)} = K_L^*.$$

From the unsteady state heat conduction equation III-4-20, we can write:

$$\begin{aligned} \left(\frac{\partial \theta_0}{\partial \tau}\right)_{t_p} - \left(\frac{\partial \theta_0}{\partial \tau}\right)_0 &= \frac{1}{\gamma_p} \left\{ \left[\frac{\partial}{\partial x} \left(K_P \frac{\partial \theta_0}{\partial x} \right) \right]_{t_p} - \left[\frac{\partial}{\partial x} \left(K_P \frac{\partial \theta_0}{\partial x} \right) \right]_0 \right\} \\ &= \frac{1}{\gamma_p} \int_0^{t_p} \frac{\partial^2}{\partial x^2} \left(K_P \frac{\partial \theta_0}{\partial x} \right) dx \quad \text{A-I-4} \end{aligned}$$

We can assume that $\frac{\partial^2}{\partial x^2} (K_p \frac{\partial \theta_0}{\partial x})$ is virtually constant within the partial layer, and we can write

$$\int_0^{t_p} \frac{\partial^2}{\partial x^2} (K_p \frac{\partial \theta_0}{\partial x}) dx = \left[\frac{\partial^2}{\partial x^2} \left\{ K_p \left(\frac{\partial \theta_0}{\partial x} \right) \right\} \right]_0 \left\{ \int_0^{t_p} dx \right\}$$

$$= t_p \left[\frac{\partial^2}{\partial x^2} (K_p \frac{\partial \theta_0}{\partial x}) \right]_0 \quad \text{A-I-5}$$

Differentiating the heat conduction equation III-4-23 with respect to x gives:

$$\frac{\partial^2}{\partial x^2} (K_p \frac{\partial \theta_0}{\partial x}) = \gamma_p \frac{\partial}{\partial x} \left(\frac{\partial \theta_0}{\partial \tau} \right) = \gamma_p \frac{\partial}{\partial \tau} \left(\frac{\partial \theta_0}{\partial x} \right) \quad \text{A-I-6}$$

At $x = 0$ this becomes:

$$\frac{\partial^2}{\partial x^2} (K_p \frac{\partial \theta_0}{\partial x})_0 = \gamma_p \frac{d}{d\tau} \left(\frac{-\dot{q}_0''}{K_0} \right)$$

Substituting the values of \dot{q}_0'' and K_0 from the equations given in section III-4 we get:

$$= \frac{\gamma_p [\dot{q}_0'']^3}{K_S^2 \theta_S^2} \left\{ \frac{f'_\theta \frac{d\theta_0}{d\tau} + f'_z}{K_0} + \frac{\dot{q}_0''}{(K_0)^2} \frac{d\theta_0}{d\tau} \right\} \quad \text{A-I-7}$$

Substituting equation A-I-7, A-I-5, A-I-3, A-I-2 in A-I-4 we get:

$$\frac{\gamma_p \dot{q}_L''}{K_L} \frac{dt_p}{d\tau} - \gamma_p \frac{\partial \theta_0}{\partial \tau} = - \frac{\gamma_p [\dot{q}_0'']^3 t_p}{K_S^2 \theta_S^2} \left\{ \left(\frac{f'_\theta}{K_0} + \frac{\dot{q}_0'' \mathcal{K}}{(K_0)^2} \right) \frac{d\theta_0}{d\tau} + \frac{f'_z}{K_0} \right\}$$

A-I-8

Rearranging and expressing in dimensionless terms gives:

$$\frac{d\theta_0^*}{d\zeta} = - \frac{\frac{q_L^*}{K_L^*} \frac{dt_p^*}{d\zeta} + \frac{t_p^* f_\zeta'}{K_0^*}}{1 + \frac{t_p^*}{K_0^*} (f_\theta' + \frac{q_0^* \kappa}{K_0^*})}$$

A-I-9

Let $F_\theta' = f_\theta' + \frac{q_0^* \kappa}{K_0^*}$

then

$$\frac{d\theta_0^*}{d\zeta} = - \frac{\frac{q_L^*}{K_L^*} \frac{dt_p^*}{d\zeta} + \frac{t_p^* f_\zeta'}{K_0^*}}{1 + \frac{t_p^*}{K_0^*} F_\theta'}$$

A-I-10

APPENDIX II

DETERMINATION OF THE LIMITING VALUE OF $\frac{dt_p^*}{d\bar{z}}$ WHEN THE PARTIAL LAYER IS EQUAL TO ZERO

As discussed in section III-4-D(v) when t_p^* is equal to zero the differential equation for the partial layer thickness becomes indeterminate. The values of the relevant parameters at the change point ($t_p^* = 0$) are:

$$\left[\theta_0^* \right]_c^{(a)} = \theta_L^*$$

$$\left[q_L^* \right]_c = \left[q_0^* \right]_c$$

$$\left[k_0^* \right]_c = k_L^*$$

Let us put

$$\bar{z} = \bar{z} - \left[\bar{z} \right]_c$$

Using Taylor series, we can expand the parameters involved in the equation III-4- as described below:

$$q_0^* = \left[q_0^* \right]_c + \left\{ f_{\theta}^{\prime} \left[\frac{d\theta_0^*}{d\bar{z}} \right]_c + f_{\bar{z}}^{\prime} \right\} \bar{z} + O(\bar{z}^2) \quad \text{A-II-1}$$

and

$$q_L^* = \left[q_0^* \right]_c + \left(g_t^{\prime} \left[\frac{dt_p}{d\bar{z}} \right]_c + g_{\bar{z}}^{\prime} \right) \bar{z} + O(\bar{z}^2) \quad \text{A-II-2}$$

(a) Notation $\left[\right]_c$ denotes the value of the various parameters at the change point, $t_p = 0$.

Since

$$\frac{dq_0^*}{d\zeta} = f'_\theta \frac{d\theta_0^*}{d\zeta} + f'_\zeta$$

and

$$\frac{dq_L^*}{d\zeta} = g'_t \frac{dt_p^*}{d\zeta} + g'_\zeta$$

$$t_p^* = \left[\frac{dt_p^*}{d\zeta} \right]_c \zeta + \theta\left(\frac{\zeta^2}{2}\right) \quad \text{A-II-3}$$

$$\theta_0^* = \theta_L^* + \left[\frac{d\theta_0^*}{d\zeta} \right]_c \zeta + \theta\left(\frac{\zeta^2}{2}\right) \quad \text{A-II-4}$$

$$K_0^* = K_L^* + \theta(\zeta) \quad \text{A-II-5}$$

Substituting into equation III-4-56, we get:

$$\frac{dt_p^*}{d\zeta}_c = \frac{\frac{3}{\gamma_p^*} \left\{ f'_\theta \left[\frac{d\theta_0^*}{d\zeta} \right]_c + f'_\zeta - g'_t \left[\frac{dt_p^*}{d\zeta} \right]_c - g'_\zeta \right\} \zeta + \theta\left(\frac{\zeta^2}{2}\right)}{- \left[\frac{d\theta_0^*}{d\zeta} \right]_c + \frac{2q_L^*}{K_L^*} \left[\frac{dt_p^*}{d\zeta} \right]_c + \theta\left(\frac{\zeta^2}{2}\right)} \quad \text{A-II-6}$$

Similarly the limiting form of the differential equation for the cooled surface temperature, III-4-53, gives

$$\left[\frac{d\theta_0^*}{d\zeta} \right]_c = - \frac{[q_L^*]_c}{K_L^*} \left[\frac{dt_p^*}{d\zeta} \right]_c \quad \text{A-II-7}$$

Substituting this equation into equation A-II-6 we get:

$$\gamma_p^* \left[\frac{dt_p^*}{d\zeta} \right]_c^2 + \left(f'_\theta + \frac{K_L^*}{[q_L^*]_c} g'_t \right) \left[\frac{dt_p^*}{d\zeta} \right]_c - \frac{K_L^*}{[q_L^*]_c} (f'_\zeta - g'_\zeta) = 0 \quad \text{A-II-8}$$

which gives:

$$\left[\frac{dt_p^*}{d\zeta} \right]_c = \frac{-(f_\theta' + \frac{K_L^*}{[q_L^*]_c} g_t') \pm \sqrt{(f_\theta' + \frac{K_L^*}{[q_L^*]_c} g_t')^2 + \frac{4\gamma_p^* K_L^*}{[q_L^*]_c} (f_{\zeta'}' - g_{\zeta'}')}}{2\gamma_p}$$

A-II-9

But $g_{\zeta'}'$ is negative if solidification is to occur when $f_{\zeta'}'$ is zero. Thus the positive root of A-II-9 is valid. As the product of the roots of a reduced quadratic equation is equal to the constant term, we can rearrange equation A-II-9 to get

$$\left[\frac{dt_p^*}{d\zeta} \right]_c = \frac{2K_L^* (f_{\zeta'}' - g_{\zeta'}')}{([q_L^*]_c f_\theta' + K_L^* g_t') + \sqrt{([q_L^*]_c f_\theta' + K_L^* g_t')^2 + 4[q_L^*]_c K_L^* (f_{\zeta'}' - g_{\zeta'}')}}}$$

A-II-10

APPENDIX III

COMPUTER PROGRAMME FOR SOLIDIFICATION OF METALS AND ALLOYS

In Chapter III a theoretical treatment has been presented to predict the progress of solidification of metals and alloys. The calculation algorithm given in Fig. III-3 lists the various ordinary differential equations for the characteristic parameters and the corresponding link equations. These equations have been solved using a Runge-Kutta method, the necessary numerical integration being done on the Imperial College I.B.M. 7094 computer, using Fortran IV.

The computer programme consists of a main programme and three subroutines. The main programme converts data relevant to each experimental run to its dimensionless form and calculates the time at which the base temperature is equal to the liquidus temperature, writing the calculated values. It then calls the first subroutine RUKUT4, which allows the integration to proceed with a variable step length while the control is transferred back to the main programme and the results are printed at a more or less regular print-interval. Subroutine RUKUT4 calls subroutine STEP4 which performs the actual numerical integration step using the Runge-Kutta method. These two subroutines have been developed by Hills⁵² and a complete description and flow diagrams for the two subroutines are given in his thesis. Subroutine STEP4 calls subroutine DIFREL in which the actual values of the differentials are calculated. Each time the control is transferred back to the main programme.

From RUKUT4 a test is made to see whether or not any of the alternate end conditions of the current solidification mode have been exceeded. If they have RUKUT4 is called again with the previous values of the solidification parameters, but with the length of the print-interval halved*.

*The integration step length used in RUKUT4 is also halved at this time.

This procedure is repeated until the relevant end condition has been reached to an accuracy of 0.1% when integration is recommenced in the new cooling mode, but with the original values of the print-interval. Information as to which of the various cooling modes is current at any one time is transferred directly from the main programme to the subroutine DIFREL by means of an integer-MODE-1- stored in common. The value of MODE 1 determines which differential expressions are evaluated by DIFREL when it is called from STEP4.

A flow diagram for the main programme is presented in Figs. A-III-1 and A-III-2, and for DIFREL in Fig. A-III-3.

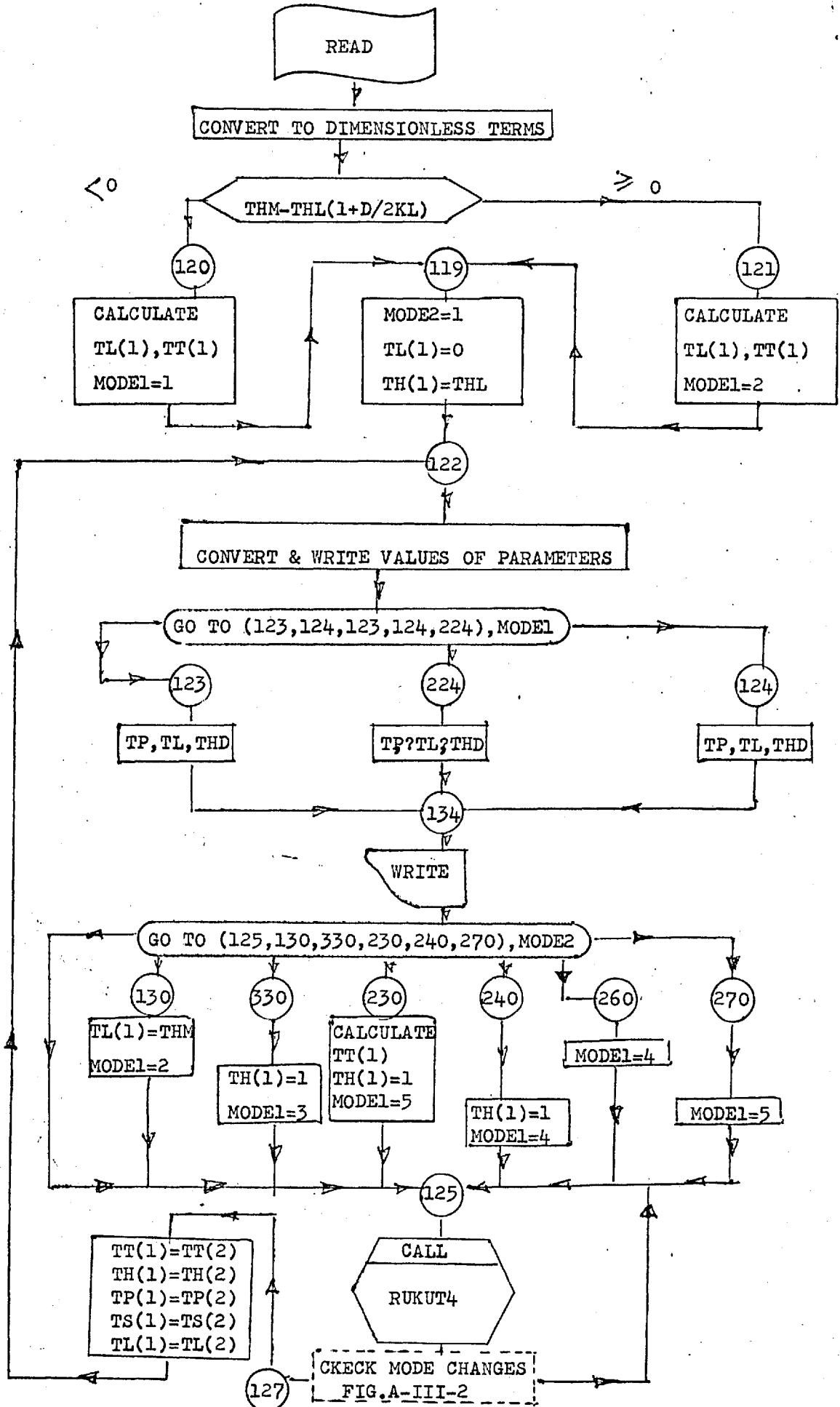


Fig. A-III-1 FLOW DIAGRAM FOR THE MAIN PROGRAMME

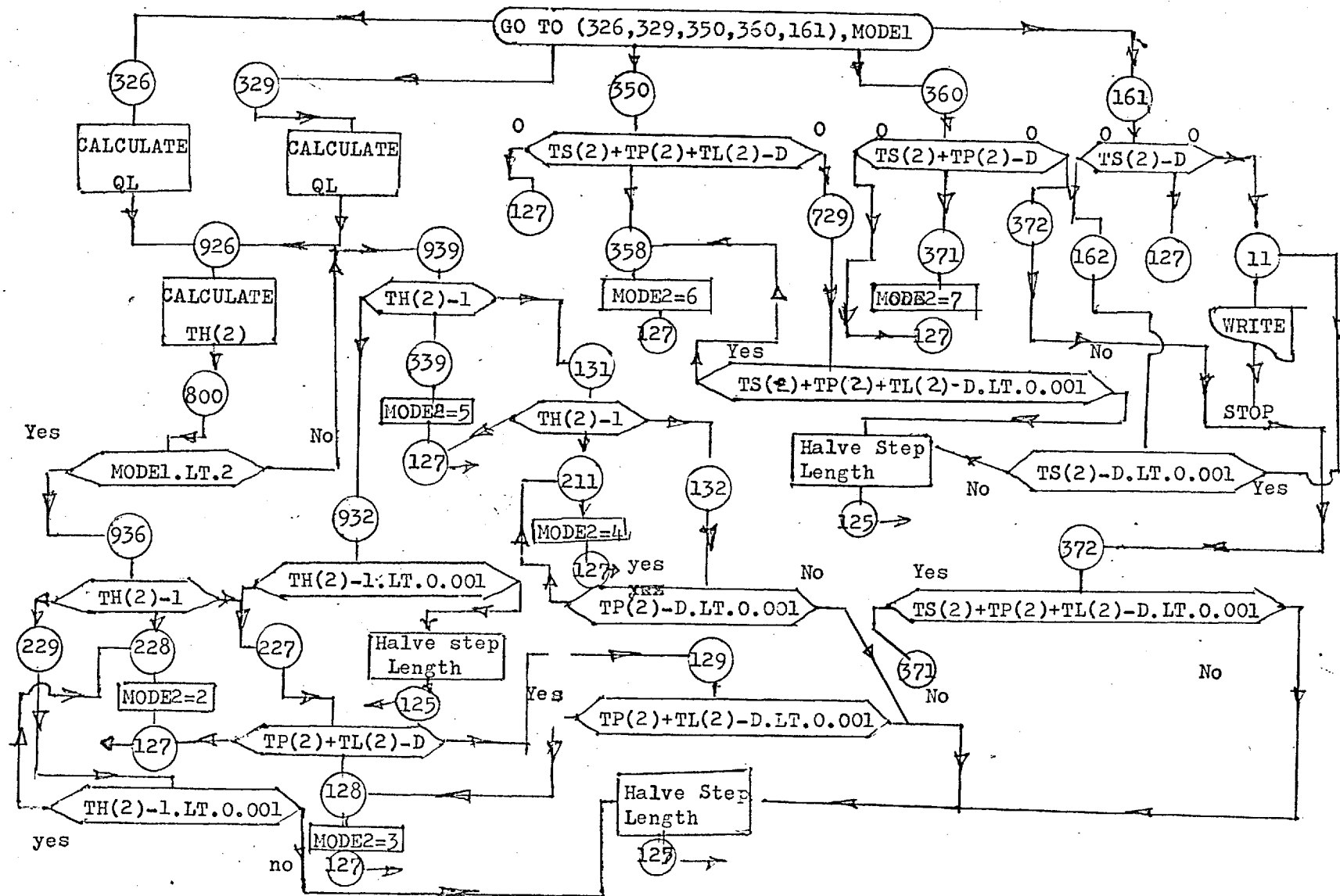


Fig. A-III-2 FLOW DIAGRAM FOR MAIN PROGRAMME (CONTINUED FROM FIG. A-III-1)

SUBROUTINE DIFREL (TS, TP, TL, TH, D1, D2, D3, D4)

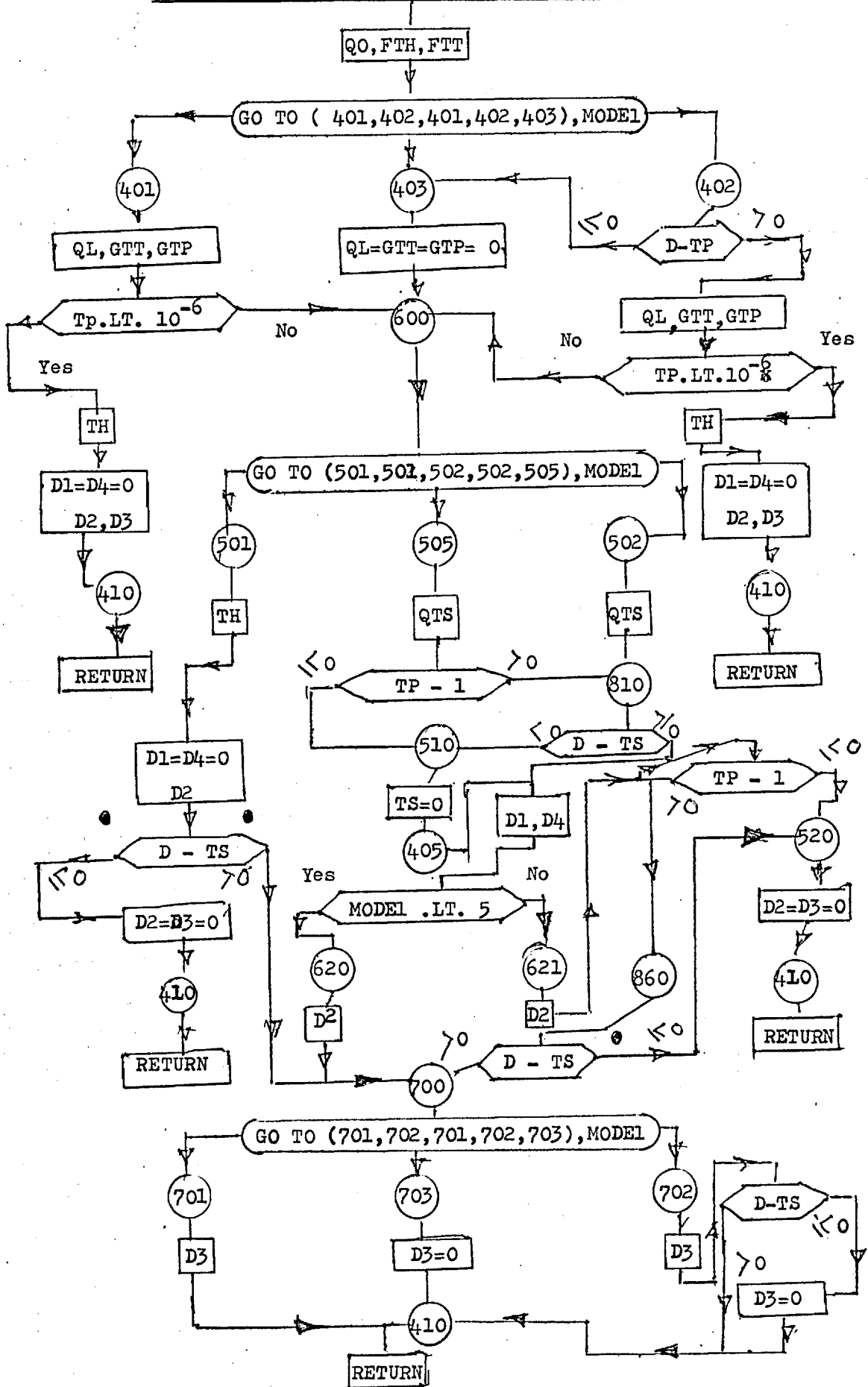


Fig. A-III-3 FLOW DIAGRAM FOR SUBROUTINE DIFREL

APPENDIX IV

SPECIMEN THEORETICAL COMPUTED RESULTS

TABLE A-IV-1

SOLIDIFICATION OF LEAD AT ZERO-SUPERHEAT

DIMENSIONLESS		HEAT TRANSFER COEFFICIENT (BTU/FT(2).HR..DEG.F									
		45.0		40.0		34.0		28.0		21.8	
THICK	TIME	THICKIN	TIME	THICKIN	TIME	THICKIN	TIME	THICKIN	TIME	THICKIN	TIME
0.0500	0.0330	0.2	0.4	0.3	0.5	0.3	0.7	0.4	1.1	0.5	1.7
0.1000	0.0696	0.5	0.9	0.5	1.1	0.6	1.5	0.8	2.2	1.0	3.7
0.1500	0.1095	0.7	1.4	0.8	1.7	1.0	2.4	1.2	3.5	1.5	5.8
0.2000	0.1524	1.0	1.9	1.1	2.4	1.3	3.3	1.6	4.9	2.0	8.0
0.2500	0.1983	1.2	2.5	1.4	3.1	1.6	4.3	1.9	6.3	2.5	10.5
0.3000	0.2470	1.5	3.1	1.6	3.9	1.9	5.4	2.3	7.9	3.0	13.0
0.3500	0.2984	1.7	3.7	1.9	4.7	2.2	6.5	2.7	9.5	3.5	15.7
0.4000	0.3525	1.9	4.4	2.2	5.5	2.6	7.6	3.1	11.3	4.0	18.6
0.4500	0.4092	2.2	5.1	2.5	6.4	2.9	8.9	3.5	13.1	4.5	21.6
0.5000	0.4684	2.4	5.8	2.7	7.3	3.2	10.2	3.9	15.0	5.0	24.7
0.5500	0.5302	2.7	6.6	3.0	8.3	3.5	11.5	4.3	17.0	5.5	28.0
0.6000	0.5944	2.9	7.4	3.3	9.3	3.9	12.9	4.7	19.0	6.0	31.4
0.6500	0.6612	3.2	8.2	3.5	10.4	4.2	14.3	5.1	21.2	6.5	34.9
0.7000	0.7303	3.4	9.0	3.8	11.4	4.5	15.8	5.5	23.4	7.0	38.5
0.7500	0.8019	3.6	9.9	4.1	12.6	4.8	17.4	5.8	25.7	7.5	42.3
0.8000	0.8759	3.9	10.8	4.4	13.7	5.1	19.0	6.2	28.0	8.0	46.2
0.8500	0.9524	4.1	11.8	4.6	14.9	5.5	20.7	6.6	30.5	8.5	50.3
0.9000	1.0311	4.4	12.8	4.9	16.2	5.8	22.4	7.0	33.0	9.0	54.4
0.9500	1.1123	4.6	13.8	5.2	17.4	6.1	24.1	7.4	35.6	9.5	58.7
1.0000	1.1958	4.9	14.8	5.5	18.7	6.4	25.9	7.8	38.3	10.0	63.1

TABLE A-IV-2

SOLIDIFICATION OF LEAD AT SUPERHEAT

TIMESTAR	TIMEMIN	THICKSTAR	THICKIN	THETASTAR	THETAC	MOLTENPRAM	THERMALIN	TOPTEMP
0.014	0.21	0.	0.	1.000	621.6	0.2106	1.14	726.0
0.056	0.86	0.0270	0.15	0.974	608.1	0.4835	2.61	726.0
0.106	1.63	0.0705	0.38	0.936	588.5	0.6220	3.35	726.0
0.131	2.01	0.0923	0.50	0.918	579.4	0.6718	3.62	726.0
0.144	2.20	0.1032	0.56	0.910	575.0	0.6940	3.74	726.0
0.150	2.30	0.1086	0.59	0.906	572.9	0.7045	3.80	726.0
0.152	2.32	0.1099	0.59	0.905	572.4	0.7071	3.81	726.0
THERMAL LAYER HAS REACHED BOUNDARY OF LIQUID REGION								
0.202	3.09	0.1514	0.82	0.875	557.0	1.1828	3.59	716.2
0.252	3.86	0.1908	1.03	0.849	543.7	1.1624	3.37	705.6
0.302	4.62	0.2288	1.23	0.826	531.8	1.1411	3.17	694.6
0.352	5.39	0.2661	1.44	0.805	520.9	1.1196	2.97	683.5
0.402	6.15	0.3031	1.63	0.786	510.9	1.0984	2.77	672.5
0.452	6.92	0.3402	1.83	0.768	501.5	1.0782	2.57	662.1
0.502	7.68	0.3775	2.04	0.751	492.7	1.0593	2.37	652.3
0.552	8.45	0.4153	2.24	0.735	484.4	1.0425	2.16	643.6
0.602	9.21	0.4536	2.45	0.720	476.5	1.0281	1.96	636.2
0.652	9.98	0.4925	2.66	0.705	469.0	1.0167	1.75	630.2
0.702	10.75	0.5317	2.87	0.692	461.9	1.0085	1.54	626.0
0.752	11.51	0.5711	3.08	0.679	455.2	1.0034	1.32	623.3
0.802	12.28	0.6103	3.29	0.666	448.9	1.0009	1.11	622.1
0.852	13.04	0.6490	3.50	0.655	443.0	1.0001	0.90	621.7
0.902	13.81	0.6870	3.70	0.644	437.5	1.0000	0.70	621.6
0.952	14.57	0.7241	3.90	0.634	432.3	1.0000	0.50	621.6
1.002	15.34	0.7606	4.10	0.625	427.4	1.0000	0.30	621.6
1.052	16.11	0.7964	4.29	0.616	422.7	1.0000	0.11	621.6
1.077	16.49	0.8140	4.39	0.612	420.5	1.0000	0.01	621.6
1.080	16.54	0.8162	4.40	0.611	420.2	1.0000	0.00	621.6

222

DATA

THERMAL CAPACITY SOLID	THERMAL CAPACITY THERMAL	THERMAL CONDUCTIVITY SOLID	THERMAL CONDUCTIVITY THERMAL	DENSITY SOLID	LATENT HEAT	LIQUID HEIGHT	HEAT TRANSFER COEFFICIENT
23.0	24.1	18.2	9.5	696.0	10.6	0.367	40.5
BTU/FT(3)	°F	BTU/FT.HR.	DEG-F	LB/FT(3)	BTU/LB	FT	BTU/FT(2).HR.DEG-F.

TEMPERATURES

INITIAL	SOLIDUS	AMBIENT
622.0 °F	517.6 °F	104.0 °F

TABLE A-IV-3

SOLIDIFICATION OF LEAD-ANTIMONY EUTECTIC AT ZERO-SUPERHEAT

DIMENSIONLESS

HEAT TRANSFER COEFFICIENT (BTU/FT²).HR..DEG.F

THICK	TIME	HEAT TRANSFER COEFFICIENT (BTU/FT ²).HR..DEG.F									
		45.0		40.0		34.0		28.0		21.8	
THICKIN	TIME	THICKIN	TIME	THICKIN	TIME	THICKIN	TIME	THICKIN	TIME	THICKIN	TIME
0.0500	0.0655	0.2	0.8	0.2	1.0	0.3	1.3	0.4	1.9	0.5	3.2
0.1000	0.1363	0.4	1.6	0.5	2.0	0.6	2.7	0.7	4.0	0.9	6.7
0.1500	0.2122	0.7	2.4	0.7	3.1	0.9	4.3	1.1	6.3	1.4	10.4
0.2000	0.2928	0.9	3.4	1.0	4.3	1.2	5.9	1.4	8.7	1.8	14.3
0.2500	0.3781	1.1	4.3	1.2	5.5	1.4	7.6	1.8	11.2	2.3	18.5
0.3000	0.4680	1.3	5.4	1.5	6.8	1.7	9.4	2.1	13.9	2.7	22.9
0.3500	0.5624	1.5	6.4	1.7	8.2	2.0	11.3	2.5	16.7	3.2	27.5
0.4000	0.6612	1.7	7.6	2.0	9.6	2.3	13.3	2.8	19.6	3.6	32.3
0.4500	0.7642	2.0	8.8	2.2	11.1	2.6	15.4	3.2	22.6	4.1	37.3
0.5000	0.8716	2.2	10.0	2.5	12.7	2.9	17.5	3.5	25.8	4.5	42.6
0.5500	0.9832	2.4	11.3	2.7	14.3	3.2	19.8	3.9	29.1	5.0	48.0
0.6000	1.0990	2.6	12.6	3.0	16.0	3.5	22.1	4.2	32.6	5.4	53.7
0.6500	1.2190	2.8	14.0	3.2	17.7	3.8	24.5	4.6	36.1	5.9	59.6
0.7000	1.3431	3.1	15.4	3.4	19.5	4.1	27.0	4.9	39.8	6.3	65.6
0.7500	1.4714	3.3	16.9	3.7	21.4	4.3	29.6	5.3	43.6	6.8	71.9
0.8000	1.6037	3.5	18.4	3.9	23.3	4.6	32.2	5.6	47.5	7.2	78.4
0.8500	1.7401	3.7	20.0	4.2	25.3	4.9	35.0	6.0	51.5	7.7	85.0
0.9000	1.8806	3.9	21.6	4.4	27.3	5.2	37.8	6.3	55.7	8.1	91.9
0.9500	2.0251	4.2	23.2	4.7	29.4	5.5	40.7	6.7	60.0	8.6	99.0
1.0000	2.1737	4.4	24.9	4.9	31.5	5.8	43.7	7.0	64.4	9.0	106.2

TABLE A-IV-4

SOLIDIFICATION OF LEAD-TIN AT ZERO-SUPERHEAT

DIMENSIONLESS		HEAT TRANSFER COEFFICIENT (BTU/FT ² ·HR.·DEG. F)									
		45.0		40.0		34.0		28.0		21.8	
THICK	TIME	THICKIN	TIME	THICKIN	TIME	THICKIN	TIME	THICKIN	TIME	THICKIN	TIME
0.0500	0.0621	0.4	1.5	0.4	1.9	0.5	2.6	0.6	3.8	0.8	6.3
0.1000	0.1292	0.8	3.1	0.9	3.9	1.0	5.4	1.3	7.9	1.6	13.1
0.1500	0.2012	1.2	4.8	1.3	6.0	1.6	8.4	1.9	12.3	2.5	20.3
0.2000	0.2779	1.6	6.6	1.8	8.3	2.1	11.5	2.5	17.0	3.3	28.1
0.2500	0.3590	2.0	8.5	2.2	10.8	2.6	14.9	3.2	22.0	4.1	36.3
0.3000	0.4445	2.4	10.5	2.7	13.3	3.1	18.5	3.8	27.2	4.9	44.9
0.3500	0.5343	2.8	12.7	3.1	16.0	3.7	22.2	4.5	32.7	5.7	54.0
0.4000	0.6284	3.2	14.9	3.6	18.9	4.2	26.1	5.1	38.5	6.5	63.5
0.4500	0.7265	3.6	17.2	4.0	21.8	4.7	30.2	5.7	44.5	7.4	73.4
0.5000	0.8288	4.0	19.7	4.5	24.9	5.2	34.4	6.4	50.8	8.2	83.8
0.5500	0.9352	4.4	22.2	4.9	28.1	5.8	38.9	7.0	57.3	9.0	94.5
0.6000	1.0455	4.8	24.8	5.3	31.4	6.3	43.4	7.6	64.1	9.8	105.7
0.6500	1.1599	5.1	27.5	5.8	34.8	6.8	48.2	8.3	71.1	10.6	117.2
0.7000	1.2782	5.5	30.3	6.2	38.4	7.3	53.1	8.9	78.3	11.4	129.2
0.7500	1.4005	5.9	33.2	6.7	42.0	7.9	58.2	9.5	85.8	12.3	141.6
0.8000	1.5267	6.3	36.2	7.1	45.8	8.4	63.4	10.2	93.5	13.1	154.3
0.8500	1.6568	6.7	39.3	7.6	49.7	8.9	68.8	10.8	101.5	13.9	167.5
0.9000	1.7907	7.1	42.5	8.0	53.8	9.4	74.4	11.5	109.7	14.7	181.0
0.9500	1.9286	7.5	45.8	8.5	57.9	10.0	80.1	12.1	118.2	15.5	194.9
1.0000	2.0703	7.9	49.1	8.9	62.2	10.5	86.0	12.7	126.9	16.3	209.3

TABLE A-IV-5

SOLIDIFICATION OF LEAD TIN EUTECTIC AT SUPERHEAT

TIMESTAR	TIMEMIN THERMAL LAYER	THICKSTAR REACHED	THICKIN BOUNDARY OF	THETASTAR LIQUID REGION	THETAC BEFORE	MOLTENPRAM SOLIDIFICATION	THERMALIN STARTED	TOPTEMP
0.261	7.79	0.	0.	1.000	361.4	1.4448	4.40	475.9
0.311	9.28	0.0062	0.06	0.994	359.8	1.3160	4.35	442.7
0.361	10.77	0.0214	0.19	0.979	356.0	1.2250	4.21	419.3
0.411	12.27	0.0424	0.38	0.960	351.0	1.1576	4.03	402.0
0.461	13.76	0.0672	0.60	0.938	345.4	1.1069	3.80	388.9
0.511	15.25	0.0946	0.84	0.915	339.6	1.0691	3.56	379.2
0.561	16.74	0.1237	1.10	0.893	333.9	1.0417	3.30	372.1
0.611	18.24	0.1538	1.37	0.871	328.3	1.0230	3.03	367.3
0.661	19.73	0.1843	1.64	0.851	323.0	1.0112	2.76	364.3
0.711	21.22	0.2147	1.91	0.832	318.1	1.0046	2.49	362.6
0.761	22.71	0.2448	2.18	0.814	313.5	1.0015	2.22	361.8
0.811	24.21	0.2743	2.44	0.797	309.2	1.0004	1.96	361.5
0.861	25.70	0.3031	2.70	0.782	305.2	1.0001	1.70	361.4
0.911	27.19	0.3311	2.95	0.768	301.6	1.0000	1.45	361.4
0.961	28.68	0.3585	3.19	0.754	298.1	1.0000	1.21	361.4
1.011	30.18	0.3852	3.43	0.742	294.9	1.0000	0.97	361.4
1.061	31.67	0.4114	3.67	0.730	291.9	1.0000	0.74	361.4
1.111	33.16	0.4371	3.89	0.719	289.1	1.0000	0.51	361.4
1.161	34.65	0.4622	4.12	0.708	286.4	1.0000	0.29	361.4
1.211	36.15	0.4869	4.34	0.699	283.8	1.0000	0.07	361.4
1.223	36.52	0.4930	4.39	0.696	283.2	1.0000	0.01	361.4

DATA

THERMAL CAPACITY SOLID	THERMAL THERMAL	THERMAL CONDUCTIVITY SOLID	THERMAL THERMAL	DENSITY SOLID	LATENT HEAT	LIQUID HEIGHT	HEAT TRANSFER COEFFICIENT
26.8	26.0	29.7	16.5	518.9	15.9	0.367	40.0
BTU/FT(3) [°] F		BTU/FT.HR.DEG-F		LB/FT(3)	BTU/LB	FT	BTU/FT(2).HR.DEG-F.

TEMPERATURES

INITIAL
511.2[°]FSOLIDUS
257.4[°]FAMBIENT
104.0[°]F

TABLE A-IV-6

SOLIDIFICATION OF 10.0 WT.0/0 TIN LEAD-TIN ALLOY
AT ZERO-SUPERHEAT

TIMESTAR	TIMEMIN	THICKSTAR	THICKIN	THETASTAR	THETAC	MOLTENPRAM	THERMALIN	TOPTEMP
PARTIAL LAYER REACHED BOUNDARY OF LIQUID REGION BEFORE SOLIDIFICATION STARTED								
0.640	15.98	0.	0.	1.000	361.4	1.3479	4.80	450.9
0.690	17.23	0.0170	0.12	0.983	357.1	1.3049	4.68	439.9
0.740	18.48	0.0474	0.34	0.955	349.9	1.2698	4.46	430.8
0.790	19.73	0.0820	0.59	0.926	342.4	1.2364	4.21	422.3
0.840	20.98	0.1196	0.86	0.897	334.9	1.2039	3.94	413.9
0.890	22.23	0.1605	1.15	0.868	327.5	1.1721	3.65	405.7
0.940	23.48	0.2051	1.47	0.840	320.3	1.1408	3.33	397.6
0.990	24.72	0.2544	1.82	0.813	313.2	1.1101	2.98	389.7
1.040	25.97	0.3097	2.22	0.786	306.3	1.0801	2.58	382.0
1.090	27.22	0.3734	2.68	0.759	299.5	1.0510	2.12	374.5
1.140	28.47	0.4494	3.22	0.733	292.7	1.0240	1.58	367.6
1.190	29.72	0.5446	3.90	0.708	286.2	1.0037	0.90	362.3
1.233	30.78	0.6414	4.60	0.687	280.9	1.0000	0.20	361.4
1.243	31.04	0.6649	4.76	0.683	279.7	1.0000	0.04	361.4
1.244	31.07	0.6683	4.79	0.682	279.6	1.0000	0.01	361.4

1
226
1

DATA

THERMAL CAPACITY		THERMAL CONDUCTIVITY		DENSITY	LATENT HEAT	LIQUID HEIGHT	HEAT TRANSFER
SOLID	PARTIAL	SOLID	PARTIAL	SOLID			COEFFICIENT
23.7	49.4	20.3	10.9	659.5	1.3	0.400	34.0
BTU/FT(3)°F		BTU/FT.HR.DEG-F		LB/FT(3)	BTU/LB	FT	BTU/FT(2).HR.DEG-F.

TEMPERATURES

LIQUIDUS
459.0°F

SOLIDUS
257.4°F

AMBIENT
104.0°F

TABLE A-IV-7

SOLIDIFICATION OF 20.0 WT.0/0 TIN LEAD-TIN ALLOY
AT ZERO-SUPERHEAT

TIMESTAR	TIMEMIN	THICKSTAR	THICKIN	THETASTAR	THETAC	MOLTENPRAM	THERMALIN	TOPTMP
PARTIAL LAYER REACHED BOUNDARY OF LIQUID REGION BEFORE SOLIDIFICATION STARTED								
0.410	8.44	0.	0.	1.000	361.4	1.3252	4.00	445.1
0.460	9.47	0.0119	0.08	0.988	358.4	1.2725	3.92	431.6
0.510	10.50	0.0377	0.25	0.964	352.1	1.2310	3.74	420.9
0.560	11.53	0.0702	0.47	0.936	344.8	1.1941	3.52	411.4
0.610	12.56	0.1072	0.72	0.906	337.3	1.1597	3.27	402.5
0.660	13.59	0.1478	1.00	0.877	329.7	1.1272	3.00	394.1
0.710	14.61	0.1924	1.30	0.848	322.3	1.0964	2.70	386.2
0.760	15.64	0.2414	1.63	0.820	315.1	1.0677	2.37	378.8
0.810	16.67	0.2956	2.00	0.793	308.0	1.0417	2.00	372.1
0.860	17.70	0.3561	2.40	0.766	301.2	1.0199	1.59	366.5
0.910	18.73	0.4236	2.86	0.741	294.7	1.0051	1.14	362.7
0.960	19.76	0.4959	3.35	0.718	288.7	1.0001	0.65	361.4
1.002	20.64	0.5568	3.76	0.700	284.2	1.0000	0.24	361.4
1.026	21.13	0.5899	3.98	0.691	281.8	1.0000	0.01	361.4

- 227 -

DATA

THERMAL CAPACITY	THERMAL CONDUCTIVITY	DENSITY	LATENT HEAT	LIQUID HEIGHT	HEAT TRANSFER
SOLID PARTIAL	SOLID PARTIAL	SOLID			COEFFICIENT
24.4 49.0	22.5 12.2	626.6	3.1	0.333	40.0
BTU/FT(3)°F	BTU/FT.HR.DEG-F	LB/FT(3)	BTU/LB	FT	BTU/FT(2).HR.DEG-F.

TEMPERATURES

LIQUIDUS	SOLIDUS	AMBIENT
415.8°F	257.4°F	104.0°F

TABLE A-IV-8

SOLIDIFICATION OF 40.0 WT.0/0 TIN LEAD-TIN ALLOY
AT ZERO-SUPERHEAT

TIMESTAR	TIMEMIN	THICKSTAR	THICKIN	THETASTAR	THETAC	MOLTENPRAM	THERMALIN	TOPTMP
PARTIAL LAYER REACHED BOUNDARY OF LIQUID REGION BEFORE SOLIDIFICATION STARTED								
0.134	3.37	0.	0.	1.000	361.4	1.3175	3.96	443.1
0.184	4.64	0.0070	0.06	0.993	359.6	1.2510	3.90	426.0
0.234	5.90	0.0241	0.19	0.977	355.4	1.2001	3.77	412.9
0.284	7.16	0.0476	0.38	0.955	349.8	1.1582	3.58	402.1
0.334	8.42	0.0756	0.60	0.931	343.6	1.1224	3.36	392.9
0.384	9.69	0.1070	0.84	0.906	337.2	1.0914	3.12	384.9
0.434	10.95	0.1412	1.11	0.881	330.7	1.0648	2.85	378.1
0.484	12.21	0.1778	1.40	0.856	324.3	1.0424	2.56	372.3
0.534	13.47	0.2165	1.71	0.832	318.2	1.0246	2.25	367.7
0.584	14.74	0.2569	2.03	0.809	312.3	1.0118	1.93	364.4
0.634	16.00	0.2984	2.35	0.788	306.7	1.0041	1.61	362.5
0.684	17.26	0.3402	2.68	0.768	301.6	1.0008	1.28	361.6
0.734	18.52	0.3811	3.01	0.749	296.9	1.0000	0.95	361.4
0.784	19.79	0.4209	3.32	0.733	292.6	1.0000	0.64	361.4
0.834	21.05	0.4595	3.63	0.718	288.7	1.0000	0.33	361.4
0.884	22.31	0.4970	3.92	0.704	285.1	1.0000	0.04	361.4
0.890	22.47	0.5016	3.96	0.702	284.7	1.0000	0.00	361.4

228

DATA

THERMAL CAPACITY	THERMAL CONDUCTIVITY	DENSITY	LATENT HEAT	LIQUID HEIGHT	HEAT TRANSFER
SOLID PARTIAL	SOLID PARTIAL	SOLID			COEFFICIENT
25.6 48.9	26.3 14.5	569.8	8.5	0.330	40.0
BTU/FT(3) °F	BTU/FT.HR.DEG-F	LB/FT(3)	BTU/LB	FT	BTU/FT(2).HR.DEG-F.

TEMPERATURES

LIQUIDUS	SOLIDUS	AMBIENT
351.0 °F	257.4 °F	104.0 °F

TABLE A-IV-9

SOLIDIFICATION OF 80.0 WT.0/0 TIN LEAD-TIN ALLOY
AT ZERO-SUPERHEAT

TIMESTAR	TIMEMIN	THICKSTAR	THICKIN	THETASTAR	THETAC	MOLTENPRAM	THERMALIN	TOPTEMP
0.060	2.00	0.	0.	1.000	361.4	0.1952	1.88	393.8
0.110	3.65	0.0163	0.16	0.984	357.3	0.2729	2.63	393.8
0.160	5.31	0.0418	0.40	0.960	351.2	0.3018	2.91	393.8
0.210	6.96	0.0685	0.66	0.937	345.2	0.3196	3.08	393.8
0.260	8.62	0.0949	0.91	0.915	339.6	0.3335	3.21	393.8
0.285	9.45	0.1079	1.04	0.905	337.0	0.3398	3.27	393.8
0.298	9.86	0.1143	1.10	0.900	335.7	0.3428	3.30	393.8
0.299	9.89	0.1147	1.10	0.900	335.6	0.3430	3.30	393.8
PARTIAL LAYER HAS REACHED BOUNDARY OF LIQUID REGION								
0.349	11.54	0.1390	1.34	0.882	330.9	1.1178	3.07	391.7
0.399	13.20	0.1617	1.56	0.865	326.8	1.1079	2.85	389.2
0.449	14.85	0.1838	1.77	0.850	322.9	1.0966	2.63	386.3
0.499	16.51	0.2061	1.98	0.836	319.1	1.0843	2.42	383.1
0.549	18.16	0.2293	2.21	0.821	315.4	1.0712	2.20	379.7
0.599	19.82	0.2540	2.45	0.807	311.6	1.0576	1.96	376.2
0.649	21.47	0.2808	2.70	0.792	307.8	1.0434	1.70	372.6
0.699	23.13	0.3108	2.99	0.776	303.7	1.0291	1.41	368.9
0.749	24.78	0.3452	3.32	0.759	299.5	1.0152	1.08	365.3
0.799	26.44	0.3858	3.72	0.742	294.9	1.0037	0.69	362.3
0.844	27.93	0.4282	4.12	0.725	290.7	1.0000	0.28	361.4
0.865	28.63	0.4486	4.32	0.718	288.7	1.0000	0.08	361.4
0.871	28.83	0.4543	4.37	0.716	288.2	1.0000	0.03	361.4
0.874	28.93	0.4572	4.40	0.715	287.9	1.0000	0.00	361.4

229

DATA

THERMAL CAPACITY	THERMAL CONDUCTIVITY	DENSITY	LATENT HEAT	LIQUID HEIGHT	HEAT TRANSFER
SOLID PARTIAL	SOLID PARTIAL	SOLID			COEFFICIENT
27.5 210.2	32.1 18.0	482.4	8.1	0.367	40.0
BTU/FT(3)°F	BTU/FT.HR.DEG-F	LB/FT(3)	BTU/LB	FT	BTU/FT(2).HR.DEG-F.

TEMPERATURES

LIQUIDUS	SOLIDUS	AMBIENT
289.8 °F	257.4 °F	104.0 °F

TABLE A-IV-10

SOLIDIFICATION OF 90.0 WT.0/0 TIN LEAD-TIN ALLOY
AT ZERO-SUPERHEAT

TIMESTAR	TIMEMIN PARTIAL LAYER	THICKSTAR REACHED	THICKIN BOUNDARY OF	THETASTAR LIQUID REGION	THETAC BEFORE	MOLTENPRAM SOLIDIFICATION	THERMALIN STARTED	TOPTEMP
0.190	6.61	0.	0.	1.000	361.4	1.2245	4.00	419.2
0.240	8.35	0.0088	0.09	0.991	359.2	1.2005	3.91	413.0
0.290	10.09	0.0262	0.26	0.975	354.9	1.1814	3.73	408.1
0.340	11.83	0.0468	0.47	0.956	350.0	1.1634	3.53	403.5
0.390	13.58	0.0695	0.69	0.936	344.9	1.1456	3.30	398.9
0.440	15.32	0.0941	0.94	0.916	339.7	1.1274	3.06	394.2
0.490	17.06	0.1210	1.21	0.895	334.3	1.1089	2.79	389.4
0.540	18.80	0.1506	1.50	0.873	328.8	1.0897	2.49	384.5
0.590	20.54	0.1838	1.84	0.851	323.1	1.0698	2.16	379.4
0.640	22.29	0.2223	2.22	0.828	317.0	1.0489	1.78	374.0
0.690	24.03	0.2690	2.69	0.802	310.5	1.0269	1.31	368.3
0.740	25.77	0.3317	3.31	0.774	303.3	1.0052	0.68	362.7
0.762	26.55	0.3694	3.69	0.760	299.7	1.0001	0.31	361.4
0.773	26.95	0.3897	3.89	0.753	297.9	1.0000	0.10	361.4
0.779	27.14	0.3997	3.99	0.750	297.1	1.0000	0.00	361.4

DATA

THERMAL CAPACITY SOLID	THERMAL CAPACITY PARTIAL	THERMAL CONDUCTIVITY SOLID	THERMAL CONDUCTIVITY PARTIAL	DENSITY SOLID	LATENT HEAT	LIQUID HEIGHT	HEAT TRANSFER COEFFICIENT
27.9	175.0	33.3	18.7	464.6	4.0	0.333	40.0
BTU/FT(3) °F		BTU/FT.HR.DEG-F		LB/FT(3)	BTU/LB	FT	BTU/FT(2).HR.DEG-F.

TEMPERATURES

LIQUIDUS
316.6 °FSOLIDUS
257.4 °FAMBIENT
104.0 °F

TABLE A-IV-11 SCLIDIFICATION OF P20S IN THE PRESENCE OF SUPERHEAT

TIMMIN	TS IN	TPSTAR	TP IN	MCLTEMP	PARAM TL IN	THETASTAR	BASETEMP	TOPTEMP	MCDE
0.33	0.	0.	0.	0.2347	1.58	1.615	519.8	609.8	1
1.31	0.	0.096	0.7	0.4103	2.77	1.428	471.6	609.8	1
1.57	0.	0.118	0.8	0.4405	2.97	1.399	464.2	609.8	1
1.70	0.	0.128	0.9	0.4544	3.07	1.386	460.9	609.8	1
1.73	0.	0.130	0.9	0.4578	3.09	1.383	460.1	609.8	1
1.74	0.	0.132	0.9	0.4595	3.10	1.382	459.7	609.8	1
1.75	0.	0.132	0.9	0.4599	3.10	1.381	459.6	609.8	1
1.75	0.	0.132	0.9	0.4601	3.11	1.381	459.5	609.8	1
THERMAL LAYER HAS REACHED BOUNDARY OF LIQUID REGION									
2.78	0.	0.200	1.3	1.8781	2.65	1.303	439.4	587.4	2
3.81	0.	0.270	1.8	1.7858	2.17	1.250	425.7	563.7	2
4.84	0.	0.362	2.4	1.6979	1.56	1.208	415.0	541.0	2
5.77	0.	0.514	3.5	1.6245	0.53	1.178	407.3	522.2	2
6.70	0.	0.592	4.0	1.6154	-0.00	1.176	406.8	519.8	2
PARTIAL LAYER HAS REACHED THE REMOTE BOUNDARY									
12.09	0.	1.325	4.0	0.	-0.00	1.000	406.8	519.8	2
BASE HAS REACHED EUTECTIC TEMPERATURE									
13.12	0.08	1.271	3.9	0.	0.	0.988	358.3	431.1	5
14.15	0.26	1.228	3.7	0.	0.	0.963	351.9	420.1	5
15.18	0.49	1.190	3.5	0.	0.	0.934	344.4	410.3	5
16.21	0.74	1.155	3.3	0.	0.	0.904	336.7	401.2	5
17.24	1.03	1.122	3.0	0.	0.	0.874	329.0	392.7	5
18.27	1.34	1.091	2.7	0.	0.	0.845	321.4	384.7	5
19.30	1.68	1.062	2.3	0.	0.	0.816	314.1	377.3	5
20.33	2.06	1.036	1.9	0.	0.	0.789	307.0	370.7	5
21.35	2.48	1.016	1.5	0.	0.	0.762	300.2	365.4	5
22.38	2.95	1.003	1.0	0.	0.	0.737	293.7	362.2	5
23.41	3.44	1.000	0.6	0.	0.	0.714	287.8	361.4	5
24.44	3.92	1.000	0.1	0.	0.	0.694	282.6	361.4	5
24.57	3.98	1.000	0.0	0.	0.	0.692	282.0	361.4	5
24.60	3.99	1.000	0.0	0.	0.	0.691	281.9	361.4	5

INITIAL TEMPERATURE = 505.8 °F HEAT TRANSFER COEFFICIENT = 40.0 BTU/FT(2).HR.°F.
 HEIGHT OF METAL = 0.33 FT.

TABLE A-IV-12 SOLIDIFICATION OF P40S IN THE PRESENCE OF SUPERHEAT

TIMMIN	TS IN	TPSTAR	TP IN	MOLTENPARAM	TL IN	THETASTAR	BASETEMP	TOPTEMP	MODE
THERMAL LAYER REACHED BOUNDARY OF LIQUID REGION BEFORE SOLIDIFICATION STARTED									
1.88	0.	0.	0.	1.9843	3.96	1.364	455.0	614.8	2
3.14	0.	0.042	0.3	1.8362	3.63	1.276	432.4	576.6	2
4.40	0.	0.092	0.7	1.7047	3.23	1.201	413.2	542.8	2
5.66	0.	0.153	1.2	1.5880	2.76	1.138	397.0	512.8	2
6.93	0.	0.231	1.8	1.4849	2.14	1.084	383.1	486.2	2
8.19	0.	0.354	2.8	1.3953	1.17	1.039	371.5	463.2	2
9.23	0.	0.502	4.0	1.3636	-0.00	1.021	366.9	455.0	2
PARTIAL LAYER HAS REACHED THE REMOTE BOUNDARY									
9.94	0.	1.330	4.0	0.	-0.00	1.000	366.9	455.0	2
BASE HAS REACHED EUTECTIC TEMPERATURE									
11.21	0.05	1.264	3.9	0.	0.	0.993	359.7	429.3	5
12.47	0.18	1.213	3.8	0.	0.	0.977	355.6	416.2	5
13.73	0.36	1.171	3.6	0.	0.	0.957	350.2	405.3	5
14.99	0.57	1.134	3.4	0.	0.	0.933	344.2	395.9	5
16.25	0.81	1.102	3.1	0.	0.	0.909	338.0	387.7	5
17.52	1.07	1.074	2.9	0.	0.	0.884	331.6	380.6	5
18.78	1.35	1.051	2.6	0.	0.	0.860	325.3	374.4	5
20.04	1.65	1.031	2.3	0.	0.	0.836	319.2	369.4	5
21.30	1.96	1.016	2.0	0.	0.	0.813	313.4	365.6	5
22.57	2.29	1.006	1.7	0.	0.	0.792	307.8	363.1	5
23.83	2.61	1.002	1.3	0.	0.	0.772	302.6	361.8	5
25.09	2.94	1.000	1.0	0.	0.	0.753	297.8	361.4	5
26.35	3.26	1.000	0.7	0.	0.	0.736	293.4	361.4	5
27.62	3.56	1.000	0.4	0.	0.	0.721	289.5	361.4	5
28.88	3.86	1.000	0.1	0.	0.	0.706	285.8	361.4	5
29.19	3.93	1.000	0.0	0.	0.	0.703	284.9	361.4	5
29.27	3.95	1.000	0.0	0.	0.	0.702	284.7	361.4	5

INITIAL TEMPERATURE = 516.6 °F
 HEIGHT OF METAL = 0.33 FT.

HEAT TRANSFER COEFFICIENT = 40.0 BTU/FT(2).HR.°F

TABLE A-IV-13 SOLIDIFICATION OF S20P IN THE PRESENCE OF SUPERHEAT

TIMMIN	TS IN	TPSTAR	TP IN	MOLTENPARAM	TL IN	THETASTAR	BASETEMP	TOPTEMP	MODE
THERMAL LAYER REACHED BOUNDARY OF LIQUID REGION BEFORE SOLIDIFICATION STARTED									
3.54	0.	0.	0.	1.5850	4.40	1.126	393.8	512.0	2
5.59	0.	0.032	0.3	1.4410	4.09	1.075	380.7	474.9	2
7.25	0.	0.072	0.7	1.3296	3.71	1.036	370.7	446.2	2
8.90	0.	0.120	1.2	1.2450	3.25	1.005	362.7	424.5	2
10.56	0.	0.181	1.7	1.1833	2.66	0.979	356.0	408.6	2
BASE HAS REACHED EUTECTIC TEMPERATURE									
12.22	0.37	0.207	2.0	1.1406	2.04	0.964	352.0	397.6	4
13.87	0.68	0.252	2.4	1.1268	1.30	0.936	344.9	394.0	4
15.53	0.98	0.274	2.6	1.1259	0.78	0.911	338.4	393.8	4
17.18	1.27	0.289	2.8	1.1259	0.35	0.887	332.4	393.8	4
18.01	1.42	0.295	2.8	1.1259	0.15	0.877	329.6	393.8	4
18.42	1.49	0.298	2.9	1.1259	0.05	0.871	328.3	393.8	4
18.63	1.53	0.299	2.9	1.1259	-0.00	0.869	327.6	393.8	4
PARTIAL LAYER HAS REACHED THE REMOTE BOUNDARY									
20.28	1.69	1.112	2.7	1.1259	0.	0.857	324.6	390.1	5
21.54	1.87	1.098	2.5	1.1259	0.	0.844	321.3	386.5	5
23.59	2.06	1.084	2.3	1.1259	0.	0.831	317.9	383.0	5
25.25	2.28	1.070	2.1	1.1259	0.	0.818	314.4	379.3	5
26.90	2.51	1.055	1.9	1.1259	0.	0.803	310.8	375.7	5
28.56	2.77	1.041	1.6	1.1259	0.	0.789	307.0	372.0	5
30.21	3.06	1.027	1.3	1.1259	0.	0.773	302.9	368.3	5
31.87	3.40	1.013	1.0	1.1259	0.	0.756	298.7	364.7	5
33.53	3.80	1.002	0.6	1.1259	0.	0.738	294.1	362.0	5
35.18	4.26	1.000	0.1	1.1259	0.	0.720	289.4	361.4	5
35.59	4.37	1.000	0.0	1.1259	0.	0.716	288.3	361.4	5
35.70	4.40	1.000	0.0	1.1259	0.	0.715	288.0	361.4	5

INITIAL TEMPERATURE = 458.8 °F
 HEIGHT OF METAL = 0.37 FT.

HEAT TRANSFER COEFFICIENT = 40.0 BTU/FT(2).HR.°F

TABLE A-IV-14 SOLIDIFICATION OF SLOP IN THE PRESENCE OF SUPERHEAT

TIMMIN	TS IN	TPSTAR	TP IN	MOLTENPARAM	TL IN	THETASTAR	BASETEMP	TOPTEMP	MODE
THERMAL LAYER REACHED BOUNDARY OF LIQUID REGION BEFORE SOLIDIFICATION STARTED									
3.83	0.	0.	0.	1.6763	4.00	1.231	420.8	535.5	2
5.58	0.	0.041	0.4	1.5049	3.58	1.163	403.3	491.3	2
7.32	0.	0.095	0.9	1.3789	3.05	1.113	390.5	458.9	2
9.06	0.	0.167	1.7	1.2902	2.33	1.074	380.5	436.1	2
10.80	0.	0.286	2.8	1.2370	1.15	1.039	371.4	422.4	2
12.21	0.	0.401	4.0	1.2308	-0.00	1.005	362.6	420.8	2
PARTIAL LAYER HAS REACHED THE REMOTE BOUNDARY									
12.76	0.	1.223	4.0	0.	-0.00	1.000	362.6	420.8	2
BASE HAS REACHED EUTECTIC TEMPERATURE									
14.51	0.08	1.197	3.9	0.	0.	0.992	359.5	412.2	5
16.25	0.24	1.177	3.8	0.	0.	0.977	355.4	407.0	5
17.99	0.44	1.158	3.6	0.	0.	0.958	350.7	402.1	5
19.73	0.66	1.140	3.3	0.	0.	0.939	345.6	397.4	5
21.48	0.91	1.122	3.1	0.	0.	0.918	340.3	392.7	5
23.22	1.17	1.103	2.8	0.	0.	0.897	334.9	387.9	5
24.96	1.47	1.084	2.5	0.	0.	0.876	329.4	383.1	5
26.71	1.80	1.065	2.2	0.	0.	0.853	323.7	378.1	5
28.45	2.17	1.045	1.8	0.	0.	0.830	317.7	373.0	5
30.19	2.61	1.025	1.4	0.	0.	0.806	311.4	367.7	5
31.94	3.17	1.006	0.8	0.	0.	0.779	304.5	363.0	5
33.50	3.82	1.000	0.2	0.	0.	0.754	298.0	361.4	5

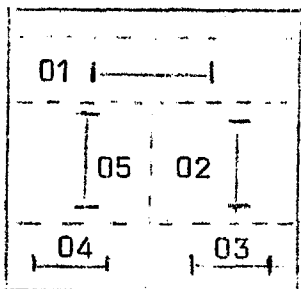
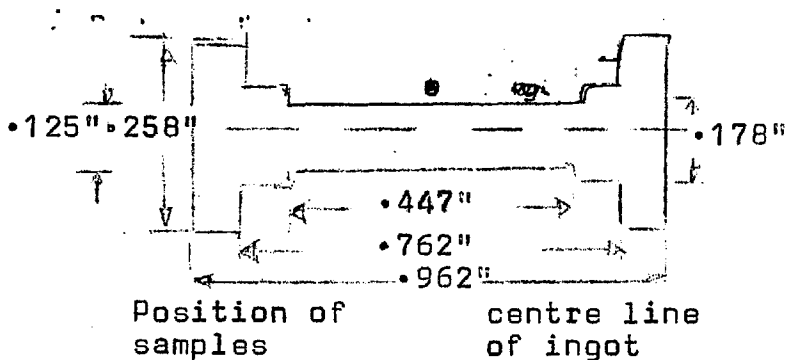
INITIAL TEMPERATURE = 496.8 °F
 HEIGHT OF METAL = 0.33 FT.

HEAT TRANSFER COEFFICIENT = 40.0 BTU/FT(2).HR.°F

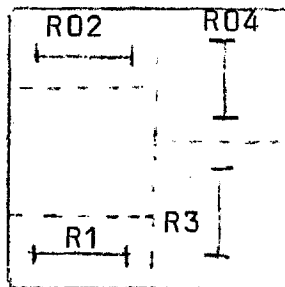
APPENDIX V

TENSILE STRENGTH OF PURE LEAD-TIN EUTECTIC

Dimension of standard sample



Normal ingot



Ingot produced by using vibrator

- O - Oriented grains along heat flow direction
- R - Random oriented
- RO - Oriented structure produced using vibrator

Sample No.	Structure	Tensile Strength (_{bs})	lb/in ²	Elongation
01	Oriented	59.5	4840	52%
02	"	83.8	6813	52%
03	"	59.5	4840	40%
04	"	58.2	4732	62%
05	"	86.0	6992	75%
R1	Random	62.6	5089	40%
R02	Oriented	64.0	5203	63%
R3	Random	78.2	6358	52%
R04	Oriented	93.7	7618	67%

ACKNOWLEDGEMENTS

Sincere appreciation is extended to Dr. A.W.D. Hills for supervision and assistance given during the course of this work. The author would like to thank Professor T.R. Anantharaman for providing the opportunity for this work.

Discussion and help of the members of The John Percy Research Group has been very useful. Valuable technical assistance of Mr. A.J. Haynes, the Workshop staff and the staff of the Analytical Services Laboratory is gratefully acknowledged.

The author is indebted to Banaras Hindu University, Varanasi, India, for the grant of the study leave; Professor F.D. Richardson for financial support during the first year of this work and the Science Research Council for providing the financial assistance for the remaining period.

The author wishes to record the help and understanding of his wife and children, without whose co-operation this work would not have been possible.

LIST OF FIGURES

<u>Fig. No.</u>		<u>Page No.</u>
II-1	Various morphologies of alloy solidification	14
III-1	Solidification Algorithm for pure metals and binary alloys	82
III-2	Calculation algorithm of pure metals and eutectic solidification	83
III-3	Calculation algorithm of alloy solidification	84
IV-1	Line diagram of the apparatus	99
IV-2	Casting Unit	100
IV-3	Multiple nozzle	105
V-1	Steady state heat transfer results plotted as $\log h(\text{Btu}/\text{ft.}^2\text{hr.}^\circ\text{F})$ versus \log air flow rate for different base temperatures	117
V-2	Solidification of Lead at zero-superheat, comparison of theoretical and experimental results using Hills' theory	122
V-3	Solidification of Lead at superheat, comparison of theoretical and experimental results	123
V-4	Solidification of lead-antimony eutectic at zero-superheat, comparison of theoretical and experimental results	124
V-5	Solidification of Lead-Tin eutectic at zero-superheat, comparison of theoretical and experimental results	125
V-6	Solidification of Lead-Tin eutectic at superheat, comparison of theoretical and experimental results	126
V-7	Cooling curves for 10 wt. % ^{Tin} Lead-Tin alloy at various distances from base	127
V-8	Cooling curves for 20 wt. % Tin, Lead-Tin alloy at various distances	128
V-9	Cooling curves for 40 wt. % Tin, Lead-Tin alloy	129

<u>Fig. No.</u>		<u>Page No.</u>
V-10	Cooling curves for 20 wt. % Lead, Tin-Lead alloy at various distances from base	130
V-11	Cooling curves for 10 wt. % Lead, Tin-Lead alloy at various distances from base	131
V-12	Lead-Tin phase diagram	132
V-13	Solidification of 10 wt. % Tin, Lead-Tin alloy at zero-superheat, comparison of theoretical and experimental results	133
V-14	Solidification of 20 wt. % Tin, Lead-Tin alloy at zero-superheat, comparison of theoretical and experimental results	134
V-15	Solidification of 20 wt. % Tin, Lead-Tin alloy at positive superheat, comparison of theoretical and experimental results	135
V-16	Solidification of 40 wt. % Tin, Lead-Tin alloy at zero-superheat, comparison of theoretical and experimental results	136
V-17	Solidification of 40 wt. % Tin, Lead-Tin alloy at positive superheat, comparison of theoretical and experimental results	137
V-18	Solidification of 20 wt. % Lead, Tin-Lead alloy at zero-superheat, comparison of theoretical and experimental results	138
V-19	Solidification of 20 wt. % Lead, Tin-Lead alloy at positive superheat, comparison of theoretical and experimental results	139
V-20	Solidification of 10 wt. % Lead, Tin-Lead alloy at zero-superheat, comparison of theoretical and experimental results	140
V-21	Solidification of 10 wt. % Lead, Tin-Lead alloy at positive superheat, comparison of theoretical and experimental results	141
V-22	Solidification of 20 wt. % Tin, Lead-Tin alloy at zero-superheat, comparison of theoretical and experimental base temperature	142
V-23	Solidification of Tin rich alloys at zero-superheat, comparison of theoretical and experimental base temperature	143

<u>Fig. No.</u>		<u>Page No.</u>
V-24	Microphotograph of Lead-Antimony eutectic	155
V-25	Microphotograph of Lead-Antimony eutectic	156
V-26	Electron probe chart showing distribution of lead and antimony in lead-antimony eutectic	157
V-27	Microphotograph of Lead-Tin eutectic	158
V-28	Microphotograph of Lead-Tin eutectic	159
V-29	Microphotograph of Lead-Tin eutectic	160
V-30	Microphotograph of 20 Wt. % Tin, Lead-Tin alloy	162
V-31	Microphotograph of 20 Wt. % Tin, Lead-Tin alloy	163
V-32	Diagrammatic representation of two phase structures obtained	164
V-33	Microphotograph of 20 wt. % Tin, Lead-Tin alloy	165
V-34	Microphotograph of 20 wt. % Tin, Lead-Tin alloy	166
V-35	Electron Probe chart showing distribution of lead and tin in light and dark phases of Fig. V-34	167
V-36	Microphotograph of 20 wt. % Tin, Lead-Tin alloy	168
V-37	Microphotograph of 20 wt. % Lead, Tin-Lead alloy	171
V-38	Microphotograph of 20 wt. % Lead, Tin-Lead alloy	172
V-39	Microphotograph of 20 wt. % Lead, Tin-Lead alloy	173
V-40	Electron Probe chart showing distribution of lead and tin in 20 wt. % Lead, Tin-Lead alloy	174
V-41	Microphotograph of 20 wt. % Lead, Tin-Lead alloy	175
V-42	Microphotograph of 20 wt. % Lead, Tin-Lead alloy	176

<u>Fig. No.</u>		<u>Page No.</u>
V-43	Microphotograph of 20 wt. % Lead, Tin-Lead alloy	177
V-44	Shape of Dendrites	178
V-45	Microphotograph of 20 wt. % Lead, Tin-Lead alloy	179
V-46	Microphotograph of 20 wt. % Lead, Tin-Lead alloy	180
V-47	Stereo Scan photograph of pour out sample	181
V-48	Microphotograph of 20 wt. % Lead, Tin-Lead alloy	182
V-49	Microphotograph of 20 wt. % Lead, Tin-Lead alloy	183
V-50	Microphotograph of 10 wt. % Lead, Tin-Lead alloy	184
V-51	Microphotograph of 10 wt. % Lead, Tin-Lead alloy	185
V-52	Electron Probe Microanalyser chart showing distribution of lead and tin in 10 wt. % Lead, Tin-Lead alloy at zero-superheat. Theoretical results (assuming fraction solidified (f) as a function of distance) are compared with experimental results	186
VI-1	Solidification of 10 wt. % Lead, Tin-Lead alloy at zero-superheat. Theoretical results (assuming fraction solidified (f_s) as a function of distance) are compared with experimental results.	194

LIST OF SYMBOLS

a_0, a_1, a_2	Coefficients in the polynomial series used to describe temperature profile in a layer
C_A, C_B	Composition of A and B constituents
C_0	Initial concentration of an alloy
C_E	Eutectic composition of an alloy
C_S^*	Composition of the solid phase at the solid/liquid interface
C_L^*	Composition of the liquid
$C_{L_S}^*, C_{L_E}^*$	Composition of liquid at solidus and liquidus temperatures respectively
C_S	Specific heat (Btu/lb.°F)
D	Initial thickness of the liquid
D_f	Diffusion coefficient
f_L	Fraction liquid present
f_{LU}	Fraction liquid present at solidus temperature
f_S	Fraction solid present
f_{SU}	Fraction solid present at solidus temperature
f'_θ	Equation III-2-19
f'_ω	Equation III-2-19
G	Temperature gradient
g'_t	Equation III-4-34
g'_ω	Equation III-4-35
h	Overall heat transfer coefficient from the surface of the metal to the cooling air (Btu/ft. ² °F)
H	Latent heat of an alloy (Btu/lb.)
H_P	Latent heat released in the partial layer = $H f_{SU}$
H_S	Latent heat released at the solidus temperature
$\Delta H_{S,E}$	Heat released during the solidification of an alloy of eutectic composition
$\Delta H_{F,L:E}$	Heat change in the formation of liquid alloys of eutectic composition

$\Delta H_{F,\alpha}$	Heat of formation of ' α ' solid solution
k	Equilibrium partition coefficient, $\frac{C_S^*}{C_L}$
K	Thermal conductivity (Btu/ft.hr. $^{\circ}$ F)
K_L	Thermal conductivity of the liquid phase
K_0	Thermal conductivity of the layer at the surface, when the temperature of the surface is θ_0 ($\theta_L > \theta_0 > \theta_S$)
K_p	Thermal conductivity of the partial layer
K_{pS}	Thermal conductivity of the partial layer when the partial layer is at the solidus temperature
K_S	Thermal conductivity of the solid phase
L	Half dendritic spacing
M	Slope of the liquidus curve
N_{Pb}, N_{Sn}	Atomic fraction lead and tin respectively
\dot{q}_0''	Heat flow from the surface, $hA(\theta_0 - \theta_a)$
$[\dot{q}_0'']_0$	Heat flow from the surface when the surface temperature is the solidus temperature ($\theta_0 = \theta_S$) = $hA(\theta_S - \theta_a)$
\dot{q}_L''	Heat flow from the liquid to the partial layer
\dot{q}_{tS}''	Heat flow from the liquid or partial layer to the solid layer
R	Rate of solidification
t_S	Thickness of the solid layer
t_L	Thickness of the thermal layer (cooled liquid)
t_p	Thickness of the partial layer
x	Distance co-ordinate along heat flow direction

GREEK SYMBOLS

τ	Time
$\bar{\tau}$	Dimensionless time
ρ	Density
γ	Thermal capacity, Btu/ft ³ . $^{\circ}$ F

γ_a	Thermal capacity of the alloy
γ_s	Thermal capacity of the solid
γ_p	Thermal capacity of the partial layer $(c_p + \frac{H_f^s \Delta T}{\theta_L - \theta_s})$
γ_L	Thermal capacity of the thermal layer
α_f	Flemings' criterion for microsegregation Equation II-1-7
θ	Temperature °F
θ_a	Ambient temperature
θ_D	Temperature of the remote boundary
θ_L	Liquidus temperature
θ_M	Initial temperature
θ_S	Solidus temperature
θ_0	Temperature of the surface

VARIABLES DEFINED BY EQUATION NO.

θ_F^*	Equation III-4-19
κ	Equation III-4-18
Ω	Equation II-2-31
Σ	Equation II-2-31
λ	Equation II-2-31
β	Equation III-4-66
ϵ	Equation III-4-61

DIMENSIONLESS VARIABLES

D^*	Dimensionless thickness of the initial liquid $= -[q_0]_0 t_s / \theta_s K_s$
K_L^*	Dimensionless thermal conductivity of the liquid $= K_L / K_S$
K_P^*	Dimensionless thermal conductivity of the partial layer $= K_P / K_S$
K_0^*	Dimensionless thermal conductivity of the surface when the surface temperature is $\theta_0 = K_0 / K_S$

q_L^*	Dimensionless heat flow from liquid = $\frac{\dot{q}_L''}{[\dot{q}_0'']_0}$
q_0^*	Dimensionless heat flow from the surface $\frac{\dot{q}_0''}{[\dot{q}_0'']_0}$
$q_{t_s}^*$	Dimensionless heat flow to the solid layer $\frac{\dot{q}_{t_s}''}{[\dot{q}_0'']_0}$
θ_D^*	Dimensionless temperature of the remote boundary θ_D/θ_S
θ_F^*	Fictitious temperature given by Equation III-4-19
θ_0^*	Dimensionless surface temperature θ_0/θ_S
θ_L^*	Dimensionless liquidus temperature θ_L/θ_S
θ_m^*	Dimensionless initial temperature of the liquid θ_m/θ_S
t_L^*	Dimensionless thickness of the thermal layer
t_P^*	Dimensionless thickness of the partial layer
t_S^*	Dimensionless thickness of the solid
	Dimensionless time $[\dot{q}_0'']_0^2/\theta_S^2 C_S K_S$
γ_P^*	Dimensionless thermal capacity of the partial layer
γ_L^*	Dimensionless thermal capacity of the thermal layer
H_S^*	Dimensionless latent heat $H_S/C_S \theta_S$

SYMBOLS USED IN THE TABLES A-IV-1 to A-IV-3

THETASTAR	Dimensionless surface temperature θ_0^*
TOP TEMP	Temperature of the remote boundary, θ_D
BASE TEMP	Surface temperature θ_0
THETAC	
TIMESTAR	Dimensionless time = τ
TIMES	
TIMEMIN	Time in minutes
TIMMIN	
TIME	
THICK	Dimensionless thickness of the solid, t_S^*
THICKSTAR	

TS IN } Thickness of the solid in inches, t_S
THICKIN }

TPSTAR Dimensionless parameter of the partial layer
TP IN Partial layer thickness in inches, t_p

MOLTEN PRAM Dimensionless parameter of the thermal layer

TL IN } Thermal layer in inches, t_L
THERMLIN }

MODE. Cooling Modes

- " 1 Mode S2
- " 2 Mode S2F
- " 3 Mode S3
- " 4 Mode S3F
- " 5 Mode Z3F

SYMBOLS USED IN THE COMPUTER PROGRAMME (Figs.A-III-1 to 3)

TS Dimensionless solid layer thickness, t_S^*

TP Dimensionless partial layer thickness, t_p^*

TL Dimensionless thermal layer thickness, t_L^*

D Dimensionless thickness of the initial liquid, D^*

THD Dimensionless temperature of the remote boundary, θ_D^*

TH Dimensionless temperature of the surface, θ_0^*

TT Dimensionless time

D1 $dt_S^*/d\bar{x}$

D2 $dt_p^*/d\bar{x}$

D3 $dt_L^*/d\bar{x}$

D4 $d\theta_0^*/d\bar{x}$

QL q_L^*

Q0 q_0^*

QTS $q_{t_S}^*$

GTP g_t^*

GTT $g_{\bar{x}}^*$

MODE 1 = 1 Mode S2
2 Mode S2F
3 Mode S3
4 Mode S3F
5 Mode Z3F

MODE 2 = 1 No change in MODE 1
2 Change from Mode S2 to Mode S2F
3 Change from Mode S2 to Mode S3
4 Change from Mode S2F to Mode S3F
5 Change from Mode S2F to Mode S3F
6 Change from Mode S3 to Mode S3F
7 Change from Mode S3F to Mode Z3F

REFERENCES*

1. Hills, A.W.D., Trans. TMS-AIME, 245, (1969), 1471.
2. Rutter, J.W. and Chalmers, B., Cand. J. Phys., 31, (1953), 15.
3. Chalmers, B., Trans. TMS-AIME, 200, (1956), 519.
4. Tiller, W.A. and Rutter, J.W., Cand. J. Phys., 34, (1956), 96.
5. Plaskett, T.S. and Winegard, W.C., Cand. J. Phys., 37, (1959), 1555.
6. Coulhard, J.C. and Elliot, R., The Solidification of Metals, ISI publication no. 110, Iron and Steel Inst., London, (1968), 61.
7. Davies, G.J., ibid., 66.
8. Mollard, F.R. and Flemings M.C., Trans. TMS-AIME, 239, (1967), 1526.
9. Cline, H.E., Trans. TMS-AIME, 242, (1968), 1613.
10. Pfann, W.G., Trans. TMS-AIME, 135, (1952), 85, Zone Melting, John Wiley and Sons, N.Y., (1958).
11. Bordy, H.D. and Flemings, M.C., Trans. TMS-AIME, 236, (1966), 615.
12. Goodman, T.R., J. Heat Transfer, Trans. ASME, series C, 89, (1967), 233.
13. Tien, R.H. and Geiger, G.E., ibid., 230.
14. Evers, N.R. et al., Phil. Trans., 240A, (1946), 1.
15. Dusinberre, G.M., Numerical Analysis of Heat Flow, McGraw-Hill, N.Y., (1949).
16. Ruddle, R.W., The Solidification of Castings, Inst. of Metals monograph and report series no. 7, Inst. of Metals, London, (1957).
17. Schneiwind, J., J. Iron and Steel Inst., 201, (1963), 594.
18. Mizikar, E.A., Trans. TMS-AIME, 239, (1967), 1747.
19. Adenis, D.J.P., Coats, K.H. and Ragone, D.V., J. Inst. Metals, 91, (1962), 3403.

*References are given in the form: Author, Journal, Volume, (year), page.

20. Peel, D.A. and Pengally, A.E., Mathematical Model in Metallurgical Process Development, Iron and Steel Inst., London, Conference, Feb. (1969), ISI reprint, 123.
21. Tien, R.H. and Geiger, G.E., J. Heat Transfer, Trans. ASME, series C, 90, (1968), 27.
22. Goodman, T.R., Trans. ASME, 30, (1948), 335.
23. Hills, A.W.D., Proc. of Symp., Chem. Engg. in the Metallurgical Industries, Inst. Chem. Engg., (1963), 123.
J. Iron and Steel Inst., 203, (1965), 18.
24. Hills, A.W.D. and Moore, M.R., Heat and Mass Transfer in Process Metallurgy, Inst. of Min. and Met., London, (1967), 141.
Trans. TMS-AIME, 249, (1969), 1481.
25. Koump, V., Tien, R.H. and Kim, W.J., Trans. TMS-AIME, 239, (1967), 1305.
26. Goodman, T.R. and Shea, J.J., J. Applied Mech., 27, (1960), 16.
27. Hrycak, P., J. A.I.Ch.E., 9, (1963), 585.
28. Tien, R.H. and Koump, V., Trans. TMS-AIME, 242, (1968), 1283.
29. Koump, V., Tien, R.H., and Perzak, T.F., ibid, 1589.
30. Kurz W. and Lux, B., Z. Metallk., 57, (1966), 70.
31. Southin, R.T., J. Inst. Metals, 94, (1966), 401.
32. Forsten, J. and Miekko-oja, J. Inst. Metals, 95, (1967), 143.
33. Chadwick, G., Acta Met., 10, (1962), 1.
34. Weinberg, F., Trans. TMS-AIME, 224, (1962), 628.
35. Muscon, D. and Hellawal, A., J. Inst. Metals, 92, (1963-64), 27.
36. Doherty, R.D. and Melford, D.A., J. Iron and Steel Inst., (1966), 1131.
37. Subramanian, S.V., Haworth, C.W. and Kirkwood, D.H., J. Iron and Steel Inst., 206, (1968), 1027 and 1124.
38. Hultgreen, R., Orr, R.L., Anderson, P.D. and Kelley, K.K., Selected Values of Thermodynamic Properties of Metals and Alloys, John Wiley & Sons Inc., London (1963).

39. Kleppa, O.J., J. Physical Chem., 59, (1955), 175.
40. Taylor, J.B., Phil. Mag., 50(5), (1900), 37.
41. Moore, M.R., Ph.D. Thesis, University of London, (1966).
42. Borelius, G., J. of Metals, 3, (1951), 477.
43. Smithells, C.J., Metals Reference Book, Butterworths, London, 3rd Edition, (1962).
44. Hansen, M., Constitution of Binary Alloys, McGraw-Hill, New York, 2nd Edition, (1958).
45. Doherty, R.D. and Feest, The solidification of metals, ISI publication no. 110, Iron and Steel Inst., London, (1968), 102.
46. Bolling, G.F. and Tiller, W.A., J. Applied Phys., 32, (1961), 2587.
47. Hunt, J.D. and Chilton, J.P., J. Inst. Metals, 92, (1963), 21.
48. Moore, A. and Elliot, R., J. Inst. Metals, 95, (1967), 369.
49. Brick, R.M. Trans. TMS-AIME, 161, (1945), 65.
50. Malinochka, Y.N., LiteinPe Proizvodstvo, 10, (1963), 28. Russian Casting Production, 10, (1963), 473.
51. Flemings, M.C., Modern Castings, July (1964), 253.
52. Hills, A.W.D., Ph.D. Thesis, University of London, (1966).